Functional studies on receptor-type protein tyrosine phosphatases of the R3 subgroup

Conn, O.

Functional studies on receptor-type protein tyrosine phosphatases of the R3 subgroup

Olga Conn

A thesis submitted in partial fulfilment of the requirements of the University of Westminster for the degree of Doctor of Philosophy

Department of Science and Technology

University of Westminster

August 2017

Acknowledgements

Firstly, I would like to extend my sincere gratitude to my supervisor Dr. Alastair Barr for giving me an exciting and valuable opportunity to study this Ph.D project. I am very grateful for his continuous support throughout my studies, for his immense knowledge, guidance and motivation. These four years have been really challenging and without his constant encouragement and sympathetic attitude this thesis would not be possible.

I am very grateful to Dr. Caroline Smith, who encouraged me to apply for this project. Thank you for always showing a great interest in the progress of my work and for giving me much appreciated valuable advice.

I would like to thank my second supervisor Dr. Miriam Dwek for her interesting suggestions, valuable comments and kind words. My sincere thanks also go to Dr. Anatoliy Markiv and Dr. Mark Odell for sharing their valuable experience and skills.

I would like to thank the University of Westminster for providing a scholarship and the British Pharmacological Society for various funds that allowed me to attend conferences and training courses.

And of course I would not be able to complete this project without the enormous support of my husband. It has been a long and rough journey. Thank you so much for being patient!

Last but not least I would like to thank my mother for always believing in me and Jeremy Alexander for endless reading and commenting on my written reports, abstracts, letters and thesis.

Table of Contents

Page Number

List of Figures

List of Tables

Abbreviations

Ab - antibody
ADP – adenosine diphosphate
Ang1 – angiopoietin-1
ATP – adenosine triphosphate
BiFC – bimolecular fluorescence complementation
BRET - bioluminescence resonance energy transfer
CTFG – connective tissue growth factor
DEP-1 - density-enhanced phosphatase-1
DSPs - dual specificity phosphatases
ECD – extracellular domain
ECM – extracellular matrix
EGF – epidermal growth factor
EGFR1 – epidermal growth factor receptor 1
EphB2 - Ephrin type-B receptor 2
FGF – fibroblast growth factor
FN - fibronectin
FRET - fluorescence resonance energy transfer
GF – growth factor
GLEPP1 - glomerular epithelial protein 1
Grb2 - Growth factor receptor-bound protein 2
HCC – hepatocellular carcinoma
HGF – hepatocyte growth factor
IGF – insulin-like growth factor
IL – interleukin
IR – insulin receptor
LAR – leukocyte common antigen related
MaMTH - mammalian-membrane two-hybrid
MAPK – mitogen-activated protein kinase
NGF – nerve growth factor
NK cells – natural killer cells
NT-3 – neurotrophin-3
NTPTPs – non-transmembrane protein tyrosine phosphatases

PDGF – platelet-derived growth factor

PI – phosphatidylinositol

PI3K – phosphatidylinositol 3 kinase

PTK – protein tyrosine kinase

PTMs – post-transfectional modifications

PTP – protein tyrosine phosphatase

RAP – receptor affinity phosphatase

ROS – reactive oxygen species

RPTK – receptor protein tyrosine kinase

RPTP – receptor protein tyrosine phosphatase

PTPRQ - protein tyrosine phosphatase receptor type Q

SAP-1 – stomach cancer-associated protein tyrosine phosphatase-1

Sdc - syndecan

SFKs - Src family kinases

SH2 – Src homology 2

SOS – Son of sevenless

SPN – sialophorin

TCR – T cell receptor

TF – transcription factor

TSP1 – thrombospondin-1

Tyr; Y – tyrosine

UV - ultraviolet

VEGF – vascular endothelial growth factor

VEGFR2 – vascular endothelial growth factor receptor 2

VE-PTP – vascular endothelial protein tyrosine phosphatase

YFP – yellow fluorescent protein

Abstract

The receptor-type protein tyrosine phosphatases (RPTPs) of the R3 subgroup play key roles in the immune, vascular and nervous system. They are characterised by an extracellular domain (ECD), comprised of multiple FNIII-like repeats, a transmembrane domain and a single intracellular phosphatase domain. Although their phosphatase domains have been Fstudied in detail the functional roles of their extracellular regions have not been clearly defined. Potential roles in ligand interaction, dimerisation and cell-cell contacts have been reported. Here I used a bimolecular fluorescence complementation (BiFC) assay in live cells to examine the molecular basis for the interaction of one of the R3 RPTP members, VE-PTP, with VE-cadherin, and explored the potential of others to interact with this protein. The potential of R3 RPTPs to homo-dimerise via extracellular domains in live cells was also addressed. Quantitative BiFC analysis using sialophorin (SPN), an unrelated membrane protein, and a membrane anchored C-terminal Venus-YFP (Myr-VC) fragment as controls revealed a specific interaction between VE-PTP and VE-cadherin using constructs expressing only the extracellular and transmembrane domains. Use of a deletion mutant indicated that, in contrast to previous studies, removal of the 17^{th} FNIII-like domain of VE-PTP is not sufficient to disrupt this interaction. Other members of the R3 RPTP family (DEP-1, GLEPP1 and SAP-1) also exhibited the potential to interact with VE-cadherin suggesting that specificity of this protein-protein interaction is not determined by the ECD alone. The direct interaction of DEP-1 with VE-cadherin is likely to be of physiological relevance since both proteins are expressed in endothelial cells. GLEPP1 and SAP-1 exhibited homo-dimerisation, whereas DEP-1 and VE-PTP did not form dimers via their extracellular and/or transmembrane domains. SPN was identified as a possible bona fide ligand for DEP-1 and their interaction is likely to be of physiological relevance since they were both shown to regulate T cell receptor activation. The interactions identified in the present study suggest a role for both the extracellular domain and transmembrane domain of R3-PTPs in interaction with VE-cadherin. The study also highlights the importance of using multiple controls in BiFC experiments and quantitative analysis of results.

Chapter 1

Introduction

1.1 Protein tyrosine phosphatases

Over the past few decades there has been a great improvement in the techniques for studying protein structures and functions. As a result there has been a great focus on processes by which newly synthesised proteins become post-translationally associated with specific organelles or are modified by folding or addition of different associated constituents, such as metals and carbohydrates (Waters, 2016). Almost all proteins undergo post-translational modifications (PTMs) that take place in different cellular compartments (e.g. nucleus, cytoplasm, endoplasmic reticulum and Golgi apparatus) and modulate functions of modified proteins. It has been proposed that overall structure and function of a mature protein in a cell could be influenced by PTMs (Blom *et al*, 2004). PTMs can be irreversible, such as proteolytic cleavage, or reversible, such as phosphorylation and glycosylation (Blom *et al*, 2004; Jensen, 2004). Protein modification by phosphorylation is considered a key event in many signal transduction pathways of biological systems and it mainly occurs on serine, threonine and tyrosine residues (Blom *et al*, 2004). For example, in cell signalling kinase cascades are turned on and off by the addition and removal of phosphate groups (Jensen, 2002; Jensen, 2004).

Many fundamental cellular processes in human cells, such as communication between and within the cells, proliferation, differentiation, metabolic homeostasis, migration and regulation of gene transcription, are coordinated by tyrosine and to a lesser extent by threonine and serine phosphorylation. Although phosphorylation of tyrosine residues represents less than 1%, tyrosine phosphorylation plays an essential role in signal transductions that regulate these cellular processes among neighbouring cells in embryogenesis, organ development, tissue homeostasis and the immune system (Alonso *et al*, 2004; Conrads and Veenstra, 2005). It is a reversible and dynamic process governed by the opposing, yet coordinated, activities of protein tyrosine kinases (PTKs) and protein tyrosine phosphatases (PTPs) (Ostman *et al*, 1994; Mustelin *et al*, 2002; Chiarugi, 2005). PTKs catalyse phosphorylation of protein, i.e. addition of a phosphate group, whereas PTPs are responsible for the removal of a phosphate group

(i.e. dephosphorylation), thus modifying biological function of their substrates (Figure 1). These two enzymatic reactions can have a variety of effects, including steric hindrance and either allosteric or conformational activation or inactivation (Hunter, 1995). It was generally considered that PTPs attenuate signal transductions generated by PTKs. However, numerous studies over a few decades demonstrated that PTPs have the potential to negatively regulate signalling by dephosphorylating autophosphorylation sites in PTKs themselves or phosphorylation sites in their downstream target as well as play a positive role by dephosphorylating an inhibitory site in a PTK, such as the C-terminal sites in Src family PTKs, thereby activating the kinase and promoting phosphorylation and signalling (Kohanski and Lane, 1986; Lin and Clinton, 1988; Ostergaard *et al*, 1989; Krebs, 1992; Thomas and Brown, 1999; Kang and Kim, 2006; Tonks, 2013). Although much more research has been focused on PTKs it is emerging that PTPs play specific, active and in some cases even dominant roles in regulating the levels of tyrosine phosphorylation in cells and in the regulation of many physiological processes (Fischer *et al*, 1991). Dysregulation of PTPs gives rise to a variety of inherited or acquired human diseases, such as cancer and immune deficiencies (Alonso *et al*, 2004). Therefore PTPs represent an important protein family the study of which would shed more light into their specific physiological functions and regulations as well as enabling development of novel therapeutic targets.

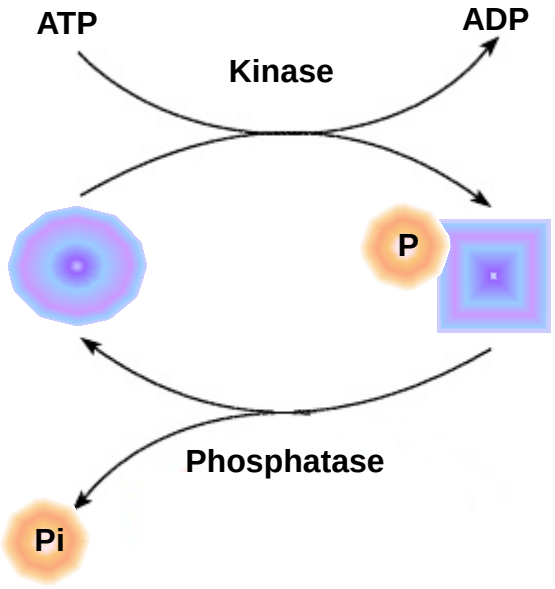

Figure 1. Phosphorylation/Dephosphorylation reactions. Protein tyrosine kinases catalyse the addition of phosphate groups (phosphorylation) by transferring the phosphate group from ATP to the hydroxyl group of a serine, threonine or tyrosine in the protein. Dephosphorylation is a reversal of phosphorylation catalysed by protein tyrosine phosphatases, which involves the removal of a phosphate group from a phosphorylated protein.

1.1.1 Dephosphorylation mechanism

Dephosphorylation of substrates by PTPs is a two-step mechanism (Figure 2). The first step involves the formation of a covalent bond between a PTP and the phosphate group of the substrate phosphotyrosine. In this process the phosphate group is displaced from the substrate's tyrosine, releasing the dephosphorylated protein. In the second step the subsequent PTP-phosphate bond (phosphoester bond) is hydrolysed, regenerating the active PTP and releasing the phosphate group (Ostman *et al*, 2006). In this step a water molecule acts as a nucleophile, which is activated by an aspartate residue by abstracting one of its hydrogens. A glutamine residue ensures the correct coordination of the hydrolytic water (Kolmodin and Aqvist, 2001).

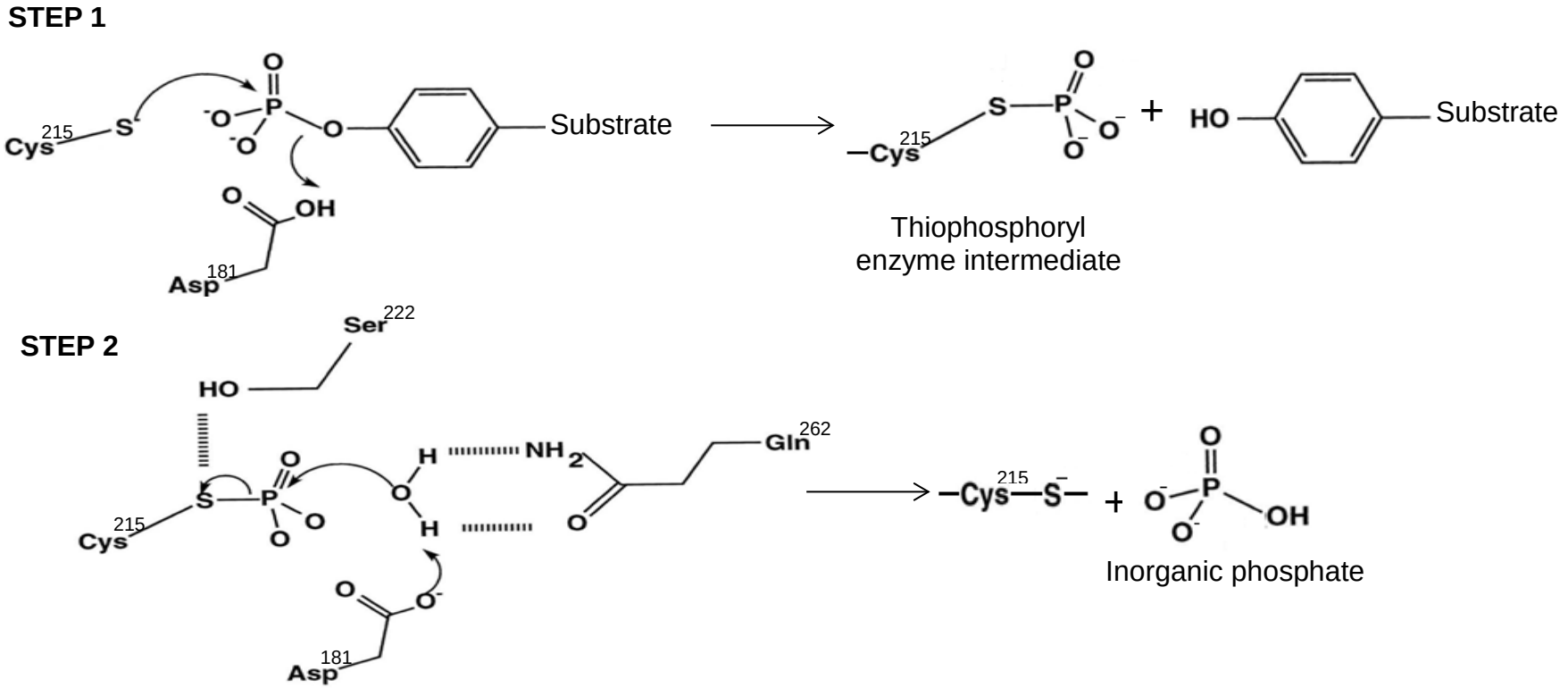

Figure 2. Two-step dephosphorylation mechanism. In the first step cysteine in the active site of a PTP acts as the attacking nucleophile, donating an electron to a phosphate group attached to a substrate, thus displacing the substrate and forming a thiophosphoryl enzyme intermediate (phospho-cysteine intermediate). The phosphoenzyme formation step is assisted by an aspartic acid, which protonates the P-O bond linking the phosphate group to the tyrosine with subsequent release of free substrate. In the second step the phosphoester bond in thiophosphoryl enzyme intermediate is hydrolysed, releasing free enzyme and inorganic phosphate. A glutamine residue coordinates a precise placement of the water nucleophile for efficient phosphoenzyme hydrolysis.

1.1.2 Classification of protein tyrosine phosphatases

Protein tyrosine phosphatases (PTPs) represent a large and diverse superfamily of related enzymes encoded by 107 PTP genes in the human genome (Alonso *et al*, 2004). The PTPs can be grouped into four families, namely Class I, II and III cysteine-based PTPs and aspartic acid-based PTPs. Based on their structure and substrate specificity Class I cysteine-based PTPs can be further divided into two major categories: the tyrosine-specific or “classical” PTPs, which are specific for phosphotyrosine (pTyr)-containing substrates and the dual specificity phosphatases (DSPs), which dephosphorylate pTyr and pSer/pThr and other substrates, such as lipids and mRNA. As demonstrated in Figure 3 classical PTPs, in turn, can be subdivided into intracellular non-transmembrane NT1-NT9 phosphatases and transmembrane receptor-like enzymes designated receptor types R1-R8 based on sequence similarity (Andersen *et al*, 2001; Alonso *et al*, 2004; Barr, 2010). This is a simplistic classification of phosphatases, which in reality is much more complex and diverse due to the use of alternative promoters, alternative mRNA splicing and post-translational modifications. Classical PTPs have one or two intracellular domains but only one membrane-proximal domain (D1) is believed to be catalytic, comprising about 280 residues. Nevertheless the structural integrity of the second PTP domain (D2) was shown to be important for the activity, specificity and stability of the RPTP as a whole and may provide docking sites for substrates and regulatory proteins (Tonks, 2006). The catalytic domain is defined by several conserved short sequence motifs, such as the signature sequence that functions as a phosphate-binding loop at the active site (Tonks, 2006). The specificity of the classical PTPs for the phosphotyrosyl residues could be partially explained by the depth of the active side cleft on the protein molecular surface. The depth of this cleft is determined by an invariant tyrosine residue from the pTyr loop. At the base of the cleft a cysteine (cys) residue is positioned within the PTP (i.e. catalytic) loop for nucleophilic attack on the phosphate moiety of the substrate (Salmeen *et al*, 2000). Non-transmembrane PTPs (NTPTPs) are rich in protein-protein interaction domains, such as the SH2 domain (Alonso *et al*, 2004). In addition the

NTPTPs contain a wide variety of structural motifs flanking the catalytic domain that are important for regulating their PTP activity, either directly by interaction with the active site or by controlling substrate specificity (Garton *et al*, 1997). The transmembrane receptor-like phosphatases (PTPs) are characterised by an extracellular domain and a membrane-spanning α-helix transmembrane. Many RPTPs display features of cell-adhesion molecules have been implicated in processes that involve cell–cell and cell–matrix contact (Tonks, 2006).

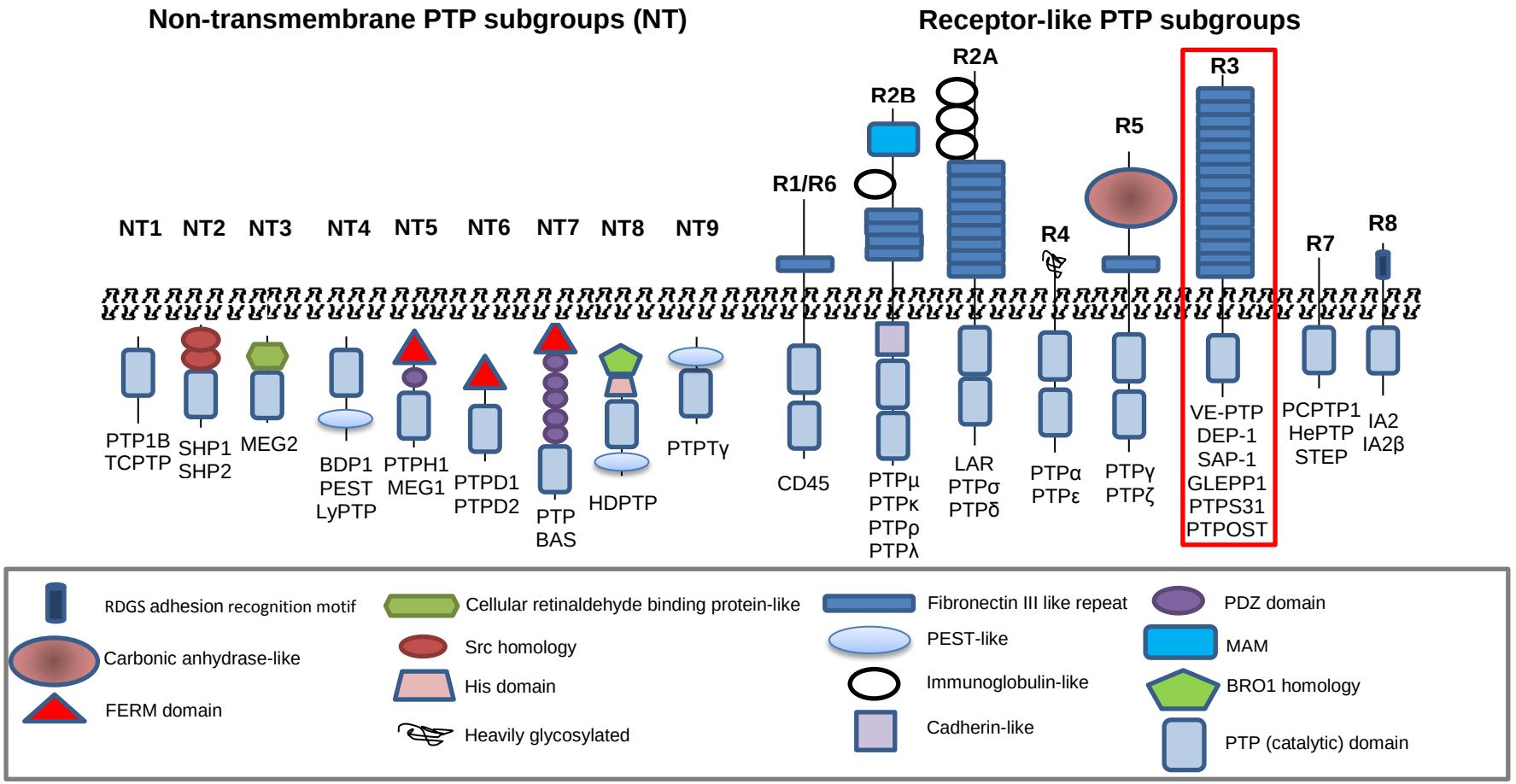

Figure 3. Schematic representation of Classical PTPs. The classical protein tyrosine phosphatases (PTPs) can be categorised as non-transmembrane (NT) or receptor-like (R) proteins. Both categories are further subdivided into NT1-NT9 groups for non-transmembrane phosphatases and R1-R8 groups for receptor phosphatases based on the structure similarities. Only the human PTPs are shown. The image was obtained and modified from Tonks (2006).

1.2 Protein tyrosine phosphatases of R3 subgroup

The focus of this thesis is on the receptor-type PTPs of R3 subgroup (R3 RPTPs) (boxed in red in Figure 3). There are five RPTP members in this subgroup in humans and mice: density-enhanced phosphatase-1 (DEP-1), vascular endothelial protein tyrosine phosphatase (VE-PTP), glomerular epithelial protein 1 (GLEPP1), stomach cancer-associated protein tyrosine phosphatase-1 (SAP- 1) and protein tyrosine phosphatase receptor type Q (PTPRQ). Only the first four members are tyrosine phosphatases. The PTPRQ protein, although it shares primary structure with the other R3 RPTPs, is a phosphatidylinositol (PI) phosphatase and has little activity towards protein substrates (Yu *et al*, 2013; Jeon, 2015). Therefore, only VE-PTP, DEP-1, SAP-1 and GLEPP1 transmembrane enzymes were investigated in this project. The schematic representation of these proteins is shown in Figure 4.

All the members of the R3 subgroup of RPTPs share a similar structure, with an extended N-terminal extracellular portion containing multiple fibronectin type III-like domains (Figure 4), a transmembrane domain and a single catalytic domain in the cytoplasmic region, which contains a highly conserved active site with a cysteine residue and the flexible WPD (Trp-Pro-Asp) loop (Murata *et al*, 2010; cited in Barr, 2010). In addition, all R3 RPTP members are highly glycosylated, containing multiple N-glycosylation sites in their extracellular region (Matozaki *et al*, 2010).

The intracellular portion of these enzymes has been studied intensively and it has been shown that they share other features as well. For example, all members of this subgroup undergo tyrosine phosphorylation at the amino acid motif YxNϕ (where x represents any amino acid and ϕ a hydrophobic amino acid) in the COOH-terminal region (Matozaki *et al*, 2010; Murata *et al*, 2010). For example, in SAP-1 two tyrosine residues at positions 945 and 953 were demonstrated to be potential phosphorylation sites. Whereas Tyr^{1220} in GLEPP1 and Tyr^{1982} in VE-PTP were shown to be required for the phosphorylation of these phosphatases (Murata *et al*, 2010). DEP-1 was shown to be phosphorylated on residues Tyr^{1311} and Tyr^{1320} in response to

vascular endothelial growth factor (VEGF) (Spring *et al*, 2014). Src family kinases are important for the tyrosine phosphorylation of R3 RPTPs. This motif was shown to act as a binding site for the Src homology-2 (SH2) domains of Src family kinases (SFKs), leading to the dephosphorylation and consequent activation of Src by the catalytic domain of R3 RPTPs (Matozaki *et al*, 2010; Murata *et al*, 2010). The same motif has been shown to be involved in interaction with an adaptor protein Grb2, which forms a complex with a guanine nucleotide exchange protein, Son of sevenless (SOS), that in turn promotes the activation of the Ras/mitogen-activated protein kinase (MAPK) pathway (Murata *et al*, 2010). However, the functional significance for the interaction between Grb2 and R3 subgroup RPTPs remains unclear. In addition R3 RPTPs are expressed in a single or limited number of cell types and unambiguously at the apical surface of polarised cells. Interestingly, in the case of VE-PTP it has been shown that with increasing cell density more VE-PTP was detected at cell contacts but the overall expression level of this phosphatase was not affected (Nottebaum *et al*, 2008).

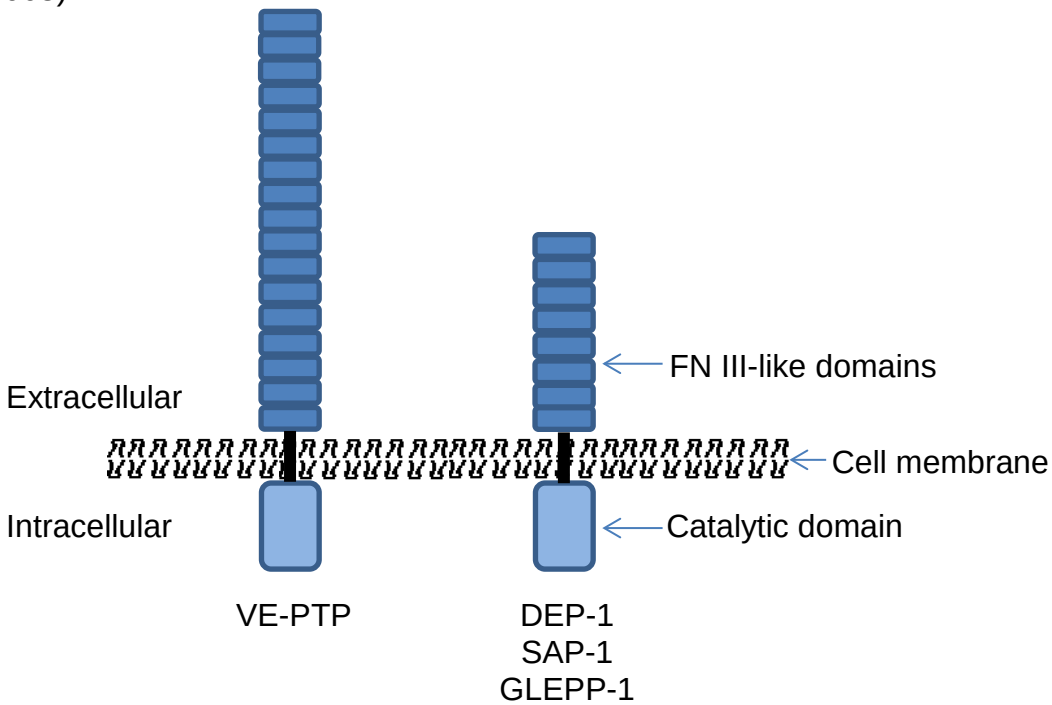

Figure 4. Schematic representation of the R3 RPTPs. VE-PTP has 17 fibronectin type III-like domains and SAP-1, GLEPP-1 and DEP-1 have eight fibronectin type III-like domains in their extracellular region. These enzymes are Ia membrane proteins that have a single transmembrane spanning domain, cleavable single peptide and a single intracellular catalytic domain.

1.2.1 Signal transduction pathways of R3 RPTPs

Some RPTPs have been reported to regulate the activity of RPTKs through dephosphorylation. Ligand-binding to the extracellular domains of RPTKs was shown to induce their dimerisation, resulting in the subsequent autophosphorylation of their cytoplasmic domains and activation of the tyrosine kinase activity. Phosphorylated tyrosine sites in the RPTKs cytoplasmic domains serve as binding sites for specific downstream signalling molecules, which, upon complex formation, initiate a specific signal transduction (Sakuraba *et al*, 2013). A study by Sakuraba *et al* (2013) using a two-hybrid system with substrate-trapping R3 RPTP mutants demonstrated that the members of the R3 subgroup share some similarities in specificity towards some RPTKs but differences towards others. All four members appeared to interact with and dephosphorylate TYRO3 and EphB2 tyrosine kinases whereas protein tyrosine kinase RET was recognised only by DEP-1, and EGFR1 and VEGFR2 kinases by SAP-1. However, the signal transduction pathways are not fully defined for all R3 RPTPs. It is interesting to note that VEGFR2 was identified as a substrate for SAP-1 in a study by Sakuraba *et al* (2013) whereas in a study by Chabot *et al* (2009) VEGFR2 was identified as a bona fide substrate for DEP-1. DEP-1 was shown to specifically dephosphorylate tyrosine residues in the activation loop of VEGFR2 and, thus, play a regulatory role in the VEGFR2-mediated angiogenic signalling response. The proposed DEP-1 regulation of VEGFR2-mediated signalling pathway is shown in Figure 5. It appears that DEP-1 exerts both negative and positive regulation of VEGFR2 activity perhaps by dephosphorylating different tyrosine residues. Upon VEGF stimulation VEGFR2 undergoes dimerisation that allows trans/autophosphorylation of several intracellular tyrosine residues. Activated VEGFR2 then associates with numerous signal transducers, resulting in endothelial cell survival, proliferation and migration (Laramee *et al,* 2007). Activated VEGFR2 was shown to associate with VE-cadherin-β-catenin complex, where it is dephosphorylated by DEP-1 (Lampugnani *et al*, 2003). This results in impaired activation of the proliferative ERK1/2 pathway and, thus, in decreased endothelial cell proliferation (Chabot *et al*, 2009). A study by

Laramee *et al* (2007) demonstrated that upon VEGF stimulation VEGFR2 also associates with and phosphorylates an adaptor protein Gab1. It has been suggested that the activated Gab1 links the DEP-1-activated Src (through dephosphorylation of the Src-inhibitory tyrosine residue Y529) to phosphatidylinositol3 kinase (PI3K) and subsequently activates Akt signalling pathway that promotes cell survival (Laramee *et al,* 2007; Chabot *et al*, 2009; Lampugnani *et al*, 2003). VE-PTP was also shown to interact with and dephosphorylate VEGFR2. However, unlike with DEP-1, this association is not direct but mediated by the Angiopoietin-1 (Ang1) receptor Tie-2 and it is accompanied by decreased VE-cadherin phosphorylation and the subsequent enhancement of lumenised vessel formation (Hayashi *et al*, 2013). VE-PTP, Tie-2 and VEGFR2 appear to form a trimeric complex that, upon stimulation by VEGF and Ang1, translocates to junctions where Tie2 and VEGFR2 are dephosphorylated and thus inactivated by VE-PTP. Downregulation of VE-PTP results in increased activation of VEGFR2 and Tie-2 and leads to VE-cadherin phosphorylation and formation of pathological vasculature (Hayashi *et al*, 2013). However, the exact signalling pathway that brings all these proteins together in regulation of VE-cadherin-mediated angiogenesis is not yet defined.

However, it is important to note that the above studies obtained their results using different methods. A study by Sakuraba *et al* (2013) used mammalian two-hybrid assay, which provides sensitivity and specificity in protein-protein interaction studies and allows the assayed proteins to undergo appropriate post-translational modifications in their native cellular context. However, caution must be taken when interpreting the results as an exogenous expression of hybrid “prey” and “bait” proteins could lead to either false positive or false negative results. For example, overexpression of proteins is common and can create the risk that the proteins interact merely due to their high concentration in the cell. Generation of hybrid proteins can also result in steric hindrance, preventing the association of the assayed proteins and thus giving rise to false negative interactions. On the other hand, fusion proteins can adopt altered conformations, which could result in exposure of an interaction domain that is normally hidden in the protein structure, facilitating

non-native interactions and resulting in false-positive signal (Lievens *et al*, 2009). In contrast, a study by Chabot *et al* (2009) used substrate-trapping experiments which, although versatile and any type of cells, tissues or organ can be used, are prone to artifactual results since isolated PTPs can be promiscuous. In addition, both studies investigated the ability of a sigle PTP to dephosphorylate VEGFR2 (i.e. SAP-1 in the Sakuraba *et al* (2013) study and DEP-1 in the Chabot *et al* (2009) study). However, since these PTPs belong to the same R3 subgroup they could both have a potential to recognise the same substrate.

A study by Shintani *et al* (2015) showed that R3 RPTPs could also be involved in insulin receptor (IR) signalling. Upon insulin stimulation the IR undergoes autophosphorylation. Activated IR subsequently phosphorylates and activates downstream signals, including PI3K and Akt (Saltiel and Kahn, 2001). All four members of R3 subgroup have been shown to suppress activation of the IR by specifically interacting with and dephosphorylating Y960 in the juxtamembrane region and Y1146 in the activation loop of the IR (Shintani *et al*, 2015). Although all four phosphatases showed similar dephosphorylating activities towards IR, only DEP-1 was found to be expressed and co-localised with IR in insulin target tissues (i.e. skeletal muscle, liver and adipose tissue) and, thus, was the most likely member to regulate insulin signalling *in vivo* (Shintani *et al*, 2015). This is an interesting observation that raises some questions about substrate specificity. If all four members have a potential to bind directly to the same substrate (as in the case with insulin receptor) *in vitro*, then it remains unclear how the substrate specificity is determined *in vivo*.

Despite many cellular targets involved in essential cellular activities, such as cell survival, proliferation and migration, the exact signalling events are not fully understood. This highlights the complexity of signal transductions and shows that one protein can trigger different signalling pathways. Even though the members of R3 RPTP subgroup show the specificity towards the same substrate, the biological downstream activities could be diverse. In addition, it is still not entirely understood how their involvement in certain signalling pathways is regulated.

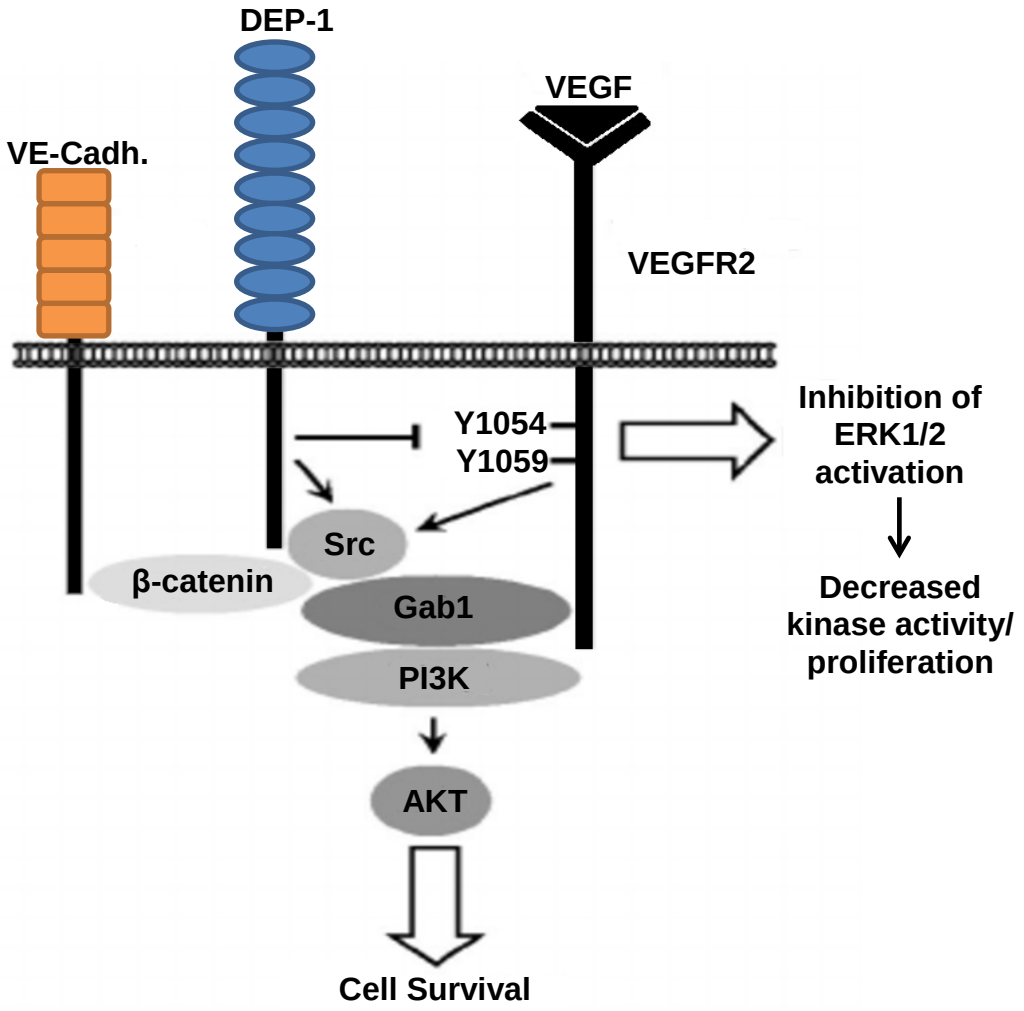

Figure 5. Regulation of signal transduction required for endothelial cell survival and proliferation by DEP-1. DEP-1 dephosphorylates VEGFR2 on tyrosine residues in the activation loop (Y1054 and Y1059), attenuating VEGFR2 kinase activity and resulting in the inhibition of the proliferative ERK1/2 pathway. At the same time DEP-1 positively regulates VEGF-induced Src and Akt activation. DEP-1 dephosphorylates the Src-inhibitory Y529, activating it. Upon VEGFR2 stimulation an adaptor protein Gab1 is rapidly phosphorylated by the activated Src and relocated to membrane, where it is recruited to the VEGFR2/VE-cadherin complex. This results in the induced association of PI3K to PH domain of Gab1 and the optimal activation of Akt and endothelial cell survival in response.

1.2.2 VE-PTP (PTPRB)

VE-PTP is expressed in vascular endothelial cells, especially in brain, lung and heart and more strongly in arterial endothelium (Fachinger *et al*, 1999). VE-PTP was shown to interact with the tyrosine kinase Tie-2 receptor (a receptor for angiopoietin that plays an important role in angiogenesis) via the intracellular parts of the proteins, causing dephosphorylation of Tie-2, which in turn results in inhibition of the proliferation of endothelial cells (cited in Matozaki *et al*, 2010; Baumer *et al*, 2006; Fachinger *et al*, 1999). Furthermore, co-precipitation experiments using COS-7 cells showed that VE-PTP also associates with the adhesion molecule of endothelial adherens junctions VE-cadherin and enhances cell-cell adhesion mediated by this molecule. But the interesting point is that this association takes place independently of their cytoplasmic tails and occurs via extracellular domains (Nawroth *et al*, 2002). Experiments using a series of truncation mutants led to the conclusion that the 5^{th} cadherin domain of VE-cadherin interacts with the 17^{th} FNIII repeat of VE-PTP. This finding raises a question as to the role of the other 16 FNIII domains in VE-PTP and other 4 domains in VE-cadherin. Taking into account that VE-PTP interacts with Tie-2 and VE-cadherin, it might play an important role in the regulation of functions of vascular adhesion molecules required for efficient angiogenesis (Matozaki *et al*, 2010). Some results showed the up-regulation of VE-PTP expression in new tumour vessels, suggesting the involvement of VE-PTP in tumour angiogenesis (Dominguez *et al*, 2007).

1.2.3 GLEPP-1 (PTPRO)

Alternative splicing of GLEPP1 mRNA generates either a cytoplasmic or transmembrane form of the enzyme (Pixley *et al*, 1995). Five spliced isoforms are known: two transmembrane-type isoforms are highly expressed in the developing nervous system, where they are involved in the regulation of axon guidance. Three truncated isoforms of GLEPP1 lacking the extracellular domain are expressed in macrophages, B cells and osteoclasts (cited in Matozaki *et al*, 2010). GLEPP1 is also expressed in the renal visceral glomerular epithelial cell (podocytes), where it may play an important role in signalling pathways required for the regulation of structure and function of the slit diaphragm of podocytes, necessary for the size-selective filtration barrier of the kidney (Thomas *et al*, 1994; Matozaki *et al*, 2010; Beltran et al, 2003). This regulation is achieved through phosphorylation/dephosphorylation of serine, threonine or tyrosine residues of the adhesion proteins nephrin and neph1, creating binding sites for SH2 domain-containing molecules and forming multiprotein complexes (Benzing, 2004). The GLEPP1 (*PTPRO* gene)-deficient mice showed reduced glomerular filtration and a tendency to hypertension (Wharram *et al*, 2000). Some evidence showed that the likely relevant substrate for GLEPP1 is the high-affinity receptor for neurotrophin-3 (NT-3) tropomyosin-related kinase C (TrkC) (Hower *et al*, 2009). GLEPP1 is co-expressed with TrkC in neurons in several locations, including sensory ganglia, cranial ganglia, spinal cord and cortex (cited in Hower *et al*, 2009). Studies on *PTPRO*$^{-/-}$ mice demonstrated that lack of GLEPP1 resulted in a disturbed axon guidance in TrkC-expressing sensory neurons, suggesting that GLEPP1 may play a role in regulation of axon outgrowth and guidance (Gonzalez-Brito and Bixby, 2009).

1.2.4 SAP-1 (PTPRH)

SAP-1 is expressed in the gastrointestinal tract, particularly in the small intestine and colon as well as stomach, and specifically localised at the microvilli of the brush border in gastrointestinal epithelial cells (Sadakata *et al*, 2009). It has been suggested that SAP-1 regulates intestinal tumorigenesis, though the exact mechanism of this regulation remains unclear (Sadakata *et al*, 2009). Using a substrate-trapping strategy it was possible to identify likely physiological substrates that are dephosphorylated by SAP-1 – prominent focal adhesion-associated proteins $p130^{Cas}$ and, to a lesser extent, paxillin. Since $p130^{Cas}$ plays an important role in the maintenance of actin stress fibres and focal adhesions through the association with the SH2 domain-containing adapter protein Crk as well as contributing to cell spreading on the extracellular matrix (ECM), SAP-1 is probably involved in regulation of the rearrangement of the actin-based cytoskeleton and cell spreading on fibronectin (Noguchi *et al*, 2001). The cytoplasmic region of SAP-1 was shown to bind to protein kinase Lck, resulting in the inhibition of the Lck kinase activity and consequent inhibition of T cell receptor-mediated T cell function (Sadakata *et al*, 2009). However, the exact mechanism of SAP-1 regulation of Lck-mediated T cell function remains unclear. SAP-1 has been shown to regulate negatively the progression of human hepatocellular carcinoma (HCC) by suppressing mitogenic and survival signalling and the expression of this protein seems to be down-regulated at the later stages of human HCC (Nagano *et al*, 2003). Similar results were obtained by studying colorectal cancer tissues, showing a decrease in SAP-1 expression with the progression of this cancer (Seo *et al*, 1997).

1.2.5 DEP-1 (PTPRJ)

DEP-1 (also known as PTPRJ and CD148) is expressed by all resting leukocytes, with the highest level of expression on monocytes, intermediate level on NK cells, B cells and $CD8^+$ T cells and the lowest level on $CD4^+$ T cells. The expression of DEP-1 on peripheral T cells is up-regulated in the presence of IL-2 and IL-15, suggesting that DEP-1 is involved in the functional regulation of activated T cells, particularly $CD8^+$ T cells. The fact that DEP-1 is also expressed on monocytes, B cells and NK cells suggests that CD148 may have a role in the biological responses of different populations of mononuclear cells and that its primary function is not restricted to T cells (Tangye *et al*, 1998). In addition, a study by Borges *et al* (1996) showed that the high expression levels of DEP-1 are also present in distal tubule epithelia and endothelial cells at sites of cell-cell interactions as well as megakaryocytes (Borges *et al*, 1996). The expression of this PTP displayed a direct relation to cell density, suggesting that it may play a role in regulation of cell contact-mediated growth inhibition (Borges *et al*, 1996; Matozaki *et al*, 2010). DEP-1 has been found to function as a tumour suppressor and deletion or mutation of a gene *PTPRJ* that encodes for this protein can be observed in colon cancer (Ostman *et al,* 2006; Barr, 2010). A study by Whiteford *et al* (2011) showed that heparin sulphate proteoglycan Syndecan-2 acts as a ligand for the DEP-1 and through the interaction of the extracellular domains of these two proteins (which requires PI3K activity downstream of Src kinase) the extracellular core protein of Syndecan-2 promotes β1 integrin-mediated fibroblast attachment and spreading. Another ligand for DEP-1 is Thrombospondin-1 (TSP1) – a glycoprotein that mediates cell-cell and cell-matrix interactions. TSP1 increases DEP-1 activity, influencing the dephosphorylation of its substrates (Takahashi *et al*, 2012).

1.3 Function of R3 RPTP extracellular domain

Even though these PTPs show functional importance in the regulation, both positive and negative, of signal transduction, the exact functions and mechanisms remain uncharacterised and require further investigation. Although the function of the intracellular catalytic domain of RPTPs has been extensively studied the function of the extracellular domain for RPTPs is less clearly defined but probably plays an important role in regulating activity. For example, the extracellular domain (ECD) of a type IIB receptor protein tyrosine phosphatase RPTPμ was shown to play a key regulatory role in modulating the stability of adherens junctions. The extracellular region of this protein is highly N-glycosylated and consists of one MAM (meprin/A5/μ) domain, one immunoglobulin (Ig)-like domain and four fibronectin (FN) type III repeats, forming rigid rod-like architecture. RPTPμ is a cell adhesion molecule that forms high affinity *trans*-dimers, the dimensions of which match cadherin-mediated cell junctions and, thus, has a potential to act as a spacer clamp, locking the phosphatase activity at the adherens junction (Aricescu *et al*, 2007).

Recent findings demonstrate that the extracellular domains of DEP-1 (also named PTPRJ and CD148) and CD45 are involved in regulation of T-cell receptor (TCR) triggering through mediating their passive (i.e. signalling independent) segregation from areas of close cell-cell contact (Cordoba *et al*, 2013). It was suggested that the segregation from the engaged TCR is enhanced by the large extracellular domains of CD148 and CD45. The results also showed that it is the large size of the CD148 extracellular domain that prevents it from inhibiting TCR signalling, whereas truncated CD148 has a strong inhibitory effect (Cordoba *et al*, 2013). Another member of R3 RPTP subgroup VE-PTP was suggested to exert its role in the regulation of the endothelial barrier via its extracellular domain. The association of VE-PTP and VE-cadherin appears to stabilise VE-cadherin-plakoglobin complex and to enhance the adhesive function of VE-cadherin. The inhibition of VE-PTP expression resulted in increased permeability of endothelial cells and leukocyte extravasation, suggesting that VE-PTP could play an important

role in regulation of immune responses and that its extracellular domain plays an active part (Nottebaum *et al*, 2008). However, the molecular basis of the association between VE-PTP and VE-cadherin in live cells has not yet been defined.

1.4 Fibronectin and FN type III-like domain

To date the role of the extracellular domain of the R3 PTPs remains unclear. However, perhaps some light can be shed from a study on a key adhesion protein fibronectin (FN) found in the blood, interstitial extracellular matrix (ECM) and pericellular matrix. Fibronectin is a high molecular weight tandem modular glycoprotein consisting of individually folded functional domains termed type I, II and III repeats (Figure 6). Fibronectin provides a substrate for cell anchorage and serves as a regulatory protein in processes such as cell adhesion, motility, differentiation and proliferation (Gao *et al*, 2003). The modular fibronectin (FN) domains function by binding to other molecules and by acting as spacers separating and orienting other domains of the protein (Carr *et al*, 1997). Two intramolecular disulfide bonds form within each type I and type II module to stabilise the folded structure (Singh *et al*, 2010). Individual FNIII modules have been proposed to unfold on mechanical stretching of fibronectin protein, providing for the elasticity of FN fibrils, which is believed to expose buried binding sites (also known as cryptic sites) that, for example, serve as nucleation sites for the assembly of FN into its fibrillar form (Gao *et al*, 2003). Fibronectin III motifs comprise 90-100 amino acids characterised by highly conserved hydrophobic residues (Brady-Kalnay and Tonks, 1995). These domains are composed of seven antiparallel β strands denoted A, B, C, C′, E, F, G, arranged into two sheets (Figure 6) (Carr *et al*, 1997). As a study by Martino *et al* (2010) showed, FN bind a wide range of growth factors (GFs) from different families, e.g. platelet-derived growth factor (PDGF) family, fibroblast growth factor (FGF) family and insulin-like growth factor (IGF) family. Some of these molecules bind to a heparin-binding domain II of the FN consisting of the 12^{th} to 14^{th} type III repeats (FNIII12-14) and others bind to the full-length FN with the exact binding

location yet to be identified. In addition there was some evidence that the neurotrophins NT-3 and BDNF, hepatocyte growth factor (HGF) and connective tissue growth factor (CTGF) also bind to FNIII12-14 with a high affinity (Martino *et al*, 2010). The physiological role of these interactions still needs to be investigated in the context of each GF and potentially they could play a role during development and tissue repair (Martino *et al,* 2010). In addition it was shown that the tenth FN-III domain of fibronectin contains the cell-adhesive triplet Arg-Gly-Asp (RGD loop) sequence, which is known to interact with integrins, and the residues outside this loop provide specificity and high affinity for each integrin-ligand pair (Carr *et al*, 1997; Takagi, 2003). A member of the integrin family α5β1 interacts with FNIII through RGD motif, mediating FN fibril formation and governing extracellular matrix assembly (Figure 6). This interaction was shown to be essential for vertebrate development (Takagi, 2004). However, none of the FN type III-like domains of R3 RPTP members has an RGD sequence but instead an XGD (where X represents any amino acid; G – glycine and D – aspartic acid) sequence was found on the expected loop in five FN type III-like domains of DEP-1, through which DEP-1 could play an important role in cell-cell interactions (Ostman *et al*, 1994).

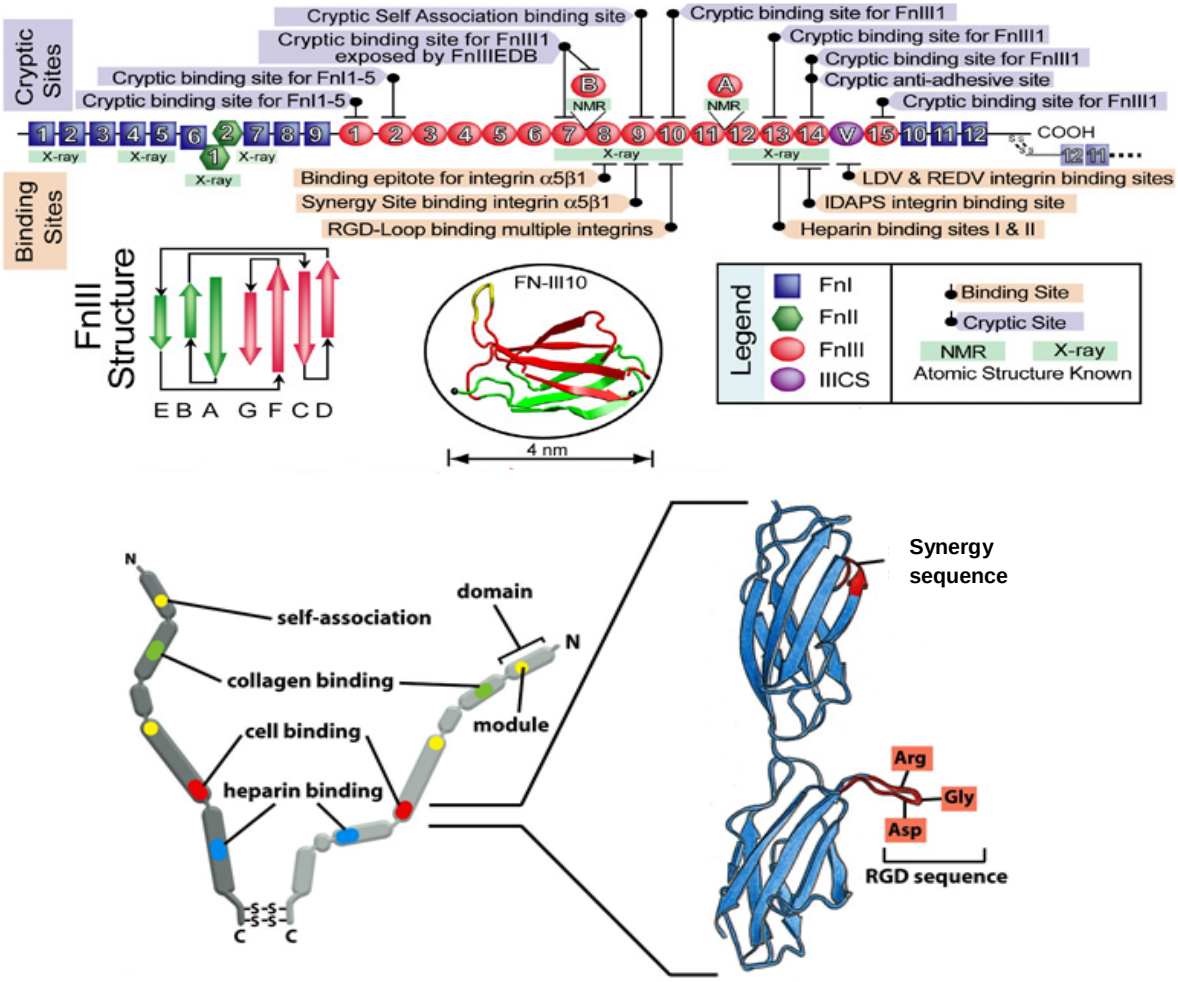

Figure 6. A structural representation of fibronectin glycoprotein. The top part of the image shows the schematic presentation of the modular structure of human fibronectin monomer, emphasising folding motifs FNI, FNII and FNIII, as well as a secondary structure of a FNIII module with accurate representation of relative β-strand lengths with respect to each other. The bottom part of the image represents a structure of the disulphide cross-linked fibronectin (FN) dimer and location of key binding sites. Fibronectin exists as a dimer of nearly identical monomers linked by a pair of disulphide bonds. It is made up of multiple FNI, FNII and FNIII domains arranged into various functional domains. The RGD sequence (Arg–Gly–Asp) is located on the 10th type III module and is the site of cell attachment via α5β1 and αVβ3 integrins on the cell surface. The "synergy site" is on the ninth type III module and has a role in modulating fibronectin's association with α5β1 integrins. The image was obtained and modified from http://www.ks.uiuc.edu/Research/fibronectin/

1.5 Regulation of R3 RPTPs

A family of enzymes that play a crucial role in the regulation of cell signalling and the fundamental cellular processes, such as cell migration, proliferation and differentiation, must be tightly controlled *in vivo* by some regulatory mechanisms. It is essential that tyrosine phosphorylation mediated by PTKs and dephosphorylation mediated by PTPs are fine-tuned since these two families of enzymes have important roles in diseases like cancer and diabetes.

1.5.1 Regulation by reversible oxidation

Recently it became apparent that reversible oxidation is one of the important regulators of RPTPs. Most RPTPs contain two conserved cytoplasmic PTP domains: D1, which contains most, if not all, catalytic activity, and D2, which has a regulatory role. Due to their microenvironment, the catalytic cysteines have a low pKa. Under normal conditions the active site cysteines are in the thiolate anion form and thus are highly susceptible to oxidation. Some studies show that reactive oxygen species (ROS), the production of which is induced by stimuli such as ultraviolet (UV) light and cytokines, oxidise the essential active site nucleophilic cysteine residue, located in the HC(X)5 signature motif, in PTPs, inactivating them (Tonks, 2006). For example, hydrogen peroxide (H_2O_2) produced in response to epidermal growth factor (EGF) has been shown to oxidise PTP1B's catalytic site cysteine to sulfenic acid, causing reversible inactivation (Lee *et al*, 1998; Mahadev *et al*, 2001). This process shifts the equilibrium between the actions of protein tyrosine kinases and protein tyrosine phosphatases towards phosphorylation, activating signal transduction pathways (Lee *et al*, 1998). A study by Krejsa *et al* (1997) showed that CD45 RPTP is also inactivated by intracellular oxidation induced by vanadium PTP inhibitors and this inactivation led to the activation of kinase signalling cascades. However, it was also shown that not all the PTPs are equally sensitive to oxidation. Based on studies of RPTPα, the D2 domain displays greater sensitivity to oxidation than the D1 domain,

suggesting that PTPs containing only the D1 domain might be less sensitive to oxidation (den Hertog *et al*, 2008).

1.5.2 Regulation by ligand-binding

RPTPs could be regulated by various mechanisms and perhaps there is more than one way to regulate the same RPTP. The extracellular domains of PTPs are typically large, highly glycosylated, structurally diverse and evolutionarily conserved, suggesting their roles in the regulation of PTP function. Recent studies have defined some RPTPs through which signal transduction may be regulated by ligand-controlled dephosphorylation of tyrosyl residues in proteins. One such RPTP is a cell-adhesion-molecule-like RPTP leukocyte common antigen related (LAR). The activity of this protein was shown to be controlled by ligand binding. A high-affinity interaction between LAR and its ligand transmembrane protein syndecan (Sdc) results in promotion of LAR's function, whereas the binding of the glycosylphosphatidylinositol-anchored protein Dallylike (Dlp) to LAR suppresses its activity (Tonks, 2006). The activity of RPTPζ was also shown to be regulated by ligand-binding. It has been demonstrated that a secreted growth factor pleiotrophin (PTN) directly binds to and inactivates the catalytic activity of RPTPζ, resulting in inability to dephosphorylate β-catenin and, thus, an increased phosphorylation of β-catenin and the subsequent loss of contact inhibition, cell adhesion and the destruction of cytoskeletal architecture (Meng *et al*, 2000). Despite different regulatory mechanisms being identified, the mechanisms regulating R3 RPTPs activity remain undefined. Although the extracellular ligand interactions were proposed to be one of the regulatory mechanisms the strong evidence for such regulation for R3 RPTPs has not yet been provided. Potential ligand proteins have been identified for only a limited number of RPTPs.

1.5.3 Regulation by dimerisation

The catalytic activity of some PTPs has been shown to be affected by dimerisation. Unlike with PTKs PTPs are believed to be inactivated by dimerisation. The artificial induction of dimerisation for CD45, RPTPα and DEP-1 clearly affected their enzymatic activity (Noordman *et al*, 2008). Some evidence suggests that the ligand-induced oligomerisation of CD148 (DEP-1; PTPRJ) could be a potential mechanism to regulate this protein and that the extracellular domain plays a crucial role. The observations by Takahashi *et al* (2006) showed that the role of CD148 in endothelial vessel formation and in cell-growth control was inhibited in the presence of a bivalent monoclonal antibody (Ab1), generated against the extracellular domain sequence of CD148. It was demonstrated that bivalent but not monovalent Ab1 inhibits endothelial cell-growth and angiogenesis. Therefore these findings demonstrate that the activity of CD148 can be potentially regulated by extracellular domain oligomerisation (Takahashi *et al*, 2006). This is an important discovery implying that CD148 could serve as a molecular target for antiangiogenesis therapy, which could be forced to oligomerise and, thus, be activated by a synthetically generated agonist.

However, whether dimerisation is a general regulatory mechanism of RPTPs is still a subject to debate. The dimerisation of R3 RPTPS is poorly understood and whether this dimerisation is related to the binding of extracellular ligands remains unclear. It has been shown that the activity of RPTPs is inhibited by ligand-induced dimerisation (Tonks, 2006). Although a study by Barr *et al* (2009) demonstrated that the members of R3 PTPs exist as monomers in solution, the dimerisation may still occur *in vivo* as a result of ligand binding to the extracellular domain. A contradictory study by Walchli *et al* (2005) showed that SAP-1 enzymes form homodimers and this dimerisation is mediated by the extracellular domains. It was also demonstrated that the monomeric form of SAP-1 is significantly more active than the dimeric one (Walchli *et al*, 2005). On the other hand, the same study by Walchli *et al* (2005) showed no dimerisation of VE-PTP and DEP1 when tested in parallel with SAP-1. The mechanism of ligand-induced dimerisation was obtained only for RPTPα and CD48, where N-terminal helix-turn-helix

wedge motif occludes the active site of the partner domain (Barr *et al*, 2009; Tonks, 2006). However, such a model of dimerisation-induced RPTP inhibition prompted by these findings cannot be extrapolated to other members of the RPTP family because the residues that occlude the active site of RPTPα and CD48 are poorly conserved among other RPTPs (Takahashi *et al*, 2006; Barr *et al*, 2009). It has been now shown that GLEPP1 could exist as a dimer in living cells and this dimerisation is partly regulated by disulphide linkages (Hower *et al*, 2009). Interestingly the presence of nerve growth factor (NGF) increases dimerisation of GLEPP1 by nearly twofold. In addition the catalytic domain of this enzyme is not involved in dimerisation whereas the extracellular domain and probably the transmembrane domain may play a role in the dimerisation. The dimerisation of GLEPP1 appeared to result in a strong decrease in its intrinsic activity (Hower *et al*, 2009).

Deregulation of R3 RPTPs' activity that results in either loss or gain of function contributes to the pathogenesis of human disease. For example, as already mentioned above, VE-PTP was shown to be an important component of the VE-cadherin-plakoglobin complex, required for the maintenance of the endothelial barrier function. VE-PTP seems to enhance plakoglobin/VE-cadherin association, suggesting that plakoglobin could be a substrate for the VE-PTP. Knocking down VE-PTP expression by RNA interference resulted in increased diepedesis of leukocytes, which demonstrates that the deregulation of VE-PTP leads to an increased inflammatory response. During inflammatory stimuli, leukocytes cause a disruption of VE-PTP/VE-cadherin association, destabilising endothelial contacts (Nottebaum *et al*, 2008). Therefore VE-PTP represents a novel therapeutic target for the treatment of inflammatory diseases. Because the selective suppression of the activity of R3 RPTPs can be essential in cells, it is important to understand how the inhibition of activity of these enzymes is regulated by dimerisation and whether this dimerisation is induced by ligands. This knowledge will shed more light on mechanisms of function and regulation of these enzymes and will help to develop novel molecular targets

for the development of medicinal reagents that possess distinct modes of action.

1.6 Membrane protein interaction technologies

Different methods have been developed to investigate membrane protein-protein interactions, such as bioluminescence resonance energy transfer (BRET) and fluorescence resonance energy transfer (FRET), which represent valuable tools but are technically challenging. BRET and FRET rely on the ability to capture fluorescent signals from the interactions of labelled molecules and have been widely used to determine the compartmentalisation and functional organisation of living cells as well as protein-protein interactions and their movement inside cells (Sekar and Periasamy, 2003). The mammalian-membrane two-hybrid (MaMTH) assay is based on split-ubiquitin technique that can be used to detect dynamic and stimulus-dependent protein-protein interactions in mammalian cells. One protein of interest is fused to the C-terminal half of ubiquitin and a chimeric transcription factor (TF) and the other is fused to the N-terminal half of ubiquitin. If the two proteins of interest interact together the split halves reconstitute functional ubiquitin protein, which is recognised by cytosolic deubiquitinating enzymes, resulting in cleavage of the TF and expression of a reporter gene, such as luciferase (Petschnigg *et al*, 2014). MaMTH assay has been successfully applied to investigate stimulus-dependent interactions of the wild-type as well as oncogenic variant of epidermal growth factor receptor (Petschnigg *et al*, 2014). However, this assay has some limitations. The activation of a reporter gene could be caused by an interaction of proteins that are not being investigated, leading to false positive results. Over-expression of proteins is common in transient transfections and it can lead to non-relevant forced protein-protein interactions and self-activation of the reporter gene by the bait protein, resulting in false positive results (Suter *et al*, 2008). Receptor alkaline phosphatase (RAP) assay is another method that can be used to identify potential extracellular binding ligands. This assay can be carried out on endogenously expressed proteins without the risk of over-expressing the proteins that could lead to false-positive results. This

method provides a direct indicator of extracellular domain binding and it is heat stable and thus can be differentiated from the heat labile alkaline phosphatases of most tissues. It is also useful when a reliable monoclonal antibody is not available for the protein of interest (Stoker, 2005).

In this study the bimolecular fluorescence complementation (BiFC) assay was chosen for the simple and direct visualisation of protein-protein interactions in live cells with minimal perturbation of their normal environment. The schematic representation of the BiFC assay is shown in Figure 7. BiFC assay can provide information about the localisation of protein-protein interactions and it has been used previously to investigate membrane protein interactions. De Virgilio *et al* (2004) used this assay to define successfully the interaction between integrin αIIbβ3 and protein tyrosine kinases C-Src and Syk in live cells. Some techniques are used for an initial screen for novel binding partners. The initial experiments on VE-PTP and VE-cadherin interaction, as well as on R3 RPTP dimerisation studies, have been carried out using affinity chromatography and co-immunoprecipitation assays (Nawroth *et al*, 2002; Hower *et al*, 2009; Takahashi *et al*, 2006). Co-immunoprecipitation provides an excellent method to purify and identify multiprotein complexes. However, during cell lysis the expressed tagged proteins could be present in a mixture of both physiological and non-physiological targets and the latter could be incorporated in the complex without any biological significance, especially if they interact with high affinity and/or slow kinetics of dissociation and thus more easily replacing the physiological targets (Berggård *et al*, 2007). In contrast to co-immunoprecipitation assays BiFC can be used to detect transient and modification-dependent protein-protein interactions.

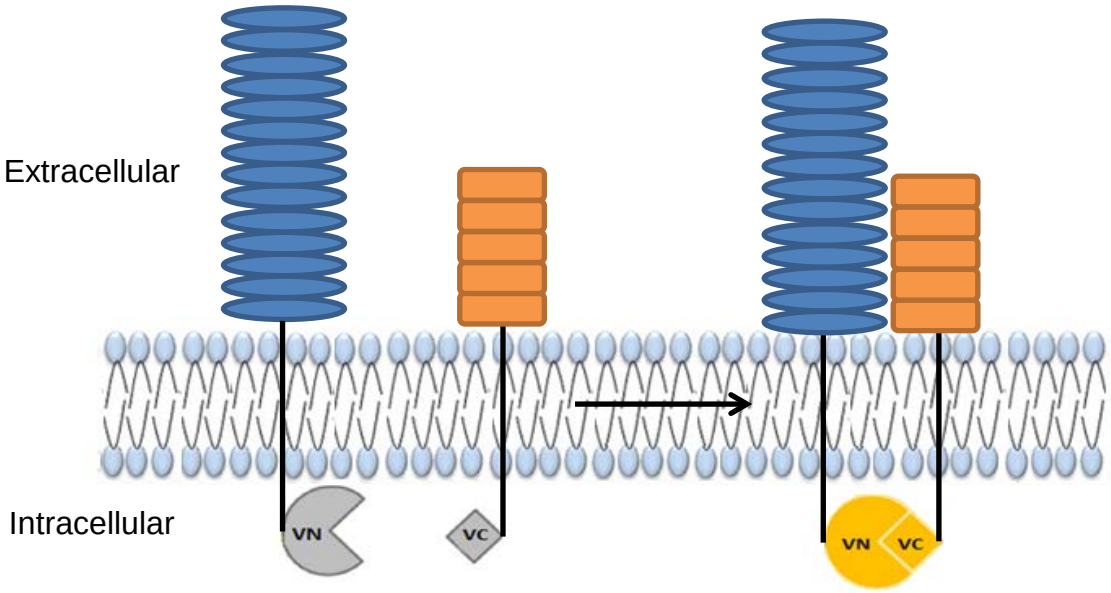

Figure 7. Schematic representation of the principle of the BiFC assay. This is based on the complementation of two non-fluorescent N- and C-terminal fragments from a Venus yellow fluorescent protein. When the two fragments are brought into proximity by an interaction between two proteins fused to the fragments the reconstituted fluorescence can be easily observed by any fluorescence microscopy.

This method is based on the formation of a fluorescent complex when two fragments of a fluorescent protein are brought together by an interaction between proteins fused to the fragments (as shown in Figure 7) and can be used for visualisation of interactions between many different proteins expressed at low concentrations (i.e. at levels comparable to endogenous counterparts) in many cell types and organisms (Kerppola, 2006). However, BiFC assay has some limitations. One common limitation of the BiFC assay is the self-assembly between the two non-fluorescent fragments, contributing to false-positive fluorescence and making data interpretation difficult (Kerppola, 2006; Kodama and Hu, 2010). This problem would be addressed in further chapters by using negative controls and by carrying out quantitative analysis instead of relying on qualitative interpretation of the data.

1.7 Aims of the thesis

The identification of ligands for R3 PTPs and the mapping of their binding sites on the extracellular domains of these enzymes will provide additional information on their functions, mechanisms of function and, perhaps, may provide tools to fine-tune the signalling pathways, mediated by these PTPs. For that reason investigation of the functional role of the extracellular domains of these proteins and identification of cognate ligands will be the main focus of this research.

The initial aim of this project was to confirm the interaction between VE-PTP and VE-cadherin via their extracellular domains in live cells as well as to investigate the molecular basis of their interaction. The second aim was to gain a better understanding of the role of R3 RPTP extracellular domains in ligand-binding specificity. This was addressed by examining whether all the members of R3 RPTP have the potential to interact with VE-cadherin via their extracellular domains in live cells. Additionally the potential dimerisation of the R3 RPTPs via their extracellular domains was investigated in live cells.

To address the aims of this thesis the bimolecular fluorescence complementation (BiFC) assay was used, which was first developed and validated with fusion proteins bJun and bFos that are known to interact. The quantitative analyses were adapted and validated from previous studies to obtain more robust data.

Chapter 2

Materials and Methods

Materials

2.1 Bacterial strains

Table 1. *E. coli* strains for cloning and associated genotypes

Strain	Genotype	Source
XL1-Blue	recA1 endA1 gyrA96 thi-1 hsdR17 supE44 relA1 lac [F´ proAB laclq ZΔM15 Tn10 (Tetr)]	Agilent
SCS110	rpsL (Strr) thr leu endA thi-1 lacY galK galT ara tonA tsx dam dcm supE44 Δ(lac-proAB) [F´ traD36 proAB laclq ZΔM15]	Agilent

Table 2. Antibiotics for bacterial cell cultures

Name	Stock Concentration	Working Concentration	Source
Ampicillin	100 mg/ml	100 µg/ml	Sigma
Chloramphenicol	34 mg/ml (80% (v/v) EtOH)	34 µg/ml	Sigma
Kanamycin	10 mg/ml	10 µg/ml	Sigma

2.2 Preparation of competent *E. coli*

Competent *E.coli* XL1-Blue and SCS110 bacterial strains were a kind gift from Dr. Markiv and were used to prepare stocks of competent cells. XL1-Blue and SCS110 cells were streaked on to LB plates and grown overnight in 37°C incubator. Single colonies from each of the plates for XL1-Blue and SCS110 cells were picked and grown in 10 ml Luria-Bertani (LB) Broth in the absence of antibiotics for 12 hours at 37°C with shaking at 180 rpm. After the incubation 10 ml of each bacterial culture was inoculated into 200 ml of fresh LB Broth and incubated at 37°C with shaking at 250 rpm until the optical density at 595 nm (OD_{595}) reached 0.4. The flasks were then chilled on ice for 30 minutes and 50 ml of each chilled bacterial culture was aliquoted into sterile chilled falcon tubes. Cells were harvested by centrifugation for seven minutes at 3500 rpm at 4°C and the supernatants were discarded. Each pellet then was resuspended in 12.5 ml 0.1 M $MgCl_2$ and centrifuged as

previously. Supernatants were discarded and each pellet was resuspended in 25 ml 0.1 M $CaCl_2$. Resuspended cells were incubated on ice for 30 minutes, centrifuged as previously and the supernatants were discarded. Each pellet was resuspended in 700 µl 0.1 M $CaCl_2$ and 300 µl 50% (v/v) glycerol and the 50 µl aliquots were stored at -80°C.

SCS110 competent cells were used when the DNA had to be digested with methylation-sensitive restriction enzymes (e.g. *Apa*I and *EcoR*I) since these cells lack DNA adenine methylation (*dam*) and DNA cytosine methylation (*dcm*) genes.

2.3 Media, buffers and solutions

Table 3. Media and buffers

Name	Composition
SOC	2% (w/v) tryptone, 0.5% w/v yeast extract, 10 mM NaCl, 2.5 mM KCl, 10 mM $MgCl_2$, 10 mM $MgSO_4$, 20 mM glucose
LB Broth	1% (w/v) Bacto tryptone, 0.5% (w/v) yeast extract, 1% (w/v) NaCl
0.1 M $MgCl_2$	2.03 g $MgCl_2.6H_2O$, 100 ml ddH_2O
0.1 M $CaCl_2$	11 g $CaCl_2.6H_2O$, 500 ml ddH_2O
50% (w/v) Glycerol	5 ml glycerol, 5 ml ddH_2O
50x Tris-acetate EDTA (TAE)	2.0 M TrisBase, 50 mM EDTA(pH8.0), 1.0 M Glacial Acetic Acid, dH_2O
6x DNA Loading Buffer	0.4% (w/v) Orange G, 0.03% (w/v) Bromophenol blue, 0.03% (w/v) xylene cyanol FF, 15% (w/v) Ficoll 400 in TAE buffer
TE Buffer	10 mM Tris-HCl, 1 mM EDTA, pH 7.5
1 M DTT	1.54 g DTT in 10 ml MilliQ water. Store 1 ml aliquots at -20°C.
3% Paraformaldehyde	2.4 ml 37% paraformaldehyde, 27.6 ml PBS (Mg^{2+}/Ca^{2+})
0.5% Triton X-100	100 µl TritonX-100, 20 ml PBS (Mg^{2+}/Ca^{2+})
5% Bovine Serum Albumin (BSA)	1 g BSA, 20 ml PBS (Mg^{2+}/Ca^{2+})
10% SDS	10 g SDS in 100 ml of MilliQ water. Store at room temperature
1 M Tris-HCl (pH 8.0)	12.114 g Tris-base in 80 ml MilliQ water. Adjust pH to 8.1 and add water to 100 ml. Store at 4°C.
Trypsin 25 mg/ml	1 g trypsin in 40 ml 25 mM NH_4HCO_3 (pH 8.1) (100x solution). Store 1 ml aliquots at -20°C.
1 M NH_4HCO_3 (pH 8.1)	7.9 g NH_4HCO_3 in 80 ml MilliQ water. Adjust pH to 8.1 and add water to 100 ml. Store at 4°C.
Lysis Buffer	20 mM Tris-HCl (pH 7.5), 150 mM NaCl, 1 mM EDTA, 1% Triton X-100, Milli Q water
2x SDS-gel loading buffer	50 mM Tris-base, 4% SDS, 100 mM DTT, 0.01% Bromophenol blue, 23% Sucrose, pH6.8.
4x Sample Buffer	240 mM Tris-HCl, pH 6.8, 8% SDS, 5% β-Mercaptoethanol, 0.04% Bromophenol blue, 40% Glycerol
10 x SDS Running Buffer (sodium dodecyl sulfate)	25 mM Tris, 192 mM glycine, 0.1% SDS, pH 8.3
1 x SDS Running Buffer	100 ml 10x SDS Running Buffer, 900 ml dH_2O
1x Transfer Buffer	25 mM Tris, 192 mM Glycine, 20% (v/v) methanol and ddH_2O up to 1.25 L
10x TBS (Tris Buffered Saline)	200 mM Tris-Base, 1.5 M NaCl, Milli Q water up to 1L, pH 7.6
1x TBS	100 ml 10x TBS, 900 ml Milli Q water
1x TBST	100 ml 1x TBS, 0.5 ml Tween 20

2.4 Standard molecular biology methods

2.4.1 Primer design

Primer design specific for each PCR template was performed using VectorNTI Advance® 11.5 software (ThermoFisher Scientific). First, the desired fusion protein sequence was generated by assembling corresponding nucleotide sequences for the chosen domains (e.g. signal peptide, extracellular and transmembrane domains) that were obtained from GenBank database (NCBI). The sequence has then been modified to include an in-frame, upstream sequence for either myc or HA epitope tags between *Apa*I and either *Xho*I or *Eco*RI restriction enzyme sequences. Primers were designed to amplify a created target sequence by choosing auto primer design in VectorNTI software and selecting the regions of analysis. The software then automatically generated a pair of primers with calculated length of primers, GC content and melting temperature. In addition the required restriction enzymes for subcloning were selected and the corresponding sequences were added to each primer. Additional bases were added where necessary to keep the polymerase reading frame between the restriction enzyme cutting sequence and the rest of the primer. Also, few more bases (e.g. GATC) were added at 5' ends of the primers to facilitate the digest close to the end of DNA regions.

2.4.2 Miniprep of DNA

Plasmid DNA was extracted and purified from bacterial cultures using a QIAprep Spin Miniprep Kit (QIAGEN) according to manufacturer's instructions. A single colony from a freshly streaked selective plate was picked and inoculated into 10 ml LB Broth supplemented with an appropriate antibiotic and incubated overnight at 37°C with 200 rpm. The bacterial cultures were then pelleted by centrifugation at 4500 rpm on a bench-top centrifuge for 10 minutes at 25°C at 8000 rpm. The supernatant was discarded and the bacterial cell pellet was resuspended in 250 µl Buffer P1 (50 mM Tris-HCl, 10 mM EDTA, 50 µg/ml RNaseA, 0.0025% (w/v)

thymolphtalein, pH 8.0) and transferred to a sterile 1.5 ml microcentrifuge tube. To lyse the cells 250 µl Buffer P2 (0.2 M NaOH, 1% (w/v) SDS) was added, mixed thoroughly by inverting the tube 4-6 times until the solution became clear (or blue if using thymolphtalein) and incubated at room temperature for up to 5 minutes. To neutralise the lysis buffer 350 µl Buffer N3 was added and mixed immediately and thoroughly by inverting the tube 4-6 times. The solution of lysed cells was then centrifuged for 10 minutes at 13000 rpm in a table-top microcentrifuge to precipitate the cell membrane, proteins and genomic DNA. The supernatant containing soluble plasmid DNA was applied to the QIAprep spin column by pipetting and centrifuged for 1 minute at 13000 rpm, discarding the flow-through. The QIAprep spin column was then washed by adding 0.5 ml Buffer PB (5 M guanidine hydrochloride, 20 mM Tris-HCl, 38% (v/v) ethanol, pH 6.6) and centrifuged for 1 minute at 13000 rpm, discarding the flow-through. The QIAprep spin column was washed again by adding 0.75 ml Buffer PE (20 mM NaCl, 2 mM Tris-HCl, 80% (v/v) ethanol, pH 7.5) and centrifuged for 1 minute at 13000 rpm, discarding the flow-through. To remove residual wash buffer the QIAprep spin column was centrifuged for additional 2 minutes at 13000 rpm. To elute DNA the QIAprep column was placed in a clean 1.5 ml microcentrifuge tube, 50 µl Buffer EB (10 mM Tris-Cl, pH 8.5) was added to the centre of the QIAprep spin column and allowed to stand for 1-2 minutes before centrifuging for 1 minute at 13000 rpm. The concentration and purity of the extracted DNA were assessed using a Nanodrop 1000 (Thermo Scientific) at 260 nm and 280 nm.

2.4.3 PCR of constructs and reaction conditions

The polymerase chain reaction (PCR) was used to amplify the coding sequences for extracellular and transmembrane domains (ECD+TM) for the R3 RPTPs, VE-cadherin and sialophorin (SPN). The details of constructs, their amplified regions and the PCR conditions are provided in Table 4. The primers used to amplify the desired regions are listed in Table 6. PCR amplification was performed using Platinum *Pfx* DNA Polymerase (Invitrogen) according to manufacturer's instructions. Reactions were carried

out using BioRad MJ Mini thermal cycler. The thermocycler programs were customised for each target sequence based on gene length and primer optimal melting temperature (refer to Table 10). The dNTP mixture (10 µl of each NTP) was obtained by mixing 1 M stock solutions for each nucleotide (New England Biolabs) in the appropriate dilution. Master mix for each PCR reaction was prepared, using 5 µM of each primer, 10 mM dNTP mixture and 2.5 ng/µl DNA template in a final volume of 20 µl in a thin-walled PCR tubes (ThermoFisher Scientific). PCR products were resolved on an agarose gel the DNA fragments were detected using a UV Transilluminator (Ultra-Violet Ltd.) as described in section 2.4.4.

Table 4. PCR conditions for ECD+TM amplification with Pfx platinum. The PCR conditions below were used to generate extracellular and transmembrane domains of the indicated proteins. For the template and primer details refer to Tables 8 and 10 respectively.

Template	Name of Construct	Areas of Amplification	PCR steps/Thermocycle conditions						Enzyme
			Initialisation	25 cycles			Final Elongation	Enhancer	
				Denaturation	Annealing	Extension			
PTPRB	VE-PTP	ECD+TM (A.A.23-1642)	94°C,5min	94°C,30sec	55°C,30sec	72°C,30sec	72°C,5min	-	Pfx
PTPRJ	DEP-1	ECD+TM (A.A.36-996)	94°C,5min	94°C,30sec	52°C,30sec	68°C,3min	72°C,10min	1x	Pfx
PTPRO	GLEPP-1	ECD+TM (A.A.30-843)	94°C,5min	94°C,30sec	55°C,30sec	68°C,3min	72°C,10min	-	Pfx
PTPRH	SAP-1	ECD+TM (A.A.28-755)	94°C,5min	94°C,30sec	60°C,30sec	68°C,3min	72°C,10min	2x	Pfx
CDH5	VE-cadherin	ECD+TM (A.A.48-620)	94°C,5min	94°C,30sec	58°C,30sec	68°C,2min	72°C,10min	-	Pfx
SPN	SPN	ECD+TM (A.A.20-276)	94°C,5min	94°C,30sec	62°C,30sec	68°C,1min	72°C,5min	2x	Pfx

2.4.4 Agarose Gel Electrophoresis

Agarose gel electrophoresis was used for visualisation and purification of DNA. Agarose gels were commonly used in concentrations of 0.7% to 1.0% w/v depending on the size of bands needed to be separated. The appropriate amount of agarose powder was measured out and placed into a microwavable flask with 100 ml of 1x TAE (Tris-acetate-EDTA) Buffer. The resulting solution was then microwaved for 1-2 minutes or until the agarose was completely dissolved. The dissolved agarose was allowed to cool down for 5 minutes at room temperature until it was comfortable to handle the flask and 1 µl SYBR® Safe DNA gel stain (Thermo Fisher Scientific) was then added that binds to DNA and allows visualisation under UV light. The agarose was poured into a gel tray with the well comb in place and was left to set at room temperature for 15-20 minutes until it had completely solidified. The well comb was removed and solidified agarose was placed into the electrophoresis unit, which was then filled with 1x TAE Buffer.

A molecular weight 1 Kb Plus DNA ladder (Thermo Fisher Scientific) and DNA samples were mixed with 6x Gel Loading Dye Purple (New England Biolabs) at a volume ratio of 5:1 and carefully loaded into the wells of the gel. Electrophoresis was set to run at 110 V constant for 30-45 minutes until the dye line was approximately 75-80% of the way down the gel.

The DNA fragments were detected using a UV Transilluminator (Ultra-Violet Ltd.) with short wavelength UV light of 200-280 nm. Long wavelength UV light of 315-400 nm was used to analyse the gel of the DNA that was used for cloning or sequencing.

2.4.5 Purification of DNA from agarose gels

To purify the DNA from the agarose gel the QIAquick gel extraction kit (Qiagen Ltd.) was used according to the manufacturer's recommendations. The DNA bands of the desired size were excised with a clean scalpel, weighed and solubilised at 50°C for 10 minutes with three volumes of Buffer QG (5.5 M Guanidine thiocyanate, 20 mM Tris-HCl, 0.0025% (w/v) Cresol Red, pH 6.6) to one volume of excised gel. One gel volume of isopropanol was added to the sample and mixed thoroughly to increase the yield of DNA fragments. To bind the DNA the sample was applied to the QIAquick column and centrifuged for one minute at 14000 rpm. To remove all traces of agarose, the flow-through was discarded and the QIAquick column was put back in the same collection tube, adding 0.5 ml of Buffer QG and centrifuging for one minute at 14000 rpm. To wash the column 0.75 ml of Buffer PE was added to QIAquick column and centrifuged for one minute at same speed, discarding the flow-through and centrifuging for further one minute at 10,000 rpm to remove all the traces of ethanol. To elute the DNA the QIAquick column was placed into a clean 1.5 ml microcentrifuge tube, adding 30 µl of Buffer EB (10 mM Tris·HCl, pH 8.5) and incubating for 2 minutes at room temperature, following by centrifugation for one minute at 14000 rpm. The concentration and purity of the extracted DNA were assessed using a Nanodrop 1000 (Thermo Scientific) at 260 nm and 280 nm. The purified DNA was stored at -20°C until further use.

2.4.6 Purification of DNA from PCR

DNA from the PCR reaction mixture was purified using the QIAquick DNA purification kit (Qiagen Ltd.) according to the manufacturer's recommendations. In short, five volumes of Buffer PB were added to one volume of the PCR reaction, mixed thoroughly and the pH was adjusted by adding 10 µl 3 M sodium acetate (or until the colour of the mixture turned yellow). To bind the DNA the resulting mixture was applied to the QIAquick column inserted into a collection tube that was spun for one minute at 14000

rpm. The flow-through was discarded and the QIAquick column was placed back in the same collection tube. To wash the column, 0.75 ml of Buffer PE was added to the QIAquick column and spun for one minute at 14000 rpm. The flow-through was discarded and the column was spun again for one minute to remove residual wash buffer. The QIAquick column with bound DNA was then placed in a sterile 1.5 ml microcentrifuge tube. To elute DNA, 30 µl Buffer EB (10 mM Tris·HCl, pH 8.5) was added to the centre of the QIAquick column and was allowed to stand for two minutes at room temperature in order to increase DNA concentration and then spun for one minute at 14,000 rpm. The concentration and A260/A280 purity ratio were assessed using a NanoDrop Lite (Thermo Scientific). The purified DNA was stored at -20°C until further use.

2.4.7 Restriction enzyme digest

Restriction enzyme digestion was used as part of the molecular cloning procedure to generate BiFC constructs. All restriction enzymes used in this project were purchased from New England Biolab (NEB) and used according to manufacturer's instructions. Information of restriction enzymes and experimental conditions used for the generation of each BiFC construct is provided in Table 5. The DNA samples and vectors were digested with 1.0 µl of the appropriate restriction enzyme in a final volume of 50 µl to create complementary sticky-ends for ligation. Double digest was done sequentially if the buffer and/or incubation temperature for restriction enzymes were not compatible (as indicated in Table 5).

Table 5. Restriction digest. Conditions for the restriction enzyme digests of the transmembrane and extracellular domains of the DNA constructs required for subcloning.

Construct	TM +ECD	Cloning Site	Buffer	T°C	Digest Duration	Heat Inactivation
VE-PTP	A.A. 23-1642	*Xho*I	CutSmart	37°C	2 hours	65°C; 20 min
DEP-1	A.A. 36-996	*Xho*I	CutSmart	37°C	2 hours	65°C; 20 min
SAP-1	A.A. 28-755	*Xho*I	CutSmart	37°C	2 hours	65°C; 20 min
GLEPP-1	A.A. 30-843	*Xho*I	CutSmart	37°C	2 hours	65°C; 20 min
VE-cadherin	A.A. 48-620	*Apa*I *Kpn*I	CutSmart NEBuffer1.1	25°C 37°C	2 hours 2 hours	65°C; 20 min NO
SPN	A.A. 20-276	*Eco*RI-HR/*Xho*I	CutSmart	37°C	2 hours	65°C; 20 min

2.4.8 Ligation

Digested PCR fragments were ligated into vectors, following insertion of the synthetic signal peptide and epitope tag sequence, (as shown in Figure 8) using T4 DNA Ligase (Roche) at vector-to-insert molar ratio of 1:3 (see calculation below) for 2 hours at room temperature to produce constructs encoding for fusion proteins with either the N- or C-terminal fragment of the Venus protein.

Since vector ends were compatible after the digest the vector DNA was first dephosphorylated with alkaline phosphatase (part of the Rapid Ligation Kit; Roche) to prevent self-ligation. The dephosphorylation of the linearised vectors was carried out according to manufacturer's instructions in a final volume of 20 µl. One microgram of each vector DNA was mixed with 2 µl 10x rApid alkaline phosphatase Buffer, 1 µl rApid alkaline phosphatase and sterile deionised water was added to make up 20 µl. The dephosphorylation reaction mixture was mixed thoroughly and incubated at 37°C for 30 minutes, followed by inactivation of the rApid Alkaline Phosphatase at 75°C for two minutes. The dephosphorylation reaction mixture was then directly used in the ligation reaction. Minimum 12 ng of each vector was used for the ligation. To calculate the amount of each insert DNA to be used for ligation the following formula was used:

$$\frac{\text{Kb of insert}}{\text{Kb of vector}} \times \text{ng of vector} = \text{ng of insert needed for a 1:1 molar ratio}$$

The ligation was performed at 3:1 insert:vector ratio, thus, the resulting value for the insert was then multiplied by three.

The appropriate amounts of vector DNA and the PCR product (insert DNA) were mixed together with 4 µl 5x Rapid Ligation Buffer, 1 µl T4 DNA Ligase (Weiss units) and nuclease-free water to final volume of 20 µl. The ligation mixture was spun briefly to collect drops and incubated for 30 minutes at

25°C. Fifteen microliters of the ligation mixture was used for transformation (as described in section 2.4.9 below).

2.4.9 Transformation of competent cells

*E.coli c*ompetent cells, strain XL1-Blue, were transformed with the resulting ligation mixtures of expression vectors, using heat-shock methodology. In short, 50 µl aliquots of bacterial suspensions were thawed out on ice for 5 minutes. One microliter of ligation mixture was added to the 16 µl of competent cells and incubated on ice for 5 minutes. The cells were heat-shocked for 1 minute in a water bath at 42°C and then allowed to recuperate on ice for 5 minutes. 250 µl of SOC medium was added and cells were incubated at 37°C for one hour with shaking at 250 rpm. The transformed cells were then aseptically plated on agar plates with 50 µg/ml of ampicillin and allowed to grow at 37°C for 14-16 hours. Colonies were then screened by colony PCR (section 2.4.10) to identify clones containing the insert in the correct orientation.

2.4.10 Colony PCR

Colony PCR, performed with MyTaqRed DNA Polymerase (Bioline), was used for screening for successful insertion of insert to vector in correct orientation. Colony PCR was performed with a combination of gene-specific and vector-specific primers. For primer sequences refer to Table 11. Single colonies were picked with sterile 10 µl pipette tips and suspended in 10 µl Milli-Q water in a clean 1.5 ml Eppendorf tube. Working on ice, 5 µl of bacterial suspension was mixed with 10 µl 5x MyTaq Red Reaction Buffer (5mM dNTPs, 15mM $MgCl_2$, stabilisers and enhancers), 1 µl of 20 µM forward primer (refer to Table 11), 1 µl of 20 µM reverse primer (refer to Table 11), 0.4 µl MyTaq Red DNA Polymerase and Milli-Q water to make up the final volume of 50 µl. The PCR parameters are shown in the Table 6.

Table 6. The PCR parameters for colony PCR. The PCR parameters used for colony PCR to screen for successful transformations.

Step	Temperature	Time	Cycles
Initial denaturation	95°C	1 min	1
Denaturation	95°C	15 s	25
Annealing	55°C	15 s	
Extension	72°C	30 s	
Final extension	72°C	5 min	1

Colonies that produced positive results were then used to inoculate 10 ml LB Broth supplemented with 100 µg/ml of ampicillin and incubated overnight at 37°C with shaking at 200 rpm. Putative positive colonies were then pelleted by centrifugation at 4500 rpm in a bench-top centrifuge for 10 minutes at 25°C. Plasmid DNA was subsequently purified from the harvested pellet as described above in section 2.4.2 and then sequenced by GATC Biotech. The sequenced DNA was aligned with the template sequence in VectorNTI software by ContigExpress assembly.

2.4.11 Purification of high yields of plasmid DNA for transfection

The correct sequenced constructs were used to generate a high yield of plasmid DNA with high purity suitable for mammalian cell transfections. The required miniprepped plasmid DNA was used to transform competent XL1-Blue bacterial cells, using the same experimental procedure as described in section 2.4.9. After the incubation a single colony was picked and suspended

in 10 ml sterile LB Broth supplemented with 100 µg/ml ampicillin and incubated for 8 hours at 37°C at 200 rpm. After the incubation period 1 ml of the bacterial culture was added to 100 ml sterile LB Broth supplemented with 100 µg/ml ampicillin and incubated for 12 hours at 37°C at 200 rpm. Plasmid DNA was extracted and purified using QIAprep Spin Midiprep Kit (QIAGEN) as described in section 2.5.1. The overnight bacterial culture was harvested by centrifuging at 6000 g for 15 minutes at 4°C. The bacterial pellet was resuspended in 4 ml Buffer P1. To lyse the bacterial cells 4 ml Buffer P2 was added, mixed thoroughly by inverting vigorously 4-6 times and incubated for 5 minutes at room temperature. To neutralise the lysis buffer 4 ml prechilled Buffer P3 was added, mixed thoroughly by inverting vigorously 4-6 times and incubated on ice for 15 minutes. A QIAGEN-tip 100 was equilibrated by applying 4 ml Buffer QBT and allowing column to empty by gravity flow. The bacterial lysate was centrifuged for 30 minutes at 20000 g at 4°C. The supernatant was then applied to the equilibrated QIAGEN-tip and allowed to enter the resin by gravity flow. The QIAGEN-tip was washed with 2 x 10 ml Buffer QC, each time allowing the column to empty by gravity flow. The DNA was eluted into a clean 15 ml vessel by adding 5 ml Buffer QF. To precipitate DNA 3.5 ml room-temperature isopropanol was added, mixed well and centrifuged at 15000 g for 30 minutes at 4°C, carefully removing supernatant. Marking the outside of the vessel helps to see what side the DNA precipitates on. The DNA pellet was washed with 2 ml room-temperature 70% (v/v) ethanol and centrifuged for 10 minutes at 15000 g, carefully removing supernatant as in the previous step. The DNA pellet was allowed to air-dry at room temperature for 10 minutes and then resuspended in 500 µl Buffer TE. The concentration and purity of the eluted DNA was assessed and the DNA samples were stored at -20°C.

2.5 Molecular cloning for generation of BiFC constructs

2.5.1 Plasmids and primers

Table 7. Addgene plasmids. Plasmids purchased from Addgene encoding for bJun-VN (fused to the NH_2-terminal fragment of the Venus yellow fluorescent protein (vYFP)), bFos-VC and bFosΔZIP (both fused to the COOH-terminal fragment of the vYFP). These plasmids were used for bimolecular fluorescence complementation method validation.

Constructs	Vector	Vector backbone	Tag	Antibiotic resistance
bJun-VN	pBiFC-VN155(I152L)	pMyc-CNV	myc	Ampicillin
bFos-VC	pBiFC-VC155	pCMV-HA	HA	Ampicillin
bFosΔZIP-VC	pBiFC-VC155	pCMV-HA	HA	Ampicillin

Table 8. Details and source of clones used.

Gene Symbol	Gene Description	Species	Alternative Name	GenBank Entry	Source	Plasmids	Antibiotic resistance
PTPRB	Protein tyrosine phosphatase, receptor type, B	*H.Sapiens*	*VE-PTP, RPTPB*	BC113463.1	SourceBioScience	pCR4-TOPO	Ampicillin (50µg/ml)
PTPRJ	Protein tyrosine phosphatase, receptor type, J	*H.Sapiens*	*DEP-1, CD148 RPTPeta*	BC063417.1	Art Weiss (UCSF)	pCR4-TOPO	Ampicillin (50µg/ml)
PTPRO	Protein tyrosine phosphatase, receptor type, O	*H.Sapiens*	*GLEPP1, RPTPO*	BC126203.1	SourceBioScience	pCR-XL-TOPO	Kanamycin (30µg/ml)
PTPRH	Protein tyrosine phosphatase, receptor type, H	*H.Sapiens*	*SAP-1, RPTPH*	BC111716.1	SourceBioScience	pCR-BluntII-TOPO	Kanamycin (100µg/ml)
CDH5	VE-cadherin (vascular endothelium)	*H.Sapiens*	*VE-Cadherin, Cadherin5, 7B4, CD144*	P33151.5	SourceBioScience	pCR-BluntII-TOPO	Kanamycin (100µg/ml)
SPN	Sialophorin	*H.Sapiens*	*CD43, LSN, GALGP, GPL115*	P16150.1	SourceBioScience	pOTB7	Chloramphenicol (20µg/ml)

Table 9. Synthetic DNA sequences and oligonucleotides used to generate signal peptides and epitope tags in expression constructs.

Protein name and epitope tag	DNA Sequence (5'->3')	Restriction sites	Delivery Vector
VE-PTP-HA	GGGCCCACCATGCTGAGCCATGGAGCCGGGTTGGCCTTGTGGATCACACTGAGCCTGCTGCAGACTGGACTGGCGGAGCCAGAGTACCCATACGATGTTCCAGATTACGCTTCTCGAG	*Apa*I - *Xho*I	pBiFC-VC155
DEP-1-HA	GGGCCCACCATGAAGCCGGCGGCGCGGGAGGCGCGGCTGCCTCCGCGCTCGCCCGGGCTGCGCTGGGCGCTGCCGCTGCTGCTGCTGCTGCTGCGCCTGGGCCAGATCCTGTGCGCAGGTGGCTACCCATACGATGTTCCAGATTACGCTTCTCGAG	*Apa*I - *Xho*I	pUC57
GLEPP1-HA	GGGCCCACCATGGGGCACCTGCCCACGGGGATACACGGCGCCCGCCGCCTCCTGCCTCTGCTCTGGCTCTTTGTGCTGTTCAAGAATGCTACAGCTTTCCATGTATACCCATACGATGTTCCAGATTACGCTTCTCGAG	*Apa*I - *Xho*I	pUC57
SAP-1-HA	GGGCCCACCATGGCTGGGGCTGGCGGGGGCCTCGGGGTCTGGGGGAACCTGGTGCTGCTGGGCCTGTGCAGCTGGACAGGGGCCAGGGCGCCTGCCCCCTACCCATACGATGTTCCAGATTACGCTTCTCGAG	*Apa*I - *Xho*I	pUC57
SPN-HA	GGGCCCACCATGGCCACGCTTCTCCTTCTCCTTGGGGTGCTGGTGGTAAGCCCAGACGCTCTGGGGAGCACAACATACCCATACGATGTTCCAGATTACGCTCGAATTC	*Apa*I -*Eco*RI	pUC57

Cont. **Table 9.** Synthetic DNA sequences and oligonucleotides used to generate signal peptides and epitope tags in expression constructs.

Protein name and epitope tag	DNA Sequence (5'->3')	Restriction sites	Delivery Vector
VE-PTP-myc*	(PTPRB-A) GATCGGGCCCACCATGCTGAGCCATGGAGCC (PTPRB-B) CTACCTCGAGACAGGTCCTCCTCTGAGATCAGCTTCTGCTC TGGCTCCGCCAGTCC	*Apa*I - *Xho*I	pBiFC-VN155(I152L)
DEP-1-myc	GGGCCCACCATGAAGCCGGCGGCGCGGGAGGCGCGGCTGCCTCCGCGCTC GCCCGGGCTGCGCTGGGCGCTGCCGCTGCTGCTGCTGCTGCTGCGCCTGGG CCAGATCCTGTGCGCAGGTGGCGAGCAGAAGCTGATCTCAGAGGAGGACCTG TCTCGAG	*Apa*I - *Xho*I	pUC57
GLEPP1-myc	GGGCCCACCATGGGGCACCTGCCCACGGGGATACACGGCGCCCGCCGCCTC CTGCCTCTGCTCTGGCTCTTTGTGCTGTTCAAGAATGCTACAGCTTTCCATGTA GAGCAGAAGCTGATCTCAGAGGAGGACCTGTCTCGAG	*Apa*I - *Xho*I	pUC57
SAP-1-myc	GGGCCCACCATGGCTGGGGCTGGCGGGGGCCTCGGGGTCTGGGGGAACCT GGTGCTGCTGGGCCTGTGCAGCTGGACAGGGGCCAGGGCGCCTGCCCCCGA GCAGAAGCTGATCTCAGAGGAGGACCTGTCTCGAG	*Apa*I – *Xho*I	pUC57
SPN-myc	GGGCCCACCATGGCCACGCTTCTCCTTCTCCTTGGGGTGCTGGTGGTAAGCC CAGACGCTCTGGGGAGCACAACAGAGCAGAAGCTGATCTCAGAGGAGGACCT GCGAATTC	*Apa*I -*Eco*RI	pUC57

* The VE-PTP-myc sequence was generated by PCR using the primers indicated

Table 10. Cloning primers for extracellular and transmembrane domains of the BiFC constructs. Underlined sequences are the restriction sites for sub-cloning.

Constructs	Forward Sequence (5'→3')	Length	Melting Tm (°C)	Reverse Sequence (5'→3')	Length	Melting T°C	Restriction sites
Cadh5	GATCGGGCCCACCATG CAGAGGCTCATGATGCT C	34	75	GATCGGTACCCCGGAGCCGC CGCCGCAGGAAG	32	75	*Apa*I-*Kpn*I
SPN	GATCCGAATTCGGGCAG TGCAGACACCCACCTC	33	74.5	GATCACCTCGAGACTGCCGC CGGCGCCACAGCA	33	75	*Eco*RI-*Xho*I
DEP-1	GATCTCTCGAGGTACCC CTAGTCCAATTCCTGA	33	70.7	GATCACCTCGAGATTTCCTCT TCTTTCTCCAGA	33	68.2	*Xho*I
SAP-1	GATCTCTCGAGGTAACC CAGGGAGGAACCTG	31	72.1	GATCACCTCGAGAATTCCTC CTCTTCAGGAAGAAAATC	38	70.5	*Xho*I
GLEPP1	GATCGGGCCCACCATG GGGCACCTGCCCAC	30	75	CTCCGGTACCTCGAGAATGC TTTTTCCTAAGAATAATGAGG	41	71.4	*Apa*I-*Xho*I
VE-PTP	AGTATCTCGAGGTAGAT GTAACTTCACCCTGGCG	34	70.7	TAGCACCTCGAGAGCTCACT TTCTGTCTGCAGATC	35	71.8	*Xho*I

Table 11. Colony PCR primers. The provided primers were used to check the insert and its orientation in the expression vector after ligation and transformation.

Construct	Insert	Forward Primer	Forward primer sequence (5'→3')	Reverse Primer	Primer sequence (5'→3')
Cadherin	ECD+TM	CMV-F	CGCAAATGGGCGGTAGGCGTG	CADH5-B	GATCGGTACCCCGGAGCCG CCGCCGCAGGAAG
VE-PTP	ECD+TM	CMV-F	CGCAAATGGGCGGTAGGCGTG	EBV-R	GTGGTTTGTCCAAACTCATC
GLEPP1	ECD+TM	CMV-F	CGCAAATGGGCGGTAGGCGTG	RO-D	
VE-PTP	SP+HA	RB-APF	GATCCCCGGGATGCTGAGCCAT GGAGCC	EBV-R	GTGGTTTGTCCAAACTCATC
DEP-1	SP+HA/SP+Myc	RJ-APF	GATCAAGCTTATGAAGCCGGCG GCGCGG	EBV-R	GTGGTTTGTCCAAACTCATC
DEP-1	ECD+TM	RJ-s	GATCTCTCGAGGTACCCCTAGTC CAATTCCTGA	EBV-R	GTGGTTTGTCCAAACTCATC
SAP-1	SP+HA/SP+myc	RH-APF	GATCAAGCTTATGGCTGGGGCTG GCGGG	EBV-R	GTGGTTTGTCCAAACTCATC
SAP-1	ECD+TM	CMV-F	CGCAAATGGGCGGTAGGCGTG	EBV-R	GTGGTTTGTCCAAACTCATC
GLEPP1	SP+HA/SP+myc	RO-APF	GATCATCGATATGGGGCACCTGC CCACG	EBV-R	GTGGTTTGTCCAAACTCATC
SPN	SP+HA/SP+myc	SPN-sp	ATGGCCACGCTTCTCCTTCT	EBV-R	GTGGTTTGTCCAAACTCATC
SPN	ECD+TM	SPN-sp	ATGGCCACGCTTCTCCTTCT	EBV-R	GTGGTTTGTCCAAACTCATC

Table 12. Sequencing primers. These primers were used for sequencing by GATC Biotech to confirm the right insert and its orientation and absence of mutations.

Name of Construct	Insert	Vector	Forward primer	Sequence (5'→3')	Reverse primer	Sequence (5'→3')
VE-PTP	SP+HA	pBiFC-VC155	CMV-F	CGCAAATGGGCGGTAGGCGTG	-	-
VE-PTP	ECD+TM	pBiFC-VN155	RBseq8	ACAATATTGCCATCACAGCTGT	RBseq9	GGTTGCCCAGAGATGCACTT
VE-PTP	ECD+TM	pBiFC-VC155	CMV-F	CGCAAATGGGCGGTAGGCGTG	EBV-R	GTGGTTTGTCCAAACTCATC
DEP-1	SP+HA	pBiFC-VC155	CMV-F	CGCAAATGGGCGGTAGGCGTG	-	-
DEP-1	SP+myc	pBiFC-VN155	CMV-F	CGCAAATGGGCGGTAGGCGTG	-	-
DEP-1	ECD+TM	pBiFC-VN155	CMV-F	CGCAAATGGGCGGTAGGCGTG	EBV-R	GTGGTTTGTCCAAACTCATC
DEP-1	ECD+TM	pBiFC-VC155	CMV-F	CGCAAATGGGCGGTAGGCGTG	EBV-R	GTGGTTTGTCCAAACTCATC
SAP-1	SP+HA	pBiFC-VC155	CMV-F	CGCAAATGGGCGGTAGGCGTG	-	-
SAP-1	SP+myc	pBiFC-VN155	CMV-F	CGCAAATGGGCGGTAGGCGTG	-	-
SAP-1	ECD+TM	pBiFC-VN155	CMV-F	CGCAAATGGGCGGTAGGCGTG	EBV-R	GTGGTTTGTCCAAACTCATC
SAP-1	ECD+TM	pBiFC-VC155	CMV-F	CGCAAATGGGCGGTAGGCGTG	EBV-R	GTGGTTTGTCCAAACTCATC
GLEPP1	SP+HA	pBiFC-VC155	CMV-F	CGCAAATGGGCGGTAGGCGTG	-	-
GLEPP1	SP+myc	pBiFC-VN155	CMV-F	CGCAAATGGGCGGTAGGCGTG	-	-
GLEPP1	ECD+TM	pBiFC-VC155	RO-FC-1F	GATCGCTAGCATGGGGCACCTGCCCA	RO-F340	AGATGAATTTGTCAGCGTAC
GLEPP1	ECD+TM	pBiFC-VN155	CMV-F	CGCAAATGGGCGGTAGGCGTG	EBV-R	GTGGTTTGTCCAAACTCATC

Cadherin	ECD+TM	pBiFC-VC155	CADH5-A	GATCGGGCCCACCATGCAGAGGCTCATGATGCTC	CADH5-B	GATCGGTACCCCGGAGCCGCCGCCGCAGGAAG
SPN	SP+HA	pBiFC-VC155	CMV-F	CGCAAATGGGCGGTAGGCGTG	-	-
SPN	SP+myc	pBiFC-VN155	CMV-F	CGCAAATGGGCGGTAGGCGTG	-	-
SPN	ECD+TM	pBiFC-VN155	CMV-F	CGCAAATGGGCGGTAGGCGTG	EBV-R	GTGGTTTGTCCAAACTCATC
SPN	ECD+TM	pBiFC-VC155	CMV-F	CGCAAATGGGCGGTAGGCGTG	EBV-R	GTGGTTTGTCCAAACTCATC
VE-PTP-17FN	ECD+TM	pBiFC-VN155	CMV-F	CGCAAATGGGCGGTAGGCGTG	EBV-R	GTGGTTTGTCCAAACTCATC

Cont. **Table 12. Sequencing primers.** These primers were used for sequencing by GATC Biotech to confirm the right insert and its orientation and absence of mutations.

2.5.2 Generation of BiFC constructs

Constructs for BiFC studies were generated by PCR and by standard molecular cloning procedures described in section 2.4 using the plasmids pBiFC-VN155(I152L) and pBiFC-VC155. A diagram of the strategy is shown below in Figure 8.

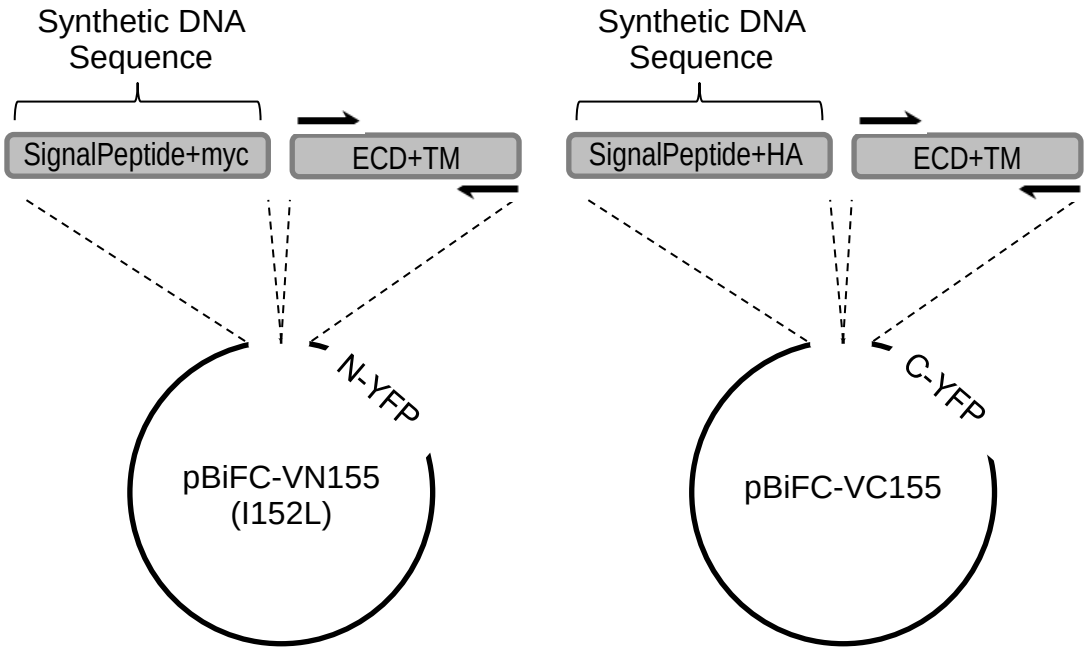

Figure 8. Schematic diagram of BiFC constructs generation. Signal peptide sequences followed by an epitope tag sequence (either HA or myc) were designed and provided by Genscript. **"** → ← **"** indicates forward and reverse primer pair used for generating the extracellular and transmembrane domains gene sequence (ECD+TM). Details of primers are provided in Table 10. The generation of BiFC constructs was done in two steps. First, signal peptide and an epitope tag were inserted into vectors, followed by the ligation of extracellular and transmembrane domains into the corresponding vector containing the N- or C-terminal sequence of Venus Yellow fluorescent protein (N-YFP, C-YFP).

Signal peptides of PTPRJ, PTPRO, PTPRH and SPN with either HA or myc tags, flanked by *Apa*I/*Xho*I restriction sites, were designed and purchased from Genscript in a pUC57 vector (refer to Table 9). DNA vectors were reconstituted in 100 µl of HPLC dH_2O. Competent SCS110 cells were

transformed with each of the pUC57 vector as described in section 2.4.9. DNA plasmids were then extracted and purified from bacterial culture as described in section 2.4.2. The synthetically generated signal peptide and myc/HA tag sequences were digested with appropriate restriction enzymes (refer to Table 9) and cloned into the BiFC expression vectors (Figure 8) as described in sections 2.4.8 and 2.4.9. Successful ligation was checked by Colony PCR as described in section 2.4.10 using vector and gene specific primers (refer to Table 11), followed by gel electrophoresis (section 2.4.4). DNA plasmids containing the correct signal peptide and an epitope tag insert were purified as described in section 2.4.2 and sequenced by GATC Biotech.

Polymerase chain reaction was used to amplify the coding sequences for extracellular and transmembrane domains for all R3 RPTPs, VE-cadherin and SPN as described in section 2.4.3. Details and sources of clones used are listed in Table 8. Cloning primers are provided in Table 10. The thermocycler programs were customised for each target sequence based on gene length and primers' melting temperature (refer to Table 4). PCR products were analysed on agarose gel and purified as described in sections 2.4.4 and 2.4.6 respectively.

Three micrograms of each of the purified PCR products and pBiFC-VN155 (27097) and pBiFC-VC155 (22011) vectors containing corresponding DNA sequences for signal peptides were digested with one unit of the appropriate restriction enzymes as described in section 2.4.7. Information on restriction enzymes used for each construct and on conditions is provided in Table 5. The digested fragments were analysed by agarose gel electrophoresis (section 2.4.4), purified (section 2.4.5) and ligated together (section 2.4.8). The resulting ligation mixture of expression vectors containing the final products was used to transform XL1-Blue strain of *E.coli* competent cells as described in section 2.4.9. Colony PCR was then performed to screen for successful ligations (section 2.4.10), which was analysed by gel electrophoresis (section 2.4.4). DNA plasmids containing the correct insert were purified as described in section 2.4.2 and sequenced by GATC Biotech.

The miniprepped plasmid DNA that corresponded to the predicted sequence was used to generate high yield of plasmid DNA with greater purity suitable for mammalian cell transfections as described in section 2.4.11.

2.5.3 Generation of VE-PTPΔ17FN mutant using a polymerase chain reaction based approach

In order to generate the VE-PTPΔ17FN construct (as illustrated in Figure 23) in which 17th fibronectin III-like domain has been removed the pBiFC-VN155 vector containing sequences for signal peptide, myc-tag, full-length extracellular and transmembrane domains followed by the N-terminal part of the YFP was used as a template. First, the sequence for the above vector was checked for all the restriction sites using VectorNTI software. The cutting sequence for the restriction enzyme *Xma*I was chosen to be included with primer sequence as there were no restriction sites for this enzyme in the above vector. Primers were designed, corresponding to the sequence on either side of the 17th FNIII domain, using VectorNTI software with an *Xma*I sequence at the start (Figure 9). The 5' ends of the primers were designed so that they would complement each other, and could be ligated together, and 3' ends oriented so that the extension would amplify the entire plasmid (see Figure 9).

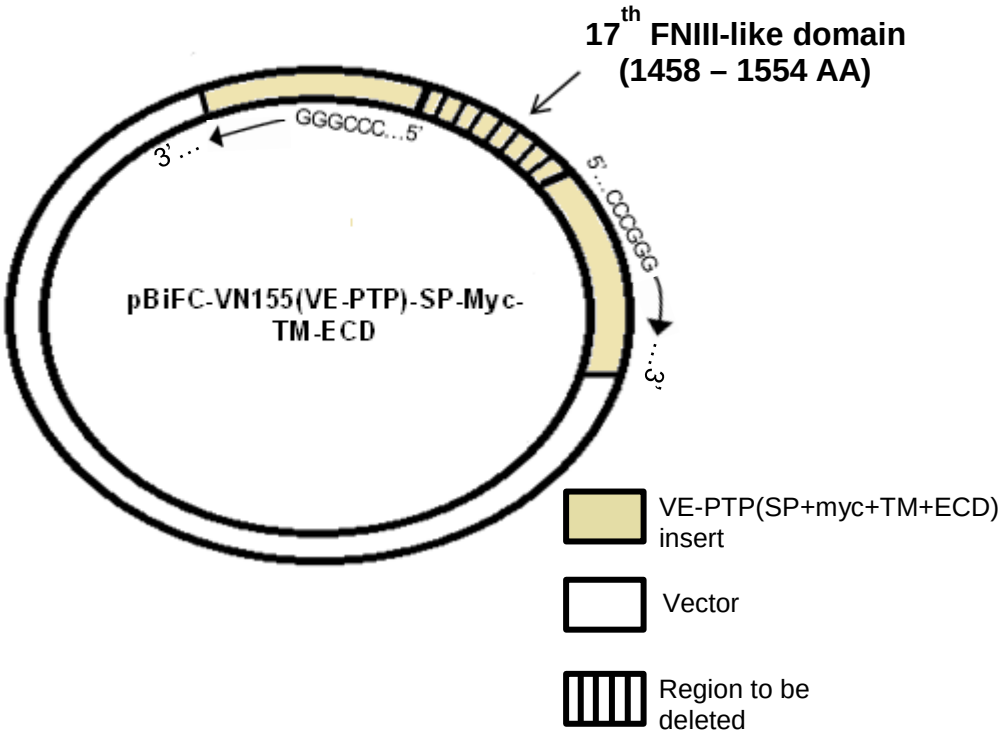

Figure 9. Schematic diagram of VE-PTPΔ17FN-VN mutant generation. This diagram illustrates the basis on which the primers were designed containing the sequence of the restriction enzyme at the 5' end and with the 3' end oriented so that polymerase would amplify the entire vector but excluding the region to be deleted.

The 5' ends of the primers contained the cutting sequence of the *Xma*I restriction enzyme (highlighted in bold in Table 13). As this cutting sequence contains six bases it was not necessary to include any additional bases to keep the polymerase reading frame between the restriction enzyme cutting sequence and the rest of the primer. Additional bases (GATC) were added at 5' ends of the primers to facilitate the restriction digest close to the end of DNA regions. The sequences of the synthesised primers are in Table 13.

Table 13. Primers for the generation of the VE-PTP mutant. Primers designed for the deletion of the 17th FN-III like domain from the previously generated VE-PTP BiFC construct. The restriction site for the *XmaI* enzyme is shown in bold.

Primer	Sequence	Length	TM	GC
VE-PTP^{-17FN}-sp	GATC**CCCGGG**CTAGG TGGAAAATGCGATCC	26	69.7°C	61.5%
VE-PTP^{-17FN}-ap	GATC**CCCGGG**CACAC GAATGTGTGGGGGTG	26	74°C	69.2%

PCR was then performed as described in section 2.4.3 in a reaction containing 100 ng template plasmid from which the 17th FNIII-like domain was to be removed. For the PCR conditions refer to Table 14.

The PCR product was analysed on agarose gel electrophoresis as described in section 2.4.4. The DNA bands of the desired size were purified from the agarose gel as described in section 2.4.5.

The gel extracted PCR product was digested with 1 U *Dpn*I (to digest template DNA) and 1 U *Xma*I restriction enzymes simultaneously in a Cutsmart Buffer at 37°C for 2 hours, followed by heat deactivation at 64°C for 20 minutes. Digested DNA was again analysed on agarose gel, extracted and purified as described above.

The ligation of *Dpn*I-*Xma*I digested DNA was performed using 110 ng of purified DNA as described in section 2.4.8. The ligation mixture was incubated at room temperature for 10 minutes, followed by heat deactivation at 65°C for 10 minutes. The resulting ligated DNA was chilled on ice for 5 minutes, followed by transformation into *E.coli* competent cells, strain XL-1 Blue, as described in section 2.4.9. Plasmids were then purified using QIAprep Spin Miniprep Kit (QIAGEN) according to manufacturer's instructions as described in section 2.4.2. The concentration and purity of the purified DNA was assessed using Nanodrop 1000 (Thermo Scientific) at 260

nm and 280 nm and then sequenced by GATC Biotech. The miniprepped plasmid DNA that corresponded to the predicted sequence, containing the deletion of the 17th FNIII-like domain, was then used to generate high yield of plasmid DNA with greater purity suitable for mammalian cell transfections as described in section 2.4.11.

Table 14. PCR parameters used for generation of VE-PTP∆17FN mutant. (A) Master Mix for one reaction to generate VE-PTP mutant was prepared according to manufacturer's recommendations. (B) Optimal PCR conditions that resulted in the correct PCR product.

A

Master Mix (one reaction)	
10x *Pfx* Buffer	10 µl
10 mM dNTPs	3 µl
50 mM $MgSO_4$	1 µl
VE-PTP^{-17FN}-sp	3 µl
VE-PTP^{-17FN}-ap	3 µl
VE-PTP-VN template	1 µl (100 ng)
Plat.*Pfx* DNA Polymerase	0.5 µl
HPLC dH_2O	28.5 µl

B

PCR Conditions

Step	Temp.	Time	Cycles
Initial Denaturation	94°C	5 min	1
Denaturation	94°C	15 sec	30
Annealing	59.6°C	30 sec	
Extension	68°C	9 min	
Final Extension	72°C	10 min	1

2.5.4 Generation of membrane anchored N- and C-terminal Venus-YFP fragments using the annealed Oligo Cloning technique

Three micrograms of each of pBiFC-VN155 (27097) and pBiFC-VC155 (22011) vectors that contain sequence for the N- and C-terminal Venus-YFP respectively were digested with 1 U *Apa*I restriction enzyme in 6 µl CutSmart Buffer and HPLC dH_2O up to the final volume of 60 µl at 25°C for 2 hours. One unit of *Eco*RI-HF was then added to the same mixture and further incubated for 2 hours at 37°C. The digested vectors were then analysed on an agarose gel as described in section 2.4.4.

Overlapping primers were designed using a trial version of VectorNTI software to contain *Apa*I and *Eco*RI restriction sites at 5' and 3' ends respectively, the membrane association sequence from the protein tyrosine kinase Lck (ATGGGCTGTGGCTGCAGCTCACACCCGGAAGATGACTG) and a myc tag (GGAGCAGAAGCTGATCTCAGAGGAGGACCT) sequence.

The oligos were re-suspended in the appropriate amount of HPLC dH_2O and 2 µg of each primer was mixed together with annealing buffer (10 mM Tris, pH7.5-8.0, 50 mM NaCl, 1 mM EDTA) up to the final volume of 50 µl. Mixed oligos were then placed in a sterile PCR tube and heated to 95°C for 2 minutes in the thermocycler and allowed to cool down gradually to 25°C at room temperature.

Five microlitres of annealed oligos was diluted with 45 µl HPLC dH_2O and the concentration and purity was assessed using Nanodrop 1000 at 260 nm and 280 nm. The annealed primers were then directly cloned into the *Apa*I/*Eco*RI sites of the previously digested and purified vectors using 5 U T4 DNA Ligase, 10 µl of 2x T4 DNA Ligation Buffer (Roche) and HPLC dH_2O up to the final volume of 20 µl at vector-to-insert molar ratio of 1:6 at 15°C for 30 minutes.

Table 15. Generation of membrane anchored N- and C-terminal Venus-YFP fragments. (A) Primers designed using VectorNTI software to generate YFP-VN155/YFP-VC155 negative control. Overlapping primers, when annealed, would create restriction sites for *Apa*I and *Eco*RI shown in bold. The protein tyrosine kinase Lck sequence and a myc tag sequence are underlined. (B) Schematic illustration of ligation of the annealed oligos into pBiFC-VN155(I152L) vector.

A

Primer	Sequence	Length
myr-F_ApaEco	**C**ACCATGGGCTGTGGCTGCAGCTCAC ACCCGGAAGATGACTGGGAGCAGAAG CTGATCTCAGAGGAGGACCTGC**G**	75
myr-R_ApaEco	**AATTC**GCAGGTCCTCCTCTGAGATCAG CTTCTGCTCCCAGTCATCTTCCGGGTG TGAGCTGCAGCCACAGCCCATGGT**GG GCC**	83

B

gggccc = *Apa*I site
gaattc = *Eco*RI site

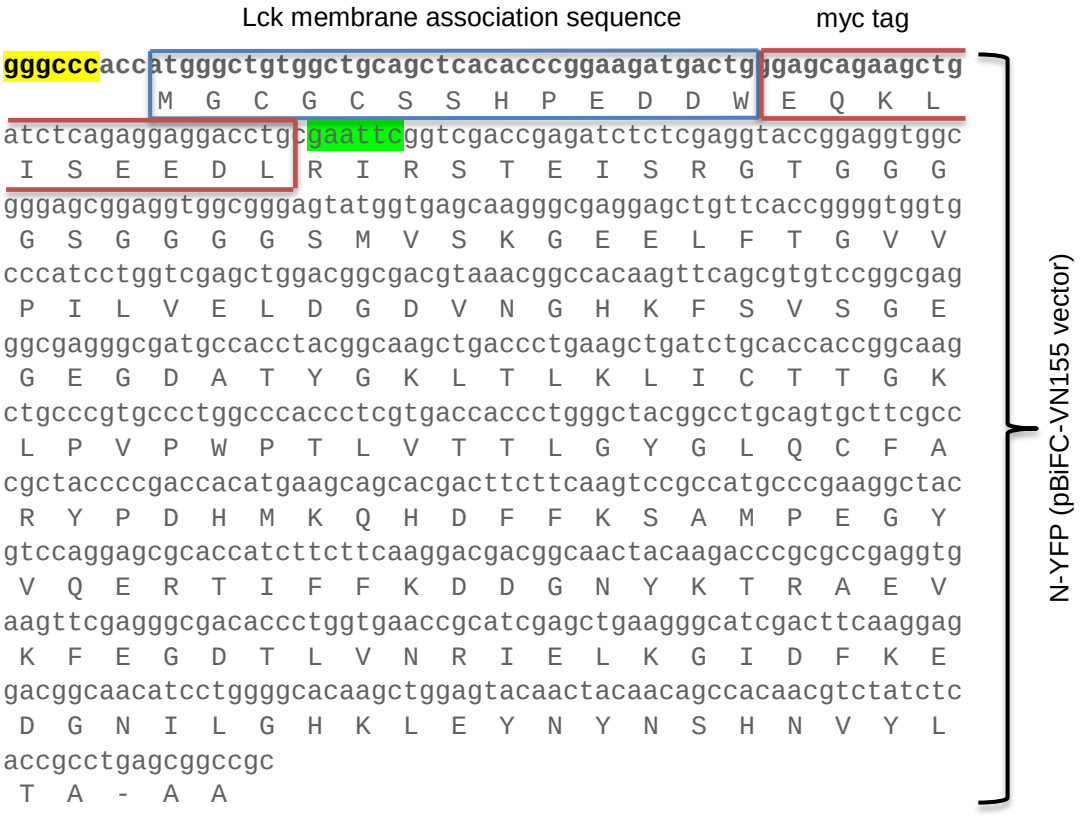

*E.coli c*ompetent cells, strain XL1-Blue, were then transformed with the resulting ligation mixtures as described in section 2.4.9. The transformed cells were then aseptically plated on agar plates with 50 µg/ml of Ampicillin and allowed to grow at 37°C for 14-16 hours, followed by the colony PCR as described above in section 2.4.10. Putative positive colonies were used to start an overnight bacterial culture (refer to section 2.4.10). Plasmid DNA was extracted and purified from the harvested pellet using QIAprep Spin Miniprep Kit (QIAGEN) as described in section 2.4.2. The concentration and purity of the eluted DNA was assessed using Nanodrop 1000 (Thermo Scientific) and then sequenced by GATC Biotech. The miniprepped plasmid DNA that corresponded to the predicted sequence was then used to generate high yield of plasmid DNA with high purity suitable for mammalian cell transfections as described in section 2.4.11.

2.5.5 Cell Culture

Human Embryonic Kidney 293 (HEK293) and 293T cells (ATCC code CRL-1573 and CRL-11268) were purchased from ATCC. Both HEK293 and HEK293T cell lines were used initially to compare the transfection and expression efficiency. The HEK293T cells are derived from 293 cells but stably express the simian virus 40 (SV40) large T antigen, which can bind to SV40 enhancer of expression vectors to increase protein production. HEK293 and HEK293T cells were maintained in Dulbecco's Modified Eagle's Medium (DMEM, with GlutaMAX, 4500 mg/L glucose; Gibco) supplemented with 10% (v/v) foetal bovine serum at 37°C in 5% CO_2 in a humidified incubator. Cells were trypsinised at 80% confluence and seeded 24 hours prior to transfection on 6-well (3×10^5 cells) plates.

2.5.6 Transfection and confocal visualisation

Transient transfections were performed using Lipofectamine® LTX Plus (Invitrogen) according to the manufacturer's instructions. Briefly, 500 µl Opti-MEM® Reduced Serum Medium, 0.5 µg of each DNA construct and PLUS™ Reagent (at the 1:1 ratio of DNA (µg) to PLUS™ Reagent (µl)) were mixed together in a sterile Eppendorf tube and allowed to incubate at room temperature for 5 minutes. Lipofectamine® LTX was mixed gently and added to the diluted DNA (2 µl per µg of DNA) and incubated at room temperature for 30 minutes. DNA-lipid complexes were then added directly to the cells in a drop-wise manner and incubated at 37°C in a CO2 incubator. After 24 hours cells were stained with CellMask™ DeepRed plasma membrane stain (ThermoFisher Scientific) for 1 hour at 37°C by directly adding 1 µl/well of the stain to live cells. The media were then removed, cells were rinsed with warm HBSS (Gibco) and images were acquired by sequential scanning using a Leica TCS SP2 confocal microscope system (Leica Microsystems) with a 63× ceramic dipping objective, using a dichroic beamsplitter DD458/514. A 514 nm argon ion laser was used to excite Venus YFP (Ex/Em 514/527 nm) with detection at 525-560 nm; and a 633 nm helium neon laser, intensity 35%, was used for the red stain (Ex/Em 649/666 nm) with detection at 660-685 nm.

2.5.7 Immunoblotting

Transfected HEK293T cells were rinsed with 2 ml/well ice-cold PBS containing Ca^{2+} and Mg^{2+} and lysed by adding 300 µl 4x Sample Buffer (240 mM Tris-HCl, pH 6.8, 8% SDS, 5% β-mercaptoethanol, 0.04% (v/v) bromophenol blue, 40% (v/v) glycerol) into each well. In some experiments some cells were lysed using 250 µl/well ice-cold lysis buffer containing complete protease inhibitor tablet (Roche). To prepare samples for loading 30 µl of cell lysates were mixed with 10 µl 4x sample buffer. The total cell lysate (20 µl) was loaded on to a 4–20% Mini-Protean TGX precast gel (Bio-Rad) and subjected to electrophoresis at 110 V for 60 minutes in 1 x SDS running buffer (for buffer composition refer to Table 3). For accurate molecular weight estimation on SDS-polyacrylamide gel and on immunoblots

pre-stained ColorBurst™ electrophoresis marker (Sigma-Aldrich) was also used. Proteins were transferred onto PVDF membranes (GE Healthcare) by tank electroblotting in 1x Transfer Buffer (25 mM Tris, 192 mM glycine, 20% (v/v) methanol and ddH_2O) for 2 hours at room temperature with an ice block and stirring to allow heat dissipation.

Each membrane was blocked with blocking buffer (3% (w/v) non-fat dry milk dissolved in 1x TBS) for one hour at room temperature with gentle shaking. An appropriate primary antibody was added directly to the blocking solution at 1 in 2000 dilution and incubated for one hour. A list of primary antibodies used in Western blotting is provided in Table 16. Membranes were then washed 3x for 5 minutes with 1x TBST and incubated with secondary anti-mouse IgG (whole molecule)-HRP linked secondary antibodies (A4416; Sigma-Aldrich) at 1 in 5000 dilution in fresh blocking buffer for 1 hour at room temperature with shaking. Membranes were washed 6x for 5 minutes with 1x TBST and developed with SuperSignal West Femto Maximum Sensitivity Substrate (ThermoScientific) according to the manufacturer's instructions and the chemiluminescence was visualised using Labworks 4.1 software.

Table 16. List of primary antibodies used in Western blotting.

Antibody	Clone	Description	Source	Dilution
Anti-myc	4A6	Mouse monoclonal to myc tag	Millipore	1:2000
Anti-HA	12CA5	Mouse monoclonal to HA tag	Abcam	1:2000
Anti-VE-cadherin	BV9	Mouse monoclonal to VE-cadherin	Abcam	1:2000
Anti-β-Actin	ab8226	Mouse monoclonal to β-Actin	Abcam	1:2000

2.5.8 Membrane localisation study by immunoprecipitation

To test that the epitope tags do not interfere with protein localisation and that the BiFC epitope-tagged proteins lacking a cytosolic domain still reach the plasma membrane the proteins were immunoprecipitated with antibodies specific to their tags, followed by detection by immunoblotting. The antibody was added directly to the cells that express the protein of interest so that only the proteins on the plasma membrane would be detected. The plasma membrane expression level could then be compared with the expression of the corresponding full-length protein as well as the expression in whole cell lysates.

HEK293T cells were transiently transfected with 2.5 µg of each DNA construct using Lipofectamine® LTX Plus as described in section 2.10. After the 24 hours of incubation at 37°C in the humidified incubator anti-myc (mouse monoclonal 4A6; Millipore) primary antibody was added to each well at 1 in 1000 dilution and incubated at room temperature for 10 minutes with gentle rocking. The media was then removed and cells were rinsed once with 1 ml/well ice-cold HBSS. The cells were lysed by adding 250 µl of ice-cold lysis buffer (refer to Table 3 for the composition) containing complete Protease Inhibitor Tablet (Roche) to each well and gently aspirating. The lysates were transferred to clean Eppendorf tubes and centrifuged at 4°C for 15 minutes at 14000 g. The supernatant was then transferred to clean Eppendorf tubes and 50 µl of the protein A-sepharose beads (GE Healthcare Life Sciences) was added to each tube. The lysate-beads mixture was agitated at 4°C for 2 hours and centrifuged for 2 minutes at 4°C, discarding the supernatant. The beads were washed 3x with 100 µl lysis buffer, centrifuging each time for 1 minute at 4°C and discarding the supernatant. After the last supernatant was removed 25 µl of 4x sample buffer was added to each tube and boiled for 5 minutes at 95°C. The tubes were centrifuged at 4°C for 2 minutes and the supernatant containing proteins was transferred to clean Eppendorf tubes.

Samples were then subjected to SDS-PAGE, followed by Western blot and visualisation as described above in section 2.5.7.

2.5.9 Generation of quantitative data and statistical analysis

ImageJ software (https://imagej.nih.gov/ij/) was used to carry out quantitative analysis of results. HEK293T cells were transiently co-transfected with an interacting fusion pair of interest, stained with CellMask™ DeepRed Plasma Membrane Stain and analysed using confocal microscope. The confocal images were then used to measure the fluorescence intensity. For BiFC quantification multiple images were taken in random distribution.

Confocal images, one from yellow channel (YFP fluorescence signal) and one from red channel (plasma membrane stain) were opened in ImageJ software. Images were then merged by selecting from Menu Bar: Image → Colour → Merge channels and then selecting the image for the red channel (C1) and for the yellow channel (C7), thus creating a composite image and keeping the source images too. The composite image was then used to select the border of each cell using a polygon selection tool and adding the selection, one at a time, in region of interest (ROI) manager (Analyse→Tools→ROI Manager). In addition, a region containing no cell was selected as a background in each confocal image analysed. The selected cells were analysed, each channel at a time, by selecting from Menu Bar option Analyse→Set Measurements→select Area, min and max grey value, integrated density and mean grey value→redirected to (a channel to be analysed)→OK. To get the values for the selected channel the Measure option in ROI Manager was chosen and the results were saved as an Excel file.

To calculate the corrected total cell fluorescence (CTCF) the following formula was used: integrated density minus (area of selected cell x mean fluorescence of background readings). This was done for all the selected cells from the yellow channel as well as the red channel. The values were then used to calculate yellow/red ratio in individual cells by dividing the corrected fluorescent intensity derived from bimolecular fluorescence complementation (e.g. YFP-VN+YFP-VC) by the corrected fluorescence signal derived from the plasma membrane stain. On average about 700 cells for each fusion protein combination were analysed from several fields in at

least three independent experiments. To determine the distribution of ratios Bin Limits were first created ranging from 0.01 to 4.01 in the interval of 0.1. Then, the frequency was determined using the Frequency function in Excel by selecting ratio values data array and bins data array and then the formula was entered as a multi-cell array by pressing Ctrl+Shift+Enter. The distributions of ratios in individual cells were then plotted in histogram.

To calculate the average yellow fluorescence intensity the border of each cell was traced in the ImageJ using a polygon selection and the average pixel intensity of the selected region, including border, was calculated. Since the cells were stained with the plasma membrane stain all the cells were selected based on the red fluorescence signal outlining the membrane, including those that did not exhibit the yellow fluorescence signal. To account for the variability in transfection efficiency the images were acquired from multiple fields per well and used for analysis. The background signal in an area with no cells was subtracted from all values as described above. BiFC fluorescence intensity values from at least three independent experiments were averaged and used for statistical analysis.

Data were analysed with ImageJ, Microsoft Excel and IBM SPSS Statistics 22 software, using Kruskal-Wallis H test and Mann-Whitney U test. A *P* value of <0.05 was considered statistically significant for any set of data.

Chapter 3

Optimisation of the Bimolecular Fluorescence Complementation (BiFC) assay and validation of the quantitation procedure

3.1 Introduction

The overall object of this thesis is to investigate receptor protein tyrosine phosphatases of R3 subgroup using bimolecular fluorescence complementation (BiFC) assay and in this chapter as a preliminary step the assay has been optimised and validated using a pair of well characterised interacting proteins. This assay enables direct visualisation of protein interactions in living cells, mimicking their normal cellular environment (Kerppola, 2006). The BiFC assay is based on the principle of protein fragment complementation, in which two non-fluorescent fragments from the Venus yellow fluorescent protein are fused to a pair of interacting partners. If these two proteins interact with each other they bring the two non-fluorescent fragments into close proximity, resulting in proper folding and assembly, thus reconstituting a fluorescent protein. Therefore the reconstituted fluorescence reflects the interaction of two proteins of interest (Kerppola, 2008). The assembled complex produces strong intrinsic fluorescence that can be detected by a confocal microscope without the need for staining with exogenous fluorogenic and chromogenic agents (Kerppola, 2006).

However, this approach has some limitations. The main two limitations are self-assembly of the two non-fluorescent fragments and irreversibility that can contribute to the false-positive fluorescence and decreases the signal-to-noise ratio, making data interpretation difficult (Kodama and Hu, 2010). To address the problem with self-assembly various mutants, such as V150L, I152L and T153M, have been introduced in fragments of a Venus yellow fluorescent protein in order to weaken the hydrophobic interaction between VN155 and VC155 and to reduce the background fluorescence (Kodama and Hu, 2010; Nakagawa *et al,* 2011). It has been previously reported that V150L resulted in very low fluorescence intensity in BiFC with bJunVN and bFosVC. The point mutation of T153M showed lower fluorescence intensity in BiFC with bJunVN and bFosVC but higher in BiFC with bJunVN and ∆bFosVC compared with I152L. However, the point mutation of I152L in VN155 of Venus significantly reduced self-assembly and decreased background fluorescence without significantly altering the overall structure (Kodama and

Hu, 2010). This improved Venus fragment should facilitate the study of protein interactions in living cells in this project.

Numerous protein interactions have been visualised using the BiFC assay in many different cell types and organisms. For example, a study by Magliery *et al* (2006) used the GFP-based BiFC assay to study protein-peptide interactions in BL21 (DE3) *Escherichia coli* cells. In their study the interactions of TPR1 and TPR2A (tetratricopeptide repeat) domains with protein chaperones Hsc70 and Hsp90 were analysed. TPR1 binds to the C-terminus of the human chaperone Hsc70 and TPR2A binds to the C-terminus of Hsp90 (Magliery *et al,* 2006). The BiFC results confirmed the known interactions and showed that protein-peptide or protein-protein interactions are clearly required for the reassembly of the GFP and that the BiFC approach was useful for discriminating strongly bound ligands from weakly bound ones (Magliery *et al* 2006).

Another study by Walter *et al* (2004) adopted the BiFC approach to address its feasibility for visualisation of the basic leucine zipper (bZIP) transcription factor bZIP63 homodimerisation in living plant cells. It has been shown previously that nuclear bZIP63 transcription factor forms homodimers and heterodimers via the C-terminal leucine zipper domain (Siberil *et al,* 2001). The BiFC results showed that the epidermal cells infiltrated with bZIP63-YFPN and bZIP63-YFPC-carrying Agrobacteria resulted in a strong fluorescence signal (Walter *et al*, 2004). The homodimerisation-induced YFP fluorescence appeared exclusively inside the nucleus which corresponded to the nuclear localisation of the bZIP63 (Walter *et al*, 2004). The same study by Walter *et al* (2004) also showed that the BiFC approach could be used to visualise cytoplasmic protein-protein interactions in plant cells. Previous experiments showed that the tobacco 14-3-3 protein T14-3c (T14) forms homodimers, which was also demonstrated by the BiFC experiments. The co-expression of T14-YFPN and T14-YFPC resulted in strong YFP fluorescence detected throughout the cytoplasm and the nucleus. The localisation of homodimer formation corresponded to the subcellular distribution of T14-3c, demonstrating that BiFC is a very efficient technology

for the analysis of protein–protein interactions in living plants cells (Walter *et al*, 2004).

Some transmembrane protein interactions have also been studied using the BiFC approach. For example, a group led by de Virgilio *et al* (2004) used BiFC to define αIIbβ3 - tyrosine kinase interactions in living cells as well as to obtain subcellular localisation of αIIbβ3 - tyrosine kinase complexes. Transmembrane platelet integrin αIIbβ3 plays a critical role in platelet aggregation by binding to soluble ligands like c-Src. BiFC analysis revealed that the co-expression of αIIbYCβ3 (fused to the C-terminal part of YFP) with SrcYN (fused to the N-terminal part of YFP) resulted in a fluorescent signal within membrane ruffles, focal complexes and focal adhesions. The localisation of BiFC corresponded with where the proteins were previously co-localised with antibody-labelled αIIbβ3 and c-Src in fixed cells (de Virgilio *et al,* 2004). The same experiments showed that αIIbβ3 can also interact with spleen tyrosine kinase Syk. The co-expression of αIIbYCβ3 and SykYN detected BiFC signal confined primarily to ruffles and nascent adhesion structures close to the cell periphery. The above results were complemented with and corresponded to the results obtained with bioluminescence resonance energy transfer (BRET) (de Virgilio *et al,* 2004).

Although the BiFC method has gained popularity in protein-protein interaction studies there is still a major downside that the non-fluorescent fragments of YFP are prone to self-assembly independent of a protein-protein interaction event. To establish whether fluorescence observed in the BiFC assay reflects a specific protein interaction, it is essential to include negative controls in each experiment. A literature survey on recent BiFC studies carried out by Horstman *et al* (2014) revealed that most studies use inappropriate controls and rely on qualitative rather than quantitative read-out of fluorescence. The validity of results from BiFC analysis must be confirmed by examining fluorescence complementation by fusion proteins in which the interaction interface has been mutated (Kerppola, 2006). However, this is possible only if there is a prior knowledge of the structural nature of the interaction interface. It was suggested by Kerppola *et al* (2006) that multiple

combinations of fusion proteins need to be tested for BiFC. Amino- and carboxyl-terminal fusions can be used to test eight distinct combinations (refer to Figure 10; obtained and modified from Kerppola (2006)) in order to find a favourable combination that would reflect the precise structures and flexibilities of the fusion proteins (Kerppola, 2006).

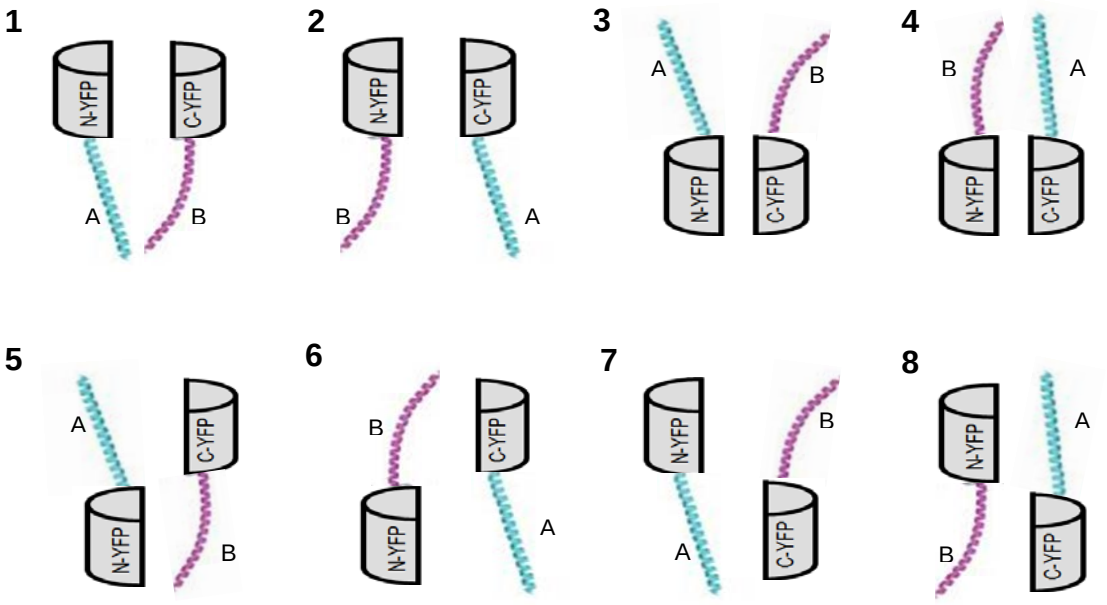

Figure 10. Schematic representation of eight different combinations of fusion proteins to be tested for BiFC. These combinations of various fusion proteins were suggested by Kerppola (2006) to be used for BiFC in order to find a favourable combination that would reflect structures and flexibility of the fusion proteins.

In addition, it is also recommended to use some of the numerous fusion proteins whose interactions have been visualised using the BiFC assay as positive controls.

Because of the self-assembly capacity of the two halves of the YFP the qualitative analysis of the BiFC method has proved problematic. Thus BiFC quantification of protein-protein interactions in living cells has been proposed in order to distinguish between a fluorescence complementation by a true protein-protein interaction and a signal due to self-assembly of the two YFP fragments (Horstman *et al*, 2014). It is necessary to compare the quantitative data obtained from the protein combination of interest and from a negative control combination. One method for BiFC quantification is to determine the average fluorescence intensity from fluorescent images. However, this method requires measurement of cells on a one-by-one basis. In addition, in transient assays it is difficult to maintain relatively uniform and constant expression levels in the entire cell population and in replicate experiments. Therefore, to determine the statistical significance between experimental and control interaction pairs a large number of cells from random fields and multiple experiments have to be analysed (Kerppola, 2006; Horstman *et al*, 2014). Additional quantification analyses performed in this thesis were adapted from Kodama and Hu (2010) and from Kerppola (2013). In previous studies the BiFC relative efficiency was quantified by determining the fluorescence intensity of BiFC complex and dividing it by the intensity of the control protein Cerulean. The distribution of ratios between the fluorescence intensities in individual cells was plotted in histogram (Kerppola, 2013). In this thesis the ratio of BiFC to cell membrane stain (rather than Cerulean) represented a measure of the efficiency of bimolecular fluorescence complementation. In addition the previous studies also looked at the signal-to-noise (S/N) ratio as a measure of BiFC specificity. The higher the S/N ratio value the more specific the interaction. The S/N ratio was calculated by dividing a median of the BiFC efficiency with the positive interaction by a median of the BiFC efficiency with the negative interaction (Kerppola, 2013; Kodama and Hu, 2010).

In this chapter the objectives were to validate a novel quantification procedure using bJun, bFos and bFosΔZIP YFP fusion proteins and to optimise the assay to enhance the BiFC signal and to minimise background noise due to self-assembly of the YFP halves. It has been previously shown that two proteins bJun and bFos interact together. bFos directly modulates bJun function by formation of a heterodimer of bFos and bJun proteins (Ransone *et al*, 1990). In previous work Hu and colleagues (2002) used the basic region-leucine zipper (bZIP) family of transcription regulatory proteins bJun and bFos to establish BiFC assay. bFos-YC (fused to the C-terminal part of the yellow fluorescent protein) and bJun-YN (fused to the N-terminal part of the yellow fluorescent protein) fusion pair exhibited high fluorescence intensity when co-expressed together in COS-1 cells. Fluorophore formation by bFos-YC/bJun-YN fusion pair showed sigmoidal kinetics, consistent with bimolecular association of the two subunits followed by fluorophore formation at the rate comparable to that observed for intact YFP. The excitation and emission spectra of the bFos-YC/bJun-YN heterodimer were also identical to those of intact YFP (Hu *et al*, 2002). The introduction of a mutation into the interaction interface of bFos (bFosΔZIP-YC) has been shown to decrease significantly the fluorescence signal under the same experimental conditions, reflecting the specific interaction between bFos-YC/bJun-YN (Hu *et al*, 2002). Based on previous studies by Hu *et al* (2002) bFos-VC/bJun-VN (fused to C- and N-terminal parts of the Venus yellow fluorescent protein respectively) and bFosΔZIP-VC/bJun-VN fusion pairs were used as positive and negative control respectively.

Figure 11 (A) shows the schematic representation of bFos-VC/bJun-VN bimolecular complex formation. Upon the interaction of these two proteins the non-fluorescent YFP fragments are brought into close proximity, reconstituting full-length functional yellow fluorescent protein. The resultant fluorescence is then detected by any confocal microscope. The mutated form of bFos-VC that lacks the interaction region (bFosΔZIP-VC), in theory, would not be able to interact with bJun-VC. As a result there is no interaction and thus no bimolecular complex formation (Figure 11, B) and in theory there should be no detectable fluorescence signal.

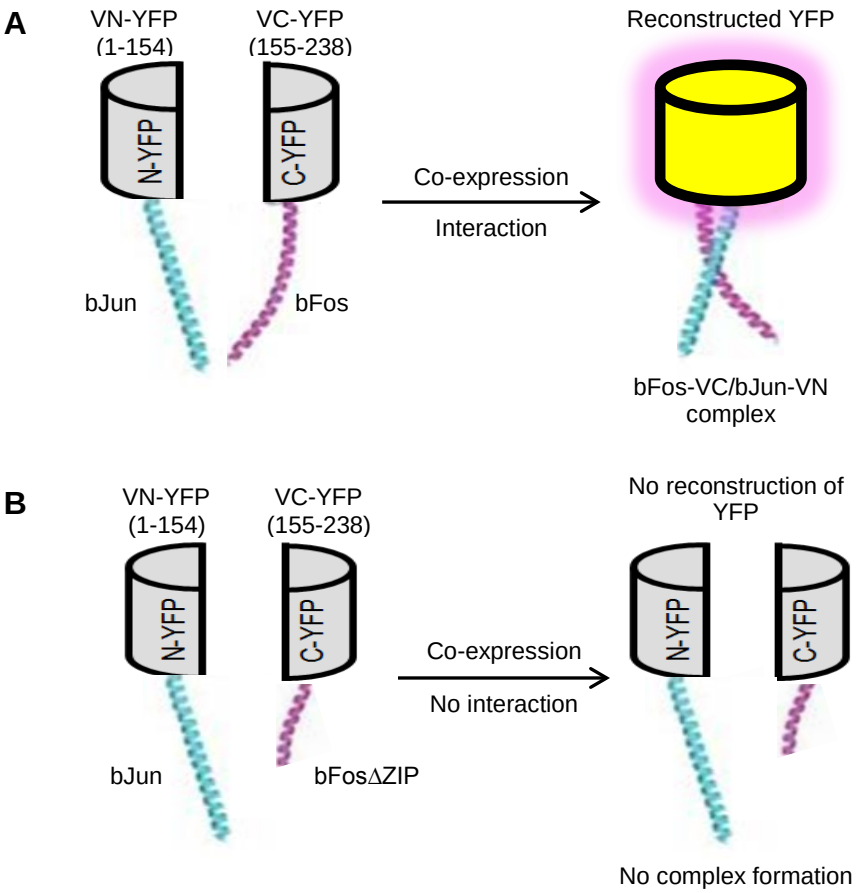

Figure 11. Schematic representation of the formation of the bFos-VC/bJun-VN bimolecular fluorescent complex. (A) Two non-fluorescent fragments (VC and VN) of a Venus yellow fluorescent protein (YFP) are fused to putative interaction partners bFos and bJun respectively. The association of the interaction partners allows formation of a bimolecular fluorescent complex. (B) Mutated bFosΔZIP-VC lacks the interaction region and thus cannot interact with bJun-VN and produce yellow fluorescence.

3.2 Results

3.2.1 Western Blot analysis to confirm the expression of bJun-VN, bFos-VC and bFosΔZIP-VC fusion proteins in HEK293T cells

To confirm the expression of bJun-VN, bFos-VC and bFosΔZIP-VC fusion proteins following transient transfection into HEK293T cells Western blot analysis was performed using whole cell lysates. Single transfections of HEK293T cells were performed using 2.5 µg of each fusion construct and after a 24-hour incubation period the cell lysates were analysed.

Western blot analysis confirmed the expression of bFos-VC and bFosΔZIP-VC (Figure 12, A) with the anticipated molecular weight of 24.77 and 23.02 kDa respectively. The deletion of leucine zipper in bFos-VC did not affect the level of expression. As can be seen in Figure 12 (A) both bFos-VC and bFosΔZIP-VC proteins are expressed at similar levels. The expression of bJun-VN was also confirmed with the anticipated molecular weight of 28.05 kDa (Figure 12, B). The expression level for bJun-VN appeared to be much higher than for bFos-VC and bFosΔZIP-VC. However, the comparison of relative expression levels of the above proteins may not be entirely reliable. A difference in band intensity could be caused by experimental variability, such as using different antibodies. Anti-myc antibody could be more sensitive in detecting myc tag compared with anti-HA antibody detecting HA tag. Using constructs fused to the same epitope tag that could be recognised by the same antibody would give a more accurate read-out of the true levels of each protein at the time of harvest and would better determine whether changes in band intensity are due to different expression levels.

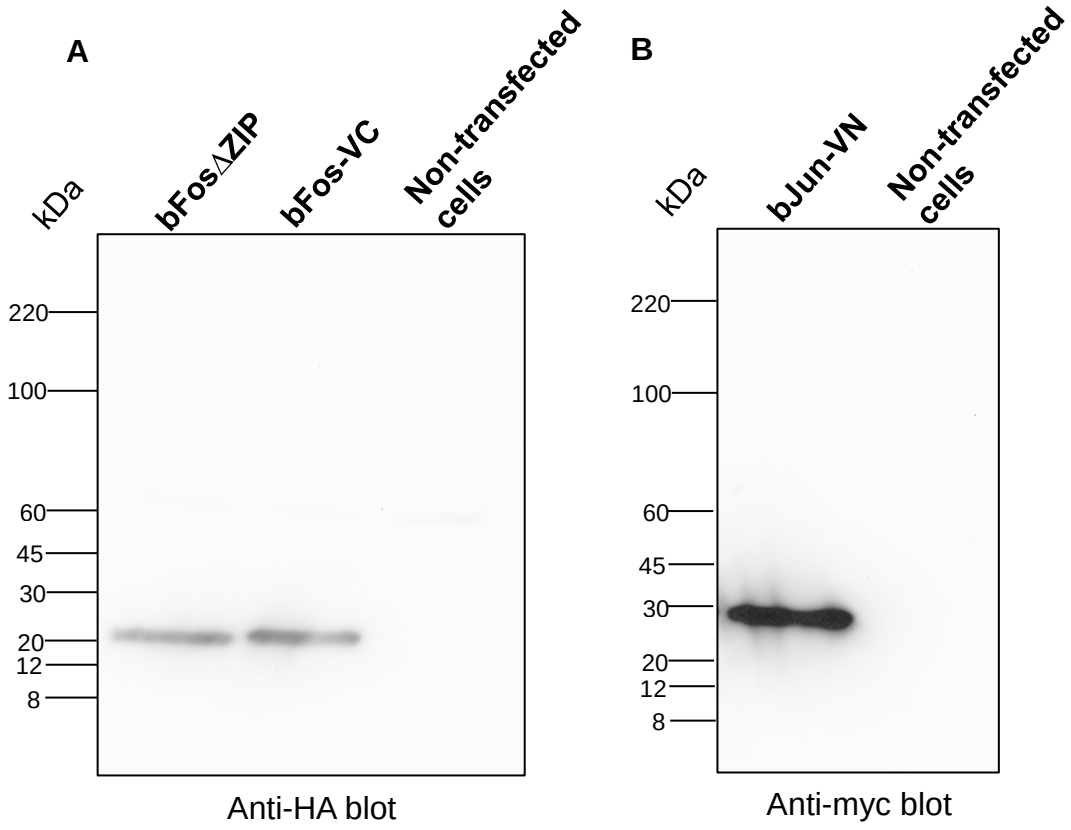

Figure 12. Western blot analysis of bJun-VN, bFos-VC and bFosΔZIP-VC fusion proteins. Transfected HEK293T cells expressing fusion proteins were harvested for the detection of fusion proteins using (A) Anti-HA and (B) Anti-myc antibodies.

3.2.2 Comparison of HEK293 and HEK293T cell lines

The human embryonic kidney 293 (HEK293) cell line is widely used in many transfection experiments due to the cells' high transfection efficiency and rapid growth. HEK293T cells are derived from HEK293 cells but have been transduced with the SV40 large T antigen (Simian Vacuolating Virus 40 Tag) that can bind to SV40 enhancer of expression vectors, promoting plasmid replication, and thus considerably increase the expression levels obtained with transient transfection.

In order to establish the cell line that results in higher BiFC signal both HEK293 and HEK293T cell lines were transiently co-transfected with bFos-VC/bJun-VN and bFosΔZIP-VC/bJun-VN fusion pairs, using 0.25 µg of each DNA fusion construct using Lipofectamine® LTX Plus. After a 24-hour incubation live cells were examined under a confocal microscope to compare fluorescence signal.

Both cell lines exhibited yellow fluorescence (Figure 13) after being co-transfected with the bFos-VC/bJun-VN fusion pair. However, qualitative assessment of at least three randomly acquired images from two independent experiments showed that the co-expression of bFos-VC/bJun-VN in HEK293T cells produced a stronger yellow fluorescence signal compared with the signal in HEK293 cells. HEK293T cells exhibited not only higher intensity of the fluorescent signal but also a higher number of cells producing the signal. Co-expression of bFosΔZIP-VC/bJun-VN in either HEK293 or HEK293T cells did not produce any fluorescence emission (Figure 13).

Based on qualitative results of this experiment it was considered that HEK293T cells exhibit higher protein expression efficiency since the transfection and confocal analysis were carried out under the same conditions and using the same parameters. In addition the experiment was repeated twice and resulted in the same outcome. Therefore the HEK293T cell line was chosen for further experiments.

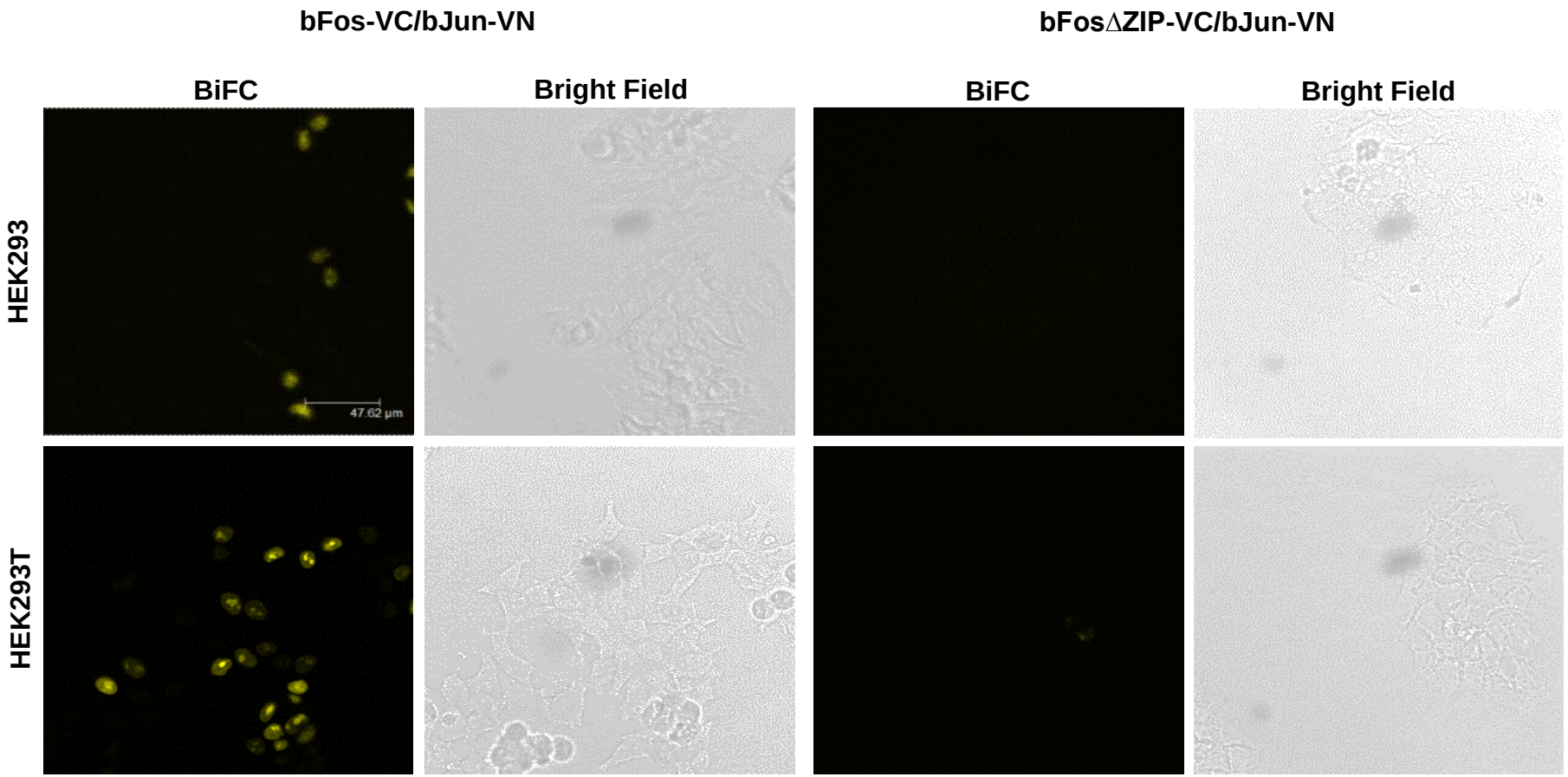

Figure 13. Confocal analysis of expression efficiency in HEK293 and HEK293T cells. Cells were co-transfected with either bFos-VC/bJun-VN or bFosΔZIP-VC/bJun-VN fusion pairs using 0.25 µg of each DNA fusion construct and images were acquired 24 hours after transfection. The scale bar is 47.62 µm.

3.2.3 Optimising quantity of DNA for HEK293T cell transfection

To minimise protein mislocalisation and formation of non-native complexes due to overexpression, the fusion proteins have to be expressed at levels comparable to the endogenous proteins. However, with transient transfections there is always a risk of overexpressing proteins. In order to establish the optimal DNA concentration HEK293T cells were transiently co-transfected with bFos-VC/bJun-VN and bFosΔZIP-VC/bJun-VN fusion pairs using 0.25 µg, 0.5 µg, 1.0 µg, 1.5 µg and 2.0 µg of each fusion construct with or without Plus (enhancer) reagent. Plus reagent is an optional reagent that was specifically designed for use in conjunction with Lipofectamine reagent and can improve transfection efficiency in adherent cell lines. After 24-hour incubation live cells were examined under a confocal microscope as indicated in Figure 14.

Co-expression of bFos-VC and bJun-VN fusion proteins in HEK293T cells, where Plus reagent was used, resulted in fluorescence complementation at all the DNA concentrations used. However, cells co-transfected with 0.25 µg of each fusion construct exhibited very low transfection efficiency. There was a significant increase in fluorescence signal in cells co-expressing bFos-VC and bJun-VN fusion proteins at 0.5 µg, 1.0 µg, 1.5 µg and 2.0 µg with no visual difference in yellow fluorescence signal among these concentrations (Figure 14).

Qualitative assessment of at least three randomly acquired images showed that without Plus reagent co-expression of bFos-VC and bJun-VN at 0.25 µg, 0.5 µg and 1.0 µg resulted in fluorescence signal but the signal appeared to be reduced compared with images when Plus reagent was added at the same concentrations. There was no fluorescence complementation when cells were transfected with 1.5 µg of each fusion construct and only one cell exhibited fluorescence signal when cells were transfected with 2.0 µg of each fusion construct (Figure 14).

bFosΔZIP-VC, which lacks the interaction region, was used as a negative control to compare the BiFC efficiency between bFos-VC and bFosΔZIP-VC when they were paired with bJun-VN fusion protein. There was no

fluorescence complementation produced when HEK293T cells were co-expressed with bFosΔZIP-VC/bJun-VN fusion pair at any concentration used when transfection was performed without Plus reagent. When HEK293T cells were transfected with the bFosΔZIP-VC/bJun-VN fusion pair with Plus reagent there was some fluorescence complementation detected at 0.5 µg concentration. However, the BiFC signal was significantly reduced compared with the signal produced by the co-expression of bFos-VC/bJun-VN at the same concentration (Figure 14).

Based on these results further experiments were conducted using 0.5 µg of each plasmid DNA with Plus reagent. This amount of DNA provided a good signal over background and minimised the amount of DNA required for each experiment.

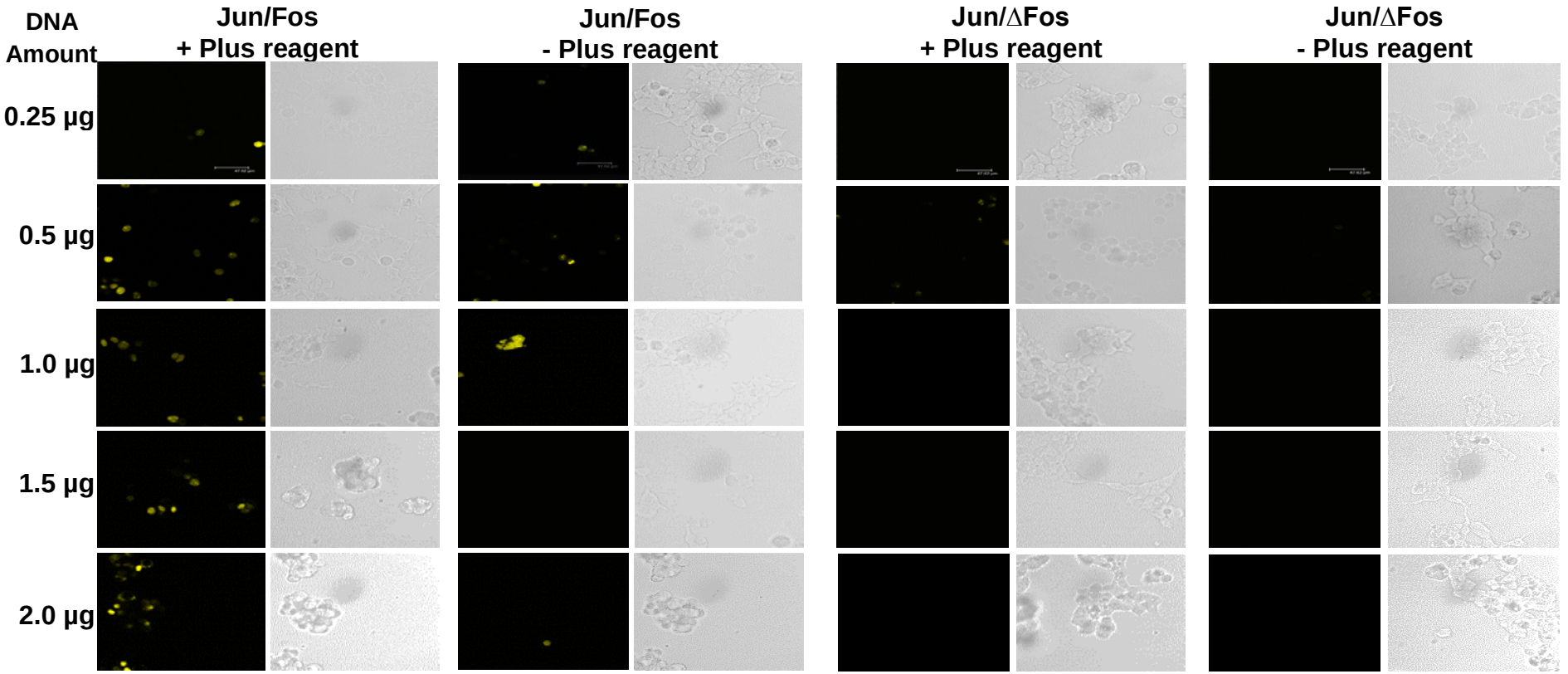

Figure 14. BiFC and bright field images of HEK293T cells transfected with either bFos-VC/bJun-VN or bFosΔZIP-VC/bJun-VN fusion pairs at various concentrations. HEK293T cells were transfected with fusion pairs at different concentration with and without Plus reagent to determine the optimum concentration for further experiments. Confocal analysis was performed 24 hours post-transfection.

3.2.4 Determining the optimal time-scale for expression of bFos-VC/bJun-VN and bFosΔZIP-VC/bJun-VN fusion pairs in HEK293T cells

In BiFC transient expression experiments fluorescence from specific interactions can generally be detected between 12 and 30 hours after transfection (Kerppola, 2006). A BiFC assay is not a “real-time” kinetic measurement of protein-protein association and the fluorescence signal increases with incubation time (Rose *et al*, 2010). However, caution must be taken as the fluorescence signal accumulates in time due to the irreversible nature of YFP complementation and the saturation of fluorescence signal influences the signal-to-noise ratio (Horstman *et al*, 2014). Therefore, it is essential to determine the optimal time-scale for expression of the BiFC fusion proteins.

The initial BiFC assay validation experiments were analysed 24 hours post transfection. It was therefore decided to compare BiFC confocal analyses at 24 and 48 hours. Longer time points (e.g. 72 hours) resulted in over-confluent detached cells. All the other image acquisition parameters, such as laser power, pinhole and detection gain, were held constant within an experiment. The BiFC signal in cells transfected with bFos-VC/bJun-VN fusion pair was higher at 24 hours post-transfection when compared with 48 hours (Figure 15, A). After 48 hours post-transfection there were fewer cells exhibiting the fluorescence signal and the signal was more saturated (Figure 15, B). A 48-hour incubation period also resulted in some weak background fluorescence signal in the YFP channel due to nonspecific interactions in cells transfected with bFosΔZIP-VC/bJun-VN fusion pair (Figure 15, B). This could be explained by the irreversible complex formation between two non-fluorescent YFP fragments and the prolonged post-transfection incubation may result in the accumulation of the fluorescence signal, leading to false-positive results and making the data interpretation difficult.

Based on these results further BiFC experiments with bJun, bFos and bFosΔZIP fusion proteins as well as with all the membrane proteins of interest were analysed at 24 hours after transfection.

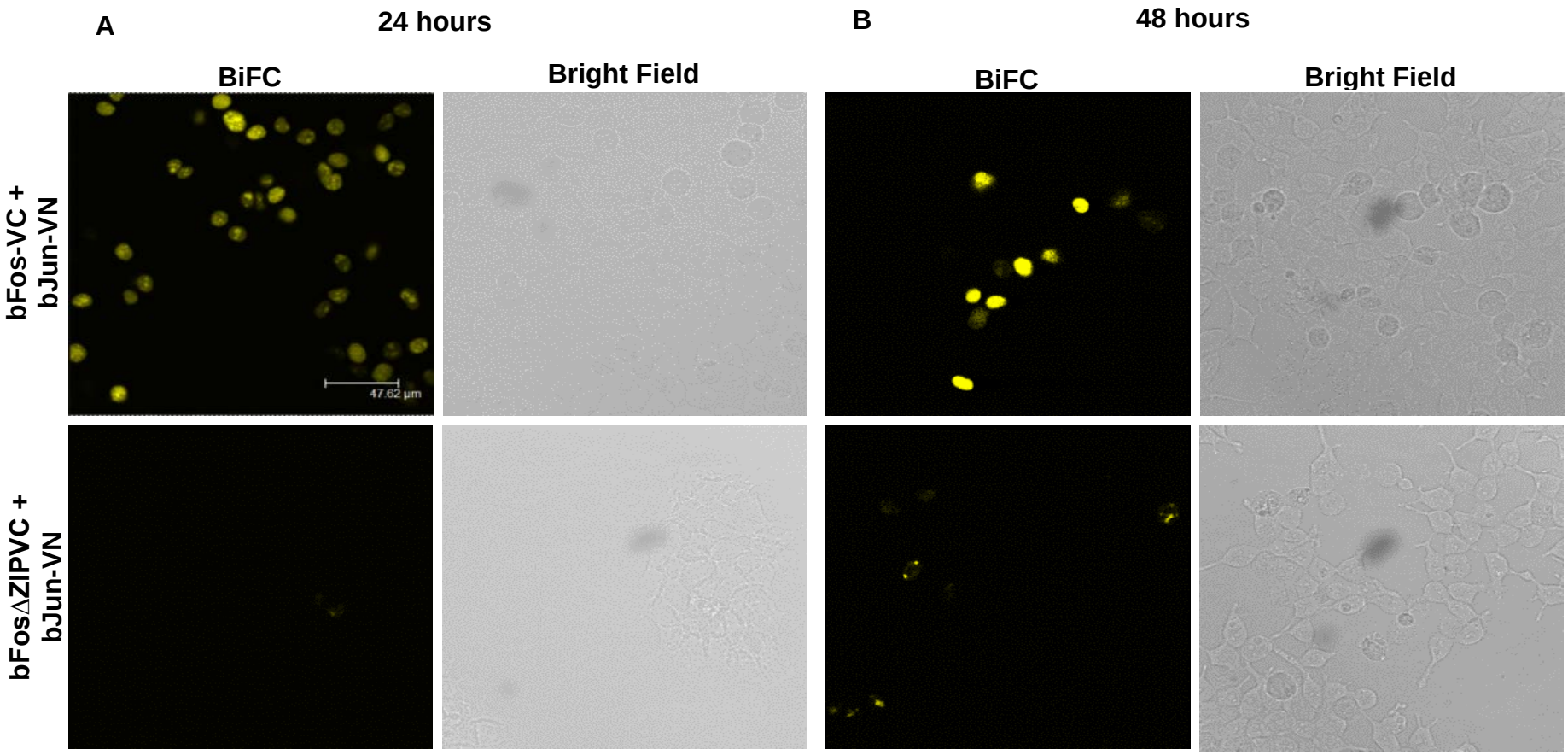

Figure 15. Visualisation of fluorescent signal after 24 and 48 hours post-transfection. HEK293T cells were transfected with bFos-VC/bJun-VN and bFosΔZIP-VC/bJun-VN fusion pairs and analysed using confocal microscope after 24 and 48 hours post-transfection.

3.2.5 Qualitative analysis and sub-cellular localisation of BiFC signal

The well-characterised interaction between bFos and bJun was used in this thesis to validate the BiFC assay before applying it to membrane protein-protein interaction studies. Mammalian expression plasmids encoding bFos-VC and bJun-VN fused to C- and N-terminal fragments of a Venus yellow fluorescent protein respectively were transfected into HEK293T cells using 0.5 µg of each plasmid. The BiFC signal was assessed by confocal microscopy 24 hours after transfection. As can be seen in Figure 16, bFos-VC and bJun-VN do indeed interact together resulting in yellow fluorescence signal. The transfected cells have been stained with CellMask™ DeepRed Plasma membrane stain prior to the visualisation to examine the localisation of bFos-VC/bJun-VN interaction. In agreement with the previous results by Hu and Kerppola (2002) fluorescence complementation by bFos-VC and bJun-VN exhibited distinct nuclear distribution. Expression of either bFos-VC or bJun-VN alone did not produce detectable fluorescence (Figure 17).

To confirm that the interaction between bFos-VC and bJun-VN is specific and is not driven by the interaction force of the two non-fluorescent fragments of a Venus yellow fluorescent protein the negative protein-protein interaction pair was included in BiFC experiments. A deletion in the leucine zipper of Fos protein has been shown to prevent Fos/Jun dimerisation *in vitro* (Gentz *et al*, 1989). Therefore, co-expression bFos∆ZIP-VC with bJun-VN in cells should not result in any yellow fluorescence signal. HEK293T cells were co-transfected with equal amounts of each expression plasmid encoding bFos∆ZIP-VC, containing mutation of the leucine zipper, and bJun-VN. The BiFC efficiency was assessed by confocal microscopy 24 hours after transfection. All the transfection and confocal analysis parameters were kept the same as in previous experiments.

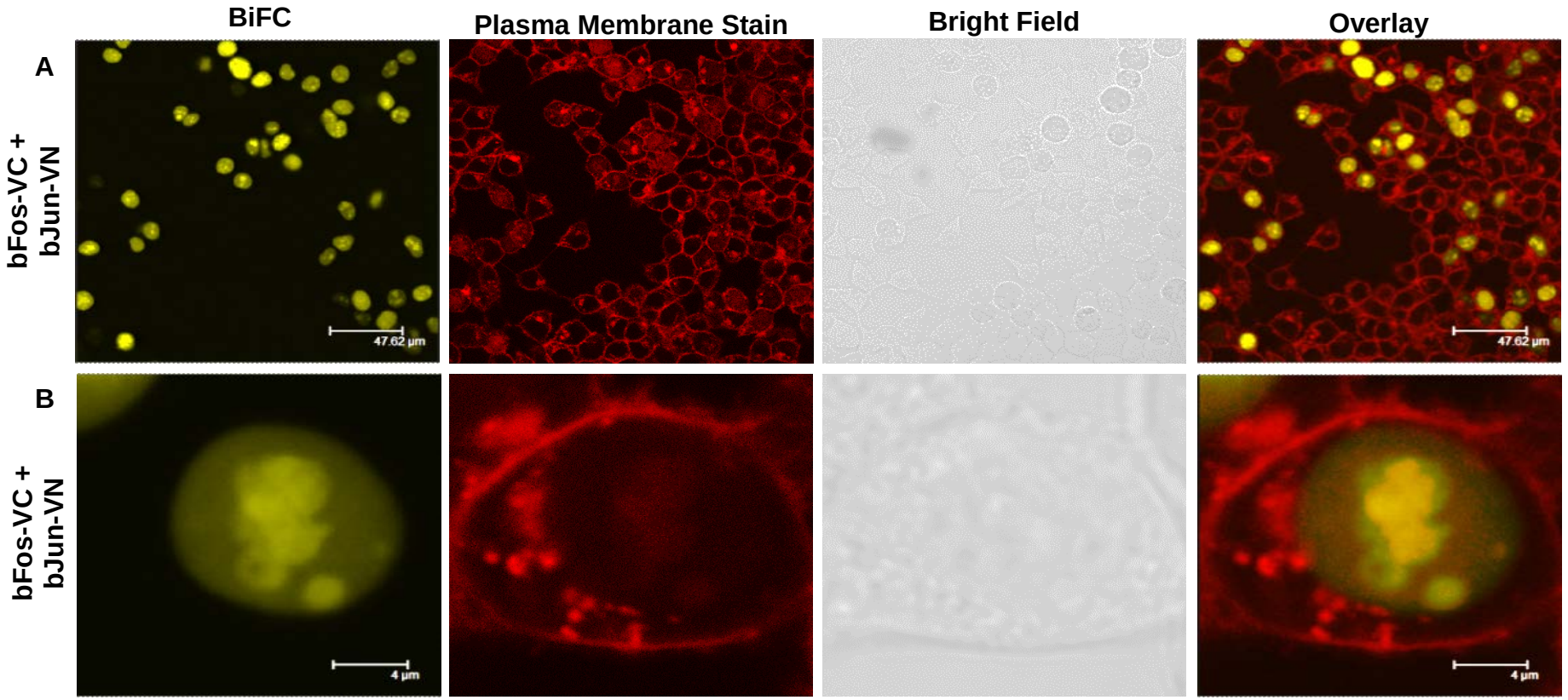

Figure 16. Visualisation of bFos-VC/bJun-VN protein interactions in living cells using BiFC analysis. Visualisation by confocal microscopy of interactions between bFos-VC and bJun-VN fusion pairs in live cells 24 hours after transfection. Confocal imaging of transiently transfected HEK293T cells obtained with a 63x objective of the Leica TCS SP2 confocal microscope shows plasma membrane (in red) stained with CellMask Deep Red plasma membrane stain and the localisation of protein – protein interaction (yellow fluorescent colour). (A) Confocal images of bFos-VC/bJun-VN interactions in cell populations. (B) Confocal images of a single cell, showing the localisation of bFos-VC/bJun-VN interactions.

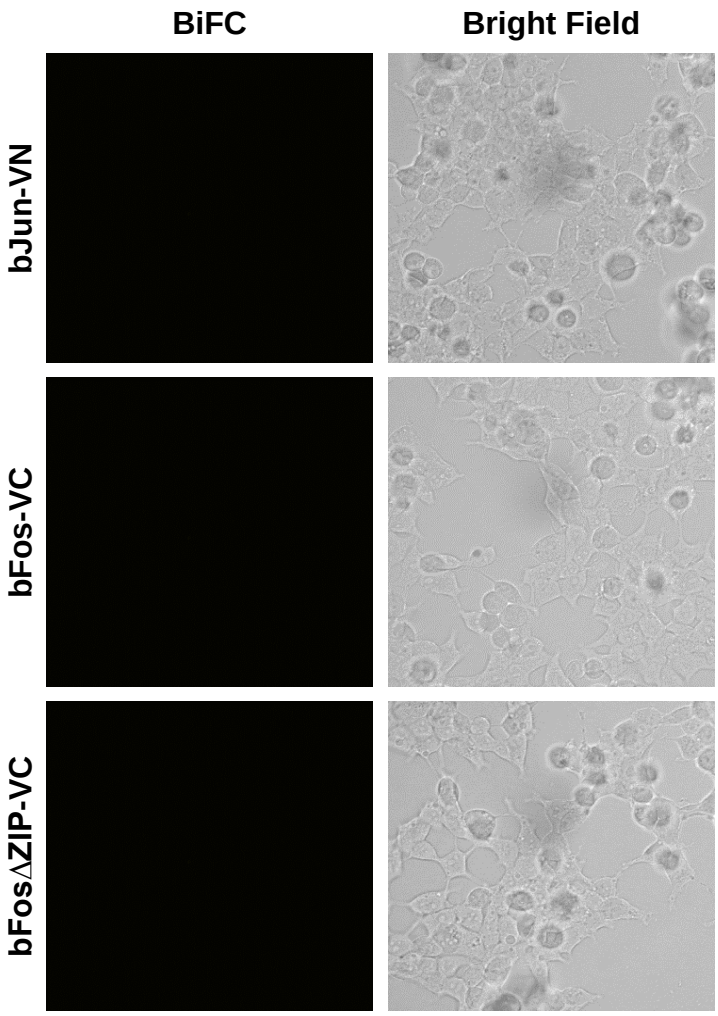

Figure 17. Confocal analysis of single transfected HEK293T cells. Confocal images of HEK293T cells expressing the proteins indicated in each panel were acquired 24 hours after transfection. None of the above proteins expressed alone exhibited fluorescence signal.

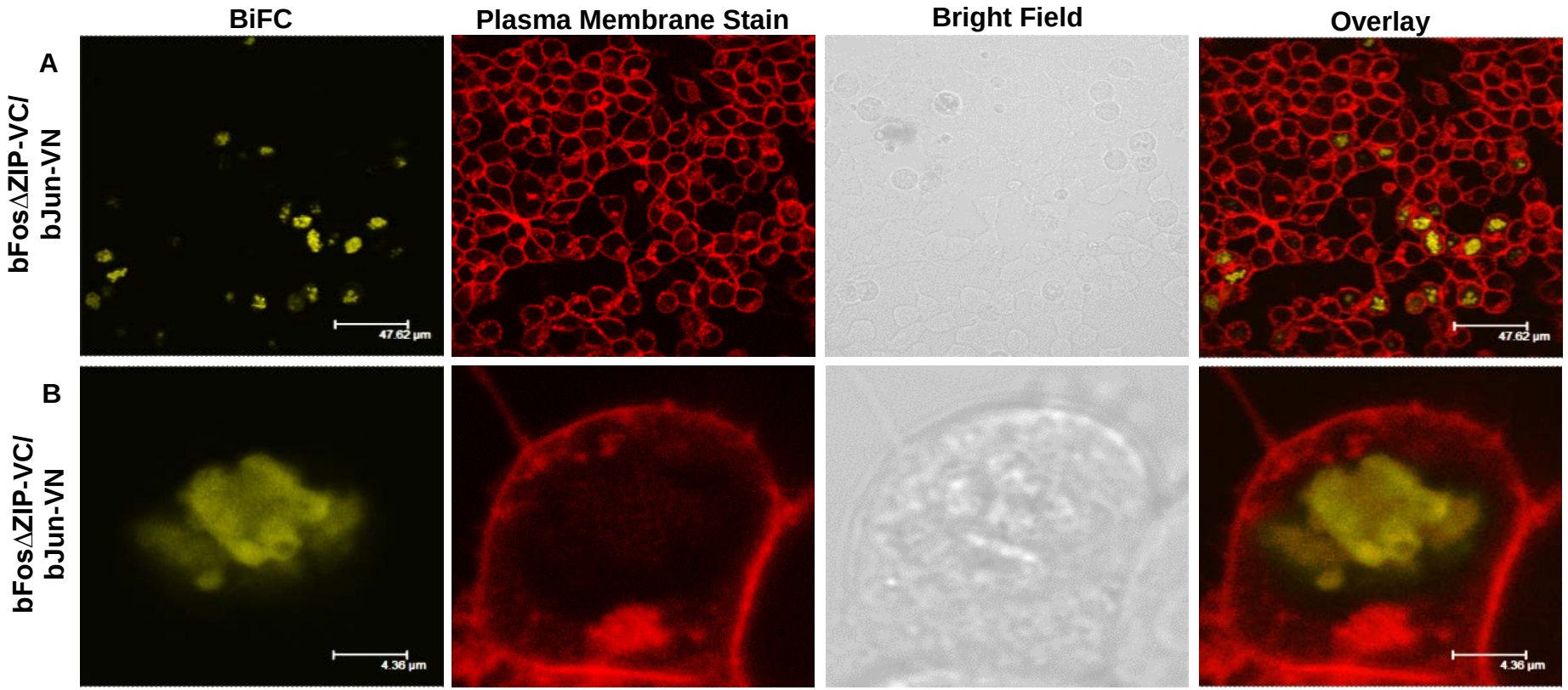

Figure 18. Visualisation of bFosΔZIP-VC and bJun-VN interactions in living cells using BiFC analysis. Visualisation by confocal microscopy of interactions between bFosΔZIP-VC and bJun-VN fusion pairs in live cells 24 hours after transfection. Confocal imaging of transiently transfected HEK293T cells obtained with a 63x objective of the Leica TCS SP2 confocal microscope shows plasma membrane (in red) stained with CellMask Deep Red plasma membrane stain and the localisation of protein – protein interaction (yellow fluorescent colour). (A) Confocal images of bFosΔZIP-VC/bJun-VN interactions in cell populations. (B) Confocal images of a single cell, showing the localisation of bFosΔZIP-VC/bJun-VN interactions

The mutation in the interacting region of bFos caused a significant reduction in the efficiency of fluorescence complementation. However, the negative bFosΔZIP-VC and bJun-VN interaction pair did not eliminate entirely the yellow fluorescence signal, which was also enriched in the nucleus (Figure 18). It has been shown previously that fluorescence complementation between bFos-VC and bJun-VN in cells required an intact leucine zipper dimerisation interface and that without this region the fluorescence signal was entirely eliminated (Hu *et al*, 2002). The results in Figure 18 contradict the previous finding, leading to the conclusion that perhaps the fluorescence complementation is formed as a result of YFP interactions, producing false-positive results. The fluorescence signal could also be caused by high expression levels of proteins that lead to an increase in fluorophore concentrations. However, images in Figure 18 are only representatives of all the BiFC experiments that have been repeated at least three times and not all images show fluorescence complementation for bFosΔZIP-VC and bJun-VN interactions. Therefore, qualitative judgment is not sufficient to draw any concrete conclusions and quantitative analyses were performed (refer to section 3.2.6).

3.2.6 Quantitative and statistical analysis

In order to confirm that the results of BiFC experiments using bFos-VC, bJun-VN and bFosΔZIP-VC fusion proteins represent specific protein-protein interactions and are not driven by the self-assembly of the two non-fluorescent YFP fragments the ImageJ software was used to analyse and quantitate the BiFC signal.

After being transfected and stained with plasma membrane stain HEK293T cells were used for confocal analysis. For BiFC quantification multiple images were taken in a random distribution from each well. The confocal images were then used for quantitative analysis using ImageJ. In each image field the staining of the plasma membrane allowed the outlining of all individual cells and the border of each cell was selected on a cell-by-cell basis. The fluorescent intensity derived from bimolecular fluorescence

complementation (e.g. YFP-VN+YFP-VC) and the red fluorescence signal derived from the plasma membrane stain were measured in individual cells and expressed as yellow/red ratio. On average about 700 cells from at least three independent experiments for each fusion protein combination were analysed. The distributions of ratios in individual cells were then plotted in histogram (Figure 19). In addition the average yellow fluorescence intensity in each cell was determined by measuring the average pixel intensity of the selected region, including border. The background signal in an area with no cells was subtracted from all values. BiFC fluorescence intensity values from at least three independent experiments were averaged and used for statistical analysis (Figure 20).

The efficiency of fluorescence complementation is determined from the fluorescence intensity. Two non-fluorescent YFP fragments are able to form fluorescent complexes at higher efficiency and at higher rate when fused to two interacting proteins. Spontaneous complementation, however, is possible but significantly reduced when the fragments are fused to proteins that do not interact with each other. Figure 19 shows the distribution of YFP fluorescence to red fluorescence signal from the plasma stain ratios, representing a measure of the efficiency of bimolecular fluorescence complementation. The interaction between bFos-VC and bJun-VN produced an increase in the efficiency of association between the fluorescent YFP fragments. HEK293T cells co-expressing bFos-VC and bJun-VN exhibit higher cell numbers that fall into a greater ratio value range compared with the cells co-expressing bFosΔZIP-VC and bJun-VN negative interacting pair. Therefore it can be concluded that bFos-VC/bJun-VN complementation complex results in a stronger YFP fluorescence signal and is more prevalent compared with negative interacting pair.

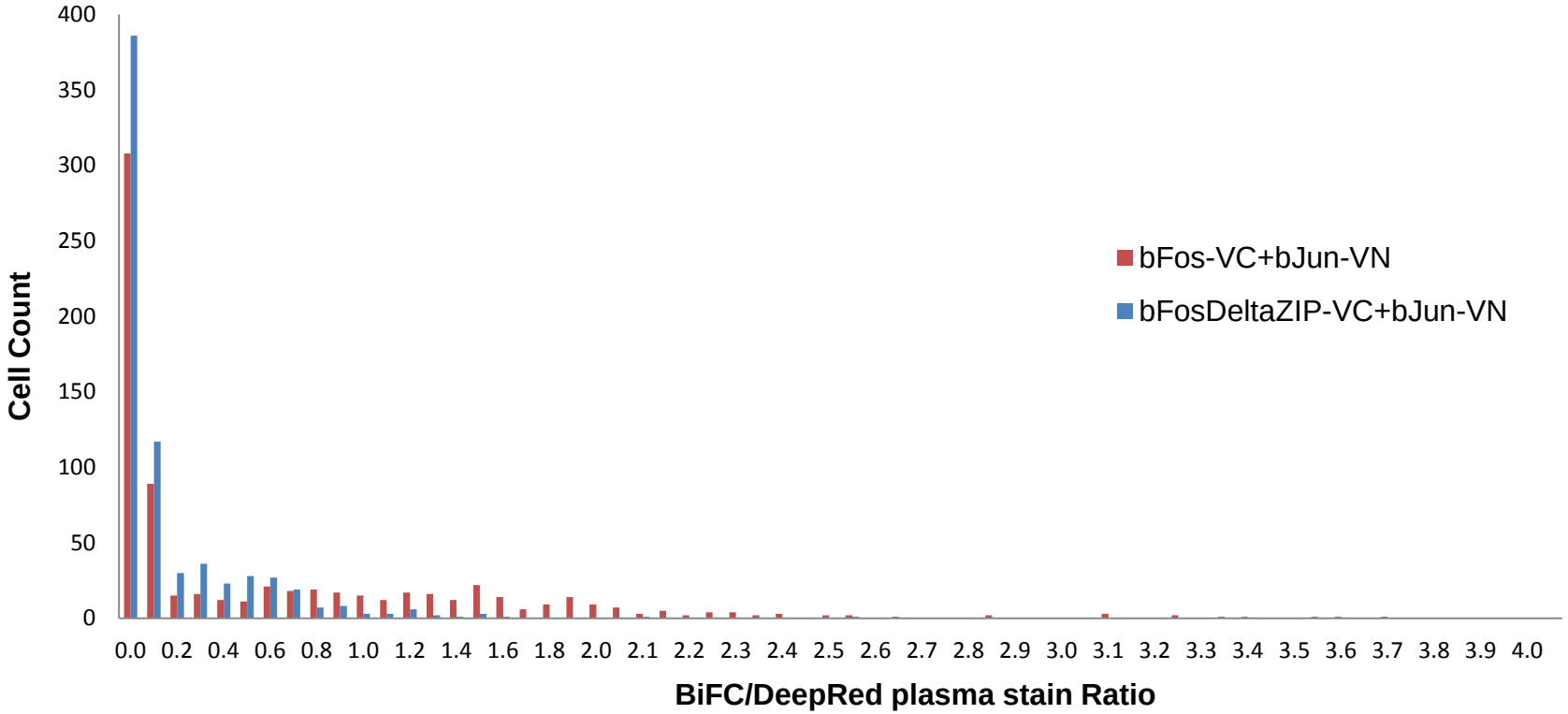

Figure 19. The distribution of BiFC/DeepRed plasma stain ratios. Plasmids encoding bJun-VN and either bFos-VC or mutated bFosΔZIP-VC (0.5 μg each) were transfected into HEK293T cells. Cells were stained with CellMask Deep Red plasma membrane stain 24 hours post-transfection. The fluorescence intensity produced by bimolecular fluorescence complementation (YN-YC) and the red fluorescence signal derived from the plasma membrane stain were measured in individual cells. The emission intensities were corrected for background fluorescence in an area of the field lacking cells. The distribution of ratios between the fluorescence intensity and red fluorescence signal in individual cells from three independent experiments was plotted in histogram.

In addition, the graph in Figure 20 also confirms that bFos-VC/bJun-VN interacting pair resulted in significantly greater fluorescence intensity than the bFos∆ZIP-VC/bJun-VN negative interacting pair. The average fluorescence intensity for bFos-VC/bJun-VN interacting pair was 6.3 x greater than for bFos∆ZIP-VC/bJun-VN negative interacting pair. Although co-expression of the negative bFos∆ZIP-VC/bJun-VN pair also produced readily detectable fluorescence the average fluorescence intensity was significantly reduced compared with positive bFos-VC/bJun-VN pair ($P<0.01$; Figure 20).

False positive fluorescence resulting from self-assembly of the non-fluorescent YFP fragments is defined by low (or reduced) signal-to-noise ratio (S/N). The S/N ratio can be used as a measure of BiFC specificity. To determine the specificity of the BiFC assay the S/N ratio was estimated using the following formula:

$$S/N = \frac{\text{Median Y/R ratio value from positive interacting pair}}{\text{Median Y/R ratio value from negative interacting pair}}$$

The bFos-VC/bJun-VN fusion pair was used as positive fusion pair and the bFos∆ZIP-VC/bJun-VN as negative fusion pair. The S/N value for the BiFC assay with bFos-VC/bJun-VN was 7.7. This result agrees with previous results obtained by Kodama and Hu (2010) in BiFC optimisation studies, showing that the S/N ratios of Venus-based BiFC assays were in a range of 3–7.

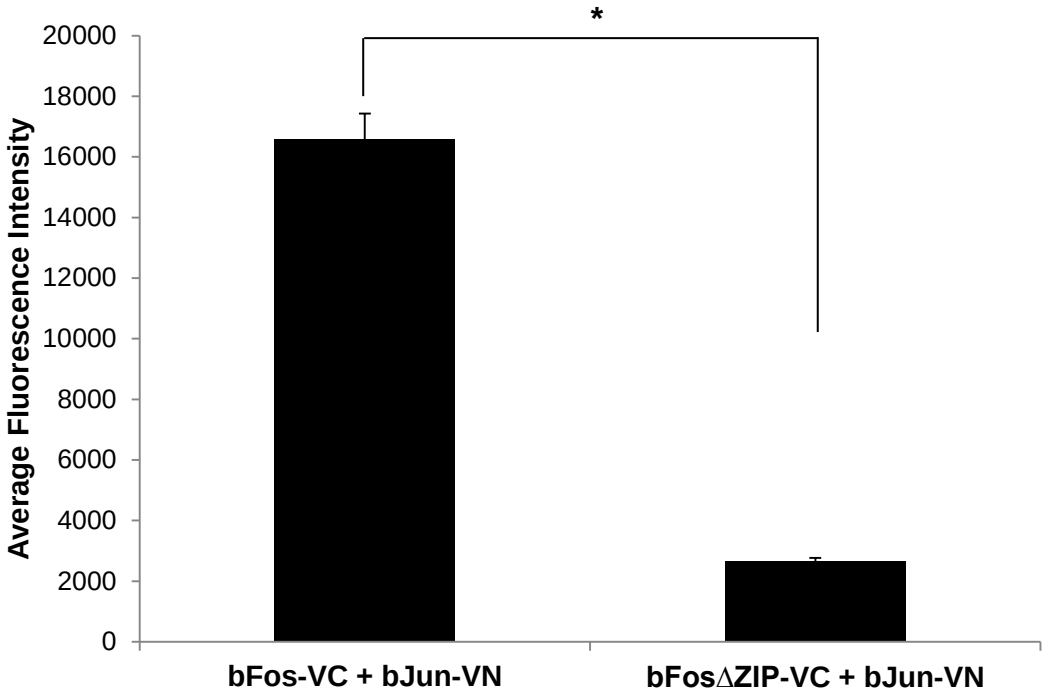

Figure 20. Validation of BiFC specificity. Quantification of fluorescence intensities that was determined with the ImageJ software using confocal images of bFos-VC/bJun-VN and bFosΔZIP-vc/bJun-VN interaction pairs in transiently transfected HEK293T cells. The mean and standard errors of three independent measurements are shown. *p<0.001 by the Mann-Whitney U test was considered significant.

3.3 Discussion

To validate and optimise the BiFC assay two interacting proteins bFos and bJun were used as the positive interacting pair and bFosΔZIP and bJun as the negative interacting pair. The interaction between bFos and bJun is well documented and these proteins have been previously used in studies developing BiFC assays (Bos *et al,* 1989; Neuberg *et al,* 1989; Kerppola, 2008; Hu *et al,* 2002). In this thesis fragments of a Venus YFP truncated at residue 155 (VN155 and VC155) were used as they exhibit a relatively high complementation efficiency when fused to interacting partners but produce low fluorescence when fused to non-interacting proteins. bJun was fused to the N-terminal part of YFP (bJun-VN) and bFos and bFosΔZIP were fused to the C-terminal part of YFP (bFos-VC and bFosΔZIP-VC) and were used first to select a cell line for BiFC experiments. In order to establish the cell line that results in a higher expression level both HEK293 and HEK293T cell lines were transiently co-transfected with bFos-VC/bJun-VN and bFosΔZIP-VC/bJun-VN fusion pairs. These cell lines were chosen for the ease of expression of mammalian proteins, cells' high transfection efficiency and ease of maintenance. The BiFC assay has been used for the analysis of protein interactions in many mammalian cells including HEK293, in which co-expression of fusion proteins exhibited similar patterns of fluorescence compared with COS-7 and NIH 3T3 cells (Fang and Kerppola, 2004). The results showed that HEK293T cells, when co-expressing bFos-VC/bJun-VN fusion pair, exhibited not only higher intensity of the fluorescent signal but also a higher number of cells producing the signal compared with HEK293 cells. This suggests that HEK293T cells exhibit higher protein expression levels, probably due to the presence of the SV40 large T antigen that can bind to SV40 enhancer of expression vectors and thus considerably increase the expression levels obtained with transient transfection. Based on these qualitative results the HEK293T cell line was chosen for further experiments with bFos and bJun as well as with transmembrane proteins discussed in following chapters.

To determine the optimal time-scale for expression of fusion proteins and BiFC complex formation the cells were analysed 24 and 48 hours post-transfection. A longer incubation period (i.e. 72 hours) was also considered but resulted in the majority of cells being detached and, thus, was not included in experimental results. In transient expression experiments fluorescence from specific interactions can generally be detected between 12 and 30 hours after transfection (Kerppola, 2006). The confocal analysis of the transfected HEK293T cells showed that the 24-hour incubation period resulted in an increased fluorescence signal. Fewer cells exhibited fluorescence signal after the 48-hour incubation period and the signal was more saturated. In addition the 48-hour incubation resulted in weak background fluorescence signal in cells co-expressing bFosΔZIP-VC/bJun-VN negative interacting pair. This could be explained by the fact that the fluorescence complex formation is irreversible and longer incubation may result in accumulation of the signal from non-specific interactions driven by the YFP fragments. Longer incubation could result in higher expression of fusion proteins that could also contribute to complementation due to non-specific interactions. Therefore, longer incubations should be avoided and, based on the qualitative analysis obtained from these experiments, it was decided that the 24-hour incubation is preferable for future experiments. For the same reason it is advisable to keep the amount of DNA used for transfection low. Although previous studies reported that BiFC generally has very low background, very high expression of fusion proteins can result in BiFC between proteins that do not interact *in vivo* (Kerppola, 2006; Kerppola, 2008). Over-expression of the fusion proteins may lead to the association of the tethered fluorescent protein fragments because of high local concentrations of the fusion proteins (Kodama and Hu, 2010). A paper on design and implementation of the BiFC assay by Kerppola (2008) recommended starting with 0.25 µg of DNA for transient transfections. However, in various papers on protein-protein interaction studies using BiFC a range of DNA amounts was used, ranging from 0.25 µg to 5.0 µg of each plasmid. To optimise the amount of DNA for transfections HEK293T cells were co-transfected with either bFos-VC/bJun-VN or bFosΔZIP-VC/bJun-VN fusion pairs, using a range of DNA amounts from 0.25 to 2.0 µg of each

plasmid. The cells transfected with bFos-VC/bJun-VN, using 0.25 µg of each plasmid, exhibited low expression efficiency and fluorescence signal. Higher amounts of DNA used for transfections produced an increase in expression efficiency and fluorescence signal compared with 0.25 µg of DNA. However, at higher amounts of DNA ranging from 0.5 to 2.0 µg, the expression efficiency and fluorescence intensity were comparable. The cells transfected with bFos-VC/bJun-VN at all the tested concentrations exhibited some background fluorescence signal. Since qualitative analysis showed no significant benefit of using higher amounts of DNA, 0.5 µg of each plasmid was used in all future experiments. This amount of DNA provided a good fluorescence signal and would save on using increased amount of transfection reagents.

To validate the BiFC assay two proteins, bFos and bJun that are known to interact together, were chosen. The qualitative analysis of HEK293T cells co-transfected with bFos and bJun, fused to C- and N-terminal fragments of a Venus yellow fluorescent protein respectively, exhibited a readily detectable fluorescence signal. The localisation of the fluorescence signal resulting from the bFos-VC/bJun-VN fusion pair interaction was predominantly in nuclei and some in cytoplasm. These results correspond to the previous studies by Bos *et al* (1989) and Neuberg *et al* (1989) that identified the location of bJun and bFos in the nucleus. Some of the complementation complex formation could probably occur during translocation of the proteins from the site of their synthesis in the cytoplasm to the nucleus. This could explain some of the fluorescence present in the cytoplasm. It has been previously reported that bFos is efficiently translocated to the nucleus when bound to bJun through their leucine zippers, and mainly by the use of the nuclear localisation signal of bJun (Chida *et al,* 1999). The negative bFosΔZIP-VC/bJun-VN interacting pair also produced a fluorescence signal when co-expressed in live cells but the signal and the BiFC efficiency were significantly reduced.

The results of these experiments correspond to the previous findings from studies on design and optimisation of a Venus-based BiFC assay with bFos and bJun. Co-expression of bFos and bJun fused to C- and N-terminal fragments of a Venus yellow fluorescent protein in live cells exhibited readily

detectable fluorescence signal with good BiFC efficiency. Confocal analysis on the localisation of the bFos-VC/bJun-VN fusion pair interaction revealed that fluorescence signal was detected merely in nuclei, which corresponds to the results of Immunofluorescence studies showing that these proteins are localised in the nucleus (Bos *et al*, 1989; Neuberg *et al*, 1989). And although the negative bFosΔZIP-VC/vJun-VN interaction pair also produced fluorescence signal when co-expressed in live cells, the signal and the BiFC efficiency appeared to be reduced.

Spontaneous assembly of VC and VN fragments provides a source of false positive results, which makes qualitative data interpretation difficult. As already mentioned above, cells experiencing physiological distress, or cells assayed at late time points when fusion proteins are in high concentration, can accumulate high levels of mislocalised fluorescent signal (Kerppola, 2008). Figures 16 and 18 show that it is not possible to rely on qualitative judgement to assess protein-protein interactions. Therefore, to reach valid conclusions on interactions, it is important to carry out quantitative and statistical analysis, comparing the intensities and numbers of fluorescent cells observed when the cells are transfected with the positive interaction pair with those observed when the cells are transfected with the negative interaction pair.

In this study the quantitative analyses were carried out as described in Chapter 2, section 2.5.9. The distribution of the BiFC/Red plasma stain ratios in Figure 19 show that more cells co-expressing bFos-VC/bJun/VN fall into a higher range of ratio values than cells co-expressing bFosΔZIP-VC/bJun-VN. When the two proteins interact the fluorescence intensity of VC and VN YFP fragments will increase, resulting in a higher fluorescence ratio, as was observed with bFos-VC/bJun-VN interaction pair. This could be explained by the fact that when proteins do not interact, most cells will have a very low fluorescence ratio, as was observed with bFosΔZip-VC/bJun-VN. In a previous study on design and complementation of BiFC assay by Kerppola (2008) the efficiency of BiFC was defined by the ratio of YN-YC (N and C terminal fragments of YFP) to Cerulean (CFP; used as the internal control) fluorescence. Although in this study the plasma membrane was stained with

fluorescent dye instead of using an internal control, the results were comparable to previous findings. In addition, to confirm BiFC specificity the signal-to noise (S/N) ratio was measured as described in a study by Kodama and Hu (2010). The self-assembly of the YFP fragments can contribute to false-positive fluorescence and decrease the S/N ratio in the BiFC assay. It has been previously reported that introduction of I152L mutation in VN155 YFP fragment dramatically reduces the self-assembly between the Venus N- and C- terminal fragments, resulting in a high S/N ratio in living cells (Kodama and Hu, 2010). The same Venus YFP fragments, containing I152L mutation in VN155, were used in this study and the S/N ratio value obtained from bFos-VC/bJun-VN interaction was 7.7. This value closely correlates to the S/N ratio value of 7 in the previous study by Kodama and Hu (2010), supporting the conclusion that the assay set-up and quantification procedure as used in this chapter are optimised and valid.

Furthermore the average yellow fluorescence signal intensities were determined for positive and negative fusion pairs from confocal images, using ImageJ as described in Chapter 2, section 2.5.9. The results obtained not only complemented the results described above but provided a robust data interpretation. There was significant 6.3 fold decrease in the yellow fluorescence signal when cells were co-expressing bFosΔZip-VC/bJun-VN fusion pair compared with positive interacting pair bFos-VC/bJun-VN. The overall quantitative assessment of the fluorescence images obtained on co-expression of either bFos-VC/bJun-VN or bFosΔZip-VC/bJun-VN constructs indicated a BiFC signal that is due to a specific interaction, rather than self-assembly of constructs and background fluorescence.

In this chapter a procedure for quantitative analysis of BiFC data was developed and validated, which could be further applied to studies of membrane proteins. This will be particularly important since the membrane protein-protein interaction studies would be more prone to self-assembly and false-positive results as the membrane proteins are “fixed” in the plane of the membrane rather than being free in cytoplasm. While it is recognised that there will be differences in expression of the membrane proteins the experiments with bFos and bJun proteins provided a good starting point,

showing that the BiFC assay is an efficient approach for visualisation of protein-protein interactions with a high specificity in live cells but further optimisation may be required with membrane proteins.

Chapter 4

Validation and characterisation of the interaction between VE-PTP and VE-cadherin in live cells

4.1 Introduction

The functions of the extracellular domain for many RPTPs are not yet well characterised. The structure of the extracellular domain of VE-PTP suggests a role as an adhesion receptor (Barford *et al*, 1995). In fact, co-immunoprecipitation studies by Nawroth and colleagues (2002) showed that VE-PTP interacts with the most prominent adhesion molecule of endothelial adherens junctions VE-cadherin. Interestingly the same research group demonstrated that VE-PTP and VE-cadherin interact together via their extracellular domains, independently of their cytoplasmic tails (Nawroth *et al*, 2002). Furthermore it has been demonstrated that the single 17th Fibronectin III-like (FNIII) domain of VE-PTP and fifth cadherin domain of VE-cadherin were sufficient for their association (Nawroth *et al*, 2002). It was proposed to be a *cis* interaction because of the membrane-proximal position of both interacting domains, making VE-PTP the first described candidate for a transmembrane protein that interacts *in cis* with a cadherin via an extracellular domain (Nawroth *et al*, 2002).

Interestingly the 17th FNIII-like domain of VE-PTP is not homologous to the other 16 repeated domains. It is not only larger than the rest of the extracellular domains, consisting of 179 amino acids as supposed to 90 amino acids for each of the 16 repeated domains, but it also contains a stretch of six prolines, which is similar to the hinge regions in immunoglobulin heavy chains. This characteristic perhaps provides the steric conformation, causing a kink in the peptide chain of the extracellular domain (Krueger *et al*, 1990).

Data from a study by Nawroth *et al* (2002) suggest the 17th membrane-proximal FNIII-like repeat is the only domain required for the interaction with VE-cadherin. However, whether other regions of the VE-PTP extracellular domain are involved remains unknown. Therefore, the purpose of this chapter was first to validate the interaction between VE-PTP and VE-cadherin via their extracellular domains in living cells using bimolecular fluorescence complementation (BiFC) assay in transiently transfected

HEK293T cells and then to investigate whether the deletion of the 17th FNIII-like domain in VE-PTP would abolish any association.

The constructs used in this study VEPTP-VN and VE-cadherin-VC, shown diagrammatically in Figure 21, consist of residues 1-1647 of VE-PTP and 1-625 of VE-cadherin, with either the modified N- or C-terminal sequence of vYFP inserted five residues after the transmembrane domain and a flexible linker sequence, as used by Kodama & Hu (2010). This approach essentially replaced the intracellular region of these proteins with non-fluorescent fragments of vYFP enabling investigation of protein-protein interactions that involve only the extracellular and transmembrane domains.

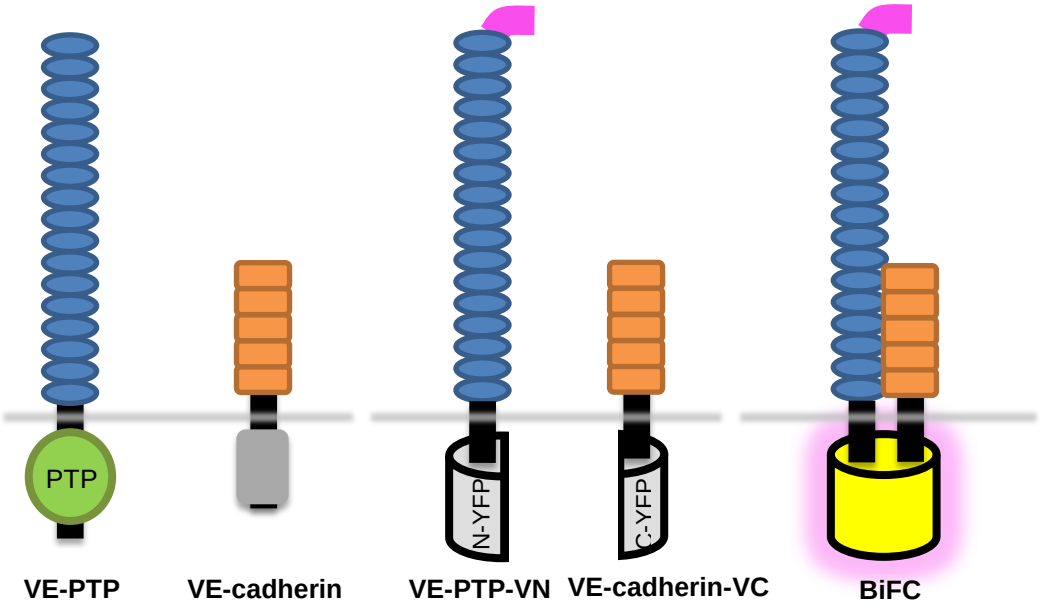

Figure 21. Schematic representation of the VE-PTP and VE-cadherin constructs used for BiFC. VE-PTP consists of multiple extracellular fibronectin III-like repeats (blue), a transmembrane domain and an intracellular protein tyrosine phosphatase domain (PTP). VE-cadherin consists of 5 extracellular cadherin domains (orange), a transmembrane sequence and an intracellular cadherin cytoplasmic region (grey). The constructs VE-PTP-VN, VE-PTP-VC and VE-cadherin-VC have a modified N- or C-terminal sequence of the Venus protein (a yellow fluorescent protein (YFP) variant; represented by a half cylinder) inserted five residues after the transmembrane domain. A myc tag (pink) has been inserted after the signal peptide of VE-PTP to facilitate analysis of expression. When brought into close proximity by a pair of interacting proteins, the fragments assemble to yield a fluorescent protein (BiFC signal).

4.1.1 Controls to determine the complementation specificity

The BiFC assay is a useful technique for the direct visualisation of protein-protein interactions in living cells. This approach allows one to study the sub-cellular localisation of interactions with minimal perturbation of their normal environment. However, because the non-fluorescent fragments of the fluorescent protein are prone to self-assembly independent of a protein-protein interaction event, leading to false positive results, it is crucial to include appropriate negative controls. In Chapter 3 (section 3.1) appropriate negative controls were discussed. Here two negative control fusion proteins were generated to determine the specificity and efficiency of BiFC. The first negative control was based on the transmembrane glycoprotein sialophorin (SPN; also known as leukosialin, CD43) and the other was a plasma membrane anchored fusion protein.

SPN control was fused to either the C- or N-terminal part of the YFP (SPN-VN or SPN-VC respectively). The SPN was chosen as a negative control since it shares no homology with any of the RPTPs of the R3 subgroup but it has an equally large extracellular domain that is highly glycosylated (Cordoba *et al*, 2013). It has been previously used as a control in studies with another R3 RPTP member DEP-1 (density enriched protein tyrosine phosphatase 1) to investigate the role of the DEP-1 extracellular domain in T cell receptor signalling (Cordoba, 2013). However, in the previous study the extracellular domain of the DEP-1 was substituted with the extracellular domain of the SPN. Therefore, there are no known possible interactions of SPN with any of the R3 RPTPs reported up to date. SPN fusion protein controls consisted of extracellular and transmembrane domains, either fused to the N-terminal part of a Venus YFP with a myc tag or the C-terminal part of Venus YFP with a HA tag (Figure 22).

The second negative control consisted of either the C- or N-terminal fragment of a Venus YFP anchored to the plasma membrane via the membrane association sequence from Lck (lymphocyte-specific protein tyrosine kinase), Myr-VC and Myr-VN respectively (i.e. myristoylated C- and N-terminal YFP fragments). Negative controls Myr-VC and Myr-VN were

generated as a backup to eliminate any possible interactions between SPN and R3 RPTPs. These negative controls had all the possible interaction domains removed (i.e. they entirely lacked any extracellular and transmembrane domains) and in theory there should be no complementation complex formation when it is co-expressed with the fusion proteins of interest. The two fusion proteins Myr-VC and Myr-VN consisted only of C- and N-terminal YFP fragments respectively that were anchored to the plasma membrane via membrane association sequence from Lck protein kinase (Figure 22). An N-terminal dual acylation motif of Lck protein kinase is necessary for correct intracellular localisation to the plasma membrane. This sequence consists of MGCGCSSHPEDDW amino acids in which the cysteines (C) become post-translationally S-acylated and the glycine-2 (G), immediately after the initiator methionine, is myristoylated (Zlatkine *et al*, 1997). Therefore, fusing this sequence to each YFP fragment should be sufficient to encode the correct lipid modification and to target the YFP fragments to plasma membrane. This dual acylation motif has been used previously to target cytosolic proteins to the plasma membrane (Zlatkine *et al*, 1997). Consequently, if any fluorescence complementation is observed after co-expressing Myr-VC or Myr-VN with any of the R3 RPTPs in mammalian cells, it is most likely due to the self-assembly of the YFP fragments. Therefore, the use of this control enables us to evaluate the specificity (i.e. whether the fluorescence complementation represents specific protein-protein interactions) and efficiency (i.e. fluorescence intensity) of association in positive interaction pairs as explained in Chapter 3, section 3.2.6.

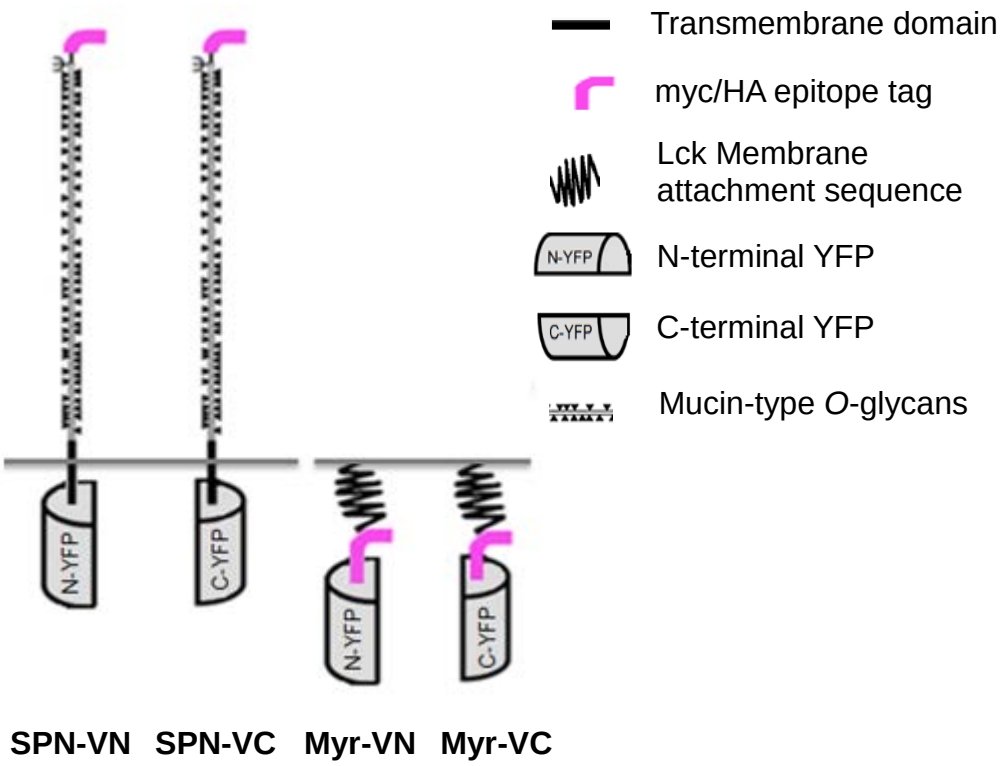

Figure 22. Schematic representation of BiFC negative controls. The full-length extracellular and transmembrane domains of SPN were fused to either C- or N-terminal parts of a Venus YFP. SPN fused to the C-terminal YFP was HA tagged, whereas SPN fused to the N-terminal YFP was myc tagged. Myr-VC and Myr-VN represented negative interaction constructs lacking any interaction domains and comprised C- and N-terminal YFP fragment respectively, followed by myc tag and the plasma membrane anchoring sequence of Lck protein kinase.

4.1.2 Investigating association of a VE-PTP∆17FN mutant with VE-cadherin

Previous *in vitro* findings of Nawroth and colleagues (2002) showed that neither the cytoplasmic nor transmembrane domains of VE-PTP are required for the interaction with VE-cadherin and that the 17th FNIII-like domain was sufficient for co-immunoprecipitation with VE-cadherin. In order to examine this finding in a BiFC live cell assay a fusion construct in which the 17th FNIII-like domain had been removed (VE-PTP∆17FN-VN) was generated (Figure 23). The objective was to investigate whether this domain is important in association with VE-cadherin in live cells. It was hypothesised that deleting the 17th FNIII-like domain of VE-PTP would be sufficient to abolish the VE-PTP interaction with VE-cadherin.

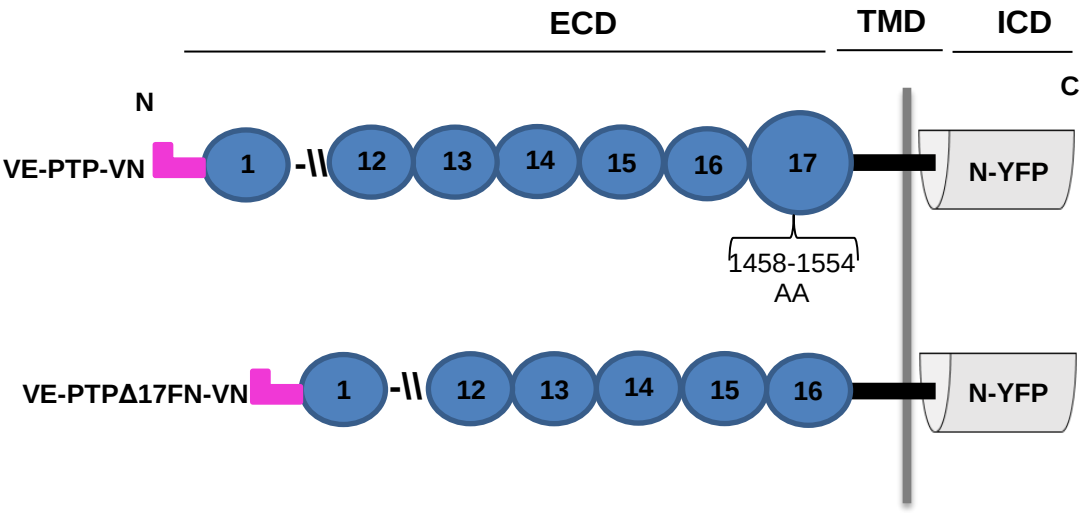

Figure 23. Schematic representation of VE-PTP mutant fusion construct. The VE-PTP-VN BiFC construct consisting of transmembrane and extracellular domains fused to the N-terminal part of the YFP was used to generate mutated VE-PTPΔ17FN-VN fusion construct in which the 17th FNIII-like domain was removed, moving the 16th FNIII-like domain proximal to the transmembrane domain. The start and the end of the 17th FNIII-like domain were based on the amino acid sequence acquired from the Uniprot Database.

4.2 Results

4.2.1 Cloning VE-PTP-VN and VE-cadherin-VC fusion proteins

VE-PTP-VC and VE-PTP-VN fusion constructs were generated as outlined in the schema in Chapter 2 (Figure 8). For the VE-PTP-VN a synthetically generated signal peptide and myc tag (EQKLISEEDL) fragment (Genscript) was inserted into *Apa*I/*Xho*I restriction sites of pBiFC-VN155(I152L) vector. The transmembrane and extracellular (TM+ECD) domains of VE-PTP construct were amplified by PCR using Platinum *Pfx* polymerase (Figure 24, A). The PCR product corresponded to the predicted size of 5.8 kb. The primers used for the generation of the VE-PTP transmembrane and extracellular domains are listed in Table 10 and the PCR conditions are provided in Table 4 (Chapter 2). The resulting PCR product was purified, digested and subsequently inserted into XhoI restriction site of the pBiFC-VN155(I152L) vector, which contained signal peptide and myc tag. Colony PCR was used to confirm the correct orientation of the insert to ensure that a fusion protein fused to the N-terminal part of YFP has been generated (Figure 25, A).

To generate the VE-PTP-VC fusion construct a synthetically generated signal peptide and HA tag fragment (Genscript) was inserted into *Apa*I/*Xho*I restriction sites of pBiFC-VC155 vector. The TM+ECD domains of VE-PTP were cut out from the previously generated VE-PTP-VN fusion construct with *Xho*I restriction enzyme, purified and ligated into the pBiFC-VC155 vector, containing signal peptide and HA tag, to create a fusion protein fused to the C-terminal part of YFP. Colony PCR was used to confirm the correct orientation of the insert (Figure 25, B).

The VE-cadherin-VC fusion construct was generated by using PCR to amplify signal peptide, transmembrane and extracellular domains of VE-cadherin. The PCR product corresponded to the predicted size of 1.9 kb for signal peptide, extracellular and transmembrane domains of VE-cadherin on an agarose gel (Figure 24, B). The resulting PCR product was ligated into *Apa*I/*Xho*I restriction sites of the corresponding pBiFC-VC155 vector and

transformed into XL1-Blue strain of *E.coli*. The presence of the correct DNA insert was determined by screening bacterial colonies by PCR using Bioline Red Taq with a combination of vector-specific and insert-specific primers (Table 11). PCR products were analysed by agarose gel (Figure 25, C) and the remaining portion of the colony containing vector with the correct insert was used to inoculate LB media with an appropriate antibiotic.

The plasmid DNA for each fusion construct was purified and sequenced to verify that the insert gene has been ligated at the correct position within the vector backbone without any mutations. The sequenced plasmids were used to prepare larger quantities of high-quality plasmid DNA for mammalian cell transfections in BiFC experiments using QIAprep Spin Midiprep Kit (QIAGEN).

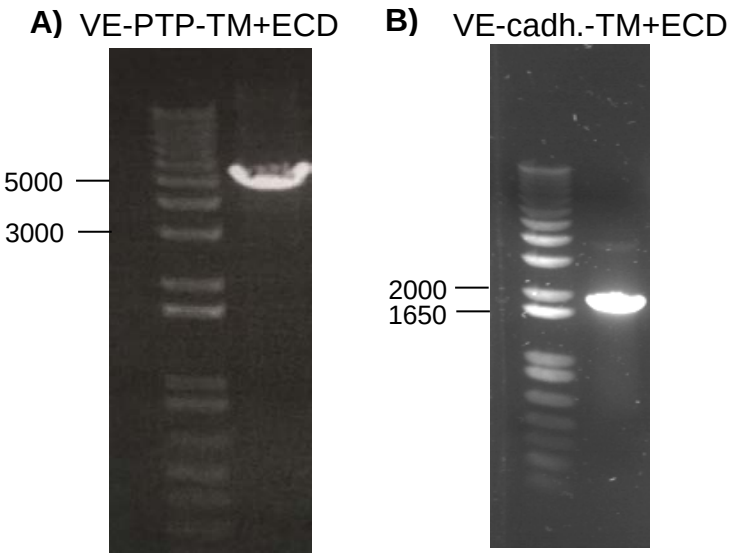

Figure 24. The generation of transmembrane and extracellular domains of VE-PTP and VE-cadherin by PCR. Electrophoresis on 0.8% agarose gel showing DNA bands corresponding to expected ECD+TM sizes for each construct: A) ~5.0 kb band for TM+ECD of VE-PTP. Running time was 35 minutes at 110 V constant, B) ~1.9 kb DNA band for TM+ECD of VE-cadherin. Primers used are listed in Chapter 2, Table 10.

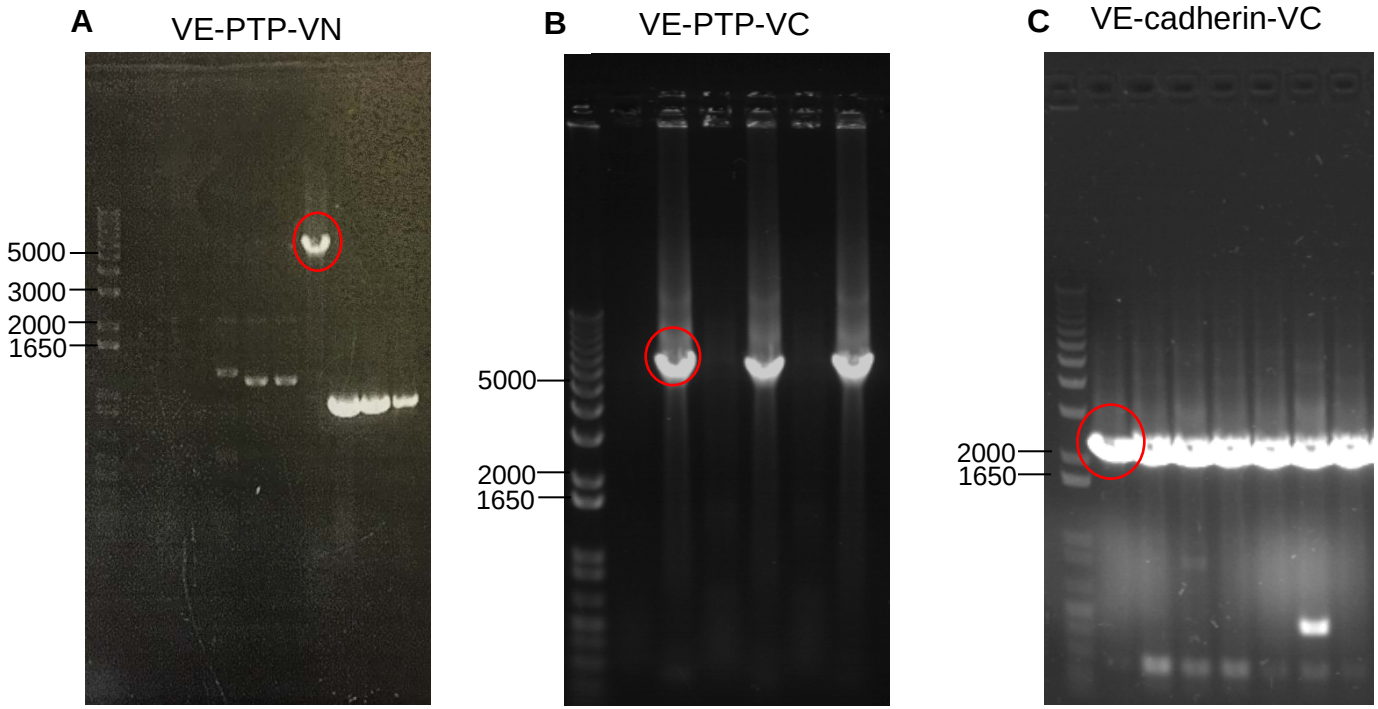

Figure 25. Colony PCR to screen for successful ligation. Following ligation and transformation colony PCR was performed with vector-specific and insert-specific primers to screen for successful ligation. (A) The DNA band corresponds to the predicted size of 5897 bp of the VE-PTP TM+ECD inserted into a pBiFC-VN155 expression vector. (B) The DNA band corresponds to the predicted size of 5613 bp of the VE-PTP TM+ECD inserted into a pBiFC-VC155 expression vector. (C) The DNA band corresponds to the predicted size of 2225 bp of the VE-cadherin TM+ECD inserted into a pBiFC-VC155 expression vector. The circled bands indicate the clones selected for sequencing.

4.2.2 Generation of negative control SPN fusion construct

To generate the SPN-VC fusion construct a synthetically generated signal peptide and HA tag fragment (Genscript) was inserted into *Apa*I/*Eco*RI restriction sites of pBiFC-VC155 expression vector. For the SPN-VN fusion construct a synthetically generated signal peptide and myc tag fragment was inserted into *Apa*I/*Eco*RI restriction sites of pBiFC-VN155(I152L) expression vector. Colony PCR was performed using REDTaq DNA Polymerase to confirm the presence of the correct insert with a combination of vector-specific and insert-specific primers. The list of primers used for colony PCR is provided in Table 11 (Chapter 2). Figure 26 shows the DNA bands corresponding to the correct sizes of 482 bp for signal peptide and HA tag in pBiFC-VC155 vector and 677 bp for signal peptide and myc tag in pBiFC-VN155(I152L) vector.

Following insertion of the appropriate signal peptide and tags into the vector the sequence corresponding to the transmembrane and extracellular domain of SPN was amplified by PCR using Platinum *Pfx* polymerase (Figure 27). The oligonucleotide primer sequences and PCR conditions are listed in Tables 10 and 4 respectively.

The resulting PCR product was subsequently digested, purified and inserted into *Eco*RI/XhoI restriction sites of the corresponding pBiFC-VC155 and pBiFC-VN155(I152L) vectors to create fusion protein fused to the C- and N-terminal parts of YFP respectively.

Colony PCR was used to confirm the presence of the correct insert (Figure 28). The oligonucleotide primer sequences and PCR conditions are listed in Tables 11 and 6 respectively.

The plasmid DNA for each fusion construct was purified and sequenced to verify that the insert gene has been ligated at the correct position within the vector backbone without any mutations. The sequenced plasmids were used to prepare larger concentrations of high-quality plasmid DNA for mammalian cell transfections in BiFC experiments using QIAprep Spin Midiprep Kit (QIAGEN).

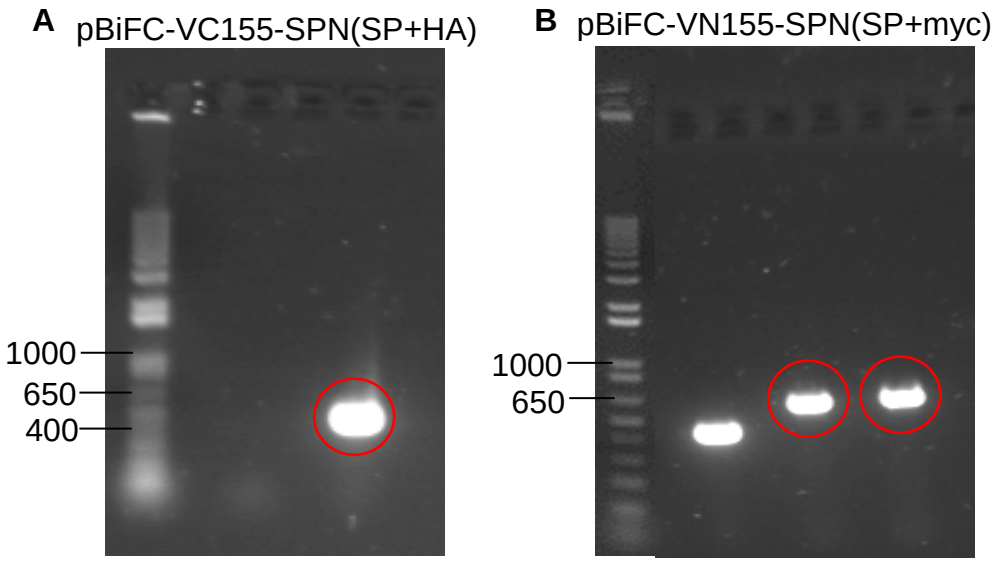

Figure 26. Colony PCR analysis. Synthetically generated signal peptide of SPN with either the HA or myc tag was ligated into *ApaI/Eco*RI restriction sites of the pBiFC-VC155 and pBiFC-VN155(I152L) vectors respectively. Colony PCR was performed with vector-specific and insert-specific primers to screen for successful ligation. (A) The DNA band of 482 bp corresponds to the predicted size of SPN signal peptide and HA tag inserted into a pBiFC-VC155 vector. (B) The DNA band of 677 bp corresponds to the predicted size of SPN signal peptide and myc tag inserted into a pBiFC-VN(I152L) vector.

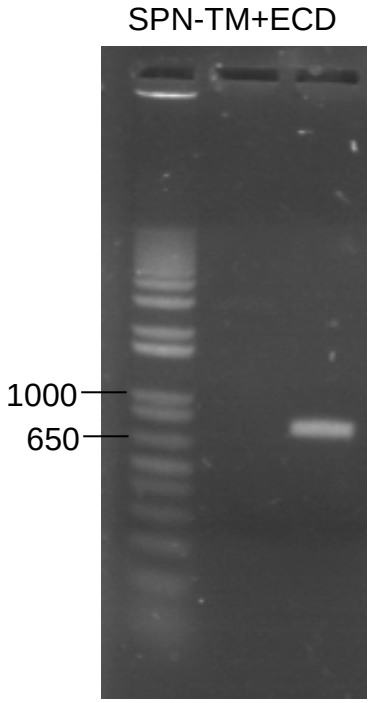

Figure 27. Generation of extracellular and transmembrane domains of SPN by PCR. Electrophoresis on 0.8% (w/v) agarose gel showing a DNA band of 771 bp that corresponds to the expected size of the SPN transmembrane and extracellular domain. Running time was 40 minutes at 110 V constant.

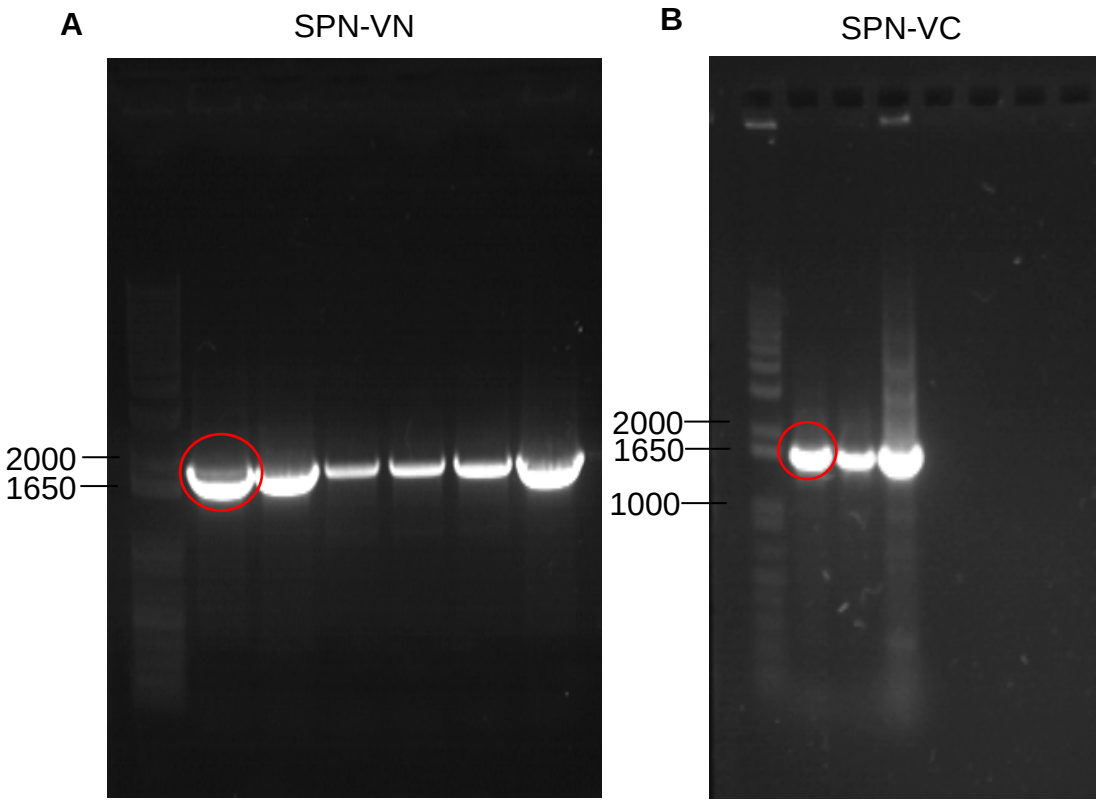

Figure 28. Colony PCR analysis. Colony PCR was performed with vector-specific and insert-specific primers to screen for successful ligation. (A) The DNA band corresponds to the predicted size of 1693 bp of the SPN TM+ECD inserted into pBiFC-VN155 vector. (B) The DNA band corresponds to the predicted size of 1551 bp of the SPN TM+ECD inserted into pBiFC-VC155 vector.

4.2.3 Cloning membrane anchored N- and C-terminal Venus-YFP fusion proteins

A membrane anchored fusion protein that entirely lacked transmembrane and extracellular domains was generated for use as a control in BiFC studies (shown schematically in Figure 15). Overlapping primers (Table 15), containing sequences corresponding to *Apa*I and *Eco*RI restriction sites, the membrane association sequence (Myr) from the protein tyrosine kinase Lck and a myc tag, were annealed together and ligated into the *Apa*I/*Eco*RI restriction sites of pBiFC-VN155 and pBiFC-VC155 expression vectors. Colony PCR was performed using REDTaq DNA Polymerase to confirm the presence of the correct DNA insert with a combination of vector-specific (CMV-F) and insert-specific (Myr-R; Table 15) primers.

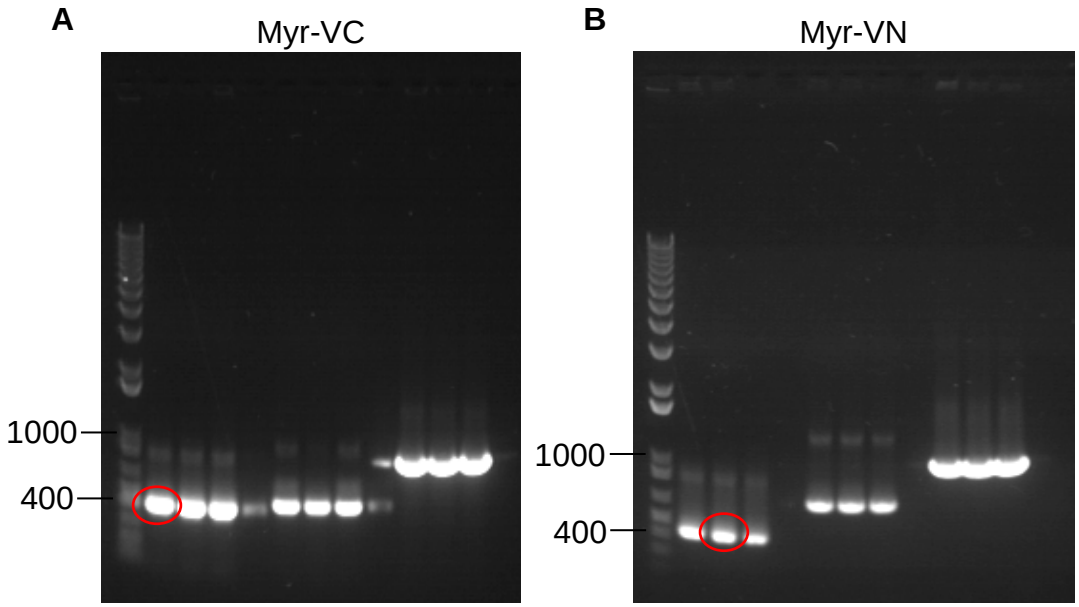

Figure 29. Colony PCR analysis for membrane anchored N- and C-terminal Venus YFP fusion proteins. Annealed overlapping primers containing the membrane association (Myr) and myc tag sequences were ligated into pBiFC-VC155 and pBiFC-VN155 expression vectors. Colony PCR was performed with vector-specific (CMV-F) and insert-specific (Myr-R) primers to screen for successful ligation. (A) The DNA band corresponds to the predicted size of 417 bp of the Myr-myc inserted into pBiFC-VC155 vector. (B) The DNA band corresponds to the predicted size of 426 bp of the Myr-myc inserted into pBiFC-VN155 vector.

4.2.4 Cloning a deletion mutant VE-PTP∆17FN

A deletion mutant of VE-PTP in which the 17th FNIII-like domain was removed was generated by PCR as shown schematically in Figure 23 for use in BiFC studies. Primers contained a non-complementary 5' *Xma*I restriction enzyme site. The primer details are provided in Table 13 and the PCR parameters are listed in Table 14. Following PCR amplification the product was digested with *Dpn*I/*Xma*I restriction enzymes and ligated to create the deletion mutant expression vector.

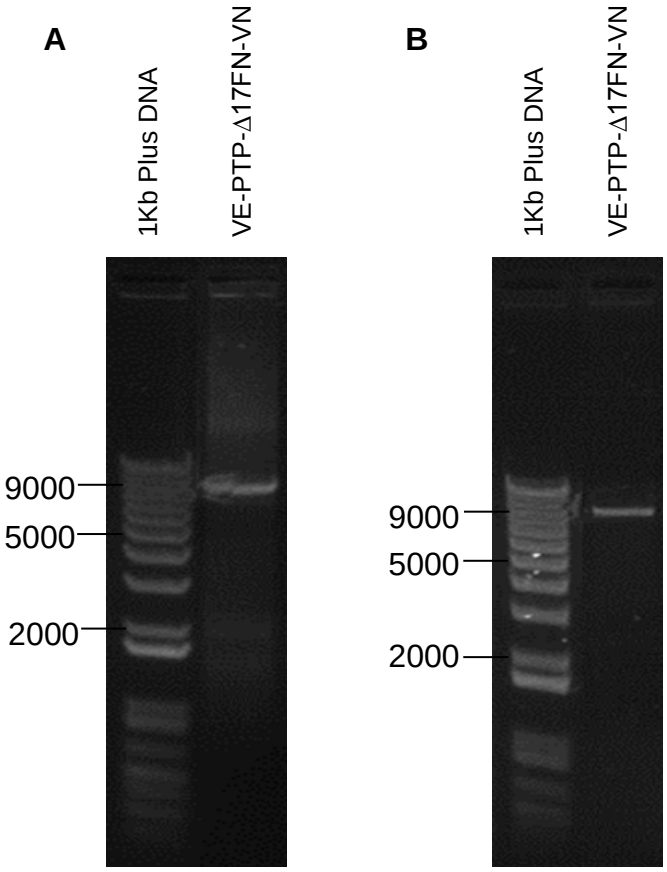

Figure 30. Deletion of the 17th FNIII-like domain in VE-PTP-VN using a PCR based approach. PCR was performed to amplify the entire sequence of the pBiFC-VN155(VE-PTP)-SP-myc-TM-ECD except for the 17th FNIII-like domain that was to be deleted. The gel extracted PCR product was digested with *Dpn*I/*Xma*I restriction enzymes and the plasmid was re-ligated together using T4DNA Ligase. (A) Gel electrophoresis analysis of the PCR product shows the band of the predicted size of ~9.0 kb. (B) Gel electrophoresis analysis of the digested PCR product confirms the right product of ~9.0 kb.

4.3 Western blot analysis of BiFC fusion proteins in HEK293T cells

Western blotting of lysates from transiently transfected HEK293T cells confirmed the expression of all the fusion proteins close to their predicted molecular weight (Figure 31). Western blotting with anti-myc antibody for the VE-PTP-VN and VE-PTP∆17FN-VN mutant, which have a myc-tag inserted following the signal peptide sequence (Figure 31, A), detected proteins with a molecular weight of approximately 220 kDa. The predicted molecular weight for VE-PTP-VN was 203 kDa. The discrepancy in molecular weight is probably accounted for by extensive glycosylation. It has previously been shown that VE-PTP has 26 potential N-glycosylation sites in its extracellular domain (Krueger et al, 1990). VE-PTP∆17FN as a fusion with the N-terminal fragment of vYFP was expressed at lower levels than VE-PTP-VN (Figure 31, A). Western blot experiments were performed at least twice and the results were consistent.

Western blotting with the VE-cadherin antibody (ab7047) detected a 130 kDa band corresponding to VE-cadherin (Figure 31, B). The band is larger than the predicted 80 kDa but this is probably due to VE-cadherin being highly glycosylated. A study by Geyer *et al* (1999) showed that the VE-cadherin has seven potential N-glycosylation sites, all localised in its five cadherin ectodomains and it has been demonstrated that indeed VE-cadherin is accompanied by oligosaccharide side chains of reduced branching pattern, which are highly sialylated. This would largely increase the size of a protein and thus affect its migration so that the actual band size observed would be different from that predicted.

Western blotting of lysates from transiently transfected HEK293T cells confirmed the expression of control proteins SPN and Myr-VC and Myr-VN at their predicted molecular weight (Figure 31, C-E). The predicted molecular weight for Myr-VC and Myr-VN was 15.3 kDa and 21.9 kDa respectively, which closely correspond to their migration points (Figure 31, C). The predicted molecular weight for SPN-VN was 48.4 kDa and 41 kDa for SPN-VC. A high-molecular weight smear, reflecting extensive glycosylation, was apparent with the SPN constructs. All control proteins were expressed at

substantially higher levels than the VE-cadherin-VC protein (Figure 31, panels A, C, D and E). However, the difference in band intensities could also be explained by the lack of sensitivity of some antibodies. Anti-VE-cadherin antibody could be less sensitive in recognising VE-cadherin compared with anti-HA antibody recognising HA tag fused to controls.

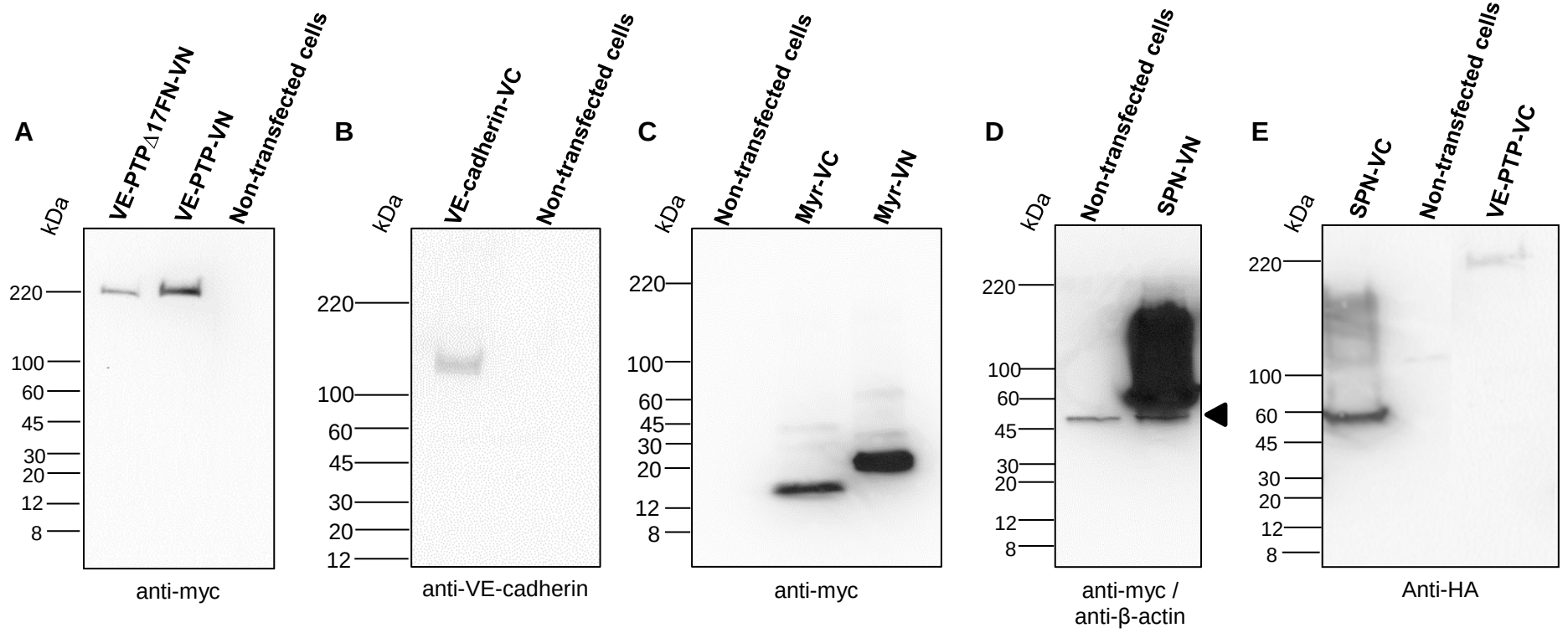

Figure 31. Protein expression analysis by Western blot. Western blotting of cell lysates from transfected HEK293T cells with either anti-myc, anti-HA or anti-VE-cadherin antibody confirmed the expression of the constructs at the expected molecular weight. β-actin (◀) was used as a loading control in some blots.

4.4 Validation of VE-PTP and VE-cadherin interaction in live cells using the BiFC technique

The involvement of the extracellular domains in the interaction between VE-PTP and VE-cadherin has been demonstrated previously by co-immunoprecipitation assay (Nawroth *et al,* 2002). However, no previous studies have been done in live cells to investigate the molecular basis of this interaction. To confirm that the interaction between these two proteins occurs via their extracellular domains in live cells the BiFC VE-PTP-VN and VE-cadherin-VC fusion proteins were constructed (refer to section 4.2.1). The fusion proteins were expressed in HEK293T cells and 24 hours post-transfection stained prior to confocal visualisation with the CellMas Plasma Membrane Stains (as detailed in method section 2.5.6). As predicted transfection of HEK293T cells with a single construct did not produce any detectable fluorescence signal, indicating that neither of the YN- and YC-fusion proteins alone is fluorescent (Figure 32).

Co-expression of the VE-PTP-VN and VE-cadherin-VC constructs in HEK293T cells resulted in the occurrence of BiFC fluorescence (Figure 33). BiFC fluorescence was observed in approximately 40% of the transfected cells. Comparison of the sub-cellular localisation of the Venus YFP (vYFP) signal with that of the CellMask deep red plasma membrane stain indicated that the fluorescence complementation signal was detected in the plasma membrane and intracellular structures, likely to be the endoplasmic reticulum or Golgi, of co-transfected cells. The localisation of the yellow fluorescence signal at the plasma membrane was also confirmed by the co-localisation analysis that was carried out using ImageJ software (Figure 34). The overlapping pixels from both signals are highlighted in white, showing that both yellow and red signals are co-localised at the plasma membrane (Figure 34, A). The histogram in Figure 34 (B) also shows that both fluorescence signals overlap to some extent, confirming that some of the BiFC signal is localised at the plasma membrane.

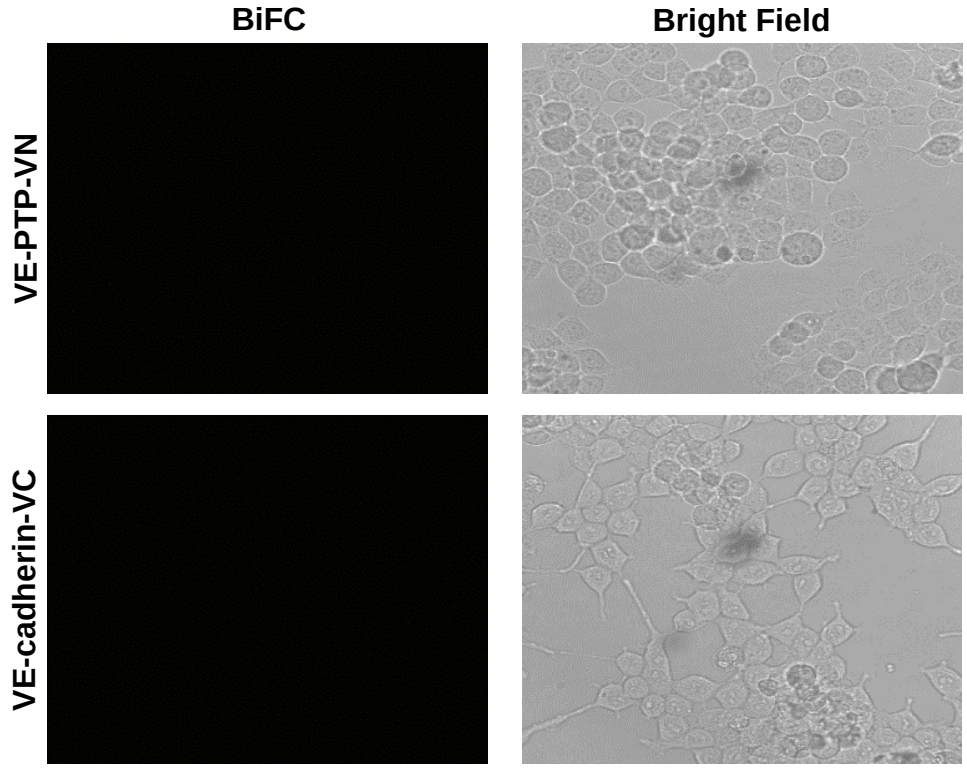

Figure 32. Confocal analysis of single construct transfected HEK293T cells. Confocal images of HEK293T cells expressing the proteins indicated in each panel were acquired 24 hours after transfection. None of the above proteins expressed alone exhibited a fluorescence signal.

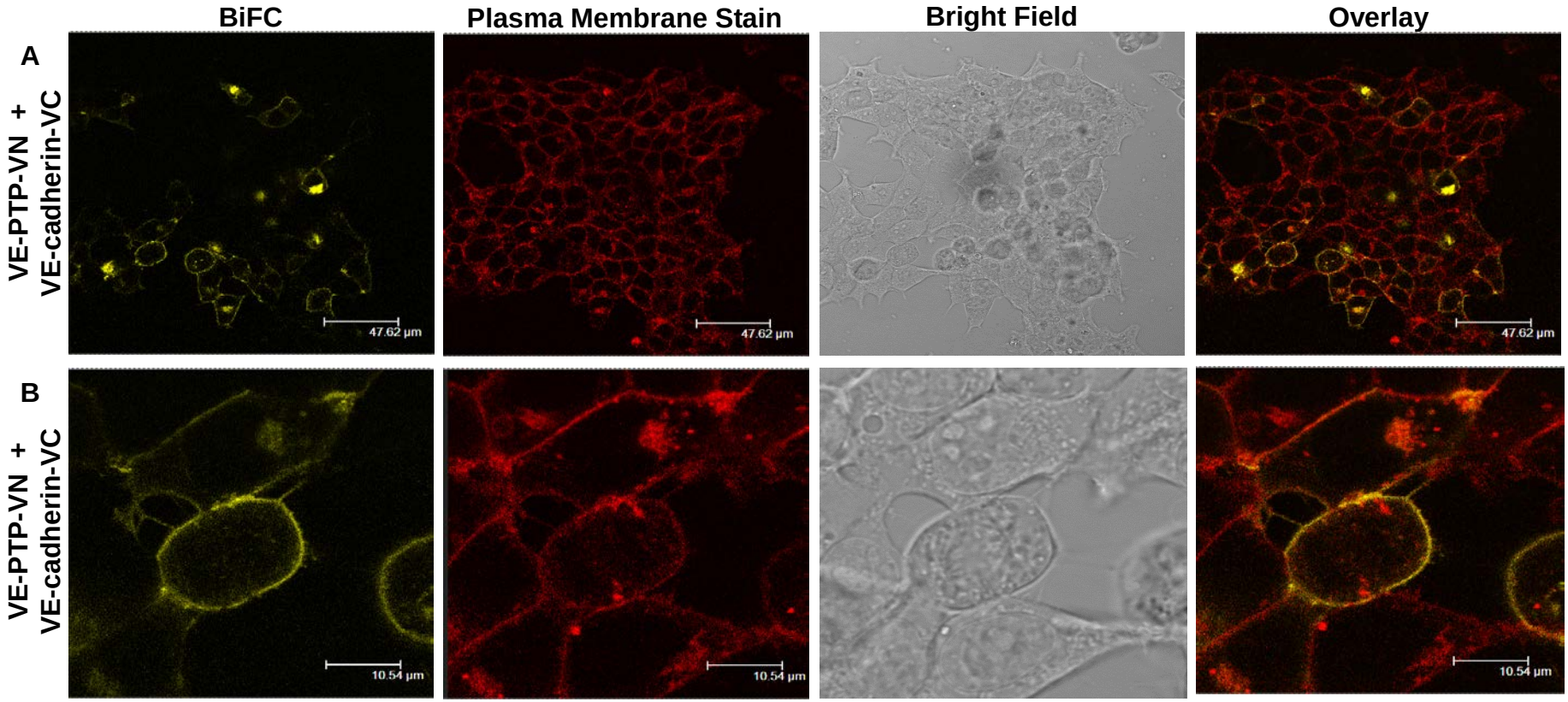

Figure 33. BiFC analysis of interaction between VE-PTP-VN and VE-cadherin-VC. Fluorescence is regained as a result of reconstitution of YFP from two non-fluorescent N- and C-terminal fragments due to an interaction between VE-PTP-VN and VE-cadherin-VC. Equal amount of expression vectors encoding VE-PTP-VN and VE-cadherin-VC were co-transfected into HEK293T cells and the resulting BiFC signal was analysed by confocal microscopy. (A) Confocal images of VE-PTP-VN/VE-cadherin-VC interactions in cell populations. (B) Confocal images of a single cell, showing the localisation of VE-PTP-VN/VE-cadherin-VC interactions.

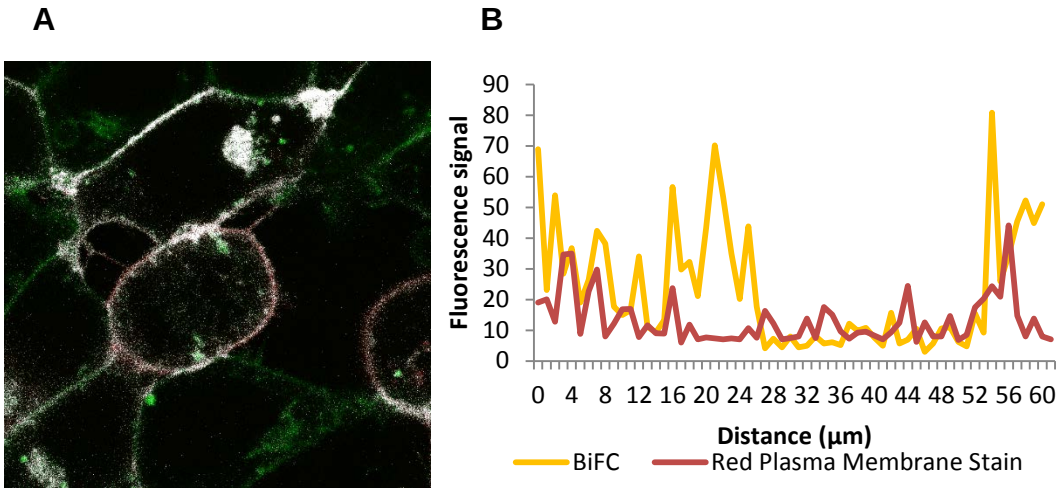

Figure 34. Co-localisation analysis of fluorescence signals from the BiFC and the red plasma membrane stain channels from HEK293T cells co-transfected with VE-PTP-VN/VE-cadherin-VC fusion pair. (**A**) Qualitative analysis highlights the overlapping pixels in white, showing that both the yellow BiFC and the red plasma membrane stain signals are co-localised at the plasma membrane. The co-localisation analysis has been performed using ImageJ software. An overlap image has been created by selecting VE-PTP-VN and VE-cadherin-VC confocal images from yellow BiFC and red plasma stain channels and selecting Image, Color, Merge Channels. The co-localisation analysis on the overlay image has been carried out by selecting Analyse, Colocalisation Thresholds. (**B**) Histogram showing fluorescence signals from BiFC (yellow) and red plasma membrane stain (red) across a single cell. Co-localisation analysis has been performed using ImageJ by drawing a line across the same cell in both BiFC and red plasma membrane stain channels and selecting Plot Profile from the drop-down menu Analyse. Fluorescence intensity values for both channels were used to graph both results on the same scale using Microsoft Excel.

4.5 Comparison of the BiFC signal from the VE-PTP and VE-cadherin pairing with VE-PTP and control constructs

In order to establish whether the BiFC signal resulting from co-expression of VE-PTP-VN and VE-cadherin-VC reflects a specific interaction between the proteins or is due to non-specific assembly of YFP fragments, the BiFC signal with VE-PTP-VN and control constructs, and pairs of control constructs, was compared with VE-PTP-VN/VE-cadherin-VC.

Figures 35-37 show that all the negative interaction pairs resulted in a BiFC fluorescence signal. However, qualitative assessment of the images suggested that VE-PTP-VN with either negative control construct resulted in a lower fluorescence signal compared with the positive VE-PTP-VN and VE-cadherin VC fusion pair (Figures 33, 35, 36 and 37). However, SPN-VN and Myr-VC exhibited a higher intensity of fluorescence signal and, in addition, more cells appeared to exhibit a BiFC signal (Figure 37) compared with VE-PTP-VN/SPN-VC (Figure 35) and VE-PTP-VN/Myr-VC (Figure 36) fusion pairs. However, all the negative control pairing appeared to exhibit reduced fluorescence intensity and the number of fluorescent cells compared with VE-PTP-VN and VE-cadherin-VC fusion pair (compare Figures 33, 35, 36 and 37). The BiFC signal appeared to be predominantly at the plasma membrane, as was predicted with membrane proteins, with some fluorescence in ER and Golgi. This was also confirmed by co-localisation analysis of BiFC and red plasma membrane fluorescence signals across a single cell (Figure 34). However, co-localisation analysis showed that the BiFC signal in cells co-expressing VE-PTP-VN with SPN-VC was mainly localised in the cytoplasm with only some signal at the plasma membrane (Figure 38, A). Cells co-expressing VE-PTP-VN and Myr-VC exhibited BiFC signal that was localised in the cytoplasm as there was minimum fluorescence signal overlap from both BiFC and red plasma membrane stain (Figure 38, B).

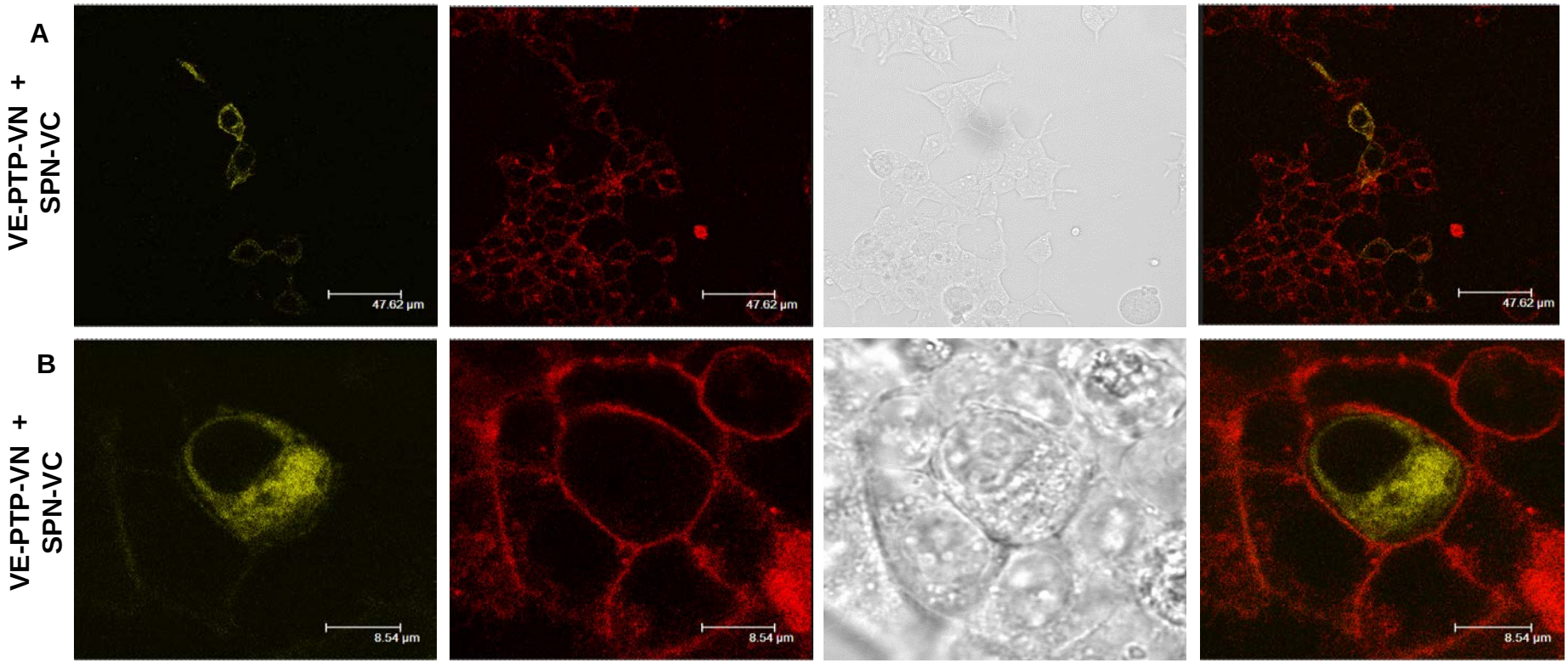

Figure 35. BiFC analysis of VE-PTP with control construct SPN-VC. To validate the specificity of the VE-PTP-VN and VE-cadherin-VC interaction, VE-PTP-VN was co-transfected with equal amount of negative control construct SPN-VC into HEK293T cells and the resulting BiFC signal was analysed by confocal microscopy after 24 hours. (A) Confocal images of VE-PTP-VN/SPN-VC interactions in cell populations. (B) Confocal images of a single cell, showing the localisation of VE-PTP-VN/SPN-VC interactions.

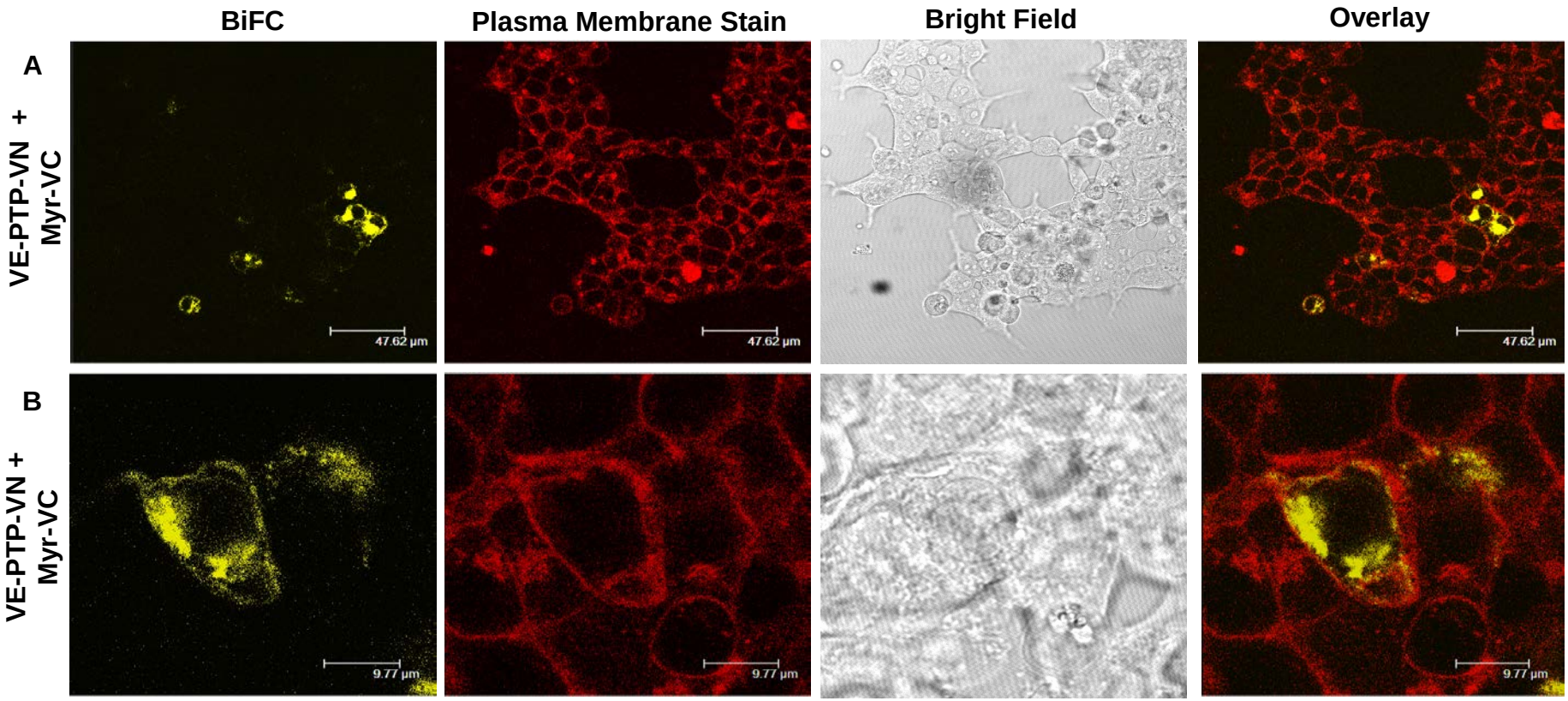

Figure 36. BiFC analysis of VE-PTP-VN with control construct Myr-VC. To validate the specificity of the VE-PTP-VN and VE-cadherin-VC interaction, VE-PTP-VN was co-transfected with an equal amount of negative control construct Myr-VC into HEK293T cells and the resulting BiFC signal was analysed by confocal microscopy after 24 hours. (A) Confocal images of VE-PTP-VN/Myr-VC interactions in cell populations. (B) Confocal images of a single cell, showing the localisation of VE-PTP-VN/Myr-VC interactions.

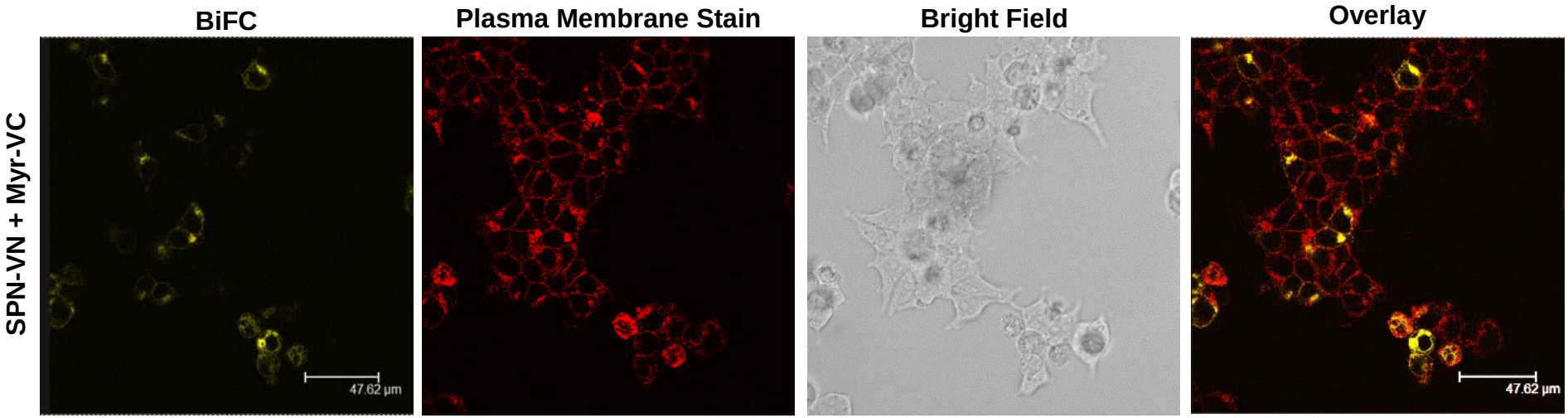

Figure 37. BiFC analysis of control constructs SPN-VN and Myr-VC. To validate the specificity of the BiFC fusion contructs interactions, an equal amount of negative control constructs SPN-VN and Myr-VC was co-transfected into HEK293T cells and the resulting BiFC signal was analysed by confocal microscopy after 24 hours.

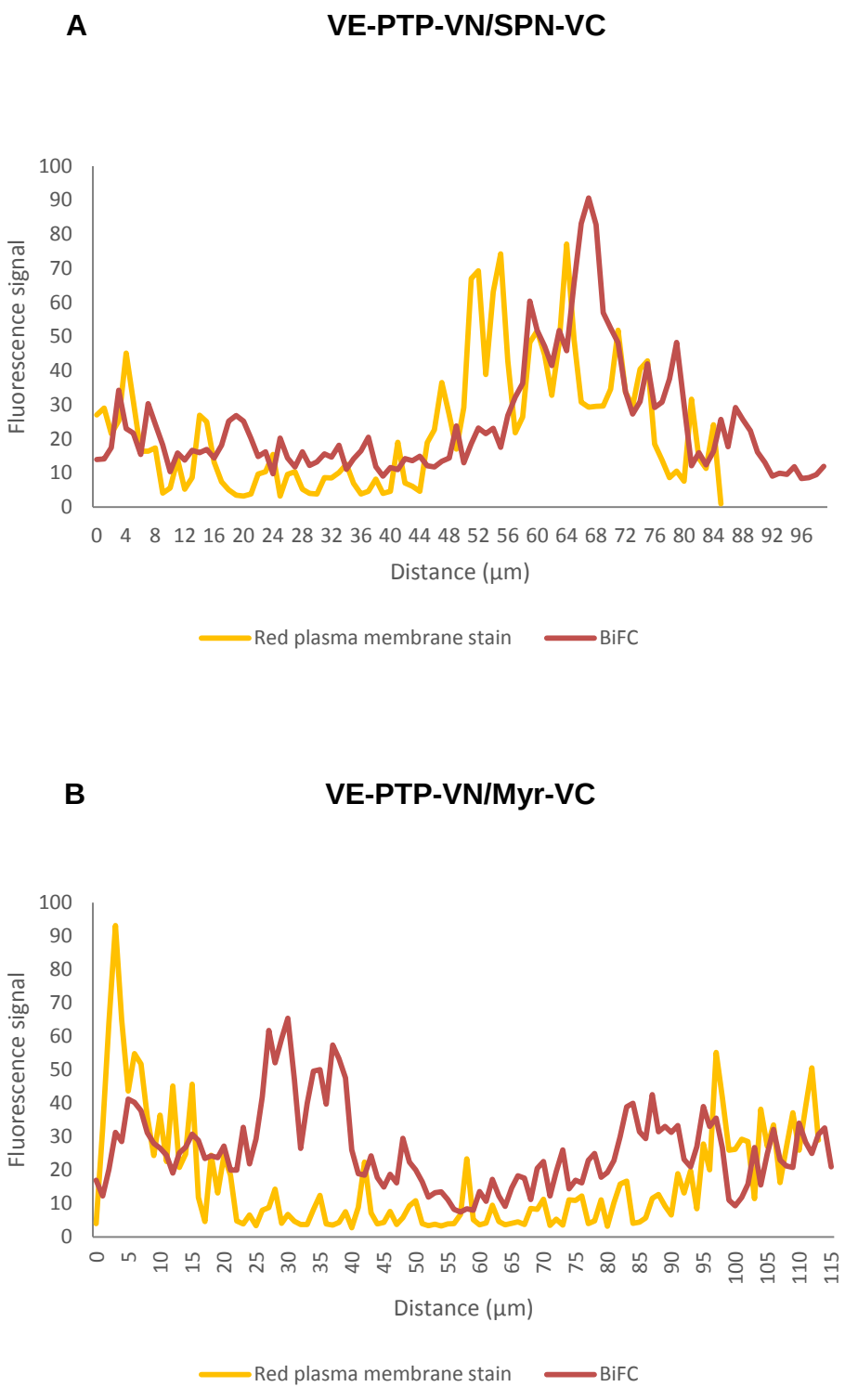

Figure 38. Co-localisation analysis of fluorescence signals from the BiFC and the red plasma mambrane stain channels. (**A**) Histogram showing fluorescence signals from BiFC (yellow) and red plasma membrane stain (red) across a single HEK293T cell co-transfected with VE-PTP-VN/SPN-VC fusion pair. (**B**) Histogram showing fluorescence signals from BiFC (yellow) and red plasma membrane stain (red) across a single HEK293T cell co-transfected with VE-PTP-VN/Myr-VC fusion pair.

4.6 Quantitative analysis of BiFC data

In order to obtain a more robust interpretation of the data and establish whether the results of BiFC experiments with VE-PTP-VN/VE-cadherin-VC represent true protein-protein interactions or are driven by the self-assembly of the two non-fluorescent YFP fragments, images were processed with ImageJ software to quantitate fluorescence signals. Quantitative comparisons of the fluorescence signal obtained with the cognate pairing and control pairings were performed. Quantitative analysis of BiFC data has previously been performed in other studies of cytosolic proteins by calculating the ratio of BiFC fluorescent intensity relative to an expressed Cerulean control protein to normalise for protein expression levels (Kerppola, 2006; Kodama and Hu, 2010). In this chapter the BiFC fluorescent intensity of individual cells was measured and the CellMask Deep Red membrane stain was used as a reference (as described in the methods section 2.5.9). This quantitative analysis approach was validated in Chapter 3 using the well characterised transcription factors bJun and bFos, which are known to form a hetero-dimer (positive control), and bJun and the deletion mutant bFos∆ZIP, which lacks the interaction domain (negative control).

Briefly, the quantitation procedure consisted of the following steps: confocal images from cells displaying a BiFC signal which had been stained with the CellMask Deep Red membrane stain were acquired in a random distribution. By tracing the outline of each cell in the ImageJ using a polygon selection the yellow fluorescent intensity derived from bimolecular fluorescence complementation and the red fluorescent signal derived from the plasma membrane stain of the selected region, including border, were calculated. The background signal in an area with no cells was subtracted from all values. The results for each cell (i.e. ImageJ region of interest) were expressed as a yellow/red ratio (i.e. vYFP fluorescence intensity/deep red fluorescence intensity). On average about 700 cells from at least three random fields from three or more independent experiments for each fusion protein combination were analysed. The ratio in individual cells was then plotted in a histogram (Figure 39).

The distribution of yellow/red ratios represents a measure of the efficiency of bimolecular fluorescence complementation. The efficiency of BiFC is defined by the fluorescent intensity that results upon bimolecular complex formation when specific fusion proteins are expressed in cells. The YFP fragments, however, have the tendency to associate with each other independently when expressed at sufficiently high concentrations but the BiFC efficiency is significantly reduced (Kerrpola, 2008). As can be seen from the histogram in Figure 39 (A) co-expressing VE-PTP-VN and VE-cadherin-VC results in higher cell numbers that have higher ratio value range compared with cells co-expressing VE-PTP-VN and Myr-VC (Figure 39, B) or SPN-VN and Myr-VC (Figure 39, D) negative interacting pairs. When comparing the distribution of ratios from VE-PTP-VN/VE-cadherin-VC and VE-PTP-VN/SPN-VC there appears to be little or no difference (Figure 39, C), suggesting that there is a possible interaction between VE-PTP and SPN. However, just based on these results it is difficult to conclude with confidence that VE-PTP-VN/VE-cadherin-VC co-expression results in higher yellow/red ratio values.

In addition, to measure the BiFC specificity the signal-to-noise (S/N) ratio was calculated as described in previous studies by Kerppola (2010). A higher S/N ratio value reflects a more specific interaction. The S/N ratio was calculated by dividing the median value of BiFC efficiency for the positive interaction (i.e. VE-PTP-VN/VE-cadherin-VC) by the median value of BiFC efficiency for the negative interaction (VE-PTP-VN/Myr-VC) (Kerppola, 2010; Kodama and Hu, 2010). Since there are no previous documented reports about VE-PTP and SPN interactions and since the yellow/red ratio distributions for VE-PTP-VN/VE-cadherin-VC and VE-PTP-VN/SPN-VC appeared to be similar, the S/N ratio was also calculated for VE-PTP-VN/SPN-VC and compared with VE-PTP-VN/VE-cadherin-VC. As can be seen from Figure 36, the VE-PTP-VN/VE-cadherin-VC pairing resulted in S/N value of 6.5 that was 2-fold higher when compared with VE-PTP-VN in combination with SPN-VC, indicating a specific interaction of VE-PTP-VN and VE-cadherin-VC.

An alternative approach to quantitate the data using only average fluorescence intensity was also used. The average yellow fluorescence intensity from at least three random fields and three or more independent experiments was calculated and used for statistical analysis (Figure 41). Quantitative analysis of the VE-PTP-VN and VE-cadherin-VC pairing resulted in an average BiFC fluorescent intensity that was significantly higher than control pairings even though control proteins appeared to be expressed at significantly higher levels than VE-PTP-VC (Figure 31). As can be seen from Figure 41 there was a significant decrease in fluorescence signal in all the control pairings ($p<0.001$). The average fluorescence signal for the VE-PTP-VN/VE-cadherin-VC fusion pair was 8141.4 that was 2-fold higher than 4099.6 for the VE-PTP-VN/SPN-VC fusion pair, 3-fold higher than 2688.5 for the VE-PTP-VN/Myr-VC and 2.5-fold higher than 3263.4 for the SPN-VN/Myr-VC.

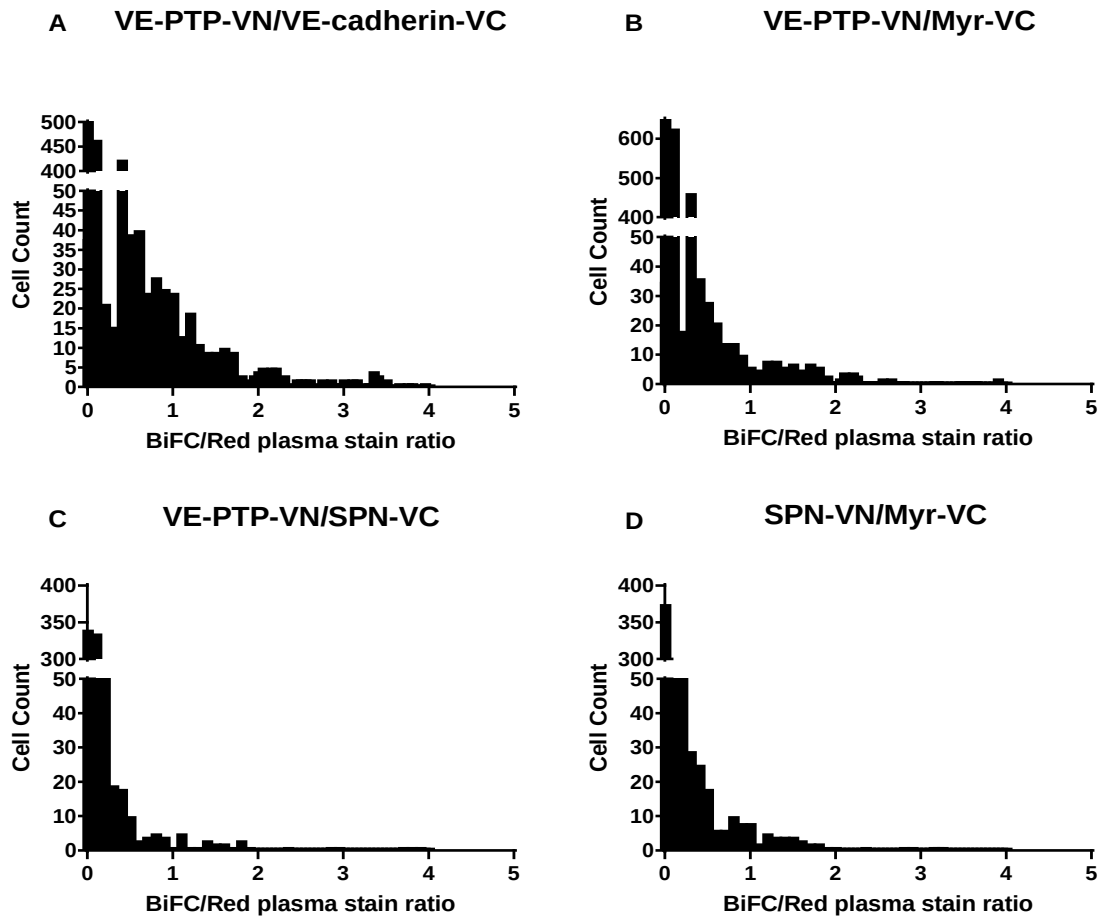

Figure 39. Validation of VE-PTP-VN/VE-cadherin-VC interaction specificity. The fluorescence intensity from BiFC (yellow) and the fluorescent signal from the plasma membrane stain (red) were measured in individual cells. The distribution of ratios between the fluorescence intensity and red fluorescent signal in individual cells was plotted in a histogram. The yellow/red ratio has been plotted for each pair of constructs as indicated above. Each histogram represents combined data from at least three independent experiments.

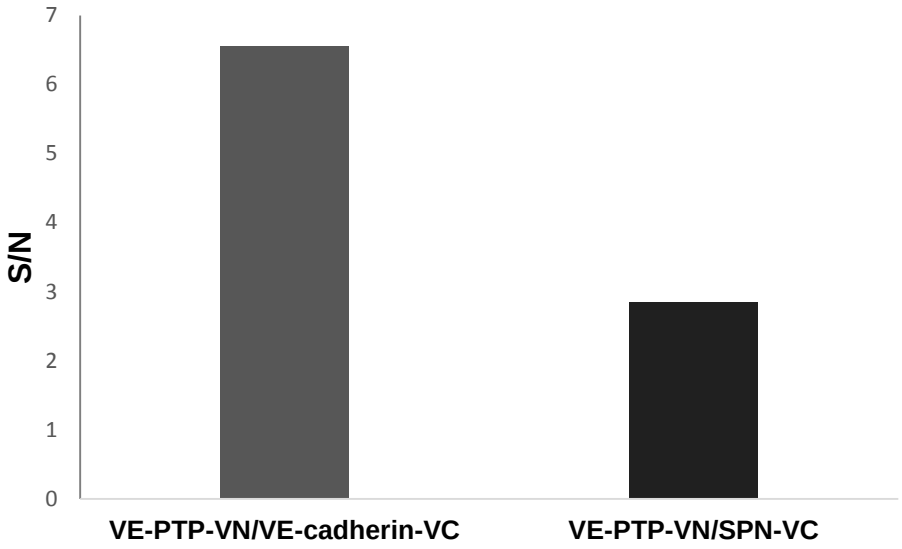

Figure 40. S/N ratio of BiFC assay in HEK293T cells. S/N for VE-PTP-VN/VE-cadherin-VC was calculated by dividing its median values of BiFC efficiency by the median value of BiFC efficiency for VE-PTP-VN/Myr-VC. S/N for VE-PTP-VN/SPN-VC was calculated by dividing its median values of BiFC efficiency by the median values of BiFC efficiency for VE-PTP/Myr-VC. The median values from at least three images taken from three independent experiments were quantitated as described in Chapter 2.

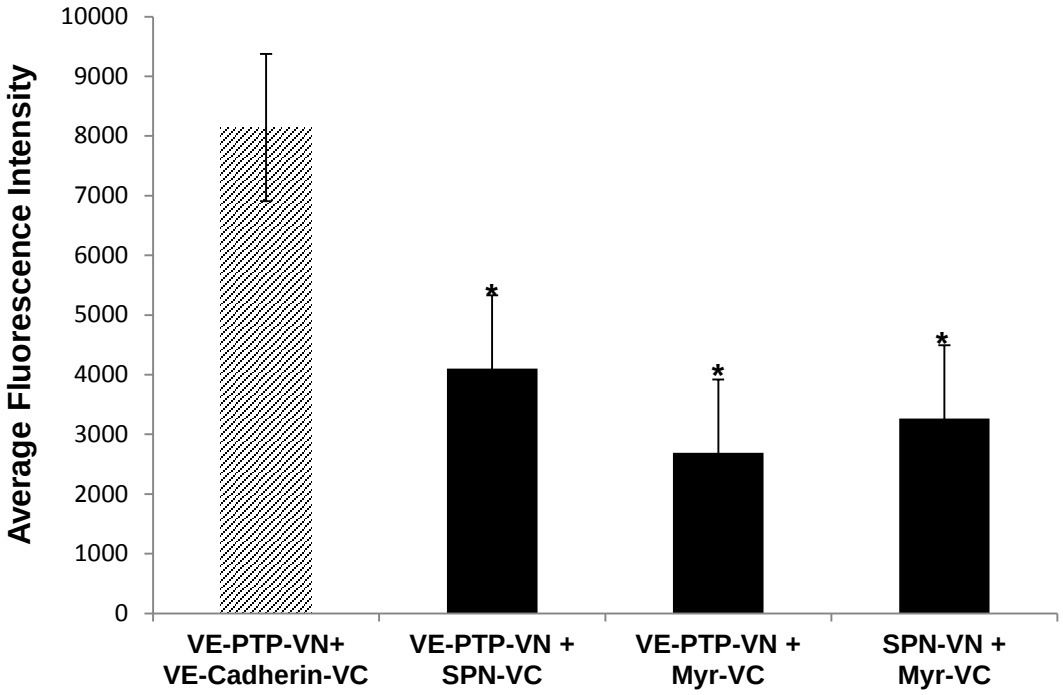

Figure 41. Quantitation of BiFC fluorescence intensities in transiently transfected HEK293T cells. Pairs of constructs as indicated were transfected into HEK293T cells and the BiFC signal assessed. Average fluorescence intensity was determined using ImageJ software. The mean and standard errors from three images taken from three independent experiments were quantitated as described in the materials and methods. *$p<0.001$ by the Kruskal-Wallis test was considered significant. Average fluorescence intensity from the positive interacting pair VE-PTP-VN/VE-cadherin-VC was compared with average fluorescence intensity from negative interacting pairs VE-PTP-VN/SPN-VC, VE-PTP-VN/Myr-VC and SPN-VN/Myr-VC.

4.7 Analysis of the VE-PTP/VE-cadherin interface

A VE-PTP deletion mutant, in which the 17th FNIII-like domain had been removed (VEPTPΔ17FN), was used in the BiFC assay to examine the region that participates in interactions between VE-PTP and VE-cadherin.

Qualitative analysis of BiFC images show that HEK293T cells co-expressing VE-PTPΔ17FN-VN and VE-cadherin-VC still exhibit a strong fluorescence signal at the plasma membrane (Figure 42) which is comparable to the signal resulting from VE-PTP-VN/VE-cadherin-VC interaction (Figure 33). However, cells co-expressing VE-PTPΔ17FN-VN and SPN-VC exhibited stronger fluorescence signal than the cells co-expressing VE-PTP-VN and SPN-VN (Figures 43 and 35), whereas cells co-expressing VE-PTPΔ17FN-VN and the negative control Myr-VC showed no or weak fluorescence signal (Figure 43) which was comparable with the signal obtained from VE-PTP-VN and Myr-VC co-expression (Figure 36).

The average BiFC fluorescence intensity resulting from co-expression of VE-PTPΔ17FN-VN with VE-cadherin-VC was not significantly different from that obtained with VE-PTP-VN in combination with VE-cadherin-VC (Figure 43, A). A similar fold increase in fluorescent intensity relative to control pairings was observed with either VE-PTP-VN or VE-PTPΔ17FN-VN. Although the BiFC qualitative analysis of VE-PTPΔ17FN-VN/SPN-VC showed strong fluorescence signal, the quantitative results showed a significant reduction of signal by 1.9-fold compared with VE-PTPΔ17FN-VN/VE-cadherin-VC ($p<0.001$; Figure 43, A). There was a significant decrease in fluorescence signal by 6.4-fold when cells were co-expressing VE-PTPΔ17FN-VN and Myr-VC compared with VE-PTPΔ17FN-VN and VE-cadherin ($p<0.001$; Figure 43, A). These results are comparable to the ones obtained with VE-PTP-VN and VE-cadherin-VC.

Figure 43 (B) shows that the VE-PTP-VN/VE-cadherin-VC pairing resulted in S/N value of 6.5 that was 1.4-fold higher than for VE-PTPΔ17FN-VN/VE-cadherin-VC and 2.4-fold higher than for VE-PTpΔ17FN-VN/SPN-VC. S/N value for VE-PTPΔ17FN-VN/VE-cadherin was 4.5, which was 1.6-fold higher than for VE-PTPΔ17FN-VN/SPN-VC.

HEK293T cells co-expressing VE-PTP-VN and VE-cadherin-VC exhibit similar cell numbers falling into a greater ratio value range compared with VE-PTP∆17FN-VN and VE-cadherin-VC (Figure 46, A and B). Co-expression of VE-PTP∆17FN-VN and SPN-VC resulted in some reduction of cell numbers that fall into a greater ratio value range (Figure 46, C). However, co-expression of VE-PTP∆17FN-VN and Myr-VC resulted in the majority of cells falling into the lower ratio value range (Figure 46, D). Therefore it can be concluded that both VE-PTP-VN/VE-cadherin-VC and VE-PTP∆17FN-VN/VE-cadherin-VC complementation complexes result in stronger fluorescence signal compared with all the negative control fusion pairs.

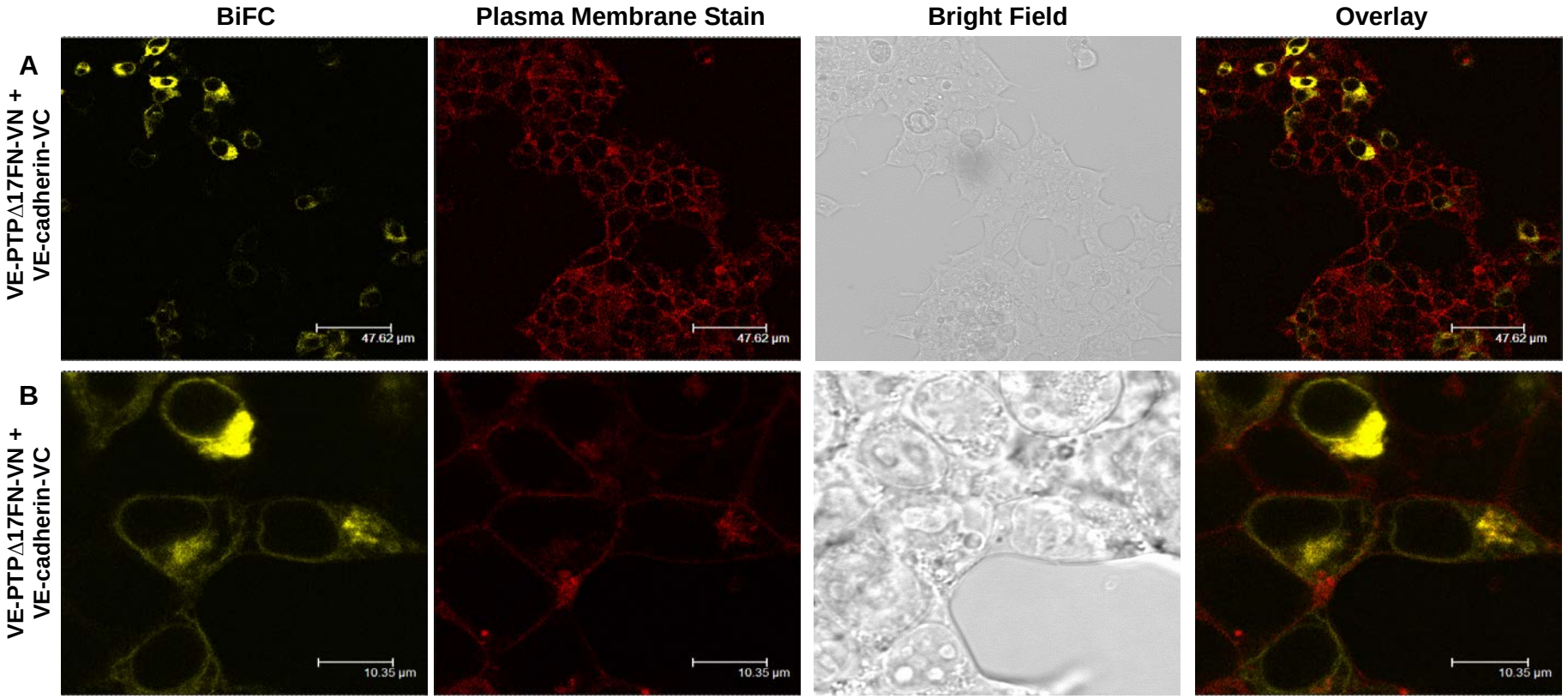

Figure 42. BiFC analysis of the deletion mutant VE-PTPΔ17FN-VN and VE-cadherin-VC. To investigate VE-PTP-VN/VE-cadherin-VC interaction interface the 17th FNIII-like domain of VE-PTP-VN was removed and the VE-PTPΔ17FN-VN mutant was co-transfected with equal amounts of either VE-cadherin-VC into HEK293T cells and the resulting BiFC signal was analysed by confocal microscopy after 24 hours. (A) Confocal images of VE-PTPΔ17FN-VN/VE-cadherin-VC interactions in cell populations. (B) Zoom in of HEK293T cells, showing the localisation of VE-PTPΔ17FN-VN/VE-cadherin-VC interactions.

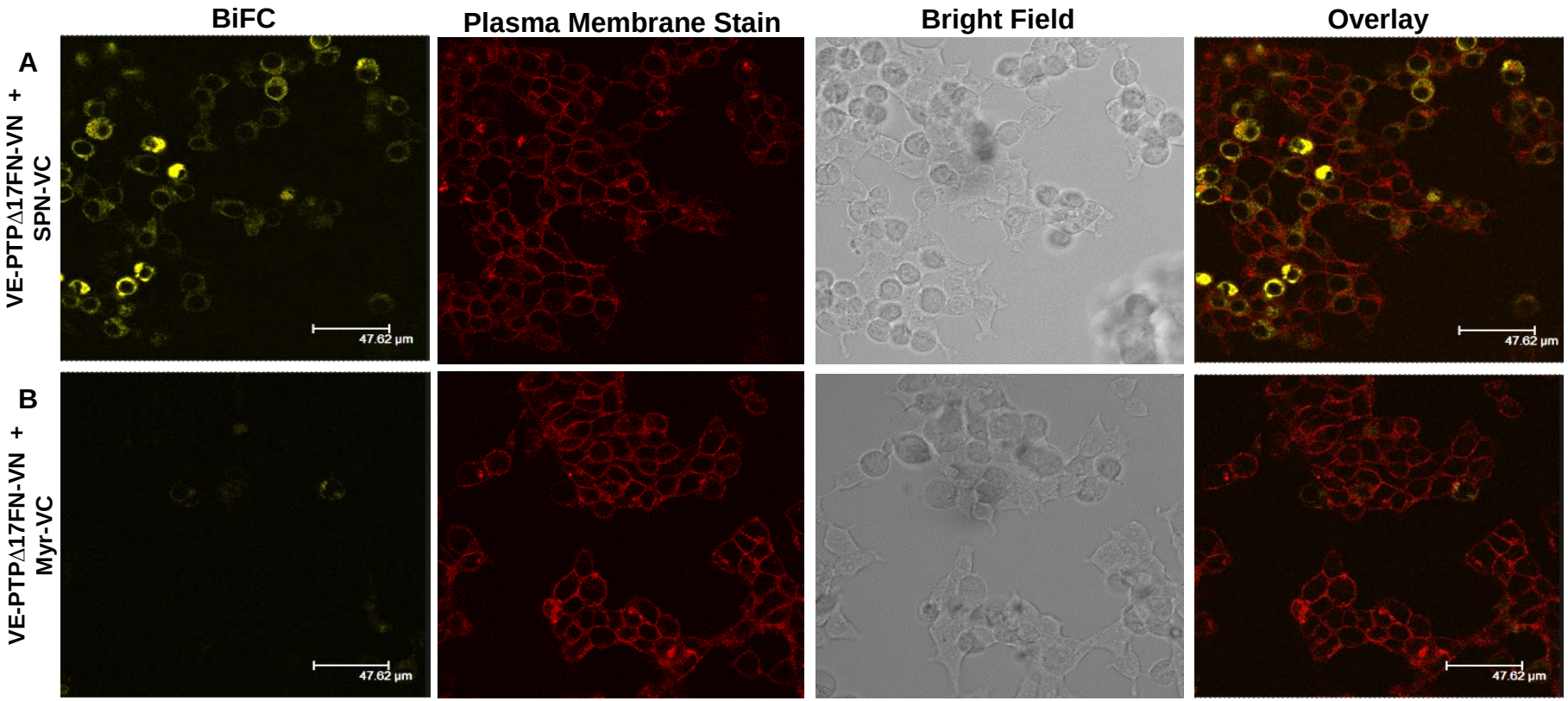

Figure 43. BiFC analysis of the deletion mutant VE-PTPΔ17FN-VN and control constructs SPN-VC and Myr-VC. To investigate the specificity of the VE-PTPΔ17FN-VN and VE-cadherin-VC interaction, VE-PTPΔ17FN-VN was co-transfected with equal amounts of either negative control construct SPN-VC or Myr-VC into HEK293T cells and the resulting BiFC signal was analysed by confocal microscopy after 24 hours. (A) Confocal images of VE-PTPΔ17FN-VN/SPN-VC interactions. (B) Confocal images of VE-PTPΔ17FN-VN/Myr-VC interactions.

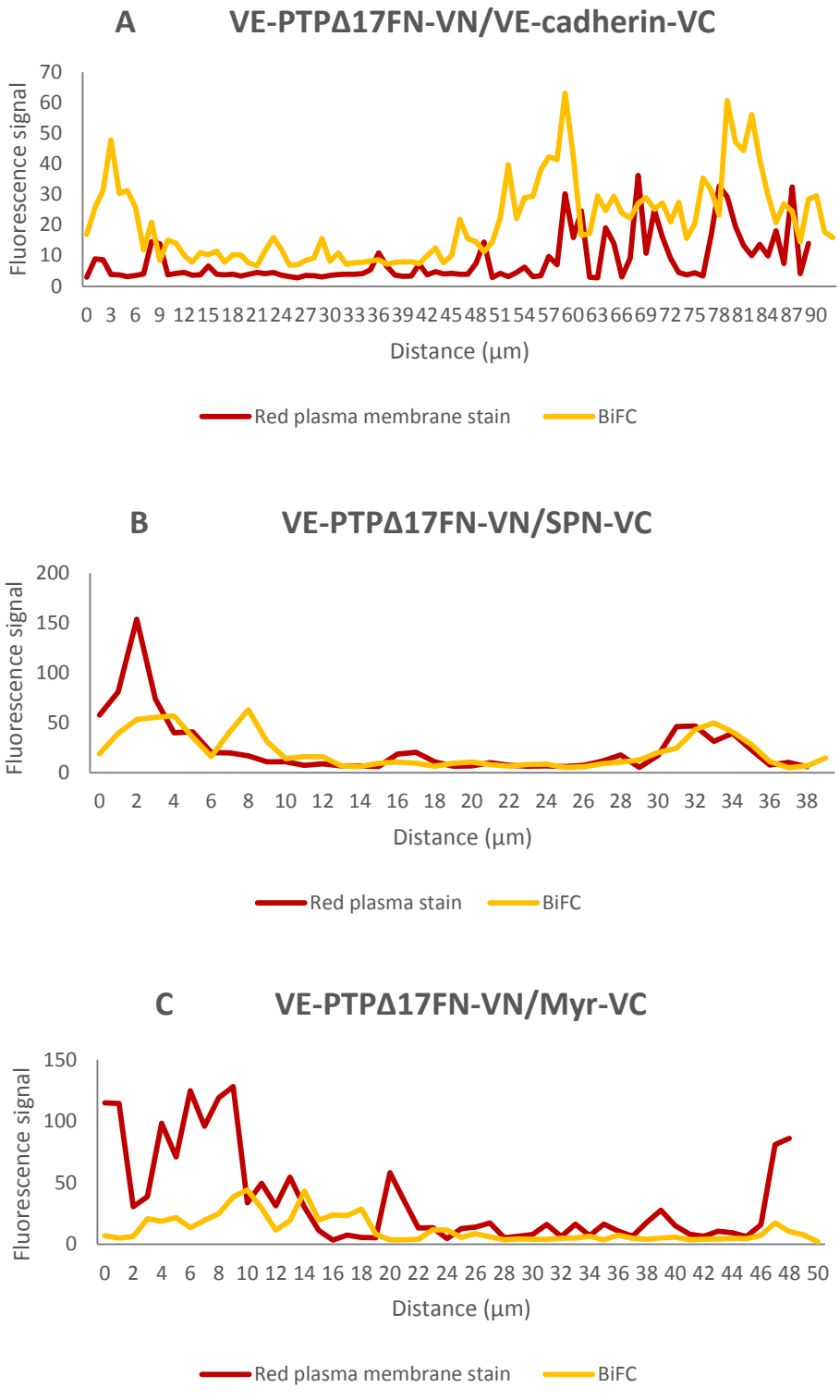

Figure 44. Co-localisation analysis of fluorescence signals from the BiFC and the red plasma membrane stain channels across a single cell. (**A**) VE-PTPΔ17FN-VN/VE-cadherin-VC (**B**) VE-PTPΔ17FN-VN/VE-SPN-VC (**C**) VE-PTPΔ17FN-VN/Myr-VC.

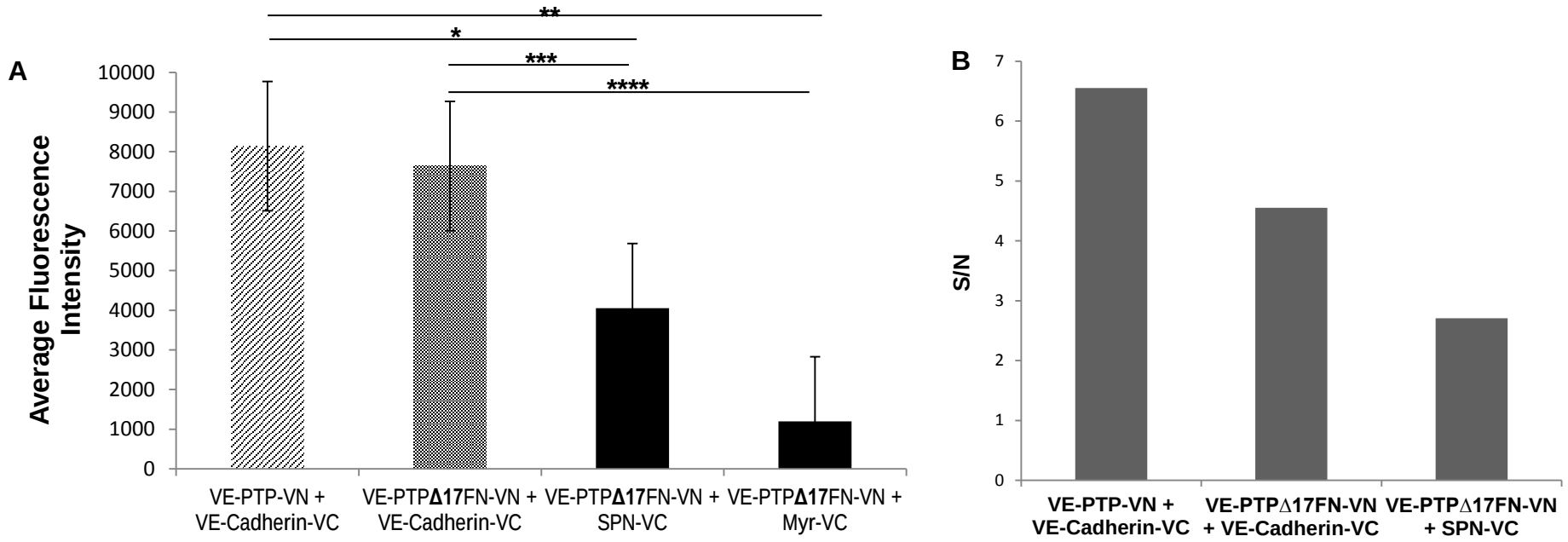

Figure 45. BiFC analysis of the VE-PTP/VE-cadherin interface. Pairs of constructs were transfected into HEK293T cells and the BiFC signal assessed. (A) Average fluorescence intensity was determined using ImageJ software. The mean and standard errors from three images taken from three independent experiments were quantitated as described in the materials and methods. *p<0.001 by the Kruskal-Wallis test was considered significant. (B) S/N ratio of BiFC assay in HEK293T cells. S/N for VE-PTP-VN/VE-cadherin-VC, VE-PTPΔ17FN-VN/VE-cadherin-VC and VE-PTPΔ17FN-VN/SPN-VC was calculated by dividing their median values by the median values from either VE-PTP-VN/Myr-VC or VE-PTPΔ17FN-VN/Myr-VC interactions.

A

Figure 46. Validation of VE-PTP-VN/VE-cadherin-VC interaction specificity. BiFC (A) VE-PTP-VN/VE-cadherin-VC, (B) VE-PTPΔ17FN-VN/VE-cadherin, (C) VE-PTPΔ17FN-VN/SPN-VC and (D) VE-PTPΔ17FN-VN/Myr-VC fusion pairs were co-expressed in HEK293T cells and 24 hours post-transfection were stained with CellMask Deep Red plasma membrane stain. The BiFC fluorescence intensity and the red fluorescent signal from the plasma membrane stain were measured in individual cells and yellow/red ratio values calculated. The distribution of ratios in individual cells was plotted in a histogram.

4.8 Discussion

Vascular endothelial protein tyrosine phosphatase (VE-PTP) is recognised to be essential for the maintenance of the endothelial barrier between blood and tissue, maintenance and remodelling of blood vessels and control of blood vessel permeability and leukocyte extravasation during inflammation by potentially regulating the adhesive function of VE-cadherin in endothelial cells (Bäumer *et al*, 2006; Nottebaum *et al*, 2008). VE-PTP is the only RPTP reported to be expressed exclusively in endothelial cells and thus attracted attention as a potential regulator of VE-cadherin (Bäumer *et al*, 2006). Co-immunoprecipitation studies by Nawroth *et al* (2002) showed that indeed VE-PTP and VE-cadherin interact together and that this interaction occurs via their extracellular domains, independently of their cytoplasmic tails. The same group demonstrated using deletion mutants that the fifth cadherin domain of VE-cadherin and the 17th FNIII-like repeat of VE-PTP were sufficient to support their interaction. While there are many studies had been done on a whole protein (e.g. using knock-out mice) no studies to date had been done in live cells on a functional role of the extracellular domain of VE-PTP in regulation of vascular permeability and angiogenesis. Here we used VE-PTP and VE-cadherin fusion constructs consisting of transmembrane and extracellular domains fused to the N- and C-terminal parts of a Venus yellow fluorescent protein (YFP) respectively to examine their interaction in live cells using the bimolecular fluorescence complementation (BiFC) assay. The qualitative BiFC analysis obtained on co-expression of VE-PTP and VE-cadherin constructs containing the transmembrane and extracellular domains of these molecules showed a strong fluorescence signal that was localised at the plasma membrane with some fluorescence in endoplasmic reticulum and probably Golgi apparatus.

To confirm that the yellow fluorescent signal originated as a result of VE-PTP-VN and VE-cadherin-VC interaction and not from self-assembly of YFP fragments we employed several controls. Although it is recommended to negate a positive interaction by introducing a point mutation, it was not practical in this project since the exact interaction site of VE-PTP and VE-cadherin is not known. One of the controls was Sialophorin (SPN) that is not

homologous to any proteins investigated in this project and has a completely different extracellular domain composition (Figure 15). It consists of a mucin-like 235-residue extracellular region highly rich in serine, threonine and proline uniformly distributed throughout the ECD region. It is also highly glycosylated, containing one N-linked carbohydrate unit and approximately 84 O-linked units (Shelley *et al,* 1989). The expression of SPN is restricted to haematopoietic cells, especially leukocytes (Fukuda and Tsuboi, 1999). The fact that the extracellular domains of SPN and VE-PTP are so different and that the two proteins are expressed in different cells made SPN a good candidate for a control. Furthermore, it has previously been used by Cardoba *et al* (2013) as a control. Fusing one of the YFP fragments to an unrelated protein that does not interact with the protein of interest should, in theory, reduce the background signal intensity. However, to eliminate any possible interactions between SPN and VE-PTP an unfused YFP fragment anchored to the plasma membrane via the membrane associated sequence from Lck (Myr-VC and Myr-VN) was generated as additional control. Since Myr-VC and Myr-VN entirely lack any transmembrane and extracellular domain sequences it was predicted that the fluorescent signal would be abolished when co-expressed with VE-PTP. Interestingly the co-expression of VE-PTP-VN with either SPN-VC or Myr-VC negative controls also resulted in fluorescence signal. Although the signal appeared to be reduced and less intense, it was not possible to conclude that the fluorescence obtained with negative interaction pairs was due to non-specific interactions or self-assembly of the two non-fluorescence YFP fragments. Due to the nature of the BiFC method the two non-fluorescence YFP fragments are able to assemble spontaneously into a functional YFP, resulting in yellow fluorescence. This could be caused by an overexpression of proteins. Under normal physiological conditions membrane (integral) proteins are molecularly dispersed and their two-dimensional translational diffusion (i.e. movement of proteins perpendicular to the plane of the membrane) occurs freely (Singer and Nicolson, 1972). However, overexpression of proteins could result in somewhat tightly packed and ordered protein molecules with limiting spacing in the plane of the membrane, thereby restricting planar diffusion. Such clustering within the membrane could enhance spontaneous collisions of the

YFP fragments and increase the probability of irreversible bimolecular fluorescent complexes and the false-positive fluorescence signal.

As reported by Horstman *et al* (2014) the vast majority of published BiFC studies report only qualitative results and show representative examples of detected interactions. Here we adapted three different quantitative analyses that were performed using ImageJ software and statistically validated data. First, the distribution of yellow/red ratio values has been determined for each interaction pair to validate the BiFC efficiency as was recommended by Kerppola (2008). Second, based on studies by Kodama and Hu (2010), the signal-to-noise ratio was calculated to validate the BiFC specificity. In addition, the average yellow fluorescence intensity for the positive interacting pair was compared with that of the negative interacting pair. The full detailed quantitative and statistical analyses are described in Chapter 2, section 2.5.9. All three quantitative methods showed similar results, complementing each other. Co-expression of VE-PTP-VN and VE-cadherin resulted in more cells exhibiting higher yellow/red ratio values, higher S/N value and a significant increase in average yellow fluorescence signal compared with all the negating interacting pairings. The fact that the VE-cadherin-VC was expressed at lower level compared with negative controls SPN-VC and Myr-VC (Figure 31, C and E) suggests that the BiFC signal from VE-PTP-VN and VE-cadherin-VC was not an artefact of overexpression. Therefore, the quantitative assessment of the fluorescence images obtained on co-expression of VE-PTP and VE-cadherin constructs indicated a BiFC signal that is due to a specific interaction, rather than self-assembly of the YFP fragments and background fluorescence. However, the disadvantage of the quantitative analyses used in this project is the measurement of whole cell fluorescence as they do not allow for the evaluation of intracellular versus membrane-localised BiFC signal. Nonetheless, the quantitation methods were based on previous BiFC studies by various research groups who used flow cytometry or ImageJ for fluorescence signal quantification (Kodama and Hu, 2010; Sung and Huh, 2010; Wong and O'Bryan, 2011).

The cells were stained with plasma membrane stain to facilitate comparison between images and identification of distinct BiFC signal localisation

patterns. Co-transfection of VE-PTP-VN and VE-cadherin-VC revealed a strong YFP fluorescence that predominantly localised at the plasma membrane as indicated by co-localisation with red plasma membrane stain (overlay image in Figure 33 and Figure 34). The BiFC signal from VE-PTP-VN/SPN-VC, VE-PTP-VN/Myr-VC and SPN-VN/Myr-VC fusion pairs also predominantly localised to the plasma membrane (overlay images in Figures 35-37). However, some BiFC signal was also detected in the cytoplasm, most likely in the endoplasmic reticulum (ER) and Golgi, for all the tested fusion pairs. Although in this study no organelle markers have been used to confirm the BiFC signal co-localisation at the ER and Golgi, the confocal images closely resemble the images from other studies that used BiFC assay to investigate membrane protein-protein interactions. For example, similar results have been demonstrated with receptor tyrosine kinases Anks1a/EphA2 in a BiFC study by Lee *et al* (2016). Most of the BiFC signal was detected in the plasma membrane but some was also present in the ER, which was confirmed by the ER marker. Interestingly a deletion of Anks1a phosphotyrosine binding domain (PTB) resulted in an increased intracellular staining for the Anks1a/EphA2 complex, suggesting that perhaps some domains are not required for the interaction but instead are needed for the correct cellular localisation (Lee *et al,* 2016). A study by Chen *et al* (2006) used the BiFC method to investigate the interaction between membrane proteins Notch2 and amyloid precursor protein (APP) in live cells. They showed that C-terminally truncated Notch2 and APP formed heterodimers that localised to the plasma membrane, ER and Golgi. The co-localisation of BiFC signal at the ER and Golgi was shown using ER CFP and Golgi-DsRed markers.

There are various reasons why the BiFC signal is present in the ER. Some domains may not be required for the interaction but might be needed for cell surface localisation (as in the case of Anks1a/EphA2 mentioned above) and without the required domain proteins would not pass quality control and thus would be retained in ER. The BiFC complex formation may also take place in the ER where the newly synthesised proteins are modified before being translocated to the plasma membrane, thereby bringing the YFP fragments

into close proximity and resulting in a fluorescence signal. Perhaps some fusion proteins are not fully processed to the cell surface and are trapped in the ER, most likely not passing the protein quality control. In addition, some proteins may be retained inactive in the ER and eventually degraded if they are not required. This was shown for the receptor tyrosine kinases (RTKs). If there is a need for high levels of RTKs on the plasma membrane, a cell may direct the ER membranes to rapidly release mature RTKs and send them towards the cell surface (Lee *et al,* 2016). As shown by Nottebaum *et al* (2008) a large fraction of the VE-PTP – containing vesicles co-localised with endocytic vesicles. Comparison with a marker for the endocytic recycling compartment (Rab11) also showed a partial overlap with the staining for VE-PTP. Their results suggested that VE-PTP resides in an endocytic compartment until it is translocated to endothelial cell contacts once the endothelial cell junctions have matured (Nottebaum *et al,* 2008). Further validation would be critical to ensure that these localisation patterns of the bimolecular fluorescent complex are physiologically relevant. To confirm the subcellular localisation of the BiFC signal numerous fluorescent organelle markers, such as KDEL-mCerulean3 fusion protein for ER or VE-cadherin-mApple fusion protein for tight junctions (both from Addgene), can be used. As the subcellular localisation of a protein is often tied to its function the comparison of localisation of full-length VE-PTP fused to the full-length YFP with that of the interaction between VE-PTP and VE-cadherin fused to the N- and C-terminal fragments of YFP would provide some information about the molecular mechanism of VE-PTP/VE-cadherin interaction.

Some proteins have been shown to internalise from the cell surface into internal membrane compartments upon interaction with other proteins, which is an important part of trafficking events in the regulation of cell signalling, receptor turnover and magnitude, duration and nature of signalling events. For example, the internalisation of the endothelial growth factor receptor (EGFR) system upon ligand stimulation has been previously demonstrated (Wilde *et al,* 1999). Epidermal growth factor (EGF) binds to its receptor epidermal growth factor receptor (EGFR),

inducing EGFR dimerisation and intracellular autophosphorylation of key tyrosine residues in the activation loop of its catalytic domain (Schlessinger, 2002). This, in turn, initiates clathrin-mediated internalisation of the EGFR, which is mediated by a RING-finger E3 ubiquitin ligase (Cbl) that binds to activated EGFR, targeting it for endocytosis (Le Roy and Wrana, 2005). Endosomally localised EGFR was shown to associate with many down-stream effectors, such as SH2-domain-containing transforming protein (SHC), leading to the recruitment and activation of signal transduction proteins Ras, Raf, MEK1 and MAPK cascade (Le Roy and Wrana, 2005). EGFR can clearly signal from endosomes, therefore showing that trafficking can control both the nature and magnitude of molecular signalling events. Furthermore VE-cadherin itself was shown to internalise upon interaction with β-arrestin. Interleukin 8 (IL9) stimulation was also shown to induce VE-cadherin internalisation in response to PAK-mediated phosphorylation of S665 on VE-cadherin (Kuppers *et al*, 2014). Therefore, it would be interesting to investigate whether the interaction between VE-PTP and VE-cadherin results in their internalisation.

Protein-protein interactions are essential for cellular functions and the majority of proteins in the cell exist as part of multicomponent assemblies. Experimentally determining and characterising VE-PTP and VE-cadherin binding interface would give a better understanding of the mechanism of their specific recognition and function. It was hypothesised, based on Nawroth *et al* study (2002), that deleting the 17th FNIII-like domain from the ectodomain of VE-PTP would be sufficient to abolish the VE-PTP interaction with VE-cadherin. However, in this study this was not observed and a similar BiFC signal was obtained with both constructs even though VE-PTPΔ17FN-VN was expressed at lower levels than VE-PTP-VN (Figure 31, A and B). One possibility that may account for this is that both constructs were expressed at levels in excess of VE-cadherin (Figure 31, A and B). Another routine possibility that may explain the difference between these findings and the Nawroth *et al* (2002) study is that there are species-dependent differences in the interaction of VE-PTP and VE-cadherin, as in this study the human cDNA

was used and the earlier study used mouse. This seems unlikely given that the human and mouse full-length amino acid sequences are 83% identical and the mechanism of interaction is likely to be conserved. To generate the VE-PTP mutant construct (VEPTPΔ17FN-VN) the 17th FNIII-like domain of VE-PTP was deleted, which brought the 16th FNIII-like domain proximal to the transmembrane domain, whereas the earlier study used either a construct in which FNIII domains 1-16 had been deleted or a construct which expressed only the 17th domain. If the FNIII-like domain proximal to the membrane is the only region involved in interaction between the two molecules, the results obtained in this study would suggest that despite the low sequence identity between the 16th and 17th domains, the 16th domain when artificially moved proximal to the membrane, is able in effect to replace the 17th domain in this position, and as a consequence the interaction is maintained. Alternatively other regions, in addition to the 17th FNIII domain, such as the transmembrane domain, of VE-PTP may be involved in the interaction with VE-cadherin. This may not have been apparent in the co-immunoprecipitation studies with detergent solubilised proteins but is of significance when performing BiFC protein-protein interaction studies in live cells as carried out in this study. There are many examples of membrane proteins forming homo- and hetero-oligomers via transmembrane domains (Strous and Gent, 2002), including receptor-type phosphatases (Tertoolen *et al*, 2001). A study by Tertoolen *et al* (2001) demonstrated that RPTPα dimerises in live cells and that the transmembrane domain alone was sufficient to drive this dimerisation. Interestingly a study by Coon *et al* (2015) showed through immunoprecipitation that VE-cadherin directly interacts with vascular endothelial growth factor receptors (VEGFR) 2 and 3 and that these interactions are mediated by their transmembrane domains (TMDs). Their results suggest that VE-cadherin contributes to the flow signalling pathway downstream of SFKs (Src family kinases) and upstream of PI3K (phosphoinositide 3-kinase) through its role as an adaptor for VEGFRs (Coon *et al,* 2015). This raises a question of whether VE-PTP also contributes to VEGFR signalling since it directly binds to VE-cadherin. Co-precipitation studies by Fachinger *et al* (1999) revealed that VE-PTP does not associate directly with VEGFR2. Nonetheless, these proteins could be

part of a functional complex involved in maintenance of blood vessels and endothelial cell barrier.

Future experiments are required to establish regions of VE-PTP that are involved in interaction with VE-cadherin. The molecular binding interface of VE-PTP and VE-cadherin interaction could be studied by generation of various deletion mutants of VE-PTP to analyse the interaction of VE-cadherin with each of the mutants. Whether the ECD drives the interaction or is required only for the initial contact and whether the TMD maintains the interaction is yet to be determined and further studies are necessary to define the relative roles of the extracellular domain and transmembrane domain in interaction of VE-PTP with VE-cadherin as well as to elucidate the precise mechanism of this interaction.

Dysregulation of PTPs is often associated with many inherited or acquired human diseases and in many cases the immune system is affected (Mustelin *et al,* 2005). Both PTKs and PTPs have been shown to have activating and inhibitory effects and the actions of both types of enzyme are required for a physiological immune response. The role of the adherens junctions and its key proteins VE-PTP and VE-cadherin and the associated signalling events in leukocyte transendothelial migration are not entirely defined. During inflammation leukocytes have to pass from the blood to the surrounding tissue through the endothelial barrier of the blood vessel wall (leukocyte extravasation or diapedesis). It is a multistep process in which many proteins are involved. VE-cadherin has been shown previously to act as a barrier in leukocyte diapedesis but it was also shown that it moves away from endothelial cell contacts to allow leukocyte extravasation. Adhesion molecules ICAM1 (intercellular adhesion molecule 1) and PECAM-1 (platelet endothelial cell adhesion molecule 1) then form a ring-like structure surrounding leukocytes at cell contact sites (Nottebaum *et al,* 2008). Tyrosine phosphorylation was also shown to play a key role in this process and tyrosine phosphorylation of adherens junction proteins has been correlated with the loosening of cadherin-mediated adhesion in various cell types (McLachlan and Yap, 2007). In contrast VE-PTP was shown to be directly implicated in the regulation of endothelial barrier, enhancing the

adhesive function of VE-cadherin and reducing leukocyte extravasation (Nottebaum *et al,* 2008). Broermann *et al* (2011) demonstrated that leukocyte docking and stimulation of endothelial cells with VEGF influence the dissociation of VE-PTP from VE-cadherin *in vivo*, resulting in the opening of the endothelial cell contacts and in increased leukocyte extravasation. The results of previous studies indicate that the VE-PTP makes an attractive candidate as a novel therapeutic target for the treatment of pathological vascular permeability and inflammation. Therefore it is essential to elucidate its physiological function, its substrates, regulation and its importance in physiological processes.

4.9 Conclusion

The quantitative data show that the BiFC signal obtained from HEK293T cells co-expressing VE-PTP-VN/VE-cadherin-VC and VE-PTP∆17FN-VN/VE-cadherin-VC was not due to non-specific YFP-fragments interactions in the plasma membrane since the negative control fusion pairs showed a significantly reduced BiFC signal even though they were expressed at much higher levels compared with positive interaction pairs. Therefore, based on these findings it can be concluded that VE-PTP and VE-cadherin have the potential to interact together via their extracellular domains. In addition, the 17^{th} FNIII-like domain of VE-PTP is not the only domain required for the interaction and the removal of this domain did not abolish the interaction with VE-cadherin. Further work is required to determine the molecular interface of VE-PTP and VE-cadherin interaction.

Chapter 5

Investigation of a potential interaction between DEP-1, SAP-1 and GLEPP1 and VE-cadherin in live cells

5.1 Introduction

Originally the sequences of receptor-type protein tyrosine phosphatases (RPTP) cytoplasmic domains were thought to be highly conserved and ectodomains more divergent between different subgroups. Further, the extracellular domains within each subgroup were thought to be homologous (for the PTPs classification refer to Figure 3) and, thus, it was suggested that members within a subgroup would share similar receptor functions. The four members of the R3 RPTP subgroup, namely VE-PTP, DEP-1, SAP-1 and GLEPP1 share structural homology of their extracellular domains, which are comprised solely of long chains of FNIII-like repeats (Tonks, 2006). However, the number of such repeats varies (Chapter 1, Figure 4). It was previously suggested that extracellular domains of R3 RPTPs could be involved in *cis*- and *trans*-interactions with extracellular domains of other receptors (e.g. RTKs) and ligands, although this has not been demonstrated in most cases (Jeon and Zinn, 2015). Most of the known substrates for the R3 RPTPs are receptor tyrosine kinases (RTKs) and Src family kinases but their interaction occurs via cytoplasmic (i.e. catalytic) domains (Jeon and Zinn, 2015). Thus the function of the extracellular domains of the R3 RPTPs is not fully understood. Co-immunoprecipitation studies by Nawroth *et al* (2002) showed that VE-PTP directly interacts with VE-cadherin via their extracellular domains (ECD). Their interaction via ECD in live cells was addressed in this project as described in Chapter 4 and it was found that VE-PTP and VE-cadherin do have the potential to interact via their extracellular domains in live cells and that the 17th FNIII-like domain of VE-PTP is not the only domain required for this interaction. Here I aimed to investigate whether other R3 RPTPs, in addition to VE-PTP, have the potential to interact with VE-cadherin, which could provide insight into the specificity and/or molecular basis of interactions with VE-PTP.

Although extracellular ligand binding has not been defined yet for all the members of R3 RPTP subgroup, some members were shown to interact with their ligands or co-receptors via their extracellular domains. DEP-1 was shown to interact with Syndecan-2. As was shown by Whiteford *et al* (2011)

DEP-1 and Syndecan-2 associate through their N-terminal extracellular parts and this interaction plays a key role in fibroblast adhesion to Syndecan-2. Affinity purification and mass spectrometry studies by Takahashi *et al* (2012) have revealed another putative ligand, a trimeric glycoprotein Thrombospondin-1 (TSP1), that binds with a high affinity and specificity to the extracellular domain of the DEP-1 in endothelial cells. Transfection experiments confirmed this association as the deletion of the DEP-1 extracellular domain abolished the interaction with TSP1 (Takahashi *et al*, 2012). The binding of the TSP1 appears to increase the catalytic activity of DEP-1 as the dephosphorylation of the DEP-1 substrates, EGFR and ERK1/2, was increased upon treatment of DEP-1 transfected cells with TSP1, which resulted in the inhibition of the endothelial cell proliferation. Interestingly, though, the TSP1 is synthesised by endothelial cells in response to injury or growth factors and thus it is likely that TSP1 acts as a ligand for DEP-1 in pathological conditions (Takahashi *et al*, 2012). The same experiments revealed that other members of R3 RPTPs did not interact with TSP1 despite having homologous extracellular domains (Takahashi *et al*, 2012). On the other hand, co-immunoprecipitation studies by Murata *et al* (2015) revealed that mouse SAP-1 associates with a transmembrane protein CEACAM20 (Carcinoembryonic Antigen-Related Cell Adhesion Molecule 20). What is more, the SAP-1 and CEACAM20 appeared to form a complex via their extracellular domains, resulting in dephosphorylation of the CEACAM20 and attenuating the CEACAM20-induced IL-8 production and thus regulating intestinal immunity (Murata *et al*, 2015). However, it is not known whether this is also the case with the human SAP-1. Co-immunoprecipitation studies by Kim *et al* (2010) showed that mouse GLEPP1 associates with extracellular cell-cell signalling molecules Wnt (Wnt-3a and Wnt1) but only when the ECD of GLEPP1 is present. The interaction of mouse GLEPP1 with Wnt via its extracellular domain resulted in inhibition of Wnt/β-catenin signalling (Kim *et al*, 2010). The activation of this signalling pathway has been linked to several human cancers (Cadigan, 2008). Therefore, GLEPP1 has been suggested to act as a tumour suppressor by inhibiting Wnt/β-catenin signalling pathway through interaction with Wnt ligand. However, whether human GLEPP1 also associates with Wnt

or it interacts with any other ligands via its extracellular domain had not been tested to date.

R3 RPTP members are comprised of repetitive fibronectin like III repeats in their extracellular domains, the physiological role of which has not been fully defined yet. Numerous studies indicate that the extracellular domain could be involved in interaction with substrates or ligands but the molecular basis of these interactions is not entirely understood. Since the members of this subfamily share similar extracellular structures, it has been proposed that they share similar physiological functions. This gives rise to some questions. Do all the R3 RPTP members have the potential to interact with the same ligands via their extracellular domains? What role does the extracellular domain of R3 RPTPs play in substrate specificity? Therefore, the purpose of this chapter was to investigate whether DEP-1, SAP-1 and GLEPP1 also have the potential to interact with VE-cadherin via their extracellular domains in living cells using bimolecular fluorescence complementation (BiFC) assay in transiently transfected HEK293T. The principle of the BiFC assay is described in Chapter 4.

To determine the specificity and efficiency of BiFC complementation two negative controls were generated: sialophorin (SPN) and either C- or N-terminal fragment of a Venus YFP anchored to the plasma membrane via the membrane association sequence from Lck (lymphocyte-specific protein tyrosine kinase), Myr-VC and Myr-VN respectively. The rationale for using these controls and their generation is described in Chapter 4.

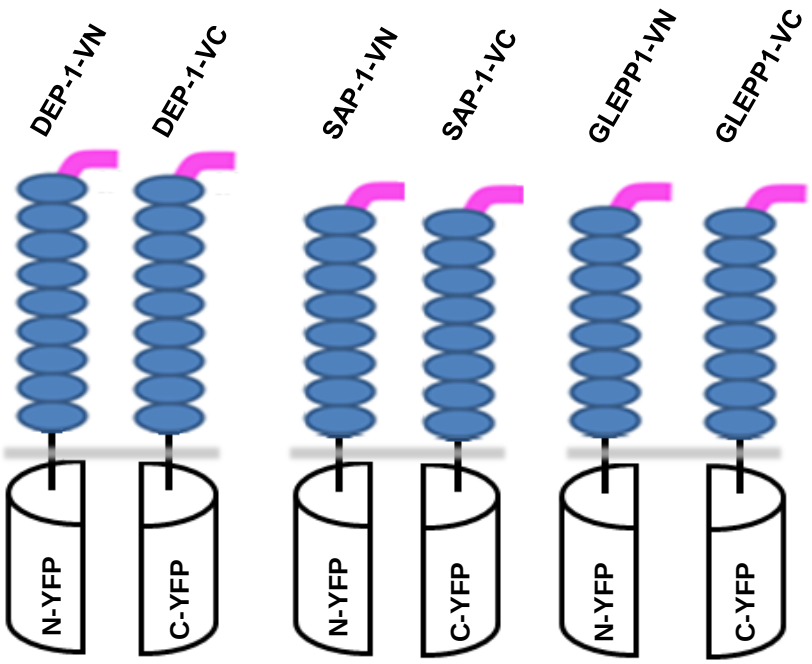

Figure 47. Schematic representation of BiFC fusion proteins. DEP-1, SAP-1 and GLEPP1 consist of multiple extracellular fibronectin III-like repeats (blue) and a transmembrane domain. The intracellular protein tyrosine phosphatase domain (PTP) was removed. The constructs DEP-1-VN, SAP-1-VN and GLEPP1-VN have a modified N-terminal sequence of the Venus protein (a yellow fluorescent protein (YFP) variant. The constructs DEP-1-VC, SAP-1-VC and GLEPP1-VC have a modified C-terminal sequence of YFP. The YFP fragments are represented by a half cylinder inserted five residues after the transmembrane domain. Constructs containing N-terminal YFP had a myc-tag (pink) and constructs containing C-terminal YFP had a HA-tag (both represented by a pink line) inserted after the signal peptide to facilitate analysis of expression.

5.2 Results

5.2.1 Cloning fusion proteins

The constructs used in this study DEP-1, SAP-1 and GLEPP1, shown diagrammatically in Figure 47, consist of residues 1-996 of DEP-1, 1-775 of SAP-1 and 1-843 of GLEPP1, with either the modified N- or C-terminal sequence of vYFP inserted five residues after the transmembrane domain and a flexible linker sequence, as used by Kodama & Hu (2010). This approach essentially replaced the intracellular region of these proteins with non-fluorescent fragments of vYFP enabling investigation of protein-protein interactions that involve only the extracellular and transmembrane domains.

DEP-1, SAP-1 and GLEPP1 fusion constructs were generated as outlined in the schema in Chapter 2 (Figure 8). For the DEP-1-VN, SAP-1-VN and GLEPP1-VN synthetically generated signal peptides and myc tag (EQKLISEEDL) fragment (Genscript) were inserted into *Apa*I/*Xho*I restriction sites of pBiFC-VN155(I152L) vector. The presence of the correct DNA insert was determined by screening bacterial colonies by PCR using Bioline Red Taq with a combination of vector-specific and insert-specific primers (Table 11). PCR products were analysed on agarose gel (Figure 48). The extracellular and transmembrane (ECD+TM) domains of DEP-1, SAP-1 and GLEPP1 constructs were amplified by PCR using Platinum *Pfx* polymerase. The PCR products corresponded to the predicted sizes of 2934 bp, 2295 bp and 2493 bp for DEP-1, SAP-1 and GLEPP1 respectively (Figure 49). The primers used for the generation of the transmembrane and extracellular domains are listed in Table 10 and the PCR conditions are provided in Table 4 (Chapter 2). The resulting PCR product was purified, digested and subsequently inserted into *Xho*I restriction site of the pBiFC-VN155(I152L) vector, which contained signal peptide and myc tag. Colony PCR was used to confirm the correct orientation of the insert to ensure that a fusion protein fused to the N-terminal part of YFP had been generated (Figure 50).

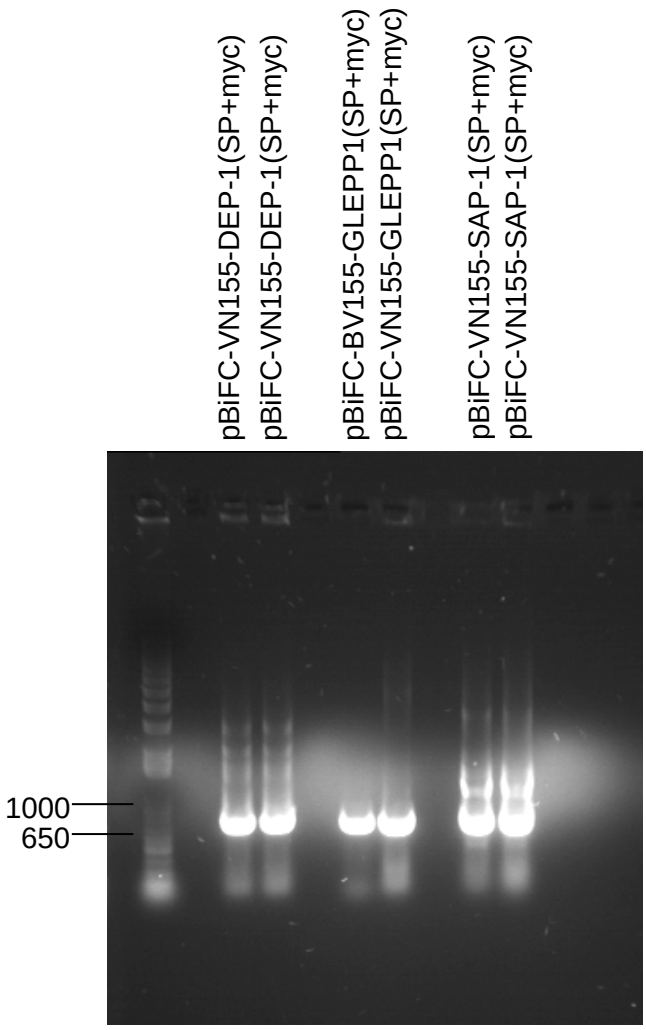

Figure 48. Colony PCR analysis. Synthetically generated signal peptides of DEP-1, GLEPP1 and SAP-1 with the myc tag were ligated into *Apa*I/*Xho*I restriction sites of the pBiFC-VN155(I152L) vector. Colony PCR was performed with vector-specific and insert-specific primers to screen for successful ligation. The DNA band of 712 bp corresponds to the predicted size of DEP-1 signal peptide and myc tag inserted into a pBiFC-VN155(I152L) vector. The DNA band of 691 bp corresponds to the predicted size of GLEPP1 signal peptide and myc tag inserted into a pBiFC-VN155(I152L) vector. The DNA band of 685 bp corresponds to the predicted size of SAP-1 signal peptide and myc tag inserted into a pBiFC-VN155(I152L) vector.

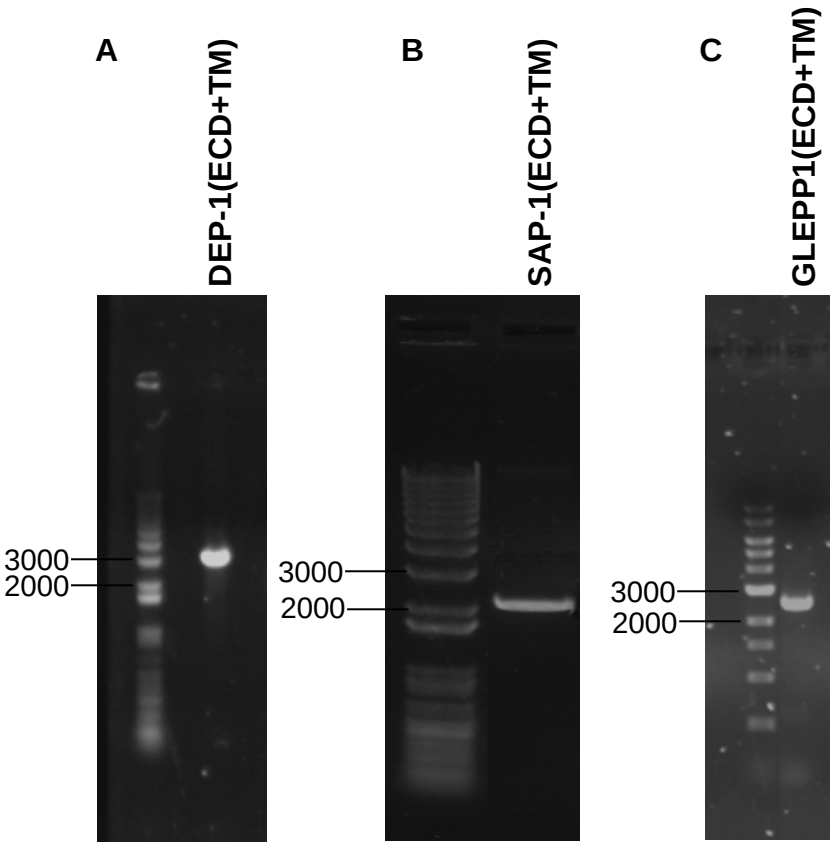

Figure 49. The generation of transmembrane and extracellular domains of DEP-1, SAP-1 and GLEPP1 by PCR. Electrophoresis on 0.8% (w/v) agarose gel showing DNA bands corresponding to expected ECD+TM sizes for each construct: A) 2934 bp band for ECD+TM of DEP-1, B) 2295 bp DNA band for ECD+TM of SAP-1 and C) 2493 bp for ECD+TM of GLEPP1. Running time was 35 minutes at 110 V constant.

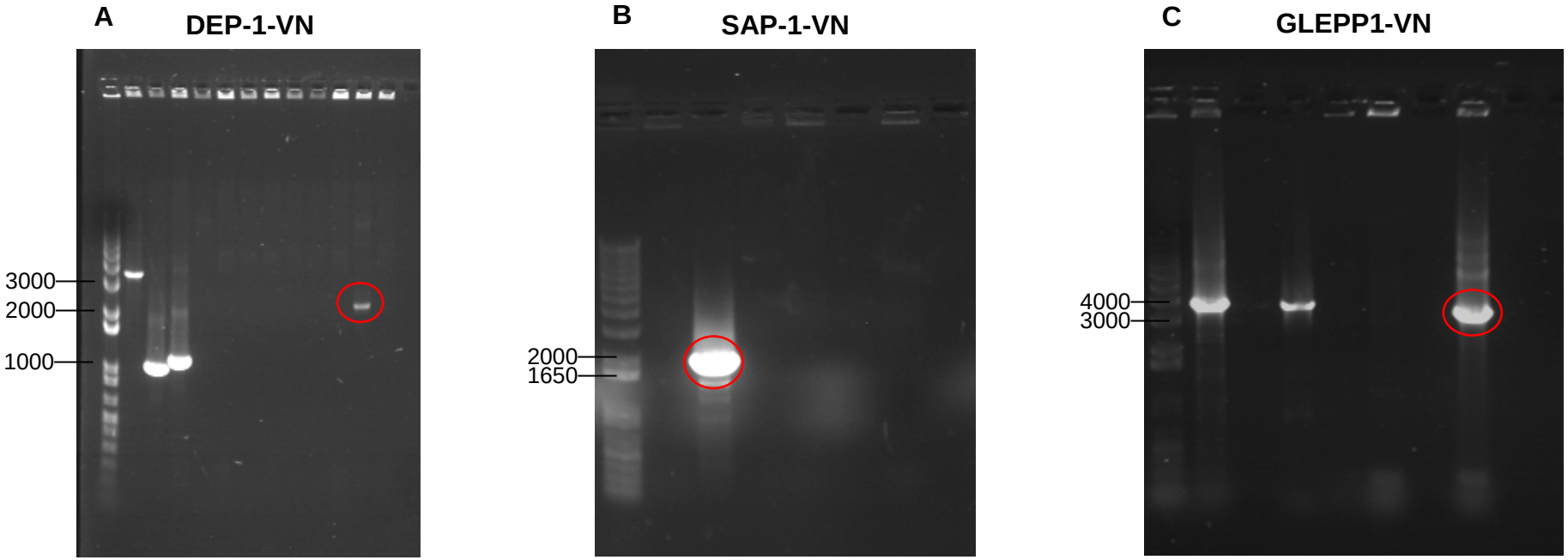

Figure 50. Colony PCR to screen for successful ligation of ECD+TM domains of DEP-1, SAP-1 and GLEPP1 into pBiFC-VN155 expression vectors. Following ligation and transformation colony PCR was performed with vector-specific and insert-specific primers to screen for successful ligation. (A) The DNA band corresponds to the predicted size of 2453 bp of the DEP-1 ECD+TM inserted into a pBiFC-VN155 expression vector. (B) The DNA band corresponds to the predicted size of 2164 bp of the SAP-1 ECD+TM inserted into a pBiFC-VN155 expression vector. (C) The DNA band corresponds to the predicted size of 3184 bp of the GLEPP1 ECD+TM inserted into a pBiFC-VN155 expression vector.

C-terminal YFP fragment fusions were generated in essentially the same way as N-terminal YFP fragment fusions. To generate DEP-1-VC, SAP-1-VC and GLEPP1-VC fusion constructs a synthetically generated signal peptide and HA tag fragment (Genscript) was inserted into *Apa*I/*Xho*I restriction sites of pBiFC-VC155 vector. The successful ligation was confirmed by PCR, using vector- and insert-specific primers, and analysed on agarose gel (Figure 51). The primers used for the Colony PCR are listed in Table 11 (Chapter 2). The previously generated ECD+TM domains of DEP-1, SAP-1 and GLEPP1 were digested with *Xho*I restriction enzyme, purified and ligated into the pBiFC-VC155 vector, containing corresponding signal peptide and HA tag, to create a fusion protein fused to the C-terminal part of YFP. Colony PCR was used to confirm the correct orientation of the insert, using either vector specific primers or a combination of vector and insert specific primers (Figure 52). The primers used for the Colony PCR are listed in Table 11 (Chapter 2).

Although each construct was generated as an N- and C-terminal fusion, only the N-terminal fusion constructs were used in combination with either VE-cadherin-VC, SPN-VC or Myr-VC in order to keep all the conditions and parameters of each experiment constant. The generation process of the VE-cadherin-VC fusion construct as well as negative control fusion constructs (SPN-VC and Myr-VC) is shown in Chapter 4.

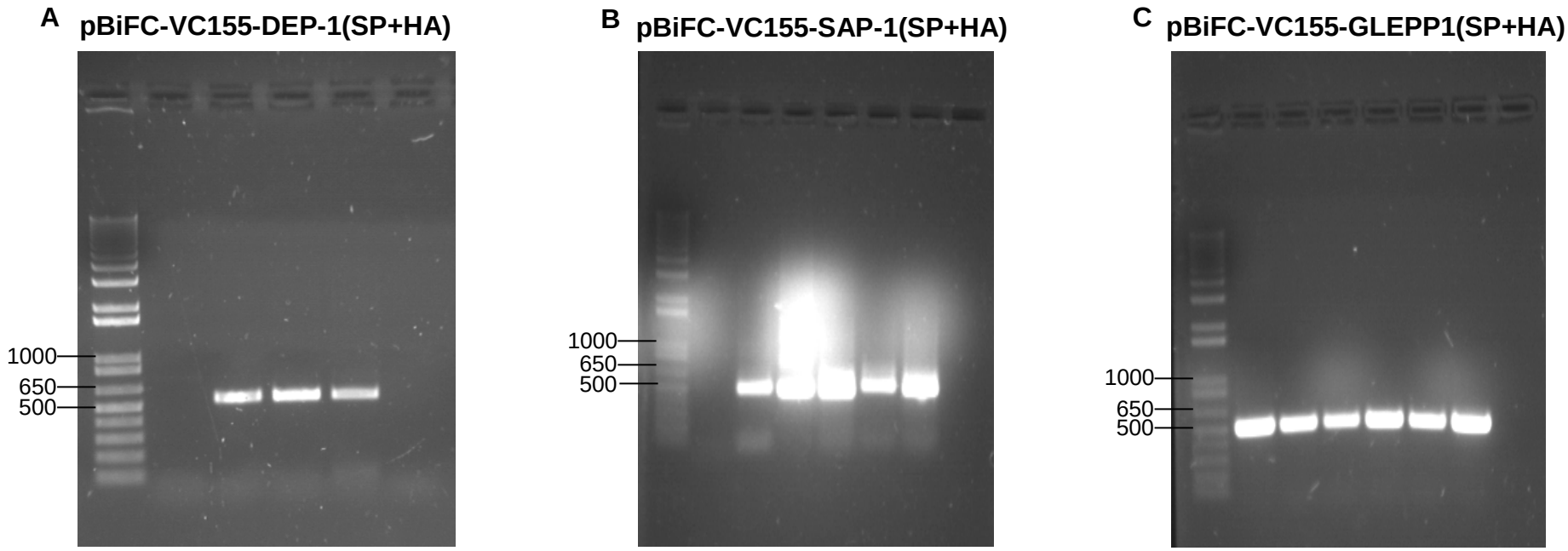

Figure 51. Colony PCR analysis to screen for successful ligation of signal peptide and HA tag of DEP-1, SAP-1 and GLEPP1 into pBiFC-VC155 expression vectors. Synthetically generated signal peptides of DEP-1, SAP-1 and GLEPP1 with the HA tag were ligated into *ApaI/XhoI* restriction sites of the pBiFC-VC155 vector. Colony PCR was performed with vector-specific and insert-specific primers to screen for successful ligation. A) The DNA band of 514 bp corresponds to the predicted size of DEP-1 signal peptide and HA tag inserted into a pBiFC-VC155 vector. B) The DNA band of 490 bp corresponds to the predicted size of SAP-1 signal peptide and HA tag inserted into a pBiFC-VC155 vector. C) The DNA band of 475 bp corresponds to the predicted size of GLEPP1 signal peptide and HA tag inserted into a pBiFC-VC155 vector.

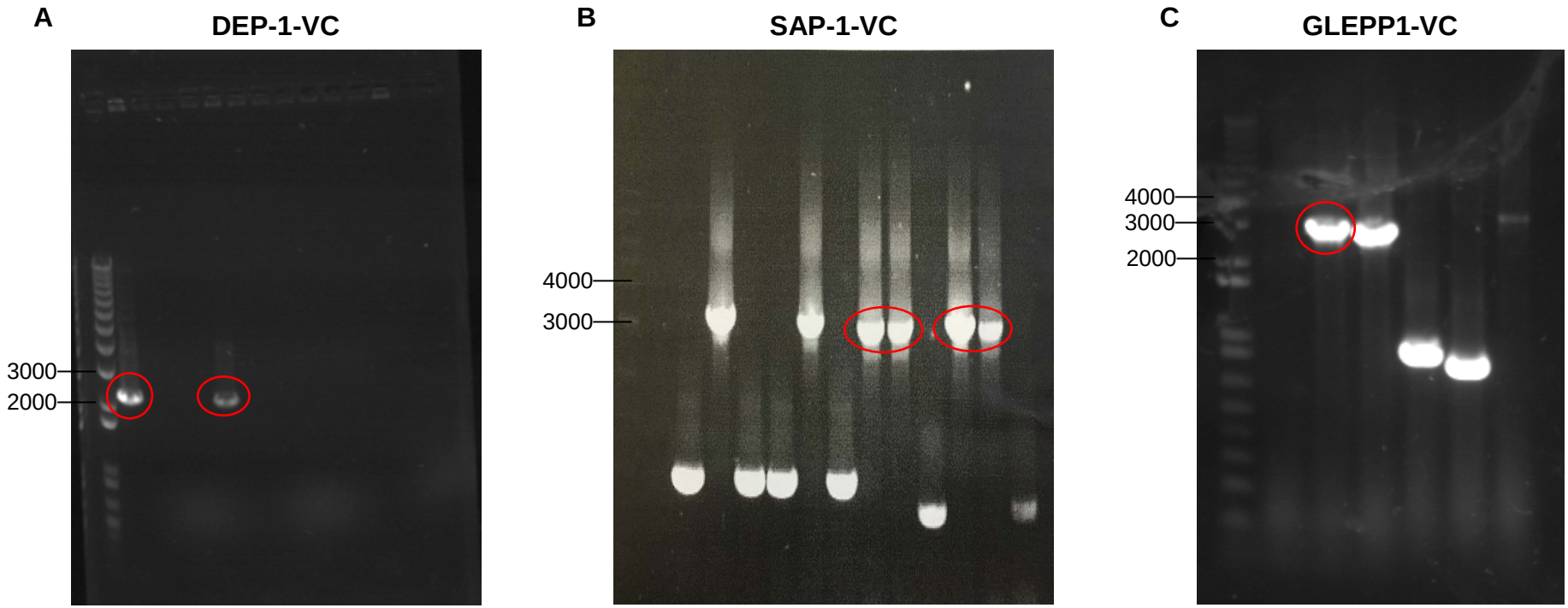

Figure 52. Colony PCR to screen for successful ligation of ECD+TM of DEP-1, SAP-1 and GLEPP1 into pBiFC-VC155 expression vectors. Following ligation and transformation colony PCR was performed with vector-specific and insert-specific primers to screen for successful ligation. (A) The DNA band corresponds to the predicted size of 2264 bp of the DEP-1 ECD+TM inserted into a pBiFC-VC155 expression vector. (B) The DNA band corresponds to the predicted size of 3125 bp of the SAP-1 ECD+TM inserted into a pBiFC-VC155 expression vector. (C) The DNA band corresponds to the predicted size of 2968 bp of the GLEPP1 ECD+TM inserted into a pBiFC-VC155 expression vector.

5.3 Western Blot analysis of BiFC fusion proteins in HEK293T cells

Western blotting of lysates from transiently transfected HEK293T cells confirmed the expression of all the fusion proteins close to their predicted molecular weight (Figure 53). Western blotting with anti-myc antibody for the DEP-1-VN, SAP-1-VN and GLEPP1-VN, which have a myc-tag inserted following the signal peptide sequence, detected two bands for each protein. For DEP-1-VN the bands with a molecular weight of approximately 180 kDa and 240 kDa were detected (Figure 53, A). For SAP-1 the bands with a molecular weight of approximately 160 kDa and 220 kDa were detected (Figure 53, A). For GLEPP1 the bands with a molecular weight of approximately 160 kDa and 230 kDa were detected (Figure 53, A). The bands for GLEPP1 appeared lighter compared with other fusion proteins on the same blot (Figure 53, A). The Western blot was repeated for the GLEPP1 fusion construct, producing the same result (Figure 53, C). The predicted molecular weights for DEP-1-VN, SAP-1 and GLEPP1 were 107 kDa, 84 kDa and 95 kDa respectively. The discrepancy in molecular weight is probably accounted for by extensive glycosylation. A study by de la Fuente *et al* (1998) confirmed that DEP-1 is highly glycosylated. Western blot analysis of DEP-1 before and after the treatment with N-linked deglycosylation enzyme N-glycosidase F detected the shift in molecular weight from 240 kDa to about 160 kDa. The treatment with O-linked deglycosylation enzyme O-Glycanase also resulted in decreased molecular weight of about 200 kDa. These results showed that the molecular weight of DEP-1 was modified by extensive glycosylation (de la Fuente *et al*, 1998). It has been previously shown that SAP-1 and GLEPP1 have 24 and 15 potential N-linked glycosylation sites respectively (Matozaki *et al*, 1994; Thomas *et al*, 1993). Western blot analyses carried out by Matozaki *et al* (1994) detected a band for SAP-1 with molecular weight of 200 kDa instead of the predicted 120 kDa. Western blot analyses of GLEPP1 from a study by Thomas *et al* (1993) also detected a higher molecular weight band of 235 kDa compared with predicted 132 kDa. In both studies the differences were accounted for by extensive glycosylation.

The double bands for DEP-1, SAP-1 and GLEPP1 could possibly represent differentially glycosylated forms of these proteins. Interestingly the higher molecular weight bands (~220 kDa) of each protein appear to be less prominent and could be due to some non-specific antibody binding.

Western blotting with anti-HA antibody for the DEP-1-VC, SAP-1-VC and GLEPP1-VC, which have a HA-tag inserted following the signal peptide sequence, detected bands with molecular weight of approximately 180, 160 and 150 kDa respectively (Figure 53, B and D). Similar to anti-myc blots the molecular weights were much higher than predicted, probably due to post-translational modification of these proteins. Both GLEPP1-VN and GLEPP1-VC fusion proteins were expressed at lower levels compared with all other fusion proteins (Figure 53, A-D). The expression of control fusion proteins SPN-VN, SPN-VC, Myr-VN and Myr-VC was shown and discussed in Chapter 4, section 4.3.

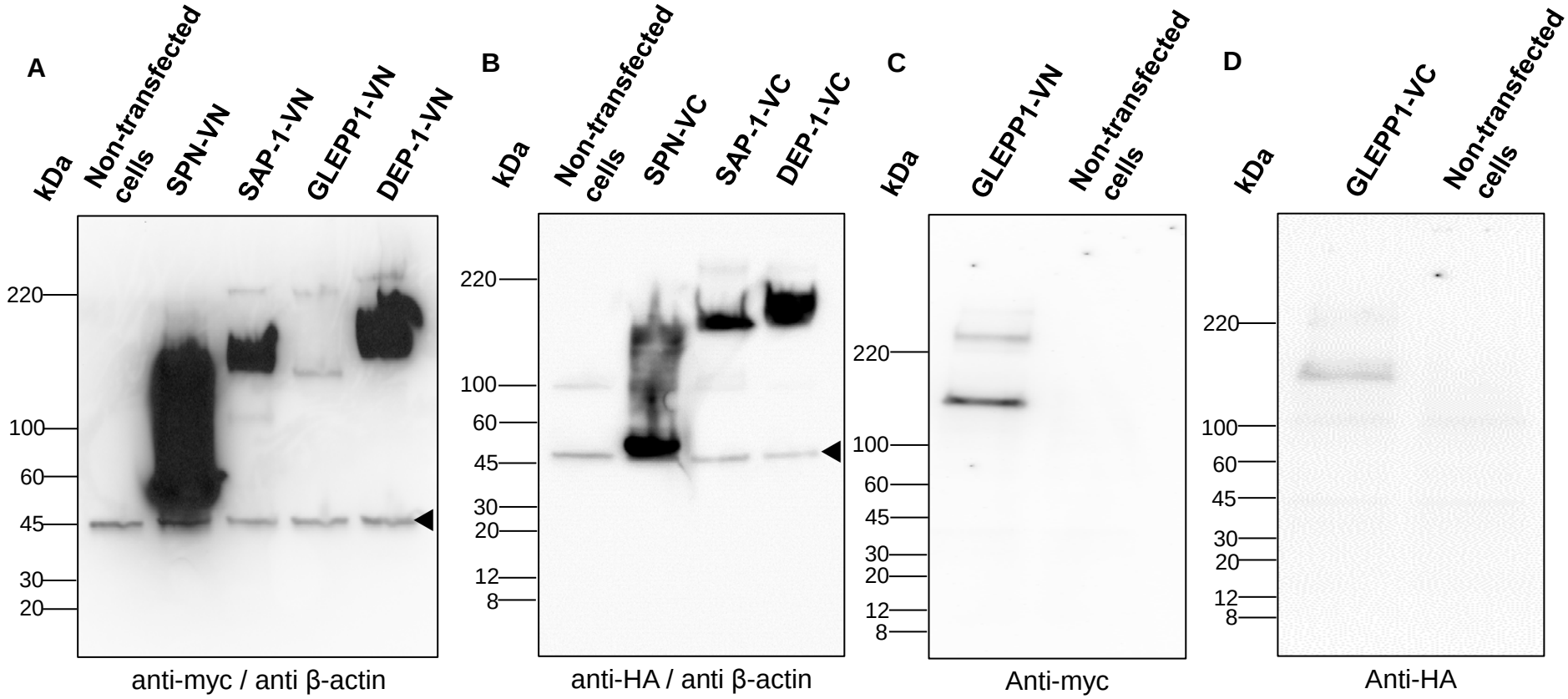

Figure 53. Protein expression analysis by Western blot. Western blotting of cell lysates from transfected HEK293T cells with either anti-myc or anti-HA antibody confirmed the expression of the constructs at close to expected molecular weight. β-actin (◀) was used as a loading control in some blots.

5.4 Investigation of DEP-1, SAP-1 and GLEPP1 interactions with VE-cadherin in live cells using the BiFC technique

To investigate whether DEP-1, SAP-1 and GLEPP1 could have the potential to interact with VE-cadherin via their extracellular domains in live cells, in a similar manner to VE-PTP, the BiFC DEP-1-VN, SAP-1-VN and GLEPP1-VN fusion proteins were generated as described above (section 5.2.1). Each fusion protein was co-expressed with VE-cadherin-VC in HEK293T cells and 24 hours post-transfection stained prior to confocal visualisation with CellMask^{TM} Plasma Membrane Stain (as detailed in method section 2.5.6). All the transfection conditions and parameters of confocal analyses were kept constant for all the experiments.

Co-expression of all three DEP-1-VN/VE-cadherin-VC, SAP-1-VN/VE-cadherin-VC and GLEPP1-VN/VE-cadherin-VC fusion pairs resulted in the occurrence of BiFC fluorescence (Figures 54, 57 and 60). For each fusion pair the comparison of the sub-cellular localisation of the Venus YFP signal with that of the CellMask deep red plasma stain indicated that the fluorescence complementation signal was detected in the plasma membrane and intracellular structures, likely to be the endoplasmic reticulum or Golgi, of co-transfected cells (Figures 56, 59 and 62).

In order to establish that the BiFC signal resulted from the interaction of DEP-1-VN/VE-cadherin-VC, SAP-1-VN/VE-cadherin-VC and GLEPP1-VN/VE-cadherin-VC fusion pairs and was not due to the non-specific assembly of YFP fragments, the R3 RPTP fusion constructs were co-expressed with each control construct. The co-expression of DEP-1-VN with either SPN-VC or Myr-VC both resulted in a BiFC fluorescence signal (Figure 55, A and B). However, the qualitative assessment of the images suggested that DEP-1-VN with a negative control construct SPN-VC appeared to exhibit a slightly reduced fluorescence signal and the number of fluorescent cells compared with the DEP-1-VN and VE-cadherin-VC fusion pair (Figures 54 and 55 (A)). In addition, the fluorescence signal that resulted from the interaction of negative fusion pairs appeared to be localised more in the cytoplasm and not in the plasma membrane. The cells co-expressed with

DEP-1-VN and Myr-VC appeared to exhibit a greater reduction in fluorescence signal compared with DEP-1-VN/VE-cadherin-VC and with DEP-1-VN/SPN-VC fusion pairs (Figures 54 and 55). The qualitative analyses of confocal images show that, similar to DEP-1-VN, SAP-1-VN and GLEPP1-VN also formed fewer complexes when co-expressed with either negative control than they did with VE-cadherin-VC. The BiFC signal resulting from the SAP-1-VN/SPN-VC complex assembly appeared to be weaker than the BiFC signal resulting from the SAP-1-VN/VE-cadherin-VC combination (Figures 57 and 58 (A)). The SAP-1-VC/Myr-VC combination appeared to result in even greater reduction of fluorescence signal compared with SAP-1-VN/VE-cadherin-VC and with SAP-1-VN/SPN-VC combinations (Figures 57 and 58). The same results were observed with the GLEPP1-VN fusion protein. The BiFC fluorescence signal appeared to be reduced when GLEPP1-VN was co-expressed with SPN-VC compared with the BiFC signal resulting from GLEPP1-VN/VE-cadherin co-expression (Figures 60 and 61 (A)). When GLEPP1-VN was co-expressed with Myr-VC the fluorescence signal appeared to be even more reduced compared with co-expression of either GLEPP1-VN/VE-cadherin-VC or GLEPP1-VN/SPN-VC fusion pairs (Figures 60 and 61 (B)). As with VE-PTP-VN and VE-cadherin co-expression (discussed in Chapter 4) the BiFC signal resulting from all the fusion pairs tested in this chapter was predominantly detected at the plasma membrane with some fluorescence in ER and Golgi (Figures 54, 55, 57, 58, 60 and 61). This was also confirmed by the co-localisation analysis of the fluorescence signals from BiFC and CellMask red plasma membrane stain (Figures 56, 59 and 62).

The qualitative results described in this chapter show that the BiFC signals for a given protein complex are difficult to interpret and a more robust quantitative analysis is required. Although the fluorescence signal with control fusion proteins appeared to be reduced it is difficult to conclude whether there is any significant difference in fluorescence intensity. In addition, the confocal images presented in Figures 54-61 are only the representatives and the number of cells exhibiting the BiFC signal and its intensity vary throughout randomly acquired images.

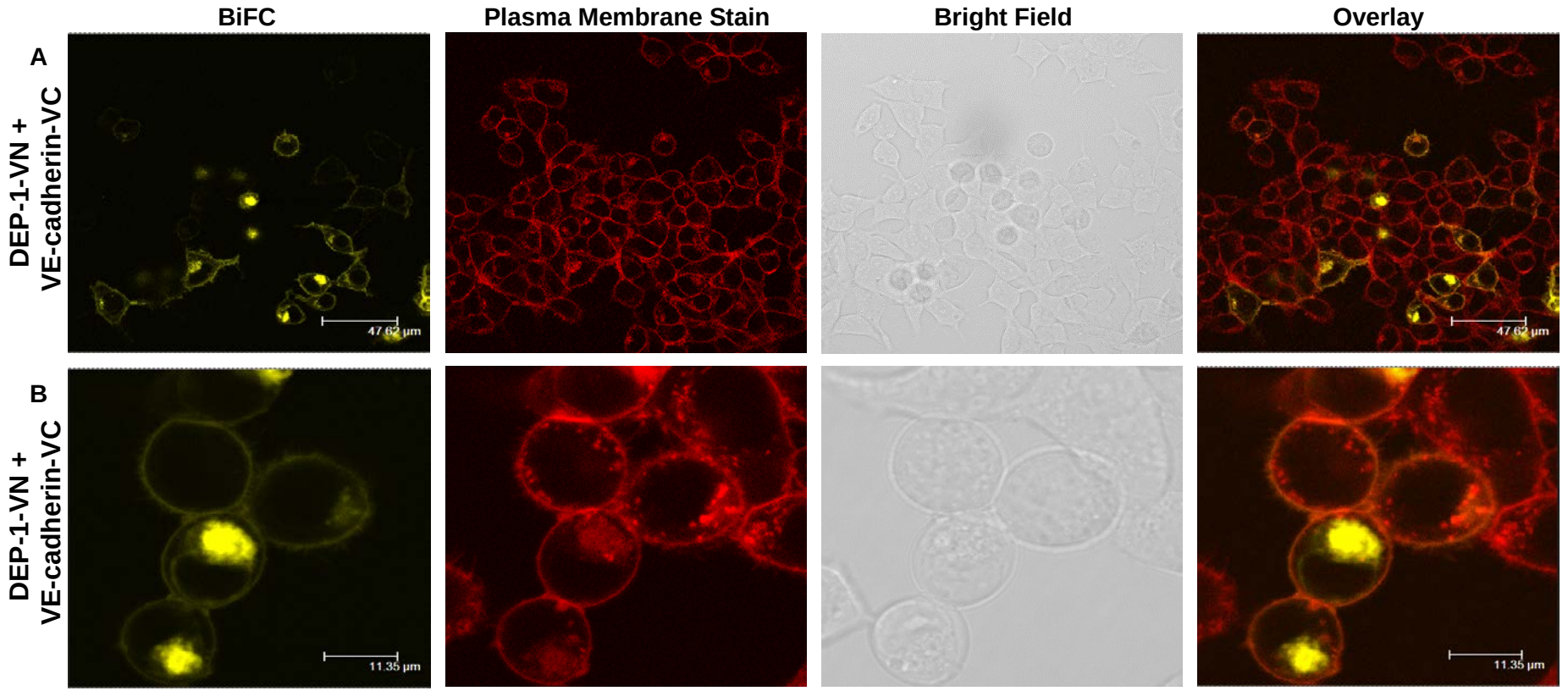

Figure 54. BiFC analysis of interaction between DEP-1-VN and VE-cadherin-VC. To investigate the potential interaction between DEP-1-VN and VE-cadherin-VC equal amounts of expression vectors encoding DEP-1-VN and VE-cadherin-VC were co-transfected into HEK293T cells and the resulting BiFC signal was analysed by confocal microscopy after 24 hours. (A) Confocal images of DEP-1-VN/VE-cadherin-VC interactions in cell populations. (B) Zoom in of HEK293T cells, showing the localisation of DEP-1-VN/VE-cadherin-VC interactions.

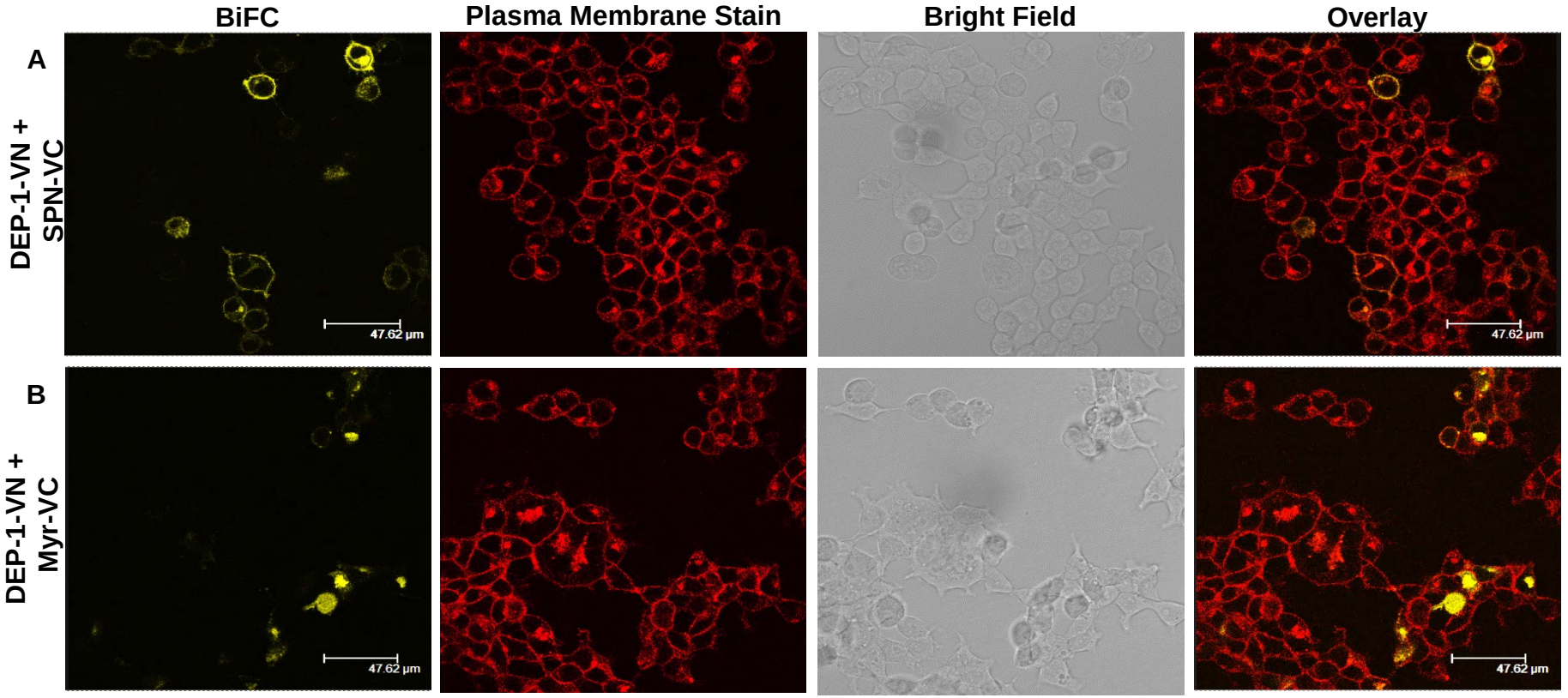

Figure 55. BiFC analysis of DEP-1-VN with control constructs SPN-VC and Myr-VC. To validate the specificity of the DEP-1-VN and VE-cadherin-VC interaction, DEP-1-VN was co-transfected with equal amounts of negative control constructs SPN-VC and Myr-VC into HEK293T cells and the resulting BiFC signal was analysed by confocal microscopy after 24 hours. (A) Confocal images of DEP-1-VN/SPN-VC interactions in cell populations. (B) Confocal images of DEP-1-VN/Myr-VC interactions in cell populations.

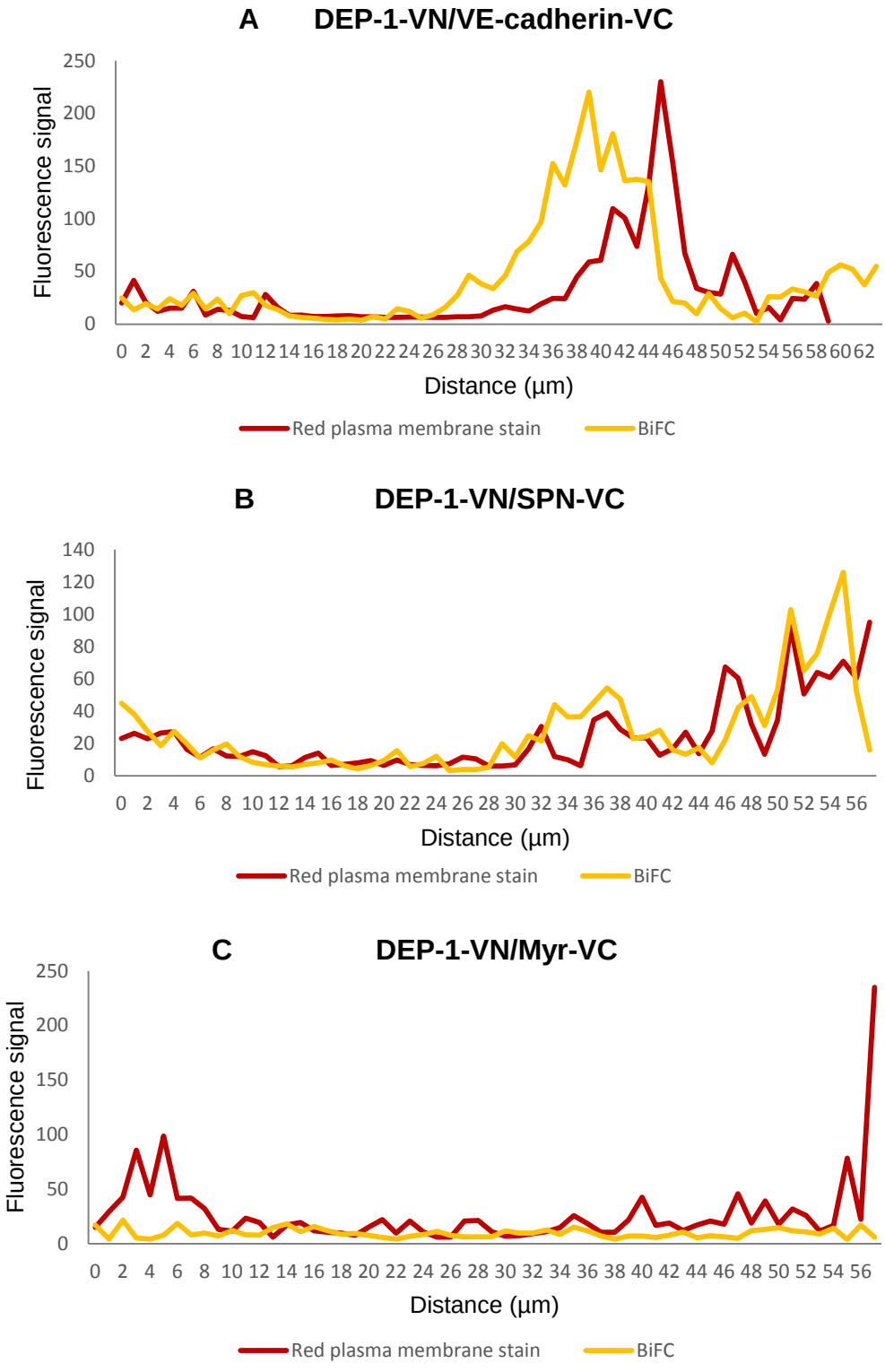

Figure 56. Co-localisation analysis of fluorescence signals across a single cell from the BiFC and the red plasma mambrane stain channels. (**A**) DEP-1-VN/VE-cadherin-VC. (**B**) DEP-1-VN/SPN-VC. (**C**) DEP-1-VN/SPN-VC.

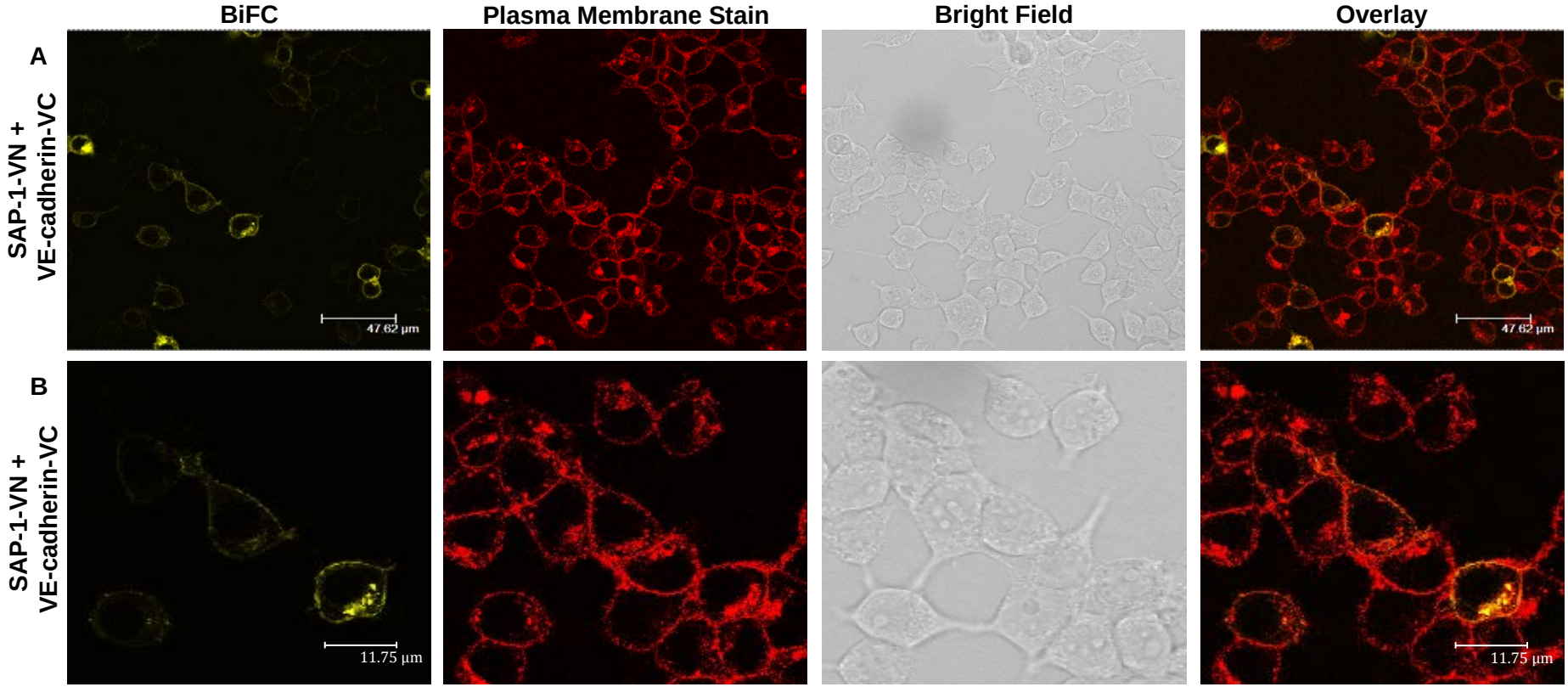

Figure 57. BiFC analysis of interaction between SAP-1-VN and VE-cadherin-VC. To investigate the potential interaction between SAP-1-VN and VE-cadherin-VC equal amounts of expression vectors encoding SAP-1-VN and VE-cadherin-VC were co-transfected into HEK293T cells and the resulting BiFC signal was analysed by confocal microscopy after 24 hours. (A) Confocal images of SAP-1-VN/VE-cadherin-VC interactions in cell populations. (B) Zoom in of HEK293T cells, showing the localisation of SAP-1-VN/VE-cadherin-VC interactions.

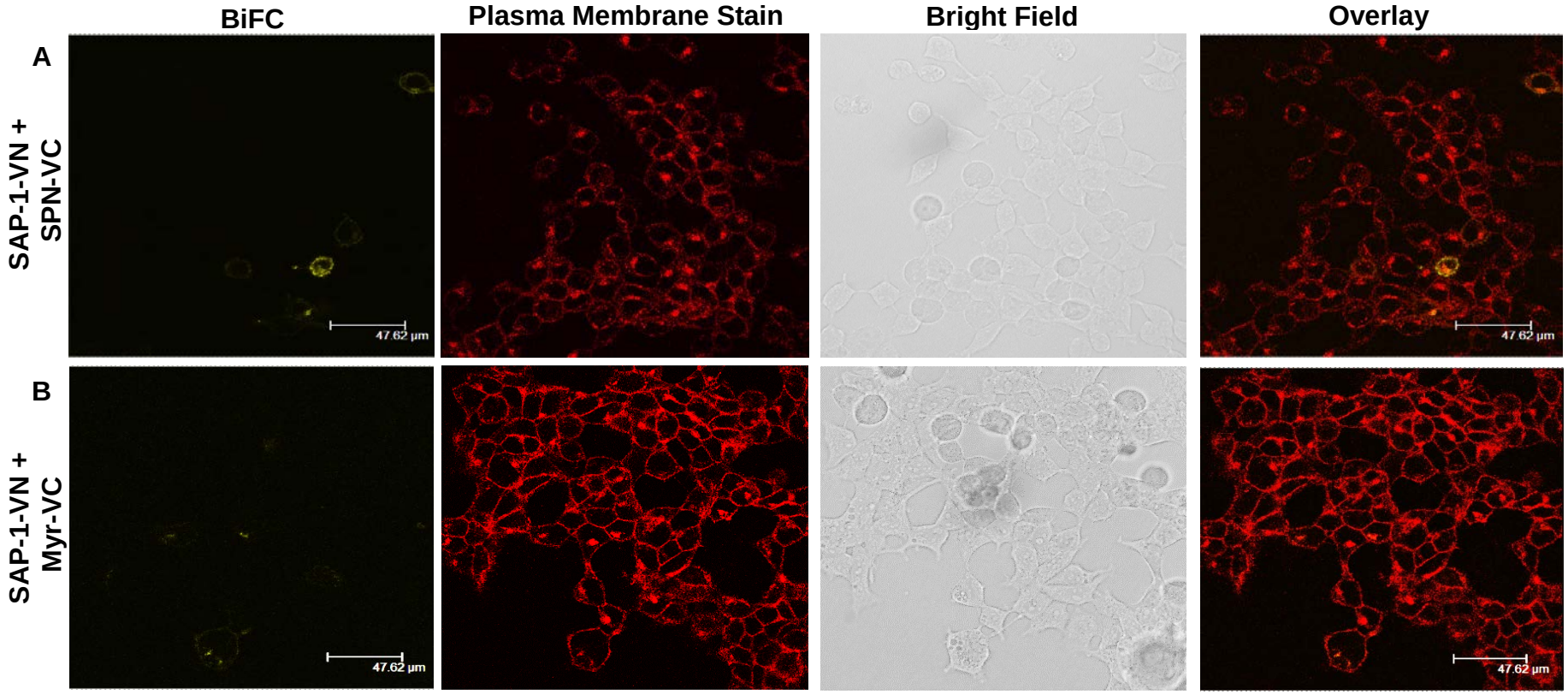

Figure 58. BiFC analysis of SAP-1-VN with control constructs SPN-VC and Myr-VC. To validate the specificity of the SAP-1-VN and VE-cadherin-VC interaction, SAP-1-VN was co-transfected with equal amounts of negative control constructs SPN-VC and Myr-VC into HEK293T cells and the resulting BiFC signal was analysed by confocal microscopy after 24 hours. (A) Confocal images of SAP-1-VN/SPN-VC interactions in cell populations. (B) Confocal images of SAP-1-VN/Myr-VC interactions in cell populations.

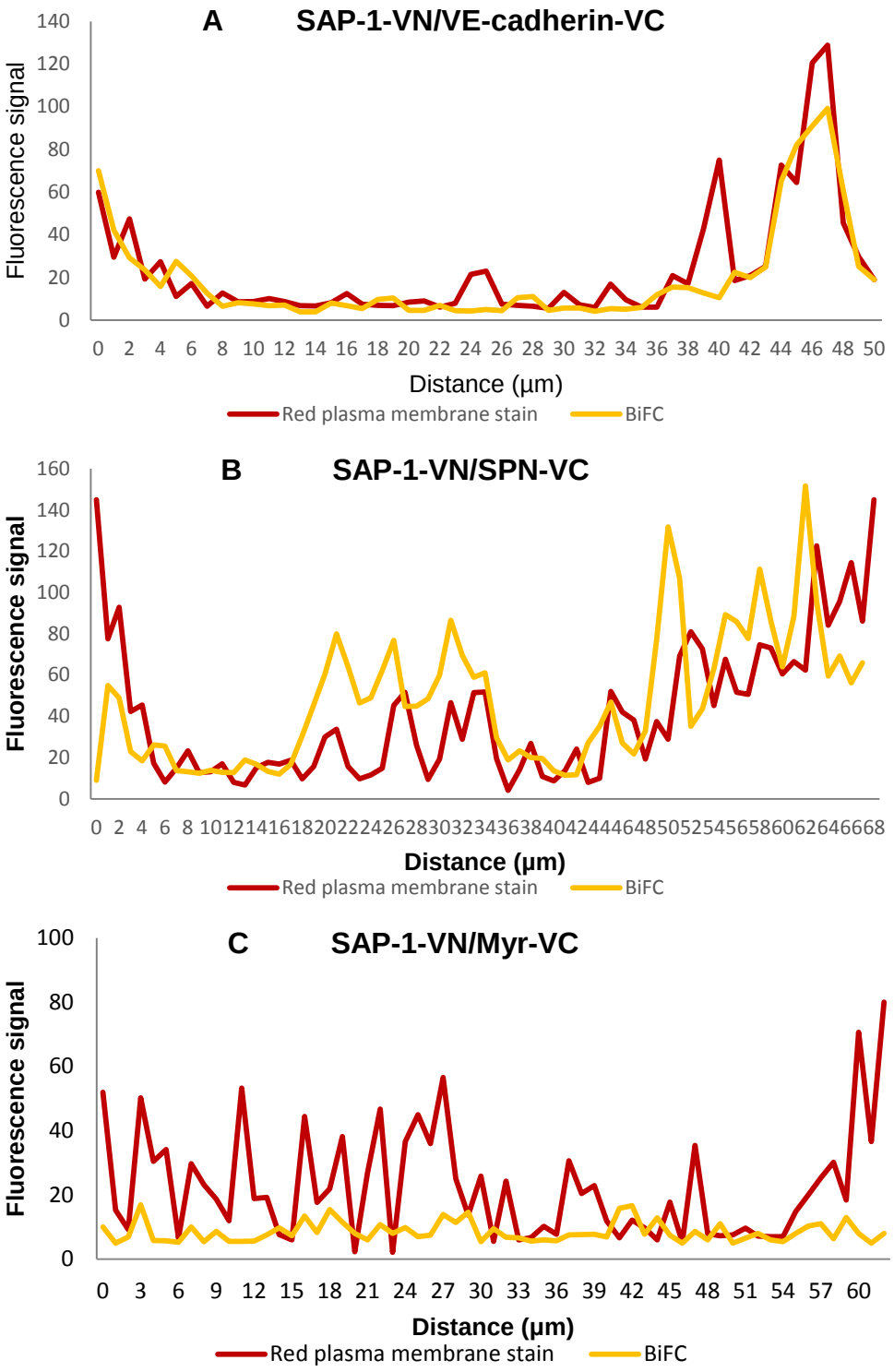

Figure 59. Co-localisation analysis of fluorescence signals across a single cell from the BiFC and the red plasma mambrane stain channels. (**A**) SAP-1-VN/VE-cadherin-VC. (**B**) SAP-1-VN/SPN-VC. (**C**) SAP-1-VN/SPN-VC.

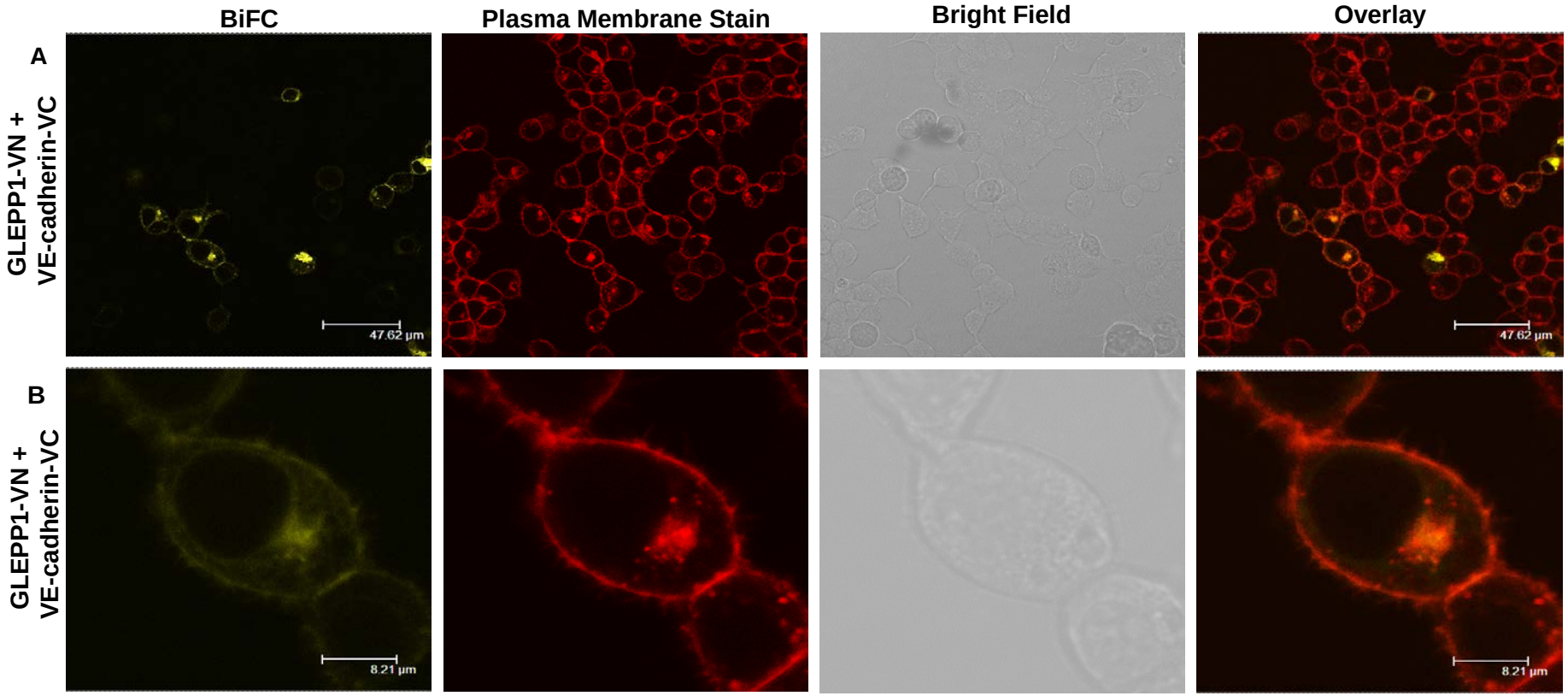

Figure 60. BiFC analysis of interaction between GLEPP1-VN and VE-cadherin-VC. To investigate the potential interaction between GLEPP1-VN and VE-cadherin-VC equal amounts of expression vectors encoding GLEPP1-VN and VE-cadherin-VC were co-transfected into HEK293T cells and the resulting BiFC signal was analysed by confocal microscopy after 24 hours. (A) Confocal images of GLEPP1-VN/VE-cadherin-VC interactions in cell populations. (B) Zoom in of HEK293T cells, showing the localisation of GLEPP1-VN/VE-cadherin-VC interactions.

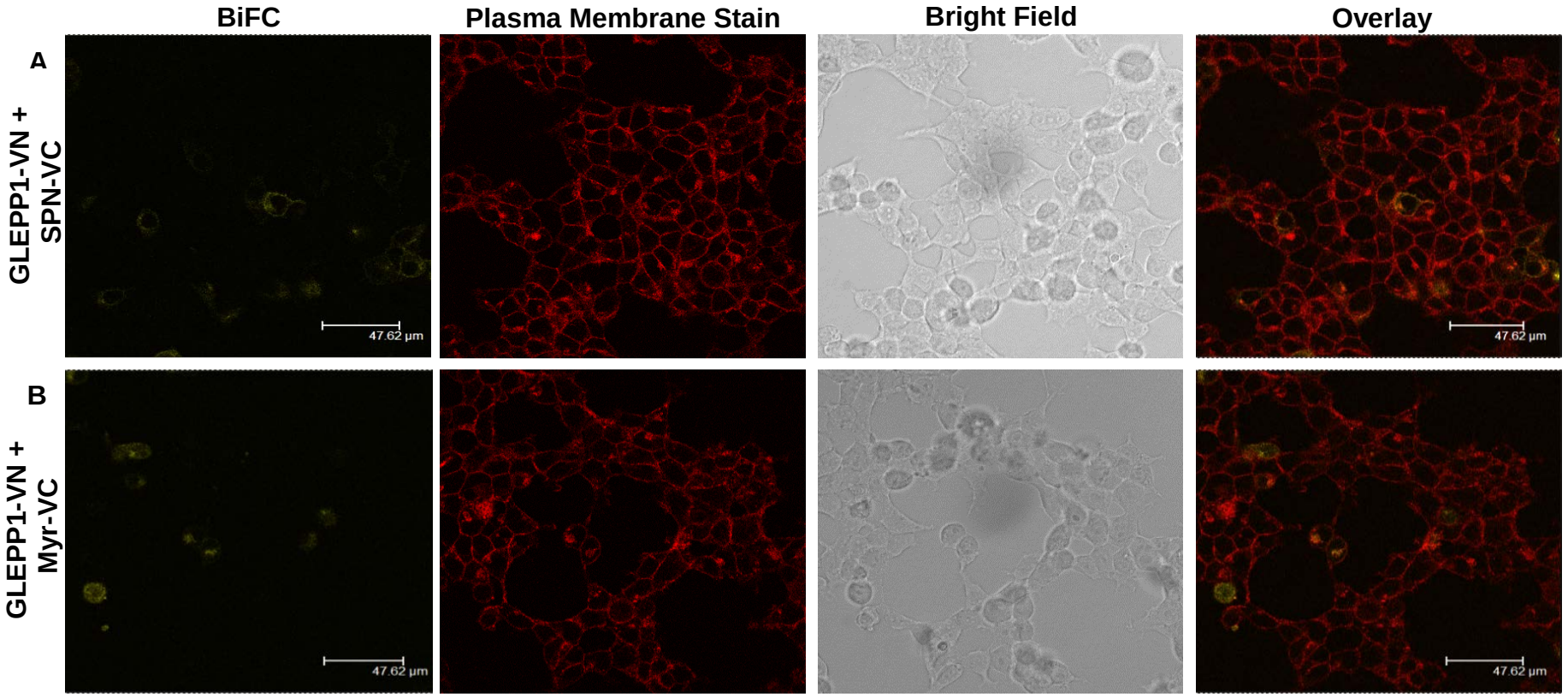

Figure 61. BiFC analysis of GLEPP1-VN with control constructs SPN-VC and Myr-VC. To validate the specificity of the GLEPP1-VN and VE-cadherin-VC interaction, GLEPP1-VN was co-transfected with equal amounts of negative control constructs SPN-VC and Myr-VC into HEK293T cells and the resulting BiFC signal was analysed by confocal microscopy after 24 hours. (A) Confocal images of GLEPP1-VN/SPN-VC interactions in cell populations. (B) Confocal images of GLEPP1-VN/Myr-VC interactions in cell populations.

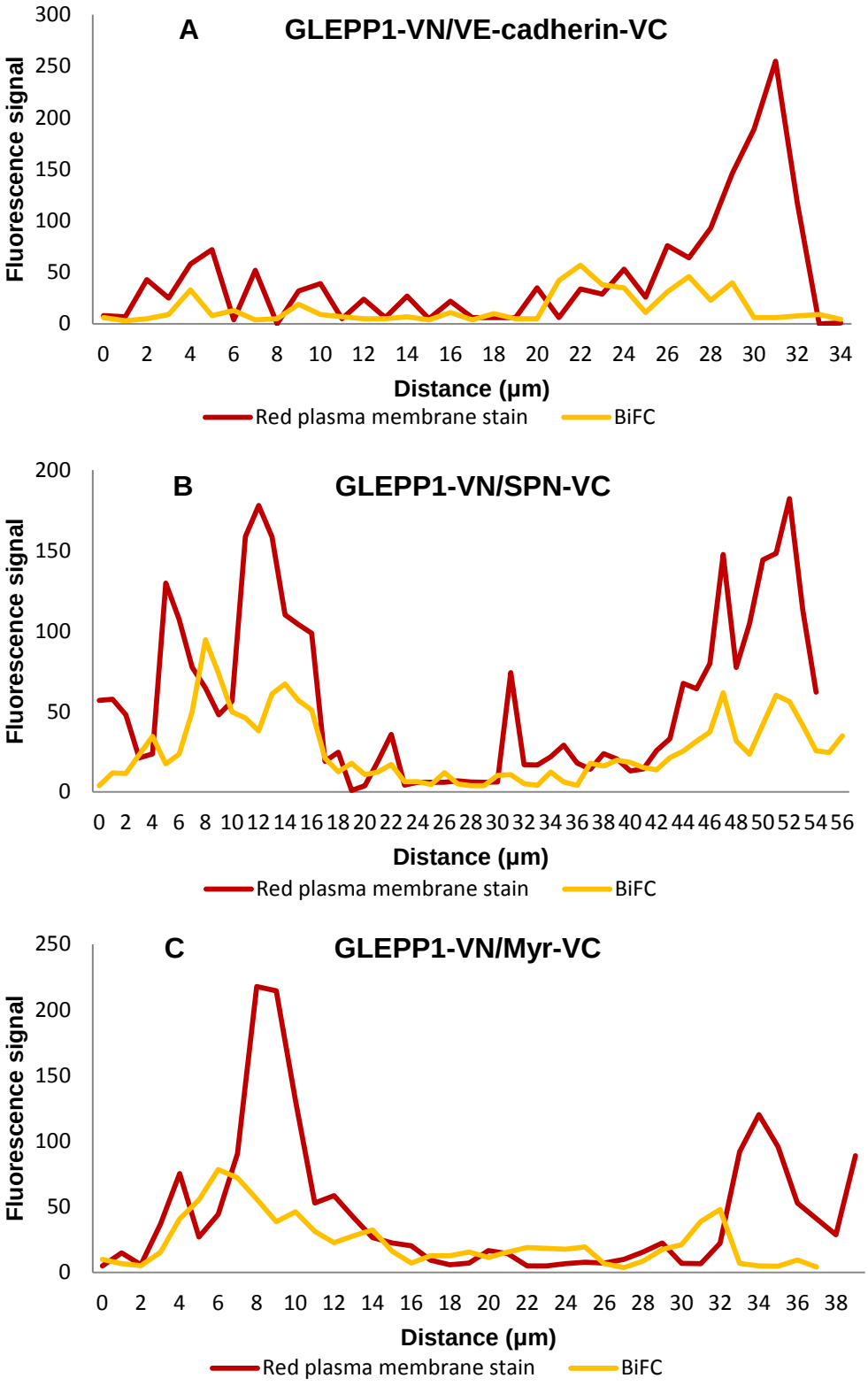

Figure 62. Co-localisation analysis of fluorescence signals across a single cell from the BiFC and the red plasma mambrane stain channels. (**A**) GLEPP1-VN/VE-cadherin-VC. (**B**) GLEPP1-VN/SPN-VC. (**C**) GLEPP1-VN/SPN-VC.

5.5 Quantitative analysis of BiFC data

In order to complement the qualitative BiFC interactions between DEP-1-VN, SAP-1-VN, GLEPP1-VN and VE-cadherin-VC described above quantitative analyses were carried out using ImageJ software. The principle and validation of the quantitative analyses with putative interacting partners bJun and bFos were described in Chapter 3. The same quantitative analyses were applied to VE-PTP-VN and VE-cadherin-VC interaction study and described in Chapter 4.

To analyse the BiFC specificity of interactions between DEP-1-VN/VE-cadherin-VC, SAP-1-VN/VE-cadherin-VC and GLEPP1-VN/VE-cadherin-VC fusion pairs the distribution of yellow/red ratios in individual cells was plotted in a histogram. If the fluorescence signal resulting from DEP-1-VN/VE-cadherin-VC, SAP-1-VN/VE-cadherin-VC or GLEPP1-VN/VE-cadherin-VC fusion pair interaction is due to specific protein-protein interactions and not due to the YFP fragments, then more cells would have higher yellow/red ratio value range compared with negative controls.

The histogram in Figure 63 (A) shows that co-expression of DEP-1-VN and VE-cadherin-VC resulted in a slightly higher number of cells that fall into higher ratio value range between 0 and 4 compared with cells co-expressing DEP-1-VN and SPN-VC (Figure 63, B) or DEP-1-VN and Myr-VC (Figure 63, C) negative interacting pairs. When comparing the distribution of ratios from DEP-1-VN/VE-cadherin-VC and DEP-1-VN/SPN-VC there appear to be fewer cells that exhibit higher yellow/red ratio values. The yellow/red ratio values for DEP-1-VN/SPN-VC mainly fall into a range between 0 and 2 (Figure 63, B). However, there appears to be little difference in yellow/red ratio distribution between DEP-1-VN/SPN-VC and DEP-1-VN/Myr-VC (Figure 63, B and C). Similar results were observed with SAP-1-VN and GLEPP1-VN fusion proteins. When SAP-1-VN was co-transfected with VE-cadherin-VC there was a higher number of cells that have higher ratio value range (between 0 and 4) than for cells co-expressing SAP-1-VN and SPN-VC or SAP-1-VN and Myr-VC control pairs (Figure 64, A-C). When cells were co-transfected with SAP-1-VN and SPN-VC there appeared to be fewer cells

exhibiting higher ratio values, falling into the distribution range between 0 and 3, than for cells co-expressing SAP-1-VN and VE-cadherin-VC fusion pair (Figure 64, A and B). When cells were co-transfected with SAP-1-VN and Myr-VC there appeared to be even greater reduction in cell numbers with higher ratio values compared with SAP-1-VN/VE-cadherin-VC or SAP-1-VN/SPN-VC fusion pairs. The majority of cells expressing SAP-1-VN and Myr-VC exhibited yellow/red ratio values that ranged from 0 to 1 (Figure 64, C). Co-expression of GLEPP1-VN and VE-cadherin-VC resulted in a higher number of cells with higher ratio value range (between 0 and 3) compared with co-expression of GLEPP1-VN/SPN-VC that resulted in cells with lower ratio value range (between 0 and 2) or GLEPP1-VN/Myr-VC that resulted in cells with even lower ratio value range (between 0 and 1) (Figure 65, A-C). However, it is difficult to conclude whether the reduction in cells exhibiting higher ratio value range is significant.

To supplement the above results and to measure the BiFC specificity the signal-to-noise (S/N) ratio was calculated as described in Chapters 3 and 4. A higher S/N ratio value reflects a more specific interaction. S/N ratio was calculated for each interacting fusion pair, including control fusion pairs to establish how much fluorescence signal was formed due to YFP fragments self-assembly. S/N ratio for DEP-1-VN/VE-cadherin-VC, DEP-1-VN/SPN-VC and DEP-1-VN/Myr-VC fusion pairs was calculated by dividing their median values by the median value of DEP-1-VN/Myr-VC. The same was done for all the other fusion pairs, dividing their median values by the median value of the corresponding Myr-VC-containing fusion pair.

There are no previous documented reports about R3 RPTPs and SPN interactions. Interestingly, while the S/N ratio value for SAP-1-VN/VE-cadherin-VC was 3.5-fold higher than for SAP-1-VN/SPN-VC and for GLEPP1-VN/VE-cadherin-VC was 2-fold higher than for GLEPP1-VN/SPN-VC, the S/N for DEP-1-VN/VE-cadherin-VC was slightly lower than for DEP-1-VN/SPN-VC control pair (Figure 66). This could suggest possible interaction between DEP-1-VN and SPN-VC. S/N value for DEP-1-VN/VE-cadherin-VC was 3-fold higher than for DEP-1-VN/Myr-VC. S/N value for

SAP-1-VN/VE-cadherin-VC was 6-fold higher compared with SAP-1-VN/Myr-VC. The S/N value for GLEPP1-VN/VE-cadherin-VC was 4.5-fold higher than for GLEPP1-VN/Myr-VC (Figure 66). These results suggest that interactions between DEP-1-VN and VE-cadherin-VC, SAP-1-VN and VE-cadherin-VC and GLEPP1-VN and VE-cadherin-VC are specific and not due to self-assembly of the YFP fragments.

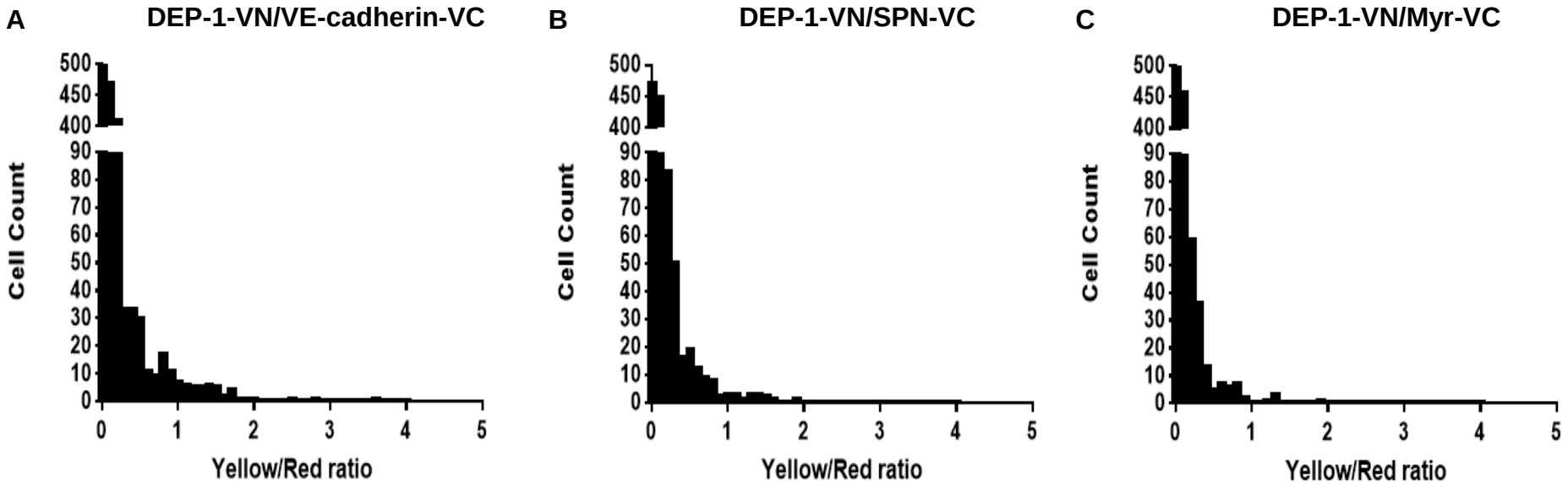

Figure 63. Validation of DEP-1-VN/VE-cadherin-VC interaction specificity. The fluorescence intensity from BiFC (yellow) and the fluorescent signal from the plasma membrane stain (red) were measured in individual cells. The distribution of ratios between the fluorescence intensity and red fluorescence signal in individual cells was plotted in a histogram. The yellow/red ratio has been plotted for each pair of constructs: (A) DEP-1-VN/VE-cadherin-VC, (B) DEP-1-VN/SPN-VC and (C) DEP-1-VN/Myr-VC.

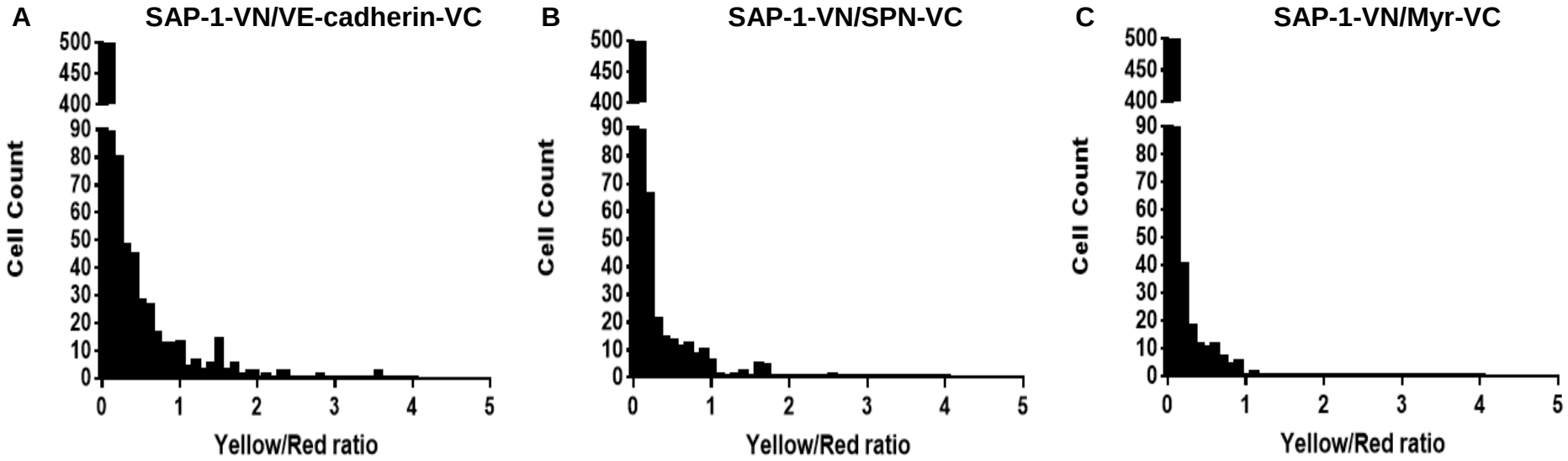

Figure 64. Validation of SAP-1-VN/VE-cadherin-VC interaction specificity. The fluorescence intensity from BiFC (yellow) and the fluorescent signal from the plasma membrane stain (red) were measured in individual cells. The distribution of ratios between the fluorescence intensity and red fluorescence signal in individual cells was plotted in a histogram. The yellow/red ratio has been plotted for each pair of constructs: (A) SAP-1-VN/VE-cadherin-VC, (B) SAP-1-VN/SPN-VC and (C) SAP-1-VN/Myr-VC.

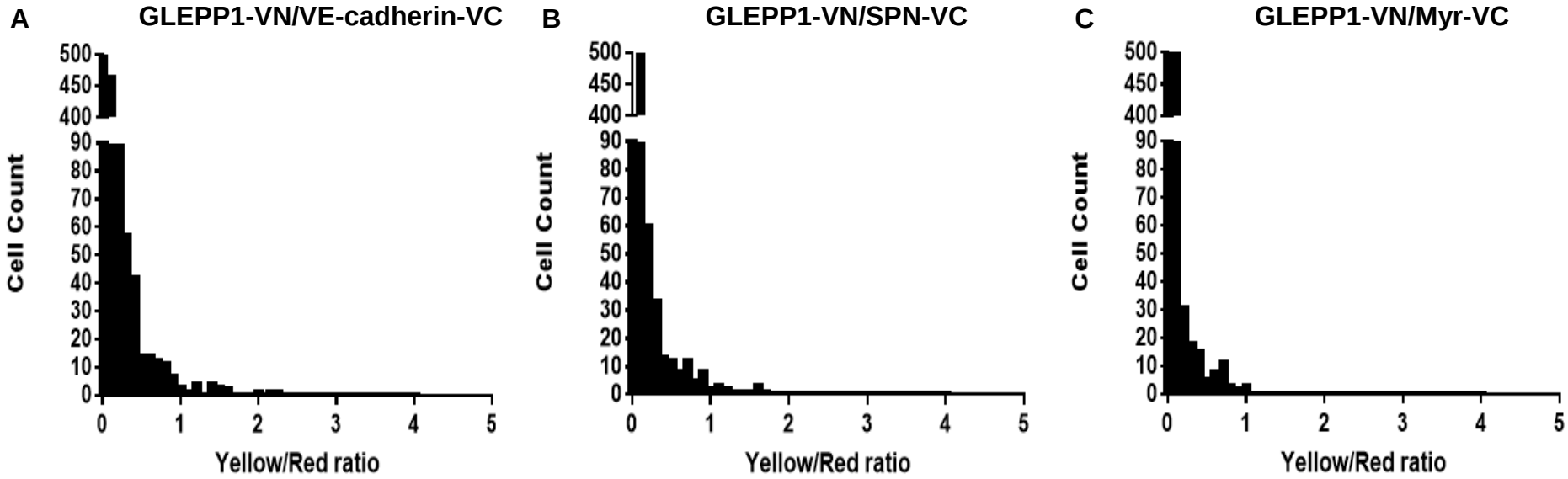

Figure 65. Validation of GLEPP1-VN/VE-cadherin-VC interaction specificity. The fluorescence intensity from BiFC (yellow) and the fluorescent signal from the plasma membrane stain (red) were measured in individual cells. The distribution of ratios between the fluorescence intensity and red fluorescence signal in individual cells was plotted in a histogram. The yellow/red ratio has been plotted for each pair of constructs: (A) GLEPP1-VN/VE-Cadherin-VC, (B) GLEPP1-VN/SPN-VC and (C) GLEPP1-VN/Myr-VC.

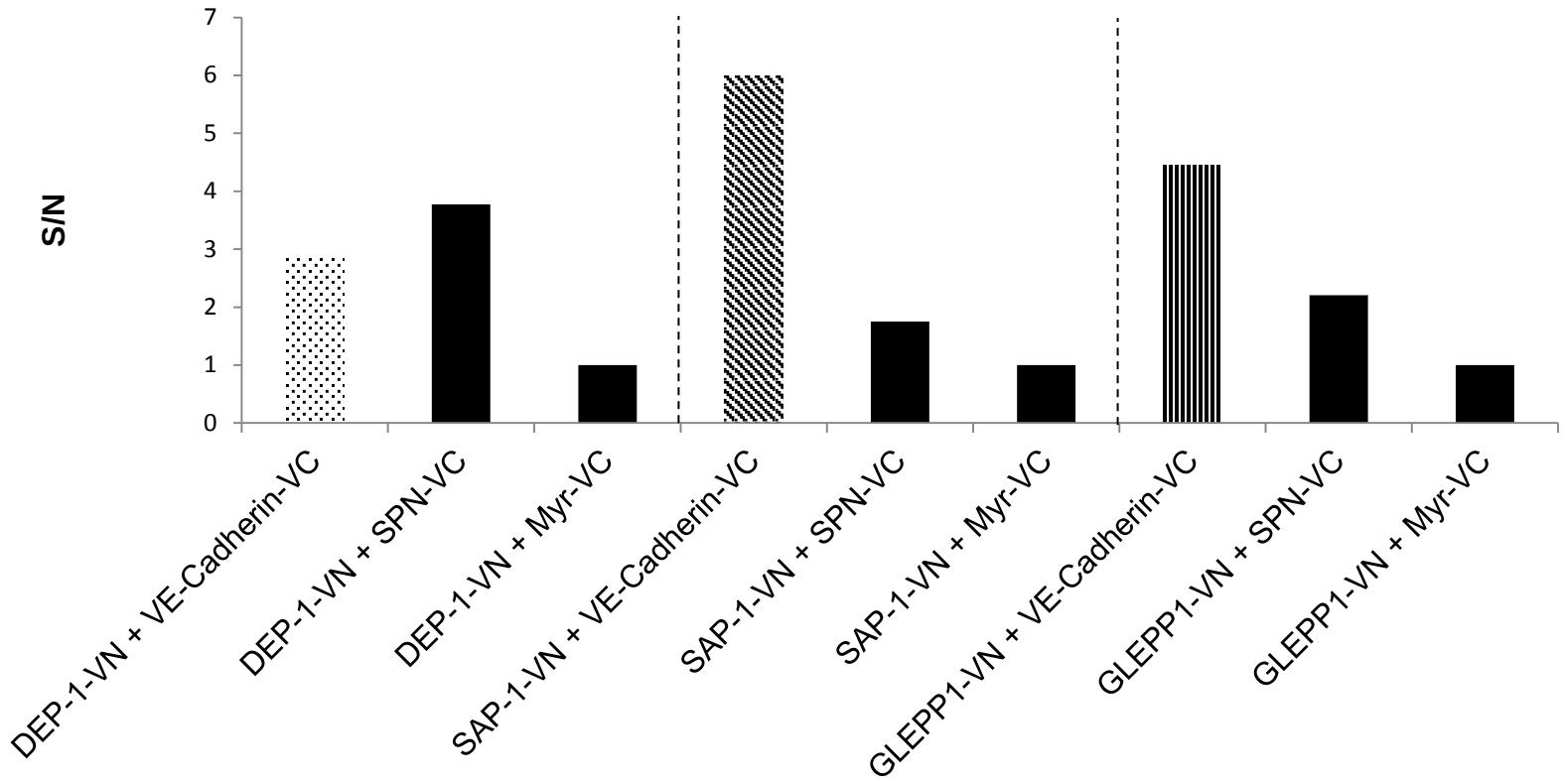

Figure 66. S/N ratio of BiFC assay in HEK293T cells. S/N for each interacting fusion pair was calculated by dividing its median value by the median value from the corresponding Myr-VC-containing fusion pair. The median value for each fusion pair was calculated based on at least three independent experiments.

An alternative approach to quantitate the data using only average fluorescence intensity was also used. The average yellow fluorescence intensity from at least three random fields and three or more independent experiments was calculated for each fusion pair and used for statistical analysis (Figure 67). Quantitative analysis of the DEP-1-VN and VE-cadherin-VC fusion pair showed that there was no significant difference in an average BiFC fluorescence intensity compared with DEP-1-VN and SPN-VC. However, when DEP-1-VN was co-expressed with Myr-VC there was a significant reduction in average fluorescence intensity by 2.5-fold and 2.2-fold than for DEP-1-VN/VE-cadherin-VC and DEP-1-VN/SPN-VC fusion pairs respectively (Figure 67). When SAP-1-VN was co-expressed with VE-cadherin-VC the average fluorescence intensity was significantly higher than for all the control pairings ($p<0.001$). As can be seen from Figure 67 there was a significant decrease in fluorescence signal by about 2- and 3-fold in SAP-1-VN/SPN-VC and SAP-1-VN/Myr-VC respectively compared with SAP-1-VN/VE-cadherin-VC fusion pair. Similarly, when HEK293T cells were co-transfected with GLEPP1-VN and VE-cadherin-VC the resulting fluorescence intensity was significantly higher than for all the control pairings ($p<0.001$). There was a significant decrease in fluorescence signal by 1.7- and 3.5-fold in GLEPP1-VN/SPN-VC and GLEPP1-VN/Myr-VC respectively than for GLEPP1-VN/VE-cadherin-VC fusion pair (Figure 67). The results of this quantitative approach correspond to results from distribution of yellow/red ratio values and S/N quantitative methods.

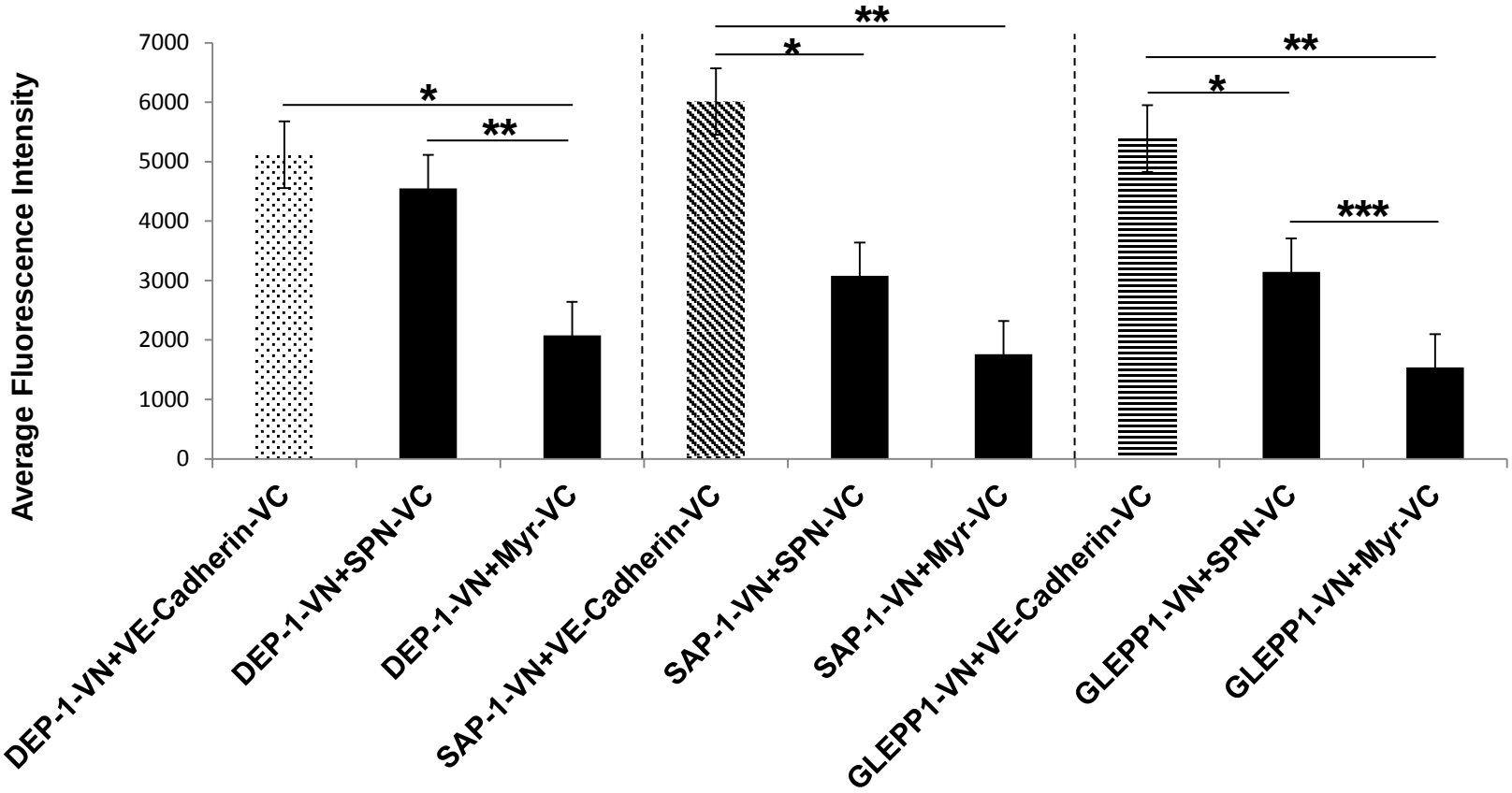

Figure 67. Quantitation of BiFC fluorescence intensities in transiently transfected HEK293T cells. Pairs of constructs as indicated were transfected into HEK293T cells using equal amounts of each expression vector and the BiFC signal assessed. Average fluorescence intensity was determined using ImageJ software. The mean and standard error from at least three independent experiments was quantitated as described in the materials and methods. $p<0.001$ by the Kruskal-Wallis test was considered significant.

5.6 Discussion

Protein tyrosine phosphatases of the R3 subgroup (R3 RPTPs) share similar structure and it has been suggested that they may share similar physiological functions. The single intracellular catalytic domain of these proteins has received much attention and it has been shown that the members of this subgroup have developmental and physiological functions in several tissues including the vascular and nervous systems (Sakuraba *et al,* 2013*)*. However, the function of the extracellular domains of R3 RPTPs that is composed of fibronectin III-like (FNIII) repeats is less well defined. Although the extracellular domains of these proteins are structurally similar, the number of FNIII-like repeats varies and some previous studies have reported little homology. Comparison of the amino acid sequence of each FNIII-like repeat in ECD performed by Matozaki *et al* (1994) revealed that SAP-1 and VE-PTP share only 24% similarity, which, in contrast to other studies, suggested that they may have different functions. Despite such low similarity, R3 RPTP extracellular domains may have similar functions. Interestingly immunofluorescence staining experiments on frozen sections from human and mouse performed by Takahashi *et al* (1999) showed that DEP-1 was expressed on luminal membranes of capillary and arterial endothelium of mature human and mouse kidney, where it accumulates at points of inter-endothelial contact. Furthermore double-labelling studies demonstrated that DEP-1 expression overlaps with localisation of VE-cadherin (Takahashi *et al*, 1999). These observations raise some speculation that perhaps DEP-1 has similar physiological functions to VE-PTP in vascular development and in endothelial cell-cell interactions through association with VE-cadherin.

In this chapter DEP-1-VN and VE-cadherin-VC fusion constructs consisting of transmembrane and extracellular domains fused to the N- and C-terminal parts of a Venus yellow fluorescent protein (YFP) respectively were used to examine their potential interaction in live cells using the bimolecular fluorescence complementation (BiFC) assay. In addition SAP-1-VN and GLEPP1-VN fusion constructs fused to the N-terminal part of YFP were also used to investigate whether all the members of R3 RPTP subgroup have the potential to interact with VE-cadherin. The qualitative BiFC analysis obtained

on co-expression of DEP-1-VN/VE-cadherin-VC, SAP-1-VN/VE-cadherin-VC or GLEPP1-VN/VE-cadherin-VC fusion pairs showed a strong fluorescence signal for each interacting pair that was localised at the plasma membrane with some fluorescence in endoplasmic reticulum and probably Golgi apparatus. These results correlate with the results obtained with VE-PTP-VN/VE-cadherin-VC interacting pair discussed in Chapter 4. To confirm the specificity of the BiFC fluorescence signal negative controls described in Chapter 4 were used with each R3 RPTP fusion. However, the co-expression of DEP-1-VN, SAP-1-VN or GLEPP1-VN with either SPN-VC or Myr-VC negative controls also resulted in fluorescence signal. Although the signal appeared to be reduced and less intense using qualitative analysis it was not possible to conclude that the fluorescence obtained with negative interaction pairs was due to non-specific interactions or self-assembly of the non-fluorescent YFP fragments that could be caused by an overexpression of proteins.

In this chapter three different quantitative analyses were performed using ImageJ software and statistically validated data as described in previous Chapters 2-4. Each quantitative analysis validates the BiFC efficiency and specificity, complementing each other to produce more robust data. The quantitative analyses demonstrated that co-expression of each member of R3 RPTP subgroup with either VE-cadherin or negative control construct resulted in a similar trend of BiFC complex formation. Co-expression of either SAP-1-VN/VE-cadherin-VC or GLEPP1-VN/VE-cadherin-VC fusion pair resulted in more cells exhibiting higher yellow/red ratio values, higher S/N value and a significant increase in average yellow fluorescence signal compared with all the negative interacting pairings. Considering that the GLEPP1-VN was expressed at lower level than for negative controls SPN-VC and Myr-VC and that DEP-1-VN and SAP-1-VN were expressed at lower level than for SPN-VC (Figures 31 and 53) suggests that the BiFC signal from either SAP-1-VN/VE-cadherin-VC or GLEPP1-VN/VE-cadherin-VC was not an artefact of overexpression. These results suggest that the interactions between SAP-1-VN and VE-cadherin-VC and between GLEPP1-VN and VE-cadherin-VC are bona fide protein-protein interactions rather than non-

specific assembly of the YFP fragments. Interestingly the fluorescence intensity obtained with the DEP-1-VN and VE-cadherin-VC pairing, although significantly different from DEP-1 with the Myr-VC control, was not significantly different from DEP-1-VN and the SPN-VC control (Figure 67) as discussed further below. In addition, the S/N value for DEP-1-VN/SPN-VC was higher than for DEP-1-VN/VE-cadherin-VC (Figure 66). These quantitative assessments of the fluorescence images obtained for each interacting pair indicated a BiFC signal that is due to a specific interaction, rather than self-assembly of the YFP fragments and background fluorescence.

In this chapter analysis of the potential of other R3 RPTPs (DEP-1, SAP-1 and GLEPP1) to interact with VE-cadherin revealed that the series of 8-9 extracellular FNIII-like domains from any of the R3-PTPs has the potential to mediate a direct interaction with VE-cadherin. This is of particular interest with regard to DEP-1 since it is expressed in endothelial cells together with VE-cadherin. It has been shown previously that DEP-1 localisation at inter-endothelial cell contacts overlaps with VE-cadherin, where it interacts with other endothelial cell tight junction proteins and, thus, it has been suggested to play a role in regulation of endothelial cell permeability (Takahashi *et al*, 1999; Sallee and Burridge, 2009; Spring *et al*, 2012). It has been previously shown that the cytoplasmic domain of VE-cadherin forms complexes with cell adhesion catenin proteins, such as plakoglobin (also known as gamma-catenin), p120-catenin and β-catenin (Lampugnani *et al*, 1995). A schematic representation of VE-cadherin/catenin complex is shown in Figure 68. This complex serves to strengthen adhesion forces and allows dynamic contacts (Azzi *et al*, 2013). Interestingly DEP-1 was also shown to associate with and dephosphorylate plakoglobin, p120-catenin and β-catenin through its cytoplasmic domain (Holsinger *et al*, 2002). But whether DEP-1 interacts directly with VE-cadherin in the same manner as VE-PTP has not been defined previously. Even if DEP-1 and VE-cadherin do not interact via their extracellular domains, the cumulative previous results suggest that these two proteins function as part of one complex. Close localisation of DEP-1 and

VE-cadherin was possibly enough for BiFC complementation to occur, resulting in fluorescence signal.

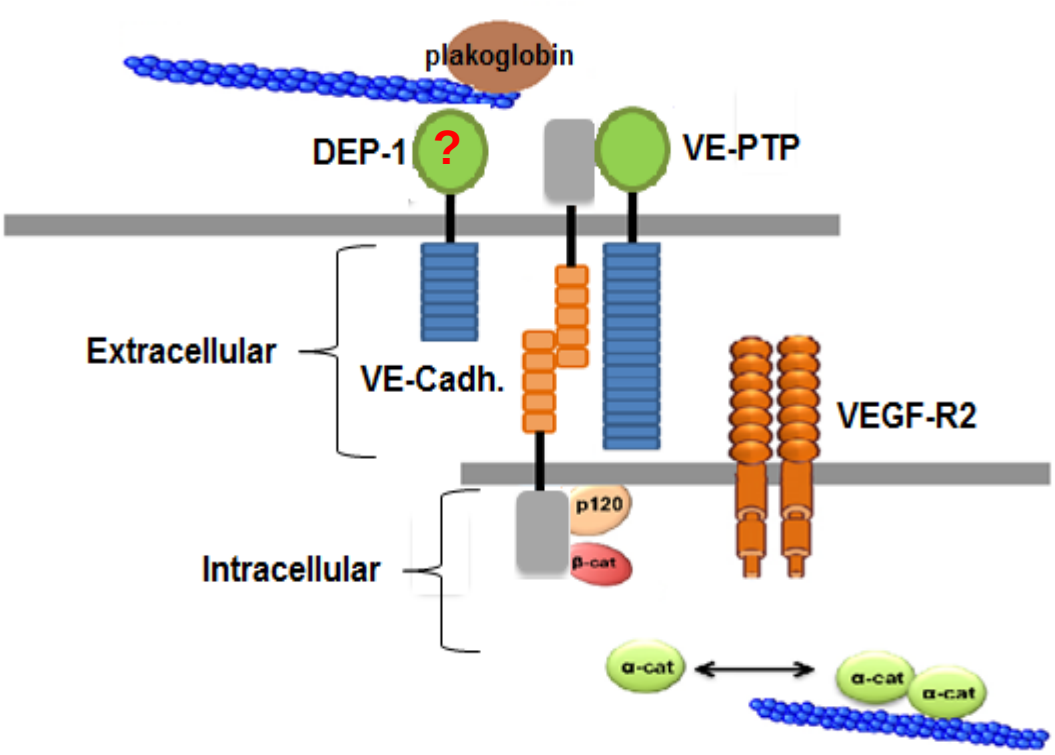

Figure 68. VE-cadherin adhesive complex. Schematic representation of VE-cadherin/catenin complex formation. This figure was adopted and modified from Azzi *et al* (2013). The cytoplasmic domain of VE-cadherin interacts with p120-catenin (p120) and β-catenin (β-cat.). Actin cytoskeleton is anchored to VE-cadherin via α-catenin (α-cat.) or plakoglobin. VE-cadherin was also shown to interact with VEGF-R2 (vascular endothelial growth factor receptor 2) and VE-PTP. It remains unclear how the DEP-1 fits in this model.

The observation that co-expression of DEP-1-VN with the SPN-VC control was not significantly different from the DEP-1-VN/VE-cadherin-VC combination but gave significantly higher levels of fluorescence than DEP-1-VN with the Myr-VC control could be interpreted as a *bona fide* interaction between DEP-1 and SPN. Both DEP-1 and SPN proteins are expressed in leukocytes. However, I am not aware of any previous reports documenting this interaction. Nonetheless, both DEP-1 and SPN have been shown to share similar physiological functions in regulation of immune responses and especially in regulation of T cell receptor (TCR) signalling. DEP-1, together with another RPTP glycoprotein CD45, was suggested to regulate TCR signalling by passive segregation from engaged TCR (kinetic-segregation model). It has been proposed that DEP-1, due to its large extracellular domain, is excluded from the vicinity of the engaged TCR, allowing TCR/MHC (major histocompatibility complex) interaction and the consequent phosphorylation of TCR ITAMs (immunoreceptor tyrosine-based activation motifs) and other substrates to take place that result in TCR signalling pathway activation (Cordoba *et al*, 2013). Fluorescent imaging revealed that truncation of DEP-1 and CD45 extracellular domains enhanced co-localisation with TCR and, as was confirmed by immunoblot analysis, enabled phosphatases to dephosphorylate membrane-proximal molecules (such as LAT) in the TCR triggering pathway (Corboda *et al*, 2013). Therefore, these results suggest that the large extracellular domain of DEP-1 prevents its tyrosine phosphatase domain from inhibiting TCR signalling. Interestingly SPN was also shown to be highly expressed in T cells and to interact with the T cell receptor to initiate signalling events (Clark and Baum, 2012). Furthermore it has been suggested that the glycosylation of SPN plays a key role in this interaction. SPN has about 80 O-linked, as well as some N-linked, glycans dispersed over the entire extracellular domain. Some studies demonstrated that the glycosylation of SPN's extracellular domain is regulated by T cells and that this differential glycosylation of SPN regulates interactions with the extracellular environment that, in turn, regulate T cell receptor signalling (Clark and Baum, 2012). As the results of this Chapter and of some previous observations suggest, there is a possibility that DEP-1 and SPN interact together via their extracellular domains. However, further

experiments are required to confirm their interaction and to investigate its molecular basis. In addition it would be interesting to examine what role the glycosylation plays in interaction between DEP-1 and SPN, as well as between R3 RPTPs and VE-cadherin. Additional experiments could be performed by enzymatically removing N- and O-linked glycans, using PNGase and O-Glycosidase.

On the other hand the physiological importance of either SAP-1 or GLEPP1 interaction with VE-cadherin is not clear. I am not aware of any reports of SAP-1 and GLEPP1 expression in endothelial cells and, since VE-cadherin expression is restricted to this cell type, the observed interaction is unlikely to be of physiological relevance. Nonetheless, the results provide insight into the molecular basis of the interaction suggesting that the interaction of VE-PTP and VE-cadherin, or other R3 RPTPs with VE-cadherin, can be mediated by several different FNIII domains and, potentially, their transmembrane domains. This finding is consistent with studies in Chapter 4 of the deletion mutant suggesting that the FNIII domains could be interchangeable. Controversially, as mentioned above, the interaction could occur through the extensive glycosylation of these proteins in the same manner as SPN interacts with proteins involved in T cell receptor regulation. Since the overall sequence identity of R3 RPTPs is very low the investigation of glycosylation involvement in protein-protein interactions would be of particular interest in future experiments. Additionally, further experiments are required to investigate mechanisms involved in regulation of R3 RPTPs' functions.

5.7 Conclusion

The results of this Chapter suggest that all members of R3 RPTP subgroup have the potential to interact with VE-cadherin via their extracellular domains in live cells. Although the physiological importance of these interactions is not yet defined, the observations of this Chapter demonstrate the importance of the extracellular domain of R3 RPTPs in regulation of their function. Perhaps substrate specificity is due not to structural similarity but to restricted expression and localisation of these proteins or could be determined by the extensive glycosylation of their extracellular domains. Conceivably a protein could combine selectivity for specific ligands with the flexibility and possibility for interaction with other ligands that would have different binding affinity and signalling outcomes. Further experiments would be required to confirm the interaction between DEP-1, SAP-1 or GLEPP1 with VE-cadherin.

Chapter 6

Investigation of potential homodimerisation of R3 RPTPs in live cells

6.1 Introduction

Dimerisation has been proposed as one of the regulatory mechanisms of receptor protein tyrosine phosphatases (RPTPs) but its regulatory role is still controversial. This proposed regulatory mechanism was based on many studies showing that receptor protein tyrosine kinases (RPTKs) transduce signals by ligand-initiated extracellular domain dimerisation to promote *in trans* cytoplasmic domain tyrosine phosphorylation and subsequent assembly of multicomponent signalling complexes. It appeared that ligand-induced receptor dimerisation brought kinase molecules into close proximity so that they could phosphorylate one another, leading to stimulation of the kinase activity (Lemmon and Schlessinger, 1998). In contrast to RPTKs, the function of RPTPs was shown to be inhibited by dimerisation. For example, receptor protein tyrosine phosphatase alpha (RPTPα) was shown to exist on the cell surface as monomers and dimers in equilibrium (Jiang *et al*, 1999). RPTPα was shown to form spontaneous dimers and that the dimerisation was mediated by the N-terminal D1 (active) catalytic domain and transmembrane region (Jiang *et al*, 1999). In addition, immunoblotting analysis revealed that the dimerised form of RPTPα was not able to dephosphorylate its biological substrate c-Src, suggesting that RPTPα is negatively regulated by dimerisation (Jiang *et al*, 1999).

Several studies have explored the potential of R3 subgroup PTPs to homo-dimerise or form homophilic interactions. However, from the available data it is difficult to develop a unifying scheme. Some members of R3 RPTPs, such as GLEPP1 and SAP-1, do show potential dimerisation but the mechanism of this dimerisation is not well defined. A study by Hower *et al* (2009) using a chimeric approach showed that GLEPP1 can form dimers in live cells and that this dimerisation results in a strong decrease of its intrinsic PTPase activity, as was confirmed using a biological substrate for GLEPP1, tropomyosin receptor kinase C (TrkC; a receptor for neurotrophin (NT)-3). In a similar way to RPTPα, the transmembrane and intracellular domains of GLEPP1 were sufficient for the observed dimerisation (Hower *et al*, 2009). Another member of R3 RPTP subgroup SAP-1 was also shown to form

stable homodimers, but in contrast to GLEPP1 the dimerisation of SAP-1 was mediated by its extracellular domain, independently of cytoplasmic and transmembrane regions. The dimerisation was suggested to be formed through at least one cysteine (but possibly more, since it has 13 cysteines in its extracellular domain) that forms disulfide bridges between two SAP-1 proteins (Walchli *et al*, 2005). Moreover, the same study by Walchli *et al* (2005) also showed that SAP-1 efficiently activates its biological substrate c-Src, but only when SAP-1 is in monomeric form, therefore suggesting that dimerisation results in reduced catalytic activity of this enzyme (Walchli *et al*, 2005). The same study by Walchli *et al* (2005) found no evidence for dimerisation of other R3 RPTP members. Immunoprecipitation and Western blot analyses by Takahashi *et al* (2006) revealed that DEP-1 can also form dimers as a result of ligand stimulation. It has been demonstrated that bivalent, but not monovalent, antibody (Ab1) was accompanied by an increase in CD148-associated PTP activity resulting in significant inhibition of cell proliferation. Therefore, in contrast to previous observations for GLEPP1 and SAP-1, DEP-1 catalytic activity seems to increase upon ligand-induced extracellular domain dimerisation. But further work is needed to elucidate the mechanism of antibody-mediated dimerisation of DEP-1 (Sorby *et al*, 2001; Takahashi *et al*, 2006). VE-PTP did not show any dimerisation under similar experimental conditions and thus it remains unclear how the function of this protein is regulated (Walchli *et al*, 2005).

All the above studies were carried out using immunoprecipitation assays. The mechanisms regulating R3 RPTPs' activity are still not fully defined and further experiments are required to investigate whether the previously used experimental procedures fully mimic natural regulation of these proteins. It still remains unclear whether the dimerisation does occur for all R3 RPTPs and whether it could be induced by an extracellular ligand binding. Based on studies described above it is becoming apparent that the extracellular domain and/or transmembrane of these phosphatases plays an important role in the regulation (either through dimerisation or by any other means) of their catalytic activities. Thus, further experiments are required to establish the role of R3 RPTP extracellular domains in dimerisation. Therefore, the aim

of this Chapter is to examine whether R3 RPTP members can form dimers via their extracellular and/or transmembrane domains in live cells using BiFC assay.

6.2 Results

6.2.1 Fusion proteins

VE-PTP, DEP-1, SAP-1 and GLEPP1 fusion constructs were generated as outlined in the schema in Chapter 2 (Figure 8). Each construct for each protein was generated as N- and C-terminal YFP fragment fusion as described in result sections of Chapters 4 and 5. The generation process of the negative control fusion constructs SPN-VC and Myr-VC is shown in Chapter 4. Throughout all BiFC experiments the same negative controls fused to the C-terminal part of the YFP were used in order to keep all the conditions constant as the position of the fused YFP fragment can affect the interaction of proteins and thus make data interpretation difficult. R3 RPTP fusion constructs are schematically shown in Figure 47 (Chapter 5).

6.3 Western blot analysis of BiFC fusion proteins in HEK293T cells

Expression of the constructs used in this chapter has been previously assessed in Chapters 4 and 5 (refer to Figures 31 and 53). Western blotting of lysates from transiently transfected HEK293T cells confirmed the expression of all the fusion proteins above their predicted molecular weight, indicating the presence of extensive glycosylation in their extracellular domains. VE-PTP-VN, DEP-1-VN, SAP-1-VN, GLEPP1-VN, SPN-VN appeared to be expressed at higher levels compared with their corresponding –VC fusions, (Figures 31 and 53). Both GLEPP1-VN and GLEPP1-VC fusion proteins appeared to be expressed at lower levels compared with all other fusion proteins (Figure 53, A-D). Western blotting was performed at least three times for each fusion construct and the results were consistent.

6.4 Investigation of homodimerisation of R3 RPTPs in live cells using BiFC technique

To investigate the role of the extracellular domain in dimerisation each construct consisting of extracellular and transmembrane domains was generated as N- and C-terminal YFP fragment fusions (as described in Chapters 4 and 5). Although the dimerisation of R3 RPTPs has been studied before, no previous studies have been done in live cells to investigate the molecular basis of dimer formation. In addition, no studies had been carried out on the specific role of R3 RPTP extracellular domain in dimerisation. Each N-terminal YFP fragment fusion protein was co-expressed with the corresponding C-terminal YFP fragment fusion protein (e.g. DEP-1-VN and DEP-1-VC) in HEK293T cells and 24 hours post-transfection stained prior to confocal visualisation with the CellMask^{TM} Plasma Membrane Stain (as detailed in method section 2.5.6). In addition, to establish the specificity of BiFC signal, each N-terminal R3 RPTP fusion construct was co-expressed with each control C-terminal fusion construct (SPN-VC and Myr-VC). All the transfection conditions and parameters of confocal analyses were kept constant for all the experiments.

Co-expression of VE-PTP-VN and VE-PTP-VC resulted in a strong fluorescence signal (Figure 69). Co-expression of VE-PTP-VN with either SPN-VC or Myr-VC also resulted in a fluorescence signal, but the intensity of the signal and the number of cells exhibiting the signal appeared to be reduced (Figure 70, A and B). The same pattern was also observed with other members of R3 RPTPs. Co-expression of DEP-1-VN/DEP-1-VC, SAP-1-VN/SAP-1-VC or GLEPP1-VN/GLEPP1-VC resulted in an abundant fluorescence signal and the signal appeared to be reduced when either DEP-1-VN, SAP-1-VN or GLEPP1-VN was co-expressed with either SPN-VC or Myr-VC (Figures 71, 72, 73, 74, 75 and 76). Comparison of the sub-cellular localisation of the yellow fluorescence signal with that of the red fluorescence signal from plasma membrane stain indicated that the fluorescence complementation signal was detected in the plasma membrane and some

intracellular structures, likely to be the endoplasmic reticulum and Golgi, of co-transfected cells.

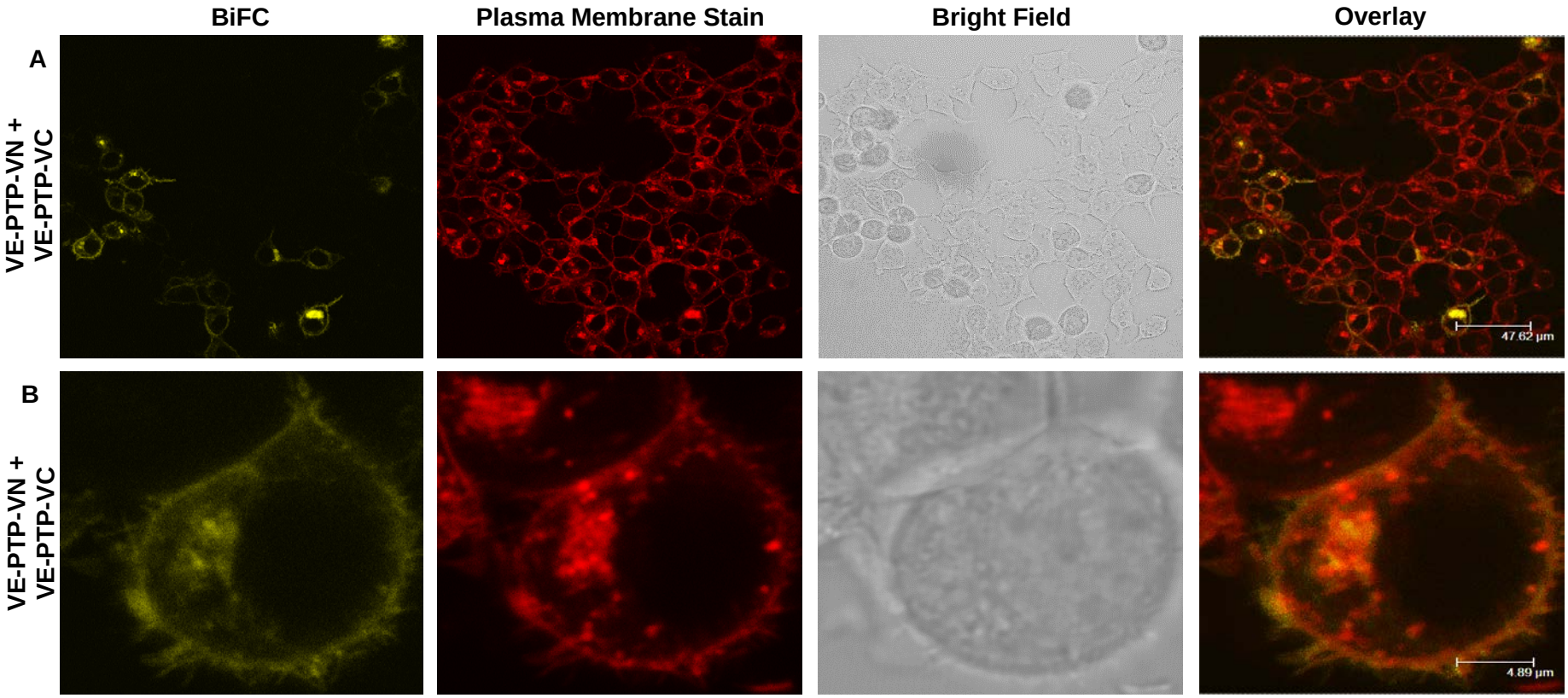

Figure 69. BiFC analysis of VE-PTP dimerisation. To investigate whether VE-PTP forms dimers in live cells, equal amounts of VE-PTP-VN and VE-PTP-VC fusions were used to co-transfect HEK293T cells and the resulting BiFC signal was analysed by confocal microscopy after 24 hours. (A) Confocal images of VE-PTP-VN/VE-PTP-VC interactions in cell populations. (B) Zoom in of HEK293T cells, showing the localisation of VE-PTP-VN/VE-PTP-VC interactions.

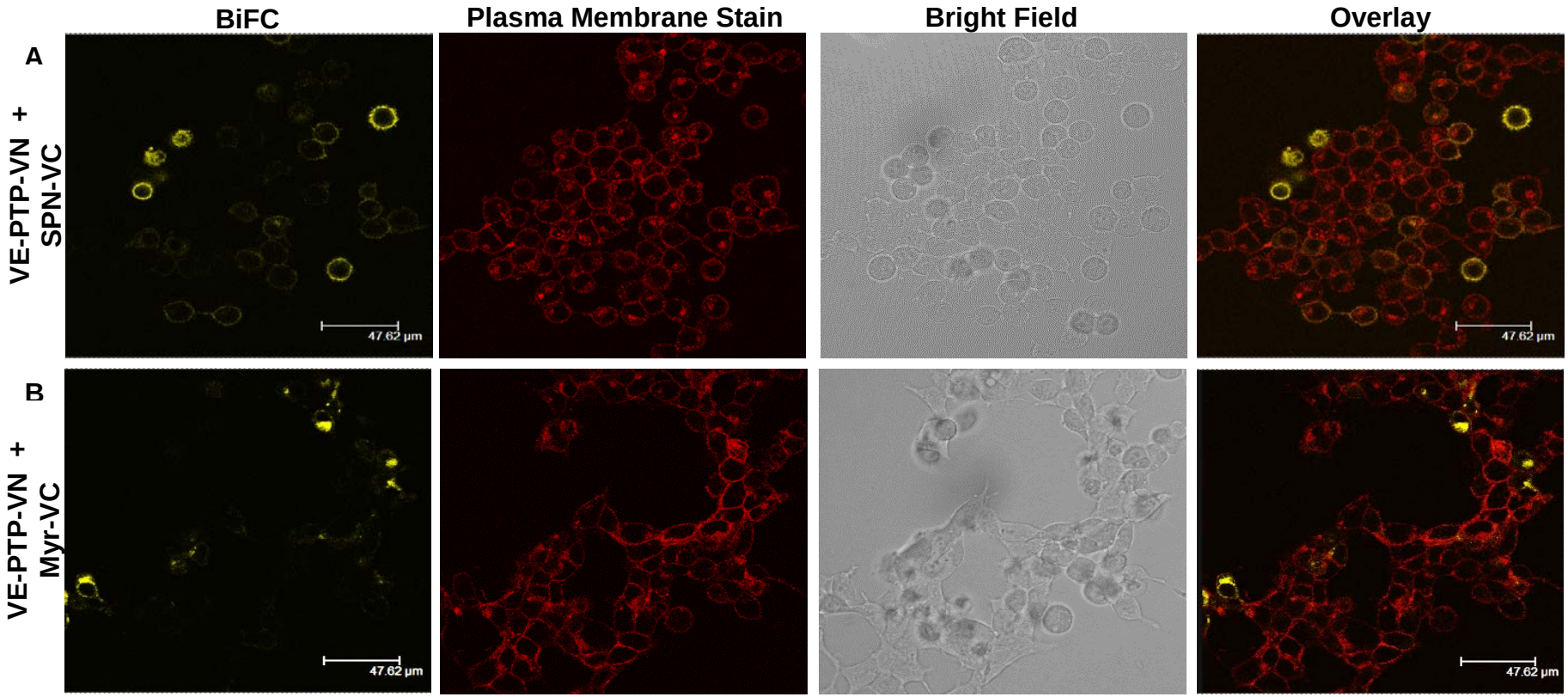

Figure 70. BiFC analysis of VE-PTP-VN with control constructs SPN-VC and Myr-VC. To validate the specificity of the VE-PTP-VN and VE-PTP-VC interaction, VE-PTP-VN was co-transfected with equal amounts of negative control constructs SPN-VC and Myr-VC into HEK293T cells and the resulting BiFC signal was analysed by confocal microscopy after 24 hours. (A) Confocal images of VE-PTP-VN/SPN-VC interactions in cell populations. (B) Confocal images of VE-PTP-VN/Myr-VC interactions in cell populations.

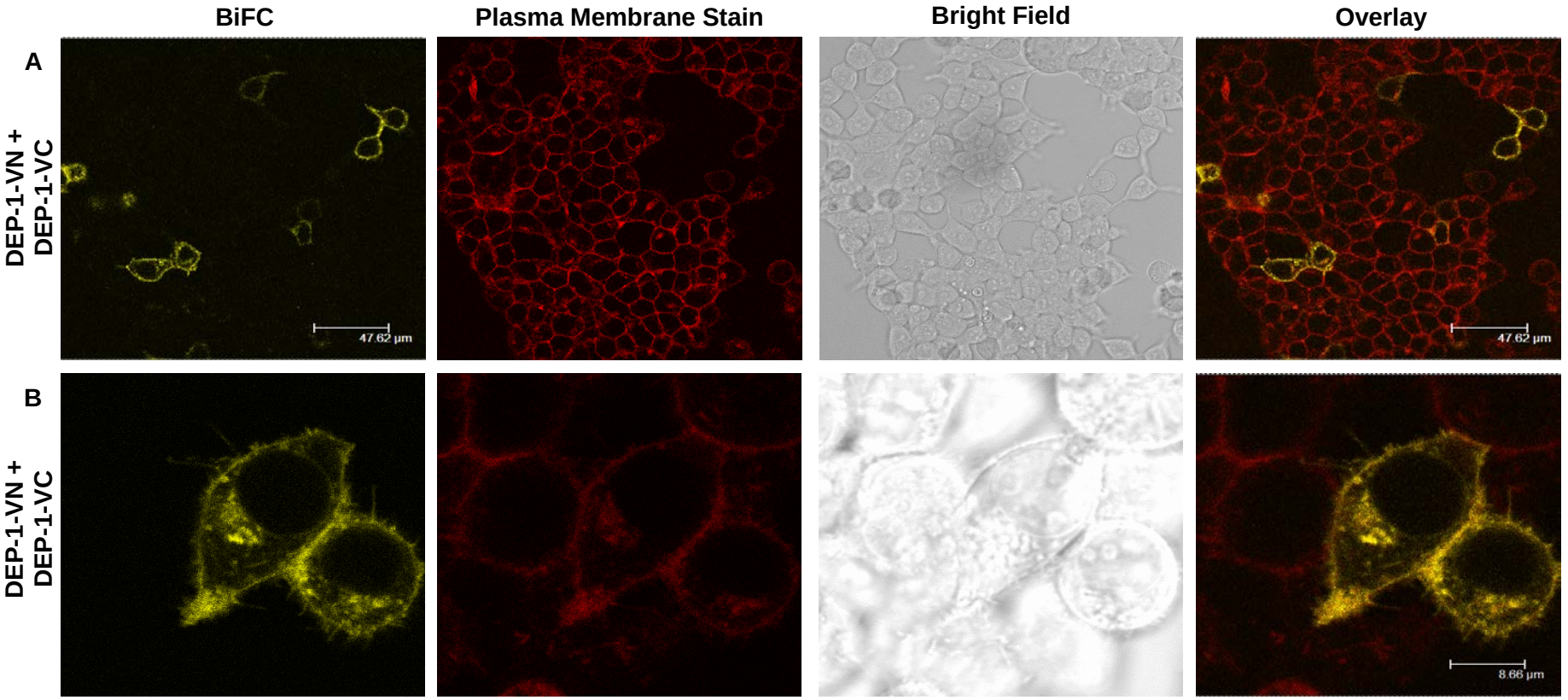

Figure 71. BiFC analysis of DEP-1 dimerisation. To investigate whether DEP-1 forms dimers in live cells, equal amounts of DEP-1-VN and DEP-1-VC fusions were used to co-transfect HEK293T cells and the resulting BiFC signal was analysed by confocal microscopy after 24 hours. (A) Confocal images of DEP-1-VN/DEP-1-VC interactions in cell populations. (B) Zoom in of HEK293T cells, showing the localisation of DEP-1-VN/DEP-1-VC interactions.

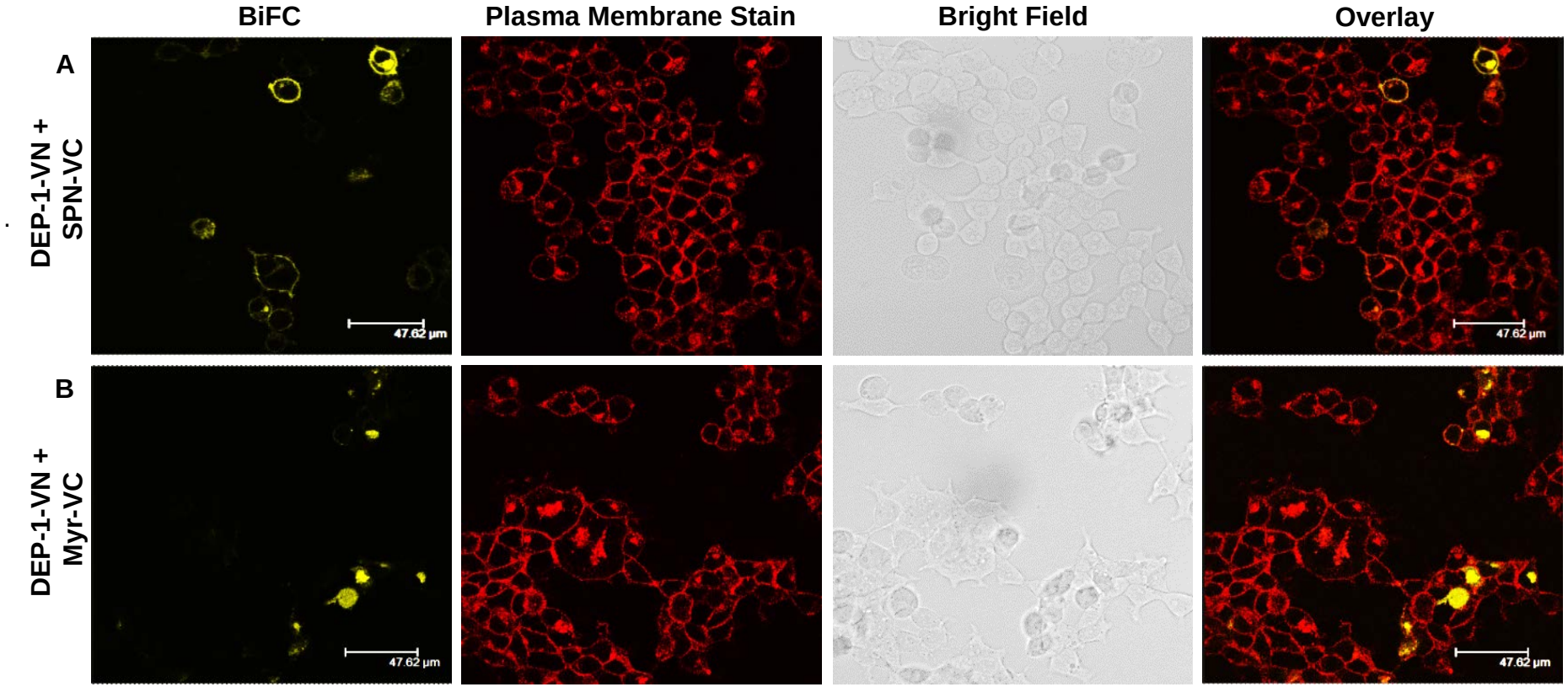

Figure 72. BiFC analysis of DEP-1-VN with control constructs SPN-VC and Myr-VC. To validate the specificity of the DEP-1-VN and DEP-1-VC interaction, DEP-1-VN was co-transfected with equal amounts of negative control constructs SPN-VC and Myr-VC into HEK293T cells and the resulting BiFC signal was analysed by confocal microscopy after 24 hours. (A) Confocal images of DEP-1-VN/SPN-VC interactions in cell populations. (B) Confocal images of DEP-1-VN/Myr-VC interactions in cell populations.

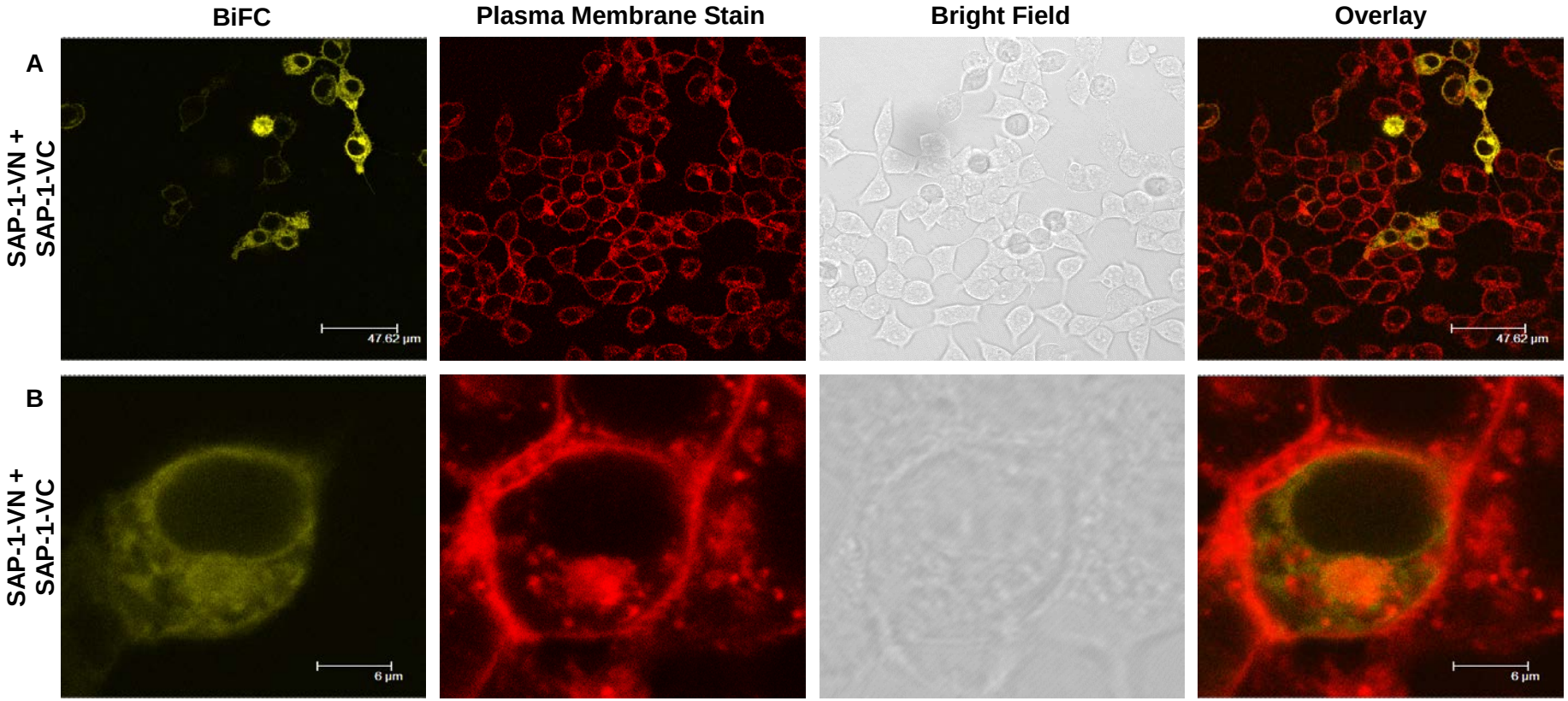

Figure 73. BiFC analysis of SAP-1 dimerisation. To investigate whether SAP-1 forms dimers in live cells, equal amounts of SAP-1-VN and SAP-1-VC fusions were used to co-transfect HEK293T cells and the resulting BiFC signal was analysed by confocal microscopy after 24 hours. (A) Confocal images of SAP-1-VN/SAP-1-VC interactions in cell populations. (B) Zoom in of HEK293T cells, showing the localisation of SAP-1-VN/SAP-1-VC interactions.

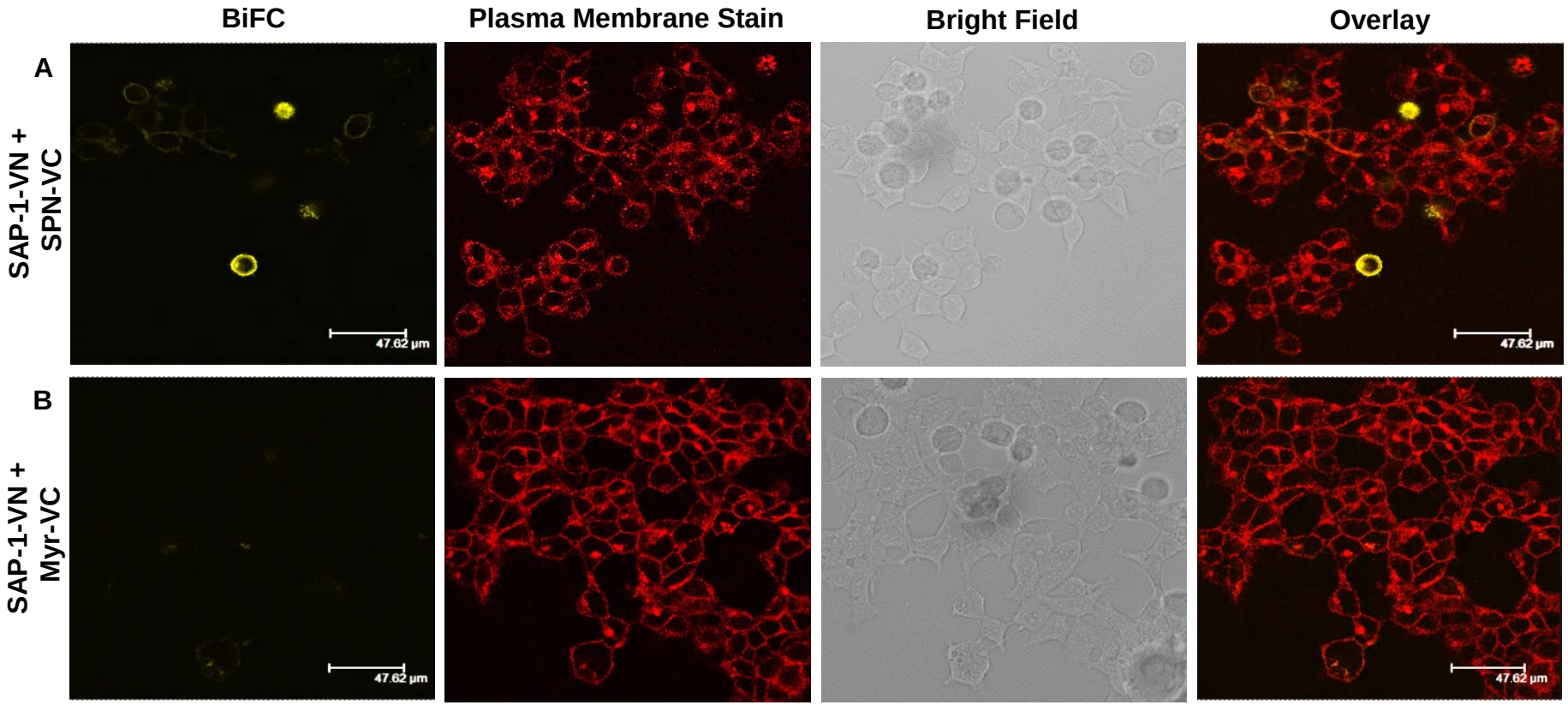

Figure 74. BiFC analysis of SAP-1-VN with control constructs SPN-VC and Myr-VC. To validate the specificity of the SAP-1-VN and SAP-1-VC interaction, SAP-1-VN was co-transfected with equal amounts of negative control constructs SPN-VC and Myr-VC into HEK293T cells and the resulting BiFC signal was analysed by confocal microscopy after 24 hours. (A) Confocal images of SAP-1-VN/SPN-VC interactions in cell populations. (B) Confocal images of SAP-1-VN/Myr-VC interactions in cell populations.

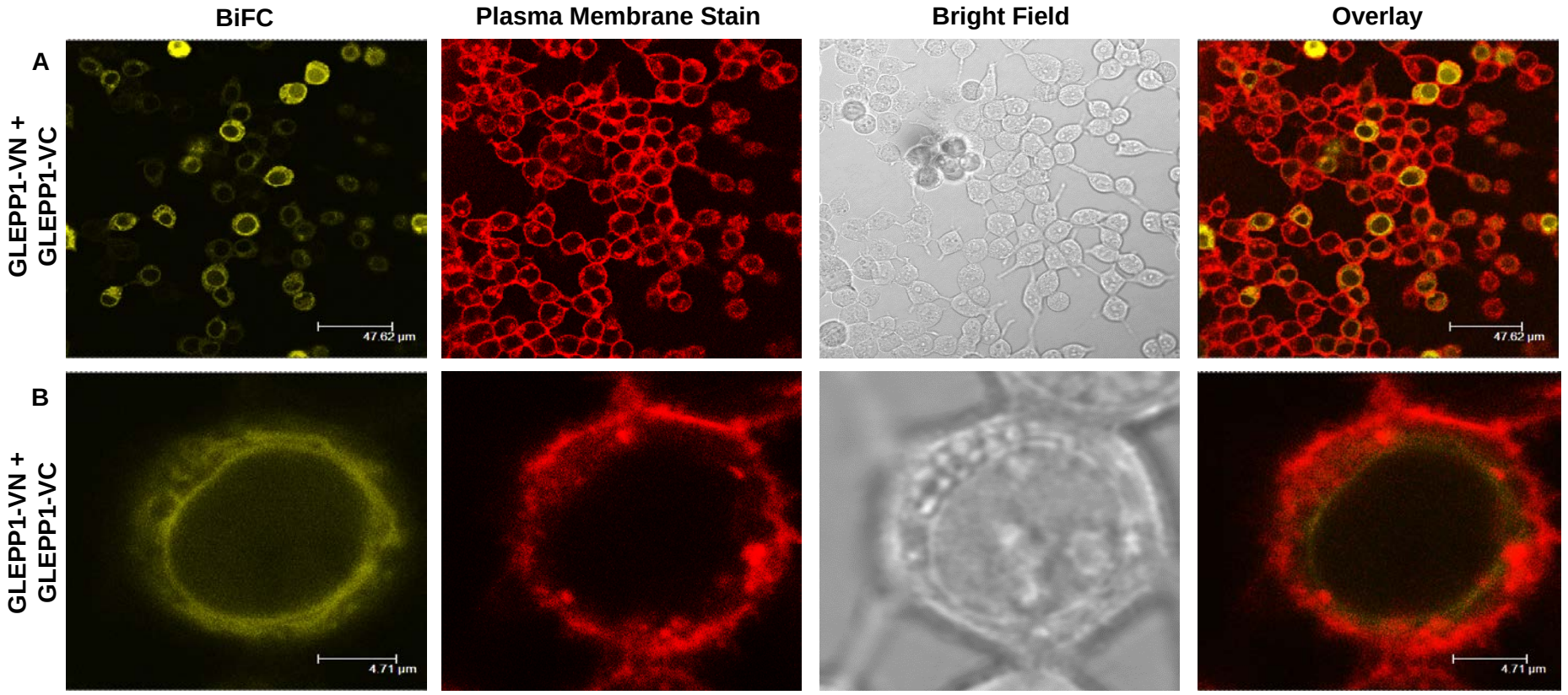

Figure 75. BiFC analysis of GLEPP1 dimerisation. To investigate whether GLEPP1 forms dimers in live cells, equal amounts of GLEPP1-VN and GLEPP1-VC fusions were used to co-transfect HEK293T cells and the resulting BiFC signal was analysed by confocal microscopy after 24 hours. (A) Confocal images of GLEPP1-VN/GLEPP1-VC interactions in cell populations. (B) Zoom in of HEK293T cells, showing the localisation of GLEPP1-VN/GLEPP1-VC interactions.

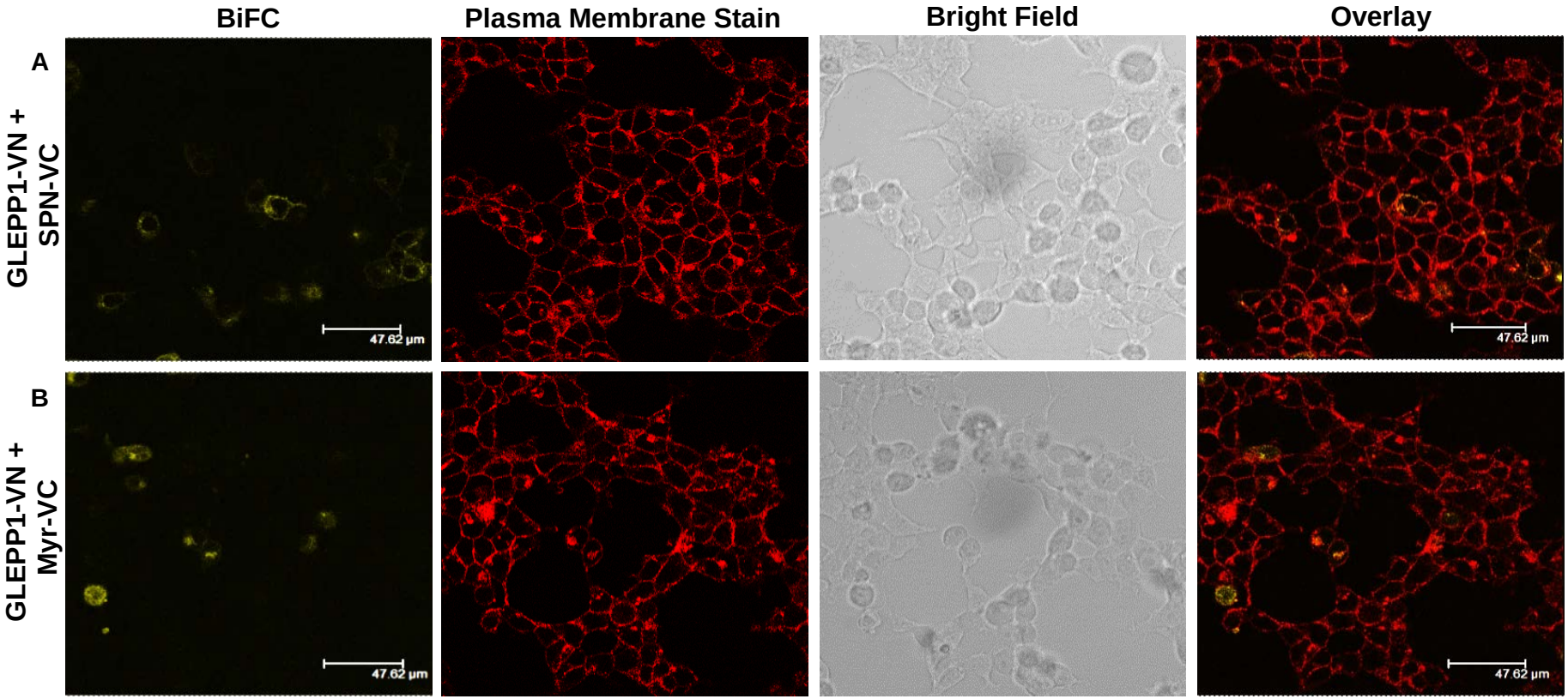

Figure 76. BiFC analysis of GLEPP1-VN with control constructs SPN-VC and Myr-VC. To validate the specificity of the GLEPP1-VN and GLEPP1-VC interaction, GLEPP1-VN was co-transfected with equal amounts of negative control constructs SPN-VC and Myr-VC into HEK293T cells and the resulting BiFC signal was analysed by confocal microscopy after 24 hours. (A) Confocal images of GLEPP1-VN/SPN-VC interactions in cell populations. (B) Confocal images of GLEPP1-VN/Myr-VC interactions in cell populations.

6.5 Quantitative analysis of R3 RPTP homodimerisation BiFC data

In order to complement the qualitative BiFC dimerisation results for each R3 RPTP fusion described above quantitative analysis was carried out using ImageJ software, as described in Chapters 2 and 3.

To analyse the BiFC specificity of R3 RPTP homodimerisation the distribution of yellow/red ratios in individual cells for each fusion pair was plotted in a histogram. In contrast to the qualitative analysis, co-expression of VE-PTP-VN and VE-PTP-VC resulted in fewer cell numbers exhibiting higher ratio values compared with cells co-expressing VE-PTP-VN and SPN-VC negative interacting pairs (Figure 77, A and B). There was very little difference in yellow/red ratio distribution between VE-PTP-VN/VE-PTP-VC and VE-PTP-VN/Myr-VC fusion pairs (Figure 77, A and C). Similarly, when comparing DEP-1-VN/DEP-1-VC and DEP-1-VN/SPN-VC interaction pairs there appears to be little difference in yellow/red ratio distribution between them (Figure 78, A and B). Co-expression of DEP-1-VN and Myr-VC resulted in more cells with lower ratio values than for DEP-1-VN/DEP-1-VC and DEP-1-VN/SPN-VC fusion pairs (Figure 78). Also, co-expression of SAP-1-VN/SAP-1-VC and SAP-1-VN/SPN-VC pairings gave rise to comparable results (Figure 79, A and B). Cells co-expressing SAP-1-VN and Myr-VC exhibited more cells with lower ratio values than for SAP-1-VN/SAP-1-VC and SAP-1-VN/SPN-VC fusion pairs (Figure 79). However, when GLEPP1-VN was co-expressed with GLEPP1-VC there were higher cell numbers with higher ratio value range in the region between 1 and 3 compared with cells co-expressing GLEPP1-VN and SPN-VC or GLEPP1-VN and Myr-VC control pairs (Figure 80). Cells co-expressing GLEPP1-VN and Myr-VC appeared to exhibit greater cell numbers with lower ratio values than for GLEPP1-VN/GLEPP1-VC or GLEPP1-VN/SPN-VC fusion pairs (Figure 80). However, it is difficult to conclude whether the reduction in cells exhibiting higher ratio value range is significant.

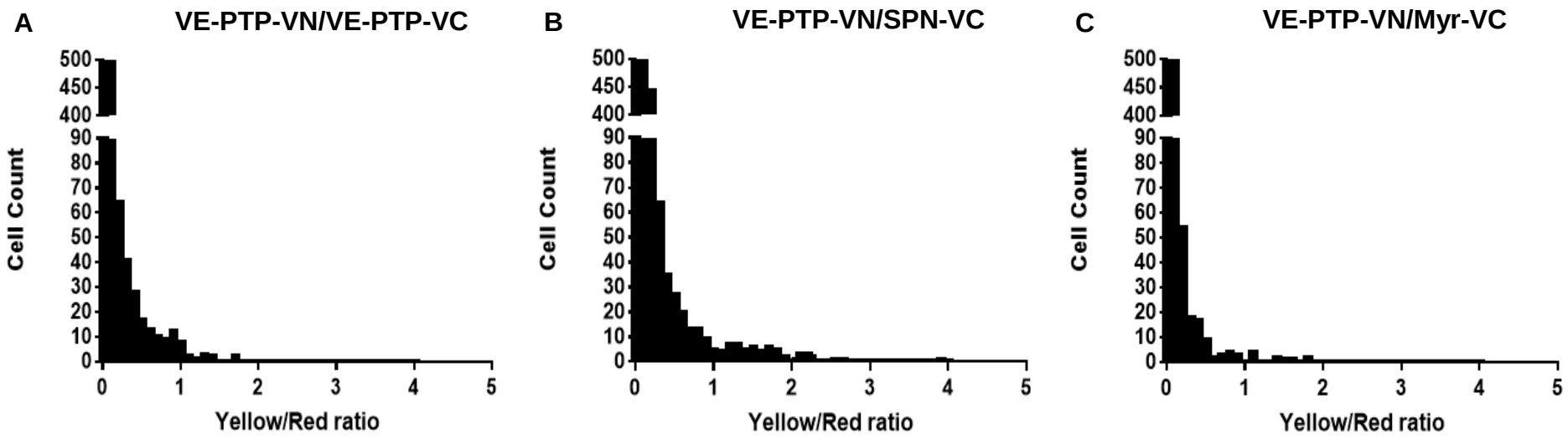

Figure 77. Validation of VE-PTP dimerisation. The fluorescence intensity from BiFC (yellow) and the fluorescent signal from the plasma membrane stain (red) were measured in individual cells. The distribution of ratios between the fluorescence intensity and red fluorescence signal in individual cells from at least three independent experiments was plotted in a histogram. The yellow/red ratio has been plotted for each pair of constructs: (A) VE-PTP-VN/VE-PTP-VC, (B) VE-PTP-VN/SPN-VC and (C) VE-PTP-VN/Myr-VC.

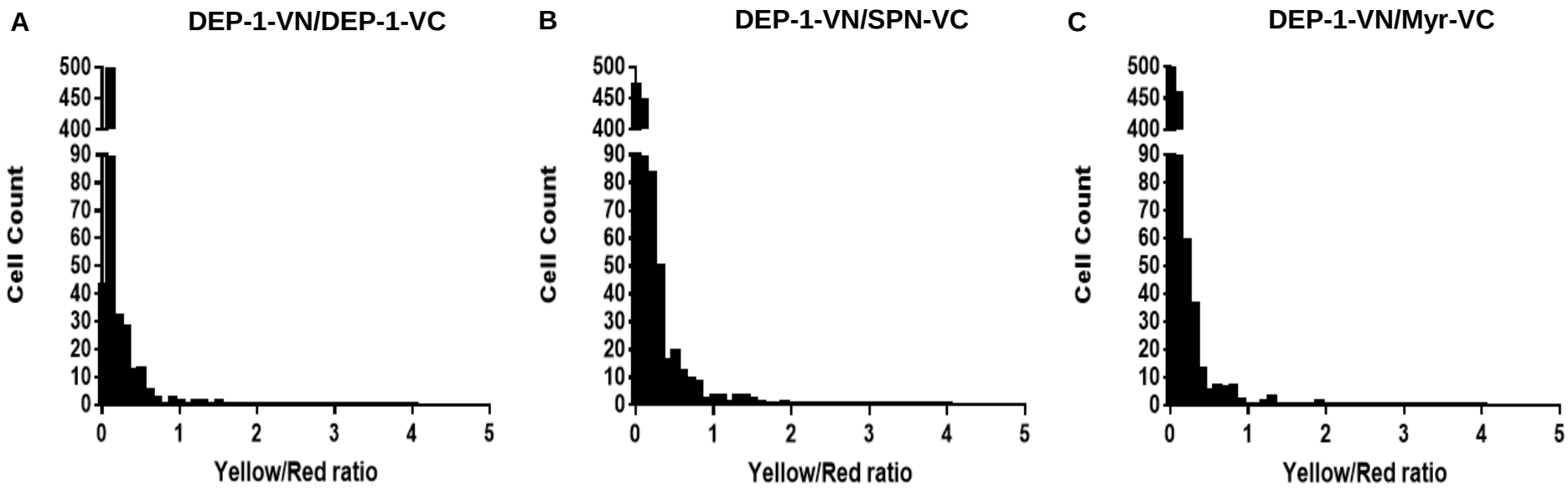

Figure 78. Validation of DEP-1 dimerisation. The fluorescence intensity from BiFC (yellow) and the fluorescent signal from the plasma membrane stain (red) were measured in individual cells. The distribution of ratios between the fluorescence intensity and red fluorescence signal in individual cells from at least three independent experiments was plotted in a histogram. The yellow/red ratio has been plotted for each pair of constructs: (A) DEP-1-VN/DEP-1-VC, (B) DEP-1-VN/SPN-VC and (C) DEP-1-VN/Myr-VC.

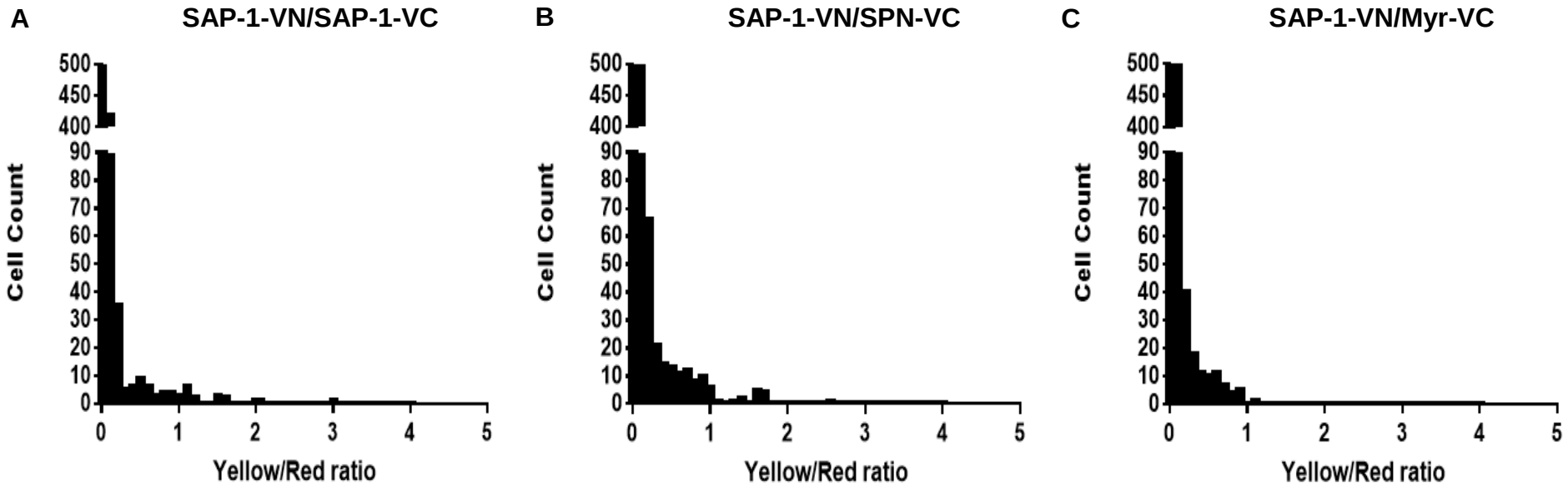

Figure 79. Validation of SAP-1 dimerisation. The fluorescence intensity from BiFC (yellow) and the fluorescent signal from the plasma membrane stain (red) were measured in individual cells. The distribution of ratios between the fluorescence intensity and red fluorescence signal in individual cells from at least three independent experiments was plotted in a histogram. The yellow/red ratio has been plotted for each pair of constructs: (A) SAP-1-VN/SAP-1-VC, (B) SAP-1-VN/SPN-VC and (C) SAP-1-VN/Myr-VC.

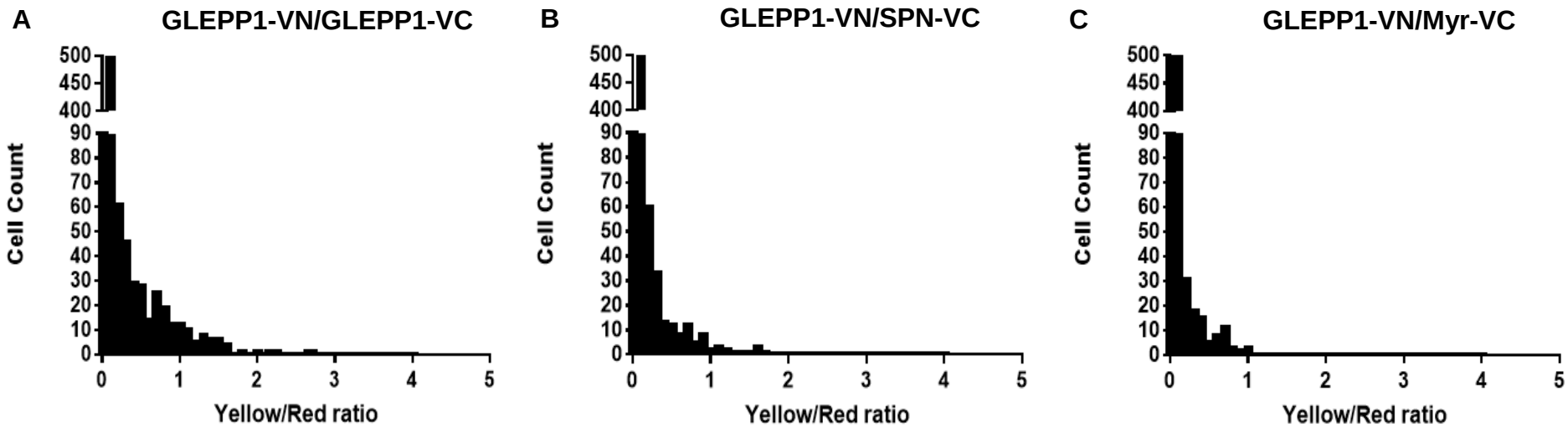

Figure 80. Validation of GLEPP1 dimerisation. The fluorescence intensity from BiFC (yellow) and the fluorescent signal from the plasma membrane stain (red) were measured in individual cells. The distribution of ratios between the fluorescence intensity and red fluorescence signal in individual cells from at least three independent experiments was plotted in a histogram. The yellow/red ratio has been plotted for each pair of constructs: (A) GLEPP1-VN/GLEPP1-VC, (B) GLEPP1-VN/SPN-VC and (C) GLEPP1-VN/Myr-VC.

The BiFC specificity was also determined by measuring signal-to-noise (S/N) ratio as described in Chapters 3 and 4 by dividing the median value of the positive interacting pair by that of the negative interacting pair. Therefore, for the Myr-VC-containing interacting pair the S/N ratio value was always 1, representing the background fluorescence. A higher S/N ratio value reflects a more specific interaction. The S/N ratio value was calculated for each interacting fusion pair, including control fusion pairs, to establish how much fluorescence signal was formed due to YFP fragments self-assembly. In addition, the average fluorescence intensities were compared in all interacting pairs as described in Chapters 3 and 4.

The S/N ratio value for VE-PTP-VN/VE-PTP-VC was 2.4 (Figure 81). Unexpectedly, although the S/N ratio value decreased to 1.5 in VE-PTP-VN/SPN-VC control pair, there was no significant difference in average fluorescence intensity between both fusion pairs (Figures 81 and 82). The S/N for VE-PTP-VN/Myr-VC control pair was 2.4 x lower than for VE-PTP-VN/VE-PTP-VC fusion pair (Figure 81). The average fluorescence intensity for VE-PTP-VN/Myr-VC was significantly reduced compared with VE-PTP-VN/VE-PTP-VC and VE-PTP-VN/SPN-VC fusion pairs (Figure 82). However, these results are considerably lower when comparing with VE-PTP-VN/VE-cadherin interacting pair, suggesting that perhaps VE-PTP does not form homodimers. The average fluorescence intensity for VE-PTP-VN/VE-cadherin-VC was 1.9 x higher and the S/N was 2.7 x higher than for VE-PTP-VN/VE-PTP-VC (Figures 40 and 41). These results suggest that VE-PTP does not homodimerise via its extracellular domain and the fluorescence signal was more likely due to non-specific YFP fragments interactions.

Interestingly the average fluorescence intensity in cells co-expressing DEP-1-VN/DEP-1-/VC was significantly lower (about 1.6 x) compared with cells co-expressing DEP-1-VN/SPN-VC (Figure 82). However, the average fluorescence intensity for both DEP-1-VN/DEP-1-VC and DEP-1-VN/SPN-VC interacting pairs was significantly higher than for DEP-1-VN/Myr-VC control pair (Figure 82). Both DEP-1-VN/DEP-1-VC and DEP-1-VN/SPN-VC fusion pairs resulted in the same S/N ratio value of 3.7, which was 3.7 x higher than

for DEP-1-VN/Myr-VC control pair (Figure 81). Similarly to VE-PTP, DEP-1-VN/DEP-1-VC co-expression resulted in a significantly lower average fluorescence intensity than for DEP-1-VN/VE-cadherin-VC (Figures 67 and 82). These results suggest that perhaps DEP-1 does not readily form homodimers.

On the other hand, S/N ratio value and average fluorescence intensity for SAP-1-VN/SAP-1-VC were significantly higher than for negative interacting pairs SAP-1-VN/SPN-VC and SAP-1-VN/Myr-VC by 1.85- and 1.6-fold respectively (Figures 81 and 82). The average fluorescence intensity in cells co-expressing SAP-1-VN/SAP-1-VC appears to be similar to fluorescence intensity in cells co-expressing SAP-1-VN/VE-cadherin/VC (Figures 67 and 82). However, S/N ratio value for SAP-1-VN/Sap-1-VC appears to be much lower than for SAP-1-VN/VE-cadherin-VC (Figures 66 and 81). These results suggest that SAP-1 has the potential to form homodimers via its extracellular domains.

S/N ratio value for GLEPP1-VN/GLEPP1-VC was 4.8-fold higher than for GLEPP1-VN/SPN-VC and 10.5-fold higher compared with GLEPP1-VN/Myr-VC (Figure 81). The average fluorescence intensity in cells co-transfected with GLEPP1-VN/GLEPP1-VC was significantly higher compared with cells co-transfected with GLEPP1-VN/SPN-VC and GLEPP1-VN/Myr-VC. The average fluorescence intensity for GLEPP1-VN/GLEPP1-VC was 2.2 x higher than for GLEPP1-VN/SPN-VC and 4.5 x higher than GLEPP1-VN/Myr-VC (Figure 82). S/N ratio value and average fluorescence intensity for GLEPP1-VN/GLEPP1-VC were both higher than the values obtained for GLEPP1-VN/VE-cadherin-VC (Figures 66, 67, 81 and 82). All three methods of analysis complement each other, suggesting that GLEPP1 has the potential to form homodimers via its extracellular domain.

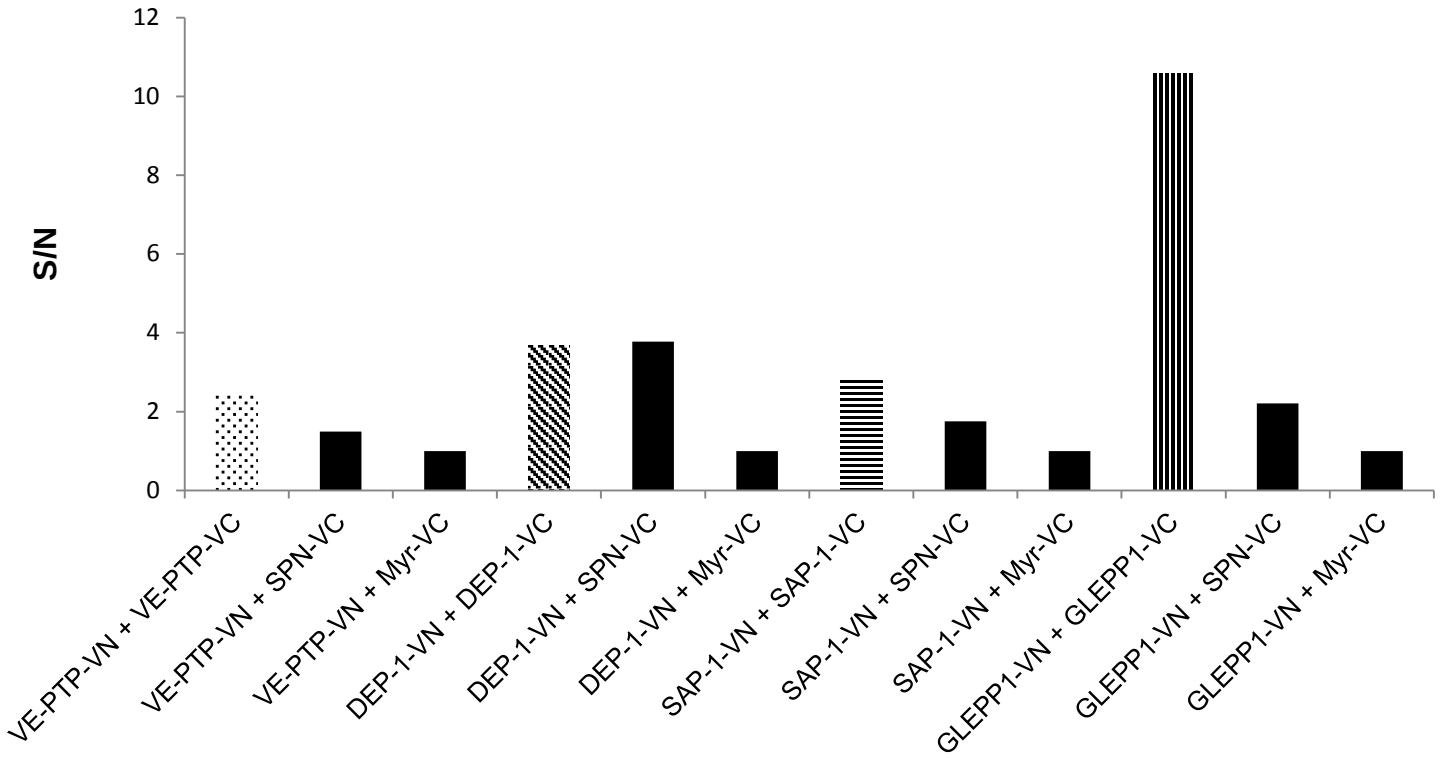

Figure 81. S/N ratio of BiFC assay in HEK293T cells in R3 RPTP dimerisation study. S/N for each interacting fusion pair was calculated by dividing its median value by the median value from the corresponding Myr-VC-containing fusion pair. The median value for each fusion pair was calculated based on at least three independent experiments.

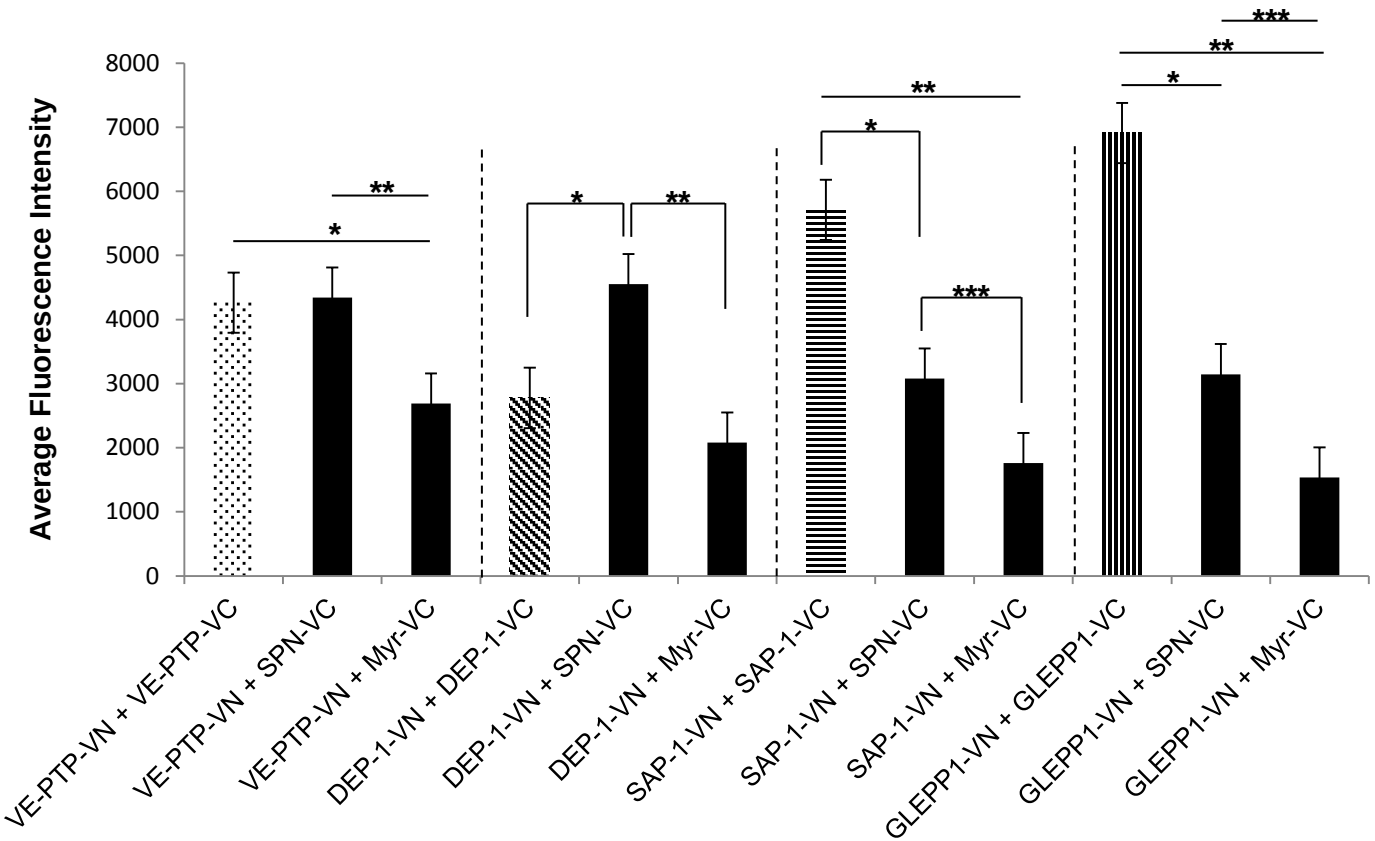

Figure 82. Quantitation of BiFC fluorescence intensities in transiently transfected HEK293T cells. Pairs of constructs as indicated were transfected into HEK293T cells using equal amounts of each expression vector and the BiFC signal assessed. Average fluorescence intensity and error bars of at least three independent experiments was determined using ImageJ software as described in the materials and methods. At least three random fields were analysed in experiments for each fusion pair tested. $p<0.001$ by the Kruskal-Wallis test was considered significant.

6.6 Evaluating the fraction of BiFC constructs in the plasma membrane

Since generation of fusion proteins and deletion of the intracellular sequence, as in this study, may affect the sub-cellular localisation of the protein, I assessed the fraction of the DEP-1-VN construct present in the plasma membrane relative to total cell expression and compared this with a full-length DEP-1 expression construct. This was achieved essentially as described in van der Wijk *et al* (2005). Briefly, using cells transfected with either DEP-1-VN or DEP-1 full-length constructs, the constructs were immunoprecipitated from whole cell lysates or immunoprecipitated after adding the anti-myc antibody to intact cells, to detect cell-surface expression only. The amount of immunoprecipitated protein was assessed by Western blotting. So far the results were obtained only for DEP-1-VN fusion construct due to availability of the corresponding full-length expression vector. Nonetheless the results could be potentially extrapolated to other similar R3 RPTP constructs.

Comparison of the fraction of cell-surface expression of the DEP-1-VN construct, relative to total DEP-1-VN expression, with the fraction of cell-surface expression of full-length DEP-1 (Fig. 83) indicated that the BiFC construct exhibited a similar fraction of cell-surface expression as DEP-1, suggesting that the generation of the fusion protein did not detract from effective trafficking of the protein. Degradation was not evident (Figure 77), indicating the cell-surface localisation and protein stability were not significantly affected by creating the fusions, although it is possible that some degradation products lacking a myc tag are not detected by this analysis. As observed in studies investigating interactions with VE-cadherin, in the studies of homodimerisation in this chapter, a BiFC signal was observed in both the plasma membrane and an intracellular structure. This is likely to be the rough endoplasmic reticulum revealing that formation of the BiFC complex between proteins of interest can occur in the endoplasmic reticulum during the post-translation modifications prior to trafficking to the plasma membrane. However, further experiments are required to confirm surface localisation of all R3 RPTP fusion constructs.

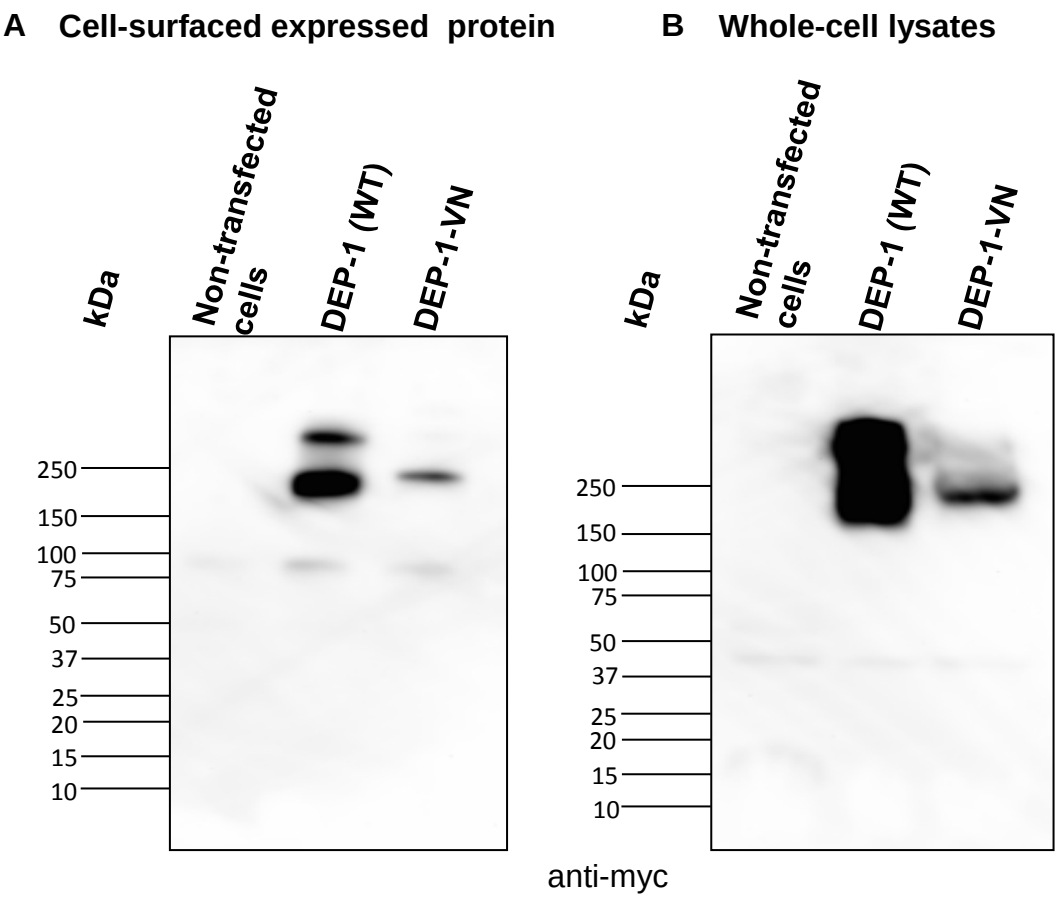

Figure 83. Evaluating the fraction of the DEP-1 BiFC construct in the plasma membrane. Comparison of DEP-1-VN construct cell surface expression relative to the full-length DEP-1 protein. HEK293T cells transfected with either DEP-1-VN or full-length DEP-1(WT). (A) Cell-surface protein was immunoprecipitated with an anti-myc antibody and detected in an anti-myc Western blot. (B) Whole cell lysates showing total protein expression.

6.7 Discussion

Dimerisation of R3 RPTPs has been previously studied by co-immunoprecipitation experiments, though it still remains unclear whether all R3 RPTP members homodimerise (Hower *et al*, 2009; Walchli *et al*, 2005; Sorby *et al*, 2001; Takahashi *et al*, 2006). It has not to date been studied in live cells and it is not known whether all the members of the R3 subgroup have the potential to form homodimers. In addition the role of the extracellular domain of R3 RPTPs in dimerisation remains undefined.

Using the bimolecular fluorescence complementation technique the potential of R3 RPTPs to homodimerise via their extracellular and transmembrane domains was examined in live cells. Each BiFC construct consisted of the ectodomain and transmembrane domain of these molecules (as shown in Figures 21 and 47). Qualitative and quantitative assessments of the fluorescence images obtained on co-expression of either VE-PTP-VN/VE-PTP-VC, DEP-1-VN/DEP-1-VC, SAP-1-VN/SAP-1-VC or GLEPP1-VN/GLEPP1-VC fusion pairs suggested potential homodimerisation of SAP-1 and GLEPP1 but not VE-PTP and DEP-1. Quantitative assessment of these interacting pairs indicated that the co-expression of either SAP-1-VN/SAP-1-VC or GLEPP1-VN/GLEPP1-VC fusion pairs resulted a BiFC signal that was due to a specific interaction, rather than self-assembly of constructs and background fluorescence.

The results of this chapter complement previous co-immunoprecipitation studies that demonstrated SAP-1 homodimerisation is mediated by its extracellular domain (Walchli *et al*, 2005). The finding that the extracellular domain of SAP-1 potentially forms homodimers is reminiscent of the previous reports on some other transmembrane proteins. For example, it has been demonstrated that RPTPα exists predominantly as homodimers and that both its extracellular and transmembrane domains were independently able to form homodimers though the exact contribution of each of the individual dimerisation domains has not yet been determined (Jiang *et al*, 2000). Interestingly, different isoforms of the same protein can undergo differential homodimerisation. A study by Xu and Weiss (2002) demonstrated that a

smaller isoform of CD45 formed homodimers more rapidly and efficiently compared with a larger CD45 isoform. The dimerisation was mediated by the extracellular domain, independently of cytoplasmic tail (Xu and Weiss, 2002). However, in this chapter the SAP-1 construct consisted of extracellular and transmembrane domain and there is a possibility that the observed dimerisation could be mediated by its transmembrane region. Dimerisation of PTPσ via its transmembrane domain was reported by Lee *et al* (2015). It has been demonstrated that the transmembrane was sufficient for at least some of the homodimerisation, though the intracellular and, to a lesser extent, the extracellular domain of the protein could also contribute (Lee *et al,* 2015). The above results suggest that the dimerisation of RPTPs could be modulated by multiple domains and the dimerisation does not fit one model. However, it is becoming apparent that extracellular and/or transmembrane domains of RPTPs play an important role in their regulation and may have physiological significance if regulated by ligands leading to changes in phosphatase activity.

It has been previously shown that GLEPP1 can potentially form homodimers mediated by its transmembrane and intracellular domains but not extracellular domain (Walchli *et al*, 2005; Hower *et al,* 2009). In a co-immunoprecipitation study by Hower *et al* (2009) a GLEPP1 construct was used in which the extracellular domain had been replaced by a NGF receptor TrkA and, thus, they could not conclude whether the extracellular domain has a role in dimerisation or not. In this chapter, however, we show that there is a potential involvement of the extracellular and transmembrane domains but not intracellular domain. Both studies (i.e. the study by Hower *et al* (2009) and the study of this chapter) were carried out using different constructs; however in both cases the transmembrane domain of GLEPP1 was present. This suggests that perhaps homodimerisation of GLEPP1 is mediated by its transmembrane domain. As already mentioned above, there are many examples of membrane proteins forming homo- and hetero-oligomers via transmembrane domains, including receptor-type phosphatases. Dimerisation of sialoglycoprotein in human erythrocyte membranes glycophorin A (GpA) was extensively studied. A pattern of seven

amino acids (L75IXXGVXXGVXXT87 (L, leucine; I, isoleucine; X, any amino acid; G, glycine; V, valine; T, threonine)) in the transmembrane of GpA was shown to be sufficient to drive its dimerisation (Lemmon *et al*, 1994). The right-handed parallel transmembrane domain α-helices cross at an angle of 40° and form a supercoil with a closely packed interface (ridges-into-grooves structure). The GXXXG motif (two glycines separated by any three residues) within the pattern of seven amino acids of GpA was shown to facilitate specific protein-protein dimerisation as glycine residues stabilise the structure through Van der Waals interactions and/or hydrogen bonding with residues on the opposite helix. This brings the interacting helices into close proximity of each other (Strous and Gent, 2002). Mutation of glycine to alanine was shown to distract dimerisation. The insertion of this motif into other hydrophobic sequence backgrounds also led to dimerisation. Genetic and statistical data suggested that the GXXXG motif is a common framework for transmembrane domain helix-helix interactions (Strous and Gent, 2002). These findings propose that many transmembrane domains may contain information that regulates specific interactions, perhaps common to many proteins, with functionally important consequences. Indeed, it has been reported that GXXXG motifs are present in about 12 % of transmembrane helices (Teese and Langosch, 2015). However, some previous observations demonstrated that the presence of GXXXG motif is not an indicator of dimerisation but influenced by sequence context presumably to ensure that non-specific interactions of transmembrane helices are avoided. Instead, the conserved transmembrane residues (such as GXXXG motif) could play a role in a variety of functions, ranging from enhancing helix flexibility, lipid interactions and cell localisation (Teese and Landosch, 2015). Interestingly, alignment of the membrane-spanning sequences performed by Chin *et al* (2005) revealed that VE-PTP, DEP-1 and SAP-1, but not GLEPP1, contain such GXXXG motif in their transmembrane domains. In the same study Chin *et al* (2005) showed that the transmembrane of DEP-1 was able to self-interact in the membrane. What is more, G979L and G983L mutations in GXXXG motif were found the most disruptive (Chin *et al*, 2005). In the same study GLEPP1 resulted in the strongest dimerisation signal despite the lack of GXXXG motif in its transmembrane domain (Chin *et al*, 2005). This

confirmed that more than one sequence motif in one or more domains could influence the interaction between proteins. In this Chapter, in agreement with previous findings, the quantitative analysis revealed that the co-expression of GLEPP1 fusion constructs resulted in the highest average fluorescence intensity as well as S/N ratio value, suggesting homodimerisation of this protein. Interestingly though, sedimentation velocity measurements carried out by Barr *et al* (2009) showed that GLEPP1 and DEP-1 were entirely monomeric in solution. The presence of GXXXG motif in the transmembrane domains of VE-PTP and SAP-1 does not seem to be involved in their dimerisation as shown by Chin *et al* (2005). As outlined above, the GXXXG motif is only a weak predictor of a dimerisation. Based on results obtained in this project, the dimerisation of SAP-1 is more likely mediated by its extracellular domain. This is in agreement with previous results obtained by Walchli *et al* (2005), showing that the extracellular domain of SAP-1 was sufficient to facilitate dimerisation, independently of its cytoplasmic and transmembrane regions. On the other hand, the results on VE-PTP dimerisation was consistent with the previous study by Chin *et al* (2005), showing that this phosphatase does not dimerise. However, similarly to DEP-1, the dimerisation could still occur on a physiological level as a result of some ligand binding.

The results obtained in this project also suggest that DEP-1 does not dimerise, which contradicts some previous findings. As mentioned in the introduction of this Chapter, the study by Takahashi *et al* (2006) showed that the extracellular domain of DEP-1 can form homodimers and that this forced dimerisation mediated by bivalent antibody increases its activity. A study by Sorby *et al* (2001) also demonstrated that DEP-1 activity can be increased as a result of ligand stimulation. Stimulation of DEP-1 with MatrigelTM (a preparation of extracellular matrix proteins secreted by Englebreth - Holm - Swarm mouse sarcoma) had a direct agonistic effect on DEP-1, which was mediated through interaction with the extracellular domain of DEP-1 (Sorby *et al*, 2001). Therefore, despite the results of this Chapter, DEP-1 could still have the potential to form extracellular ligand-mediated dimers *in vivo*. Ligand-induced dimerisation was shown for a cell surface receptor

glycoprotein CD36. A study by Daviet *et al* (1997) demonstrated that CD36 exists predominantly as a monomer, but undergoes homodimerisation upon extracellular binding of Thrombospondin-1. Thrombospondin-1-induced dimerisation of CD36 was shown to be implemented in signal transduction of angiogenic pathways (Daviet *et al*, 1997).

Dimerisation, whether it is homodimerisation or heterodimerisation, represents a powerful regulatory mechanism that can have a variety of functional consequences. Dimerisation between the same members of a family could have distinct functional specificity, whereas dimerisation between different members of a protein family can result in functional diversity, when different protein combinations have distinct regulatory properties. It is an attractive idea that RPTPs could be regulated by dimerisation similarly to RPTKs. Understanding the molecular mechanisms of the regulation of R3 RPTP would potentially assist in drug development for R3 RPTPs for some diseases, such as some immune, cardiovascular and neurological disorders or some types of cancers. For example, ligand-fusion proteins or antibodies to the extracellular domain of R3 RPTPs could be potentially used to regulate their activity. R3 RPTPs have been described as tumour suppressors and dysregulation of these phosphatases has been implicated in a variety of diseases. For example, GLEPP1 has been found to be lost in malignant cells in colon cancer and in hepatocellular carcinomas (Tautz *et al*, 2006). GLEPP1 was shown to play a role in terminal differentiation, apoptosis and cell cycle arrest, which are some of the hallmarks of tumour suppressor (Aguiar *et al*, 1999; Seimiya and Tsuruo, 1998). Using restriction landmark genome scanning (RLGS) in an animal model of multistage tumorigenesis induced by folate/methyl-deficiency revealed that GLEPP1 gene was silenced due to immediate promoter methylation during hepatocarcinogenesis progression resulting in significant reduction of GLEPP1 expression (Motiwala *et al*, 2003). These findings suggested that the silencing of PTPRO in the liver could facilitate tumour promotion either by relaxing cell cycle arrest, preventing cell contact inhibition or developing resistance to apoptosis (Motiwala *et al*, 2003). A truncated isoform of GLEPP1 (PTPROt) is expressed in B-lymphoid cells.

More recent study by Motiwala *et al* (2015) showed that PTPROt is significantly down-regulated in the most common adult leukaemia, Chronic Lymphocytic Leukaemia (CLL). The expression of PTPROt was shown to prevent infiltration of inflammatory cells, such as monocytes and T-lymphocytes that support the growth of CLL cells, into the spleen (the study was concentrating on spleen tissue as an increased spleen weight and accumulation of leukaemic CD5/CD19 cell population are the characteristics of CLL) (Motiwala *et al*, 2015). In addition, the expression of PTPROt appeared to suppress the leukaemic phenotype by mediating activation of a cellular tumour protein p53 and the resultant suppression of an oncogenic transcription factor Foxm1 expression (Motiwala *et al*, 2015). The collective results suggest that GLEPP1 could be a good therapeutic target for novel drugs against some types of cancer.

SAP-1 expressed in intestinal epithelial cell was shown to be involved in the regulation of the intestinal immunity, partially by controlling the expression of proinflammatory cytokines and chemokines, such as interferon-γ and IL-17, in the colonic mucosa (Kotani *et al*, 2016). It has been suggested that SAP-1 regulates the intestinal immunity through its physiological substrate CAECAM20 (carcinoembryonic antigen-related cell adhesion molecule 20). Tyrosine phosphorylation of CAECAM20 is an intestinal microvilli-specific membrane protein that was shown to promote the binding of spleen tyrosine kinase (Syk) and activation of nuclear factor-κB (NF-κB) in cultured cells. This leads to the production of IL-8 chemokine that, in turn, results in neutrophil infiltration, both of which were shown to be characteristics of inflammatory bowel disease (Murata *et al*, 2015). It has been shown that SAP-1 and CAECAM20 can associate together via their extracellular domains, independently of their cytoplasmic tails. However, full-length of SAP-1 is required to exert its effect on CAECAM20 as it has been shown to dephosphorylate CAECAM20 and, thus, counteract CAECAM20-mediated proinflammatory effects (Murata *et al*, 2015). Therefore, SAP-1 represents a therapeutic potential in inflammatory bowel diseases. The therapeutic potential of VE-PTP and DEP-1 as targets for anti-inflammatory drugs was discussed in previous Chapters 4 and 5 with regards to their regulatory roles

in leukocytes extravasation and T-cell receptor signalling respectively. DEP-1 also represents an attractive therapeutic target for the treatment of the cardiovascular diseases associated with diabetes and obesity. A study by Shintany *et al* (2015) demonstrated that R3 RPTPs suppressed the insulin-induced tyrosine phosphorylation of the insulin receptor (IR), inhibiting insulin signalling and negatively regulating energy metabolism. However, DEP-1 is the only R3 RPTP that is expressed in insulin target tissues such as the skeletal muscle, liver and adipose tissue, where it was shown to co-localise with insulin receptor in the plasma membrane (Shintany *et al*, 2015). Selective DEP-1 inhibitors could have the potential to enhance the insulin-induced activation of IR and the downstream Akt signalling, thus improving glucose and insulin tolerance in type 2 diabetes patients.

Although R3 RPTPs represent an attractive drug target many difficulties limit the development of PTPs' inhibitors due to a highly charged and highly conserved active site. Highly potent inhibitors often target multiple PTPs that can lead to tremendous adverse effects. Despite this major drawback, there was an influx of new strategies in developing competitive orthosteric and allosteric PTP inhibitors to target specific PTPs (Stanford and Bottini, 2017). One of the exciting developments in the PTP field is the development of the first-in-class selective orthosteric small molecule VE-PTP inhibitor AKB-9778 (Campochiaro *et al*, 2015). This small molecule was shown to be effective in diabetic retinopathy and retinal vein acclusion treatments as well as other eye diseases, including neovascular age-related macular degeneration, characterised by excessive vascular permeability and ocular neovascularisation and it is now in clinical trials (Shen *et al*, 2014). VE-PTP was shown to negatively regulate the activity of the angiopoietin-1 receptor Tie2, which together with VE-cadherin and plakoglobin play a role in maintaining the integrity of endothelial junctions (Fachinger *et al*, 1999). VE-PTP regulation of vascular integrity via Tie2 and VE-cadherin appear to be independent of each other. VE-PTP was shown to inhibit Tie2, resulting in increased vascular leakage and, thus, inhibiting VE-PTP would represent an attractive therapeutic target to decrease vascular leakage associated with certain eye diseases as well as type 2 diabetes. Small molecule AKB-9778

appeared to inhibit VE-PTP catalytic activity, leading to the increased phosphorylation of Tie2 and activation of downstream Akt signalling and subsequent reduction in vascular leakage and occular neovascularisation (Shen *et al*, 2014).

In most cases the ligands for the R3 RPTPs, the regulation of their dimerisation state and the effects of dimerisation on their activity are not fully defined. Nonetheless, increasing evidence shows that dimerisation can determine enzyme activity and growing data demonstrates that generally protein tyrosine phosphatases are inhibited by dimerisation. However, in some cases, as was seen with DEP-1, the catalytic activity was enhanced by artificial dimerisation. Therefore, the correlation between dimerisation and regulation of catalytic activity should be established specifically for each RPTP and cannot be extrapolated even to members of the same sub-type of RPTPs. Understanding regulatory mechanisms of R3 RPTPs will shed light on physiological roles of this subfamily and aid in development of novel therapeutic targets. Further studies are required to define the relative roles of the extracellular and transmembrane domains in R3 RPTP dimerisation and perhaps explore other possible mechanisms of their regulation, such as extracellular ligand binding or reversible oxidation.

6.8 Conclusion

Although there is growing evidence that the dimerisation of R3 RPTPs can regulate their functions and that their extracellular and/or transmembrane domains could be involved in the formation of dimers, the results of this chapter clearly demonstrate that the phosphatases of this subgroup do not behave in similar ways and, thus, it is difficult to present a unifying theme. Based on the results obtained in this project GLEPP1 and SAP-1 have a potential to dimerise, which is mediated by their extracellular and/or transmembrane domains. However, the exact molecular interface of such interactions remains unclear and requires further investigation. VE-PTP and DEP-1 did not show the potential to dimerise via their extracellular and

transmembrane domains, though dimerisation can perhaps still occur under physiological conditions through different domains (e.g. cytoplasmic domain or full-length protein is required) or as a result of extracellular ligand binding. There could be another regulatory mechanism altogether. Therefore, further experiments are required to establish the potential of these phosphatases to dimerise and to investigate other means of their regulation in order to gain better understanding of their functions.

Chapter 7

Summary and Future Directions

This thesis uses a live cell bimolecular fluorescence complementation (BiFC) assay and the results provide insight into functional roles and the importance of the extracellular and transmembrane domains of protein tyrosine phosphatases of the R3 subgroup (R3 RPTPs). This method enabled me to confirm the interaction between VE-PTP and VE-cadherin via their extracellular domains in live cells, representing a major step forward from previous immunoprecipitation studies. In addition this method was used to investigate extracellular domain interactions of other members of the R3 subgroup, namely DEP-1, SAP-1 and GLEPP1 with VE-cadherin. Despite little homology within their extracellular domains all members of the R3 subgroup showed the potential to interact with VE-cadherin via their extracellular and/or transmembrane domains in live cells, although the physiological importance of these interactions remains to be defined. The molecular basis of these interactions has to be further investigated. It is possible that the extensive glycosylation of their extracellular domains could also play a role in the interaction with other proteins. This project also demonstrated that the 17th FNIII-like domain of VE-PTP is not the only domain involved in interaction with VE–cadherin as was reported by previous studies by Nawroth *et al* (2002). This raises a question whether these protein-protein interactions are specific. Collective results over the decade showed that phosphatases appear to exhibit high specificity towards their substrates (Zhang *et al*, 1993; Zhang *et al*, 2002). However, whether the specificity applies towards ligand binding is not fully defined. Based on the expression analysis of R3 RPTPs it has been proposed that the ligand binding specificity is determined by specific tissue and/or cell type expression. More recent studies highlight the importance of extracellular and transmembrane domains of R3 RPTPs in protein-protein interaction. In itself extracellular ligand binding was proposed to be one of the regulatory mechanisms that governs substrate specificity of RPTPs, thus regulating their catalytic activity (den Hertog *et al*, 2008). Perhaps there are combinatorial factors that determine specificity of R3 RPTP interactions. Homophilic binding interactions have been shown for some R3 RPTPs in

previous immunoprecipitation studies and have been proposed as another regulatory mechanism.

The results of this project showed that fusion constructs SAP-1 and GLEPP1 indeed have the potential to form dimers via their extracellular and/or transmembrane domains. On the other hand, fusion constructs VE-PTP and DEP-1 appeared not to homodimerise. However, in this project the generated BiFC fusion constructs consisted of extracellular and transmembrane domains fused to either N- or C-terminal part of a yellow fluorescent protein, lacking the intracellular domain entirely. Perhaps, VE-PTP and DEP-1 still have the potential to form homodimers in their normal physiological environment via their intracellular domains or every domain is required for the dimerisation to occur. In addition, the dimerisation could occur in response to extracellular ligand binding. Based on the results of this project and on many previous studies it appears that the regulation of R3 RPTP could be specific to each member and the results for one phosphatase cannot be extrapolated to another even though they belong to one subgroup. Further work is necessary to investigate the detailed molecular basis of interactions between R3 RPTP and VE-cadherin as well as the molecular basis of homodimerisation. We have already begun further experiments with VE-PTP and VE-cadherin, using the same methodology. In order to understand what particular region is essential for this interaction various mutants of VE-PTP are being generated, each lacking two different extracellular domains, which would be then co-expressed with VE-cadherin. Moreover, it would be of particular interest to investigate the role of glycosylation of the extracellular domains of R3 RPTPs in protein-protein interactions.

The BiFC assay remains a popular tool for direct visualisation of protein-protein interactions in live cells due to its simplicity and the ability to carry out experiments with regular confocal microscopy. Despite many improvements of BiFC assay the results require careful evaluation. Due to the nature of this method split fragments of a yellow fluorescent protein (YFP) have the tendency to self-associate spontaneously without the interaction between proteins fused to the YFP fragments resulting in false-positive fluorescence

signal, especially if proteins are overexpressed, which is common in transient transfections (Kerppola, 2006). Therefore it is advisable not to rely on only the qualitative confocal analysis but carry out thorough quantitative and statistical analysis that would provide more robust data. Here I adapted three different ways of quantitative analysis to measure the average fluorescence intensity, signal-to-noise (S/N) ratio and the distribution of yellow/red fluorescence signal ratio. All three methods gave very similar results, complementing each other and confirming the specificity of the BiFC method.

Furthermore, as this thesis highlights, I believe the choice of appropriate negative controls is essential. As a control in the BiFC experiments a transmembrane protein sialophorin (SPN) (also termed leukosialin and CD43) was used as a fusion with the N- or C-terminal YFP sequence (designated SPN-VN and SPN-VC respectively). The SPN protein is similar to R3 RPTPs in that it has a large highly glycosylated extracellular domain and a single transmembrane spanning region; however, it has no homology to any R3 RPTPs and for these reasons has previously been used as a control in other studies of DEP-1 function (Cordoba *et al*, 2013). Moreover, a control construct that entirely lacked the extracellular domain and transmembrane regions and was associated with the cell membrane via the Lck myristoylation sequence (designated Myr-VC) was used as an additional negative control. Despite negative interacting pairs exhibiting some fluorescence signal the quantitative analysis revealed that the signal was significantly reduced compared with positive interacting fusion pairs, indicating specific interactions. However, one exception was the interaction of DEP-1 with SPN control. It is interesting to note that the fluorescence intensity obtained with the DEP-1 and VE-cadherin pairing, although significantly different from DEP-1 with the Myr-VC control, was not significantly different from DEP-1 and the SPN-VC control. And the fluorescence intensity obtained from DEP-1 and SPN interaction was higher compared with DEP-1 and DEP-1 interaction. These observations could be interpreted as a *bona fide* interaction between DEP-1 and SPN. Although both proteins are expressed in leukocytes I am not aware of any previous reports documenting this interaction. Further experiments would be required

to investigate whether the interaction between DEP-1 and SPN has any physiological significance. The findings highlight the importance of using several controls in BiFC studies with membrane proteins which are more prone to artefactual results than studies of freely diffusing cytoplasmic proteins, since the sub-cellular location of these proteins is restricted to the plane of the membrane.

An important area of future investigation in the field of R3 RPTPs is identification of potential ligands and exploration of ligand-induced dimerisation. With respect to R3 RPTPs, since ligands have been documented for DEP-1 (Takahashi *et al*, 2012; Whiteford *et al*, 2011), it is reasonable to assume that ligands exist for other R3 RPTP family members. One approach to identify ligands involves the receptor alkaline phosphatase (RAP) assay. This method provides a direct indicator of extracellular domain binding and it is heat stable and, thus, can be differentiated from the heat labile alkaline phosphatases of most tissues (Stoker, 2005). We have already generated R3 RPTP alkaline phosphatase (AP) fusion proteins and confirmed their expression by Western blotting. These AP fusion proteins can be used as affinity probes to identify ligand- or receptor-expressing cells in tissue culture or in tissue sections and the binding can be directly visualised through simple chromogenic assays without purification, radioactive labelling or secondary reagents. However, these results are not included in this thesis since the experiments are still at the preliminary stage but would be addressed in future work.

References

Aguiar, R. C., Yakushijin, Y., Kharbanda, S., Tiwari, S., Freeman, G. J. & Shipp, M. A. (1999) PTPROt: an alternatively spliced and developmentally regulated B-lymphoid phosphatase that promotes G0/G1 arrest. *Blood*, 94(7), 2403-13.

Alonso, A., Sasin, J., Bottini, N., Friedberg, I., Osterman, A., Godzik, A., Hunter, T., Dixon, J. & Mustelin, T. (2004) Protein tyrosine phosphatases in the human genome. *Cell*, 117(6), 699-711.

Andersen, J. N., Mortensen, O. H., Peters, G. H., Drake, P. G., Iversen, L. F., Olsen, O. H., Jansen, P. G., Andersen, H. S., Tonks, N. K. & Muller, N. P. (2001) Structural and evolutionary relationships among protein tyrosine phosphatase domains. *Mol Cell Biol*, 21(21), 7117-36.

Aricescu, A. R., Siebold, C., Choudhuri, K., Chang, V. T., Lu, W., Davis, S. J., van der Merwe, P. A. & Jones, E. Y. (2007) Structure of a tyrosine phosphatase adhesive interaction reveals a spacer-clamp mechanism. *Science*, 317(5842), 1217-20.

Azzi, S., Hebda, J. K. & Gavard, J. (2013) Vascular permeability and drug delivery in cancers. *Front Oncol*, 3, 211.

Barford, D., Jia, Z. & Tonks, N. K. (1995) Protein tyrosine phosphatases take off. *Nat Struct Biol*, 2(12), 1043-53.

Barr, A. J. (2010) Protein tyrosine phosphatases as drug targets: strategies and challenges of inhibitor development. *Future Med Chem*, 2(10), 1563-76.

Barr, A. J., Ugochukwu, E., Lee, W. H., King, O. N., Filippakopoulos, P., Alfano, I., Savitsky, P., Burgess-Brown, N. A., Muller, S. & Knapp, S. (2009) Large-scale structural analysis of the classical human protein tyrosine phosphatome. *Cell*, 136(2), 352-63.

Beltran, P. J., Bixby, J. L. & Masters, B. A. (2003) Expression of PTPRO during mouse development suggests involvement in axonogenesis and differentiation of NT-3 and NGF-dependent neurons. *J Comp Neurol*, 456(4), 384-95.

Benzing, T. (2004) Signaling at the slit diaphragm. *J Am Soc Nephrol*, 15(6), 1382-91.

Berggard, T., Linse, S. & James, P. (2007) Methods for the detection and analysis of protein-protein interactions. *Proteomics*, 7(16), 2833-42.

Blom, N., Sicheritz-Ponten, T., Gupta, R., Gammeltoft, S. & Brunak, S. (2004) Prediction of post-translational glycosylation and phosphorylation of proteins from the amino acid sequence. *Proteomics*, 4(6), 1633-49.

Borges, L. G., Seifert, R. A., Grant, F. J., Hart, C. E., Disteche, C. M., Edelhoff, S., Solca, F. F., Lieberman, M. A., Lindner, V., Fischer, E. H., Lok, S. & Bowen-Pope, D. F. (1996) Cloning and characterization of rat density-enhanced phosphatase-1, a protein tyrosine phosphatase expressed by vascular cells. *Circ Res*, 79(3), 570-80.

Bos, T. J., Rauscher, F. J., Curran, T. & Vogt, P. K. (1989) The carboxy terminus of the viral Jun oncoprotein is required for complex formation with the cellular Fos protein. *Oncogene*, 4(2), 123-6.

Brady-Kalnay, S. M. & Tonks, N. K. (1994a) Identification of the homophilic binding site of the receptor protein tyrosine phosphatase PTP mu. *J Biol Chem*, 269(45), 28472-7.

Brady-Kalnay, S. M. & Tonks, N. K. (1994b) Protein tyrosine phosphatases: from structure to function. *Trends Cell Biol*, 4(3), 73-6.

Brady-Kalnay, S. M. & Tonks, N. K. (1995) Protein tyrosine phosphatases as adhesion receptors. *Curr Opin Cell Biol*, 7(5), 650-7.

Broermann, A., Winderlich, M., Block, H., Frye, M., Rossaint, J., Zarbock, A., Cagna, G., Linnepe, R., Schulte, D., Nottebaum, A. F. & Vestweber, D. (2011) Dissociation of VE-PTP from VE-cadherin is required for leukocyte extravasation and for VEGF-induced vascular permeability in vivo. *J Exp Med*, 208(12), 2393-401.

Baumer, S., Keller, L., Holtmann, A., Funke, R., August, B., Gamp, A., Wolburg, H., Wolburg-Buchholz, K., Deutsch, U. & Vestweber, D. (2006) Vascular endothelial cell-specific phosphotyrosine phosphatase (VE-PTP) activity is required for blood vessel development. *Blood*, 107(12), 4754-62.

Bohmer, F., Szedlacsek, S., Tabernero, L., Ostman, A. & den Hertog, J. (2013) Protein tyrosine phosphatase structure-function relationships in regulation and pathogenesis. *FEBS J*, 280(2), 413-31.

Cadigan, K. M. (2008) Wnt-beta-catenin signaling. *Curr Biol*, 18(20), R943-7.

Campochiaro, P.A. (2015) Treatment of diabetic macular edema with an inhibitor of vascular endothelial-protein tyrosine phosphatase that activates Tie2. *Ophthalmology* 122, 545–554.

Carmeliet, P. & Collen, D. (2000) Molecular basis of angiogenesis. Role of VEGF and VE-cadherin. *Ann N Y Acad Sci*, 902, 249-62; discussion 262-4.

Carr, P. A., Erickson, H. P. & Palmer, A. G. (1997) Backbone dynamics of homologous fibronectin type III cell adhesion domains from fibronectin and tenascin. *Structure*, 5(7), 949-59.

Chabot, C., Spring, K., Gratton, J. P., Elchebly, M. & Royal, I. (2009) New role for the protein tyrosine phosphatase DEP-1 in Akt activation and endothelial cell survival. *Mol Cell Biol*, 29(1), 241-53.

Chen, C. D., Oh, S. Y., Hinman, J. D. & Abraham, C. R. (2006) Visualization of APP dimerization and APP-Notch2 heterodimerization in living cells using bimolecular fluorescence complementation. *J Neurochem*, 97(1), 30-43.

Chen, R., Jiang, X., Sun, D., Han, G., Wang, F., Ye, M., Wang, L. & Zou, H. (2009) Glycoproteomics analysis of human liver tissue by combination of multiple enzyme digestion and hydrazide chemistry. *J Proteome Res*, 8(2), 651-61.

Chiarugi, P. (2005) PTPs versus PTKs: the redox side of the coin. *Free Radic Res*, 39(4), 353-64.

Chida, K., Nagamori, S. & Kuroki, T. (1999) Nuclear translocation of Fos is stimulated by interaction with Jun through the leucine zipper. *Cell Mol Life Sci*, 55(2), 297-302.

Chin, C. N., Sachs, J. N. & Engelman, D. M. (2005) Transmembrane homodimerization of receptor-like protein tyrosine phosphatases. *FEBS Lett*, 579(17), 3855-8.

Clark, M. C. & Baum, L. G. (2012) T cells modulate glycans on CD43 and CD45 during development and activation, signal regulation, and survival. *Ann N Y Acad Sci*, 1253, 58-67.

Coon, B. G., Baeyens, N., Han, J., Budatha, M., Ross, T. D., Fang, J. S., Yun, S., Thomas, J. L. & Schwartz, M. A. (2015) Intramembrane binding of VE-cadherin to VEGFR2 and VEGFR3 assembles the endothelial mechanosensory complex. *J Cell Biol*, 208(7), 975-86.

Conrads, T.P. & Veenstra, T.D. (2005). An enriched look at tyrosine phosphorylation. *Nature Biotechnology*, 23(1), 36-37.

Cordoba, S. P., Choudhuri, K., Zhang, H., Bridge, M., Basat, A. B., Dustin, M. L. & van der Merwe, P. A. (2013) The large ectodomains of CD45 and CD148 regulate their segregation from and inhibition of ligated T-cell receptor. *Blood*, 121(21), 4295-302.

Daviet, L., Malvoisin, E., Wild, T. F. & McGregor, J. L. (1997) Thrombospondin induces dimerization of membrane-bound, but not soluble CD36. *Thromb Haemost*, 78(2), 897-901.

de la Fuente-Garcia, M. A., Nicolas, J. M., Freed, J. H., Palou, E., Thomas, A. P., Vilella, R., Vives, J. & Gaya, A. (1998a) CD148 is a membrane protein tyrosine phosphatase present in all hematopoietic lineages and is involved in signal transduction on lymphocytes. *Blood*, 91(8), 2800-9.

de Virgilio, M., Kiosses, W. B. & Shattil, S. J. (2004) Proximal, selective, and dynamic interactions between integrin alphaIIbbeta3 and protein tyrosine kinases in living cells. *J Cell Biol*, 165(3), 305-11.

Dejana, E., Lampugnani, M. G., Martinez-Estrada, O. & Bazzoni, G. (2000) The molecular organization of endothelial junctions and their functional role in vascular morphogenesis and permeability. *Int J Dev Biol*, 44(6), 743-8.

Dejana, E., Orsenigo, F. & Lampugnani, M. G. (2008) The role of adherens junctions and VE-cadherin in the control of vascular permeability. *J Cell Sci*, 121(Pt 13), 2115-22.

den Hertog, J., Ostman, A. & Bohmer, F. D. (2008) Protein tyrosine phosphatases: regulatory mechanisms. *FEBS J*, 275(5), 831-47.

Dominguez, M. G., Hughes, V. C., Pan, L., Simmons, M., Daly, C., Anderson, K., Noguera-Troise, I., Murphy, A. J., Valenzuela, D. M., Davis, S., Thurston, G., Yancopoulos, G. D. & Gale, N. W. (2007) Vascular endothelial tyrosine phosphatase (VE-PTP)-null mice undergo vasculogenesis but die embryonically because of defects in angiogenesis. *Proc Natl Acad Sci U S A*, 104(9), 3243-8.

Fachinger, G., Deutsch, U. & Risau, W. (1999) Functional interaction of vascular endothelial-protein-tyrosine phosphatase with the angiopoietin receptor Tie-2. *Oncogene*, 18(43), 5948-53.

Fang, D. & Kerppola, T. K. (2004) Ubiquitin-mediated fluorescence complementation reveals that Jun ubiquitinated by Itch/AIP4 is localized to lysosomes. *Proc Natl Acad Sci U S A*, 101(41), 14782-7.

Fischer, E. H., Charbonneau, H. & Tonks, N. K. (1991) Protein tyrosine phosphatases: a diverse family of intracellular and transmembrane enzymes. *Science*, 253(5018), 401-6.

Frye, M., Dierkes, M., Kuppers, V., Vockel, M., Tomm, J., Zeuschner, D., Rossaint, J., Zarbock, A., Koh, G. Y., Peters, K., Nottebaum, A. F. & Vestweber, D. (2015) Interfering with VE-PTP stabilizes endothelial junctions in vivo via Tie-2 in the absence of VE-cadherin. *J Exp Med*, 212(13), 2267-87.

Fukuda, M. & Tsuboi, S. (1999) Mucin-type O-glycans and leukosialin. *Biochim Biophys Acta*, 1455(2-3), 205-17.

Gao, M., Craig, D., Lequin, O., Campbell, I. D., Vogel, V. & Schulten, K. (2003) Structure and functional significance of mechanically unfolded fibronectin type III1 intermediates. *Proc Natl Acad Sci U S A*, 100(25), 14784-9.

Garton, A. J., Burnham, M. R., Bouton, A. H. & Tonks, N. K. (1997) Association of PTP-PEST with the SH3 domain of p130cas; a novel

mechanism of protein tyrosine phosphatase substrate recognition. *Oncogene*, 15(8), 877-85.

Gentz, R., Rauscher, F. J., Abate, C. & Curran, T. (1989) Parallel association of Fos and Jun leucine zippers juxtaposes DNA binding domains. *Science*, 243(4899), 1695-9.

Geyer, H., Geyer, R., Odenthal-Schnittler, M. & Schnittler, H. J. (1999) Characterization of human vascular endothelial cadherin glycans. *Glycobiology*, 9(9), 915-25.

Giannotta, M., Trani, M. & Dejana, E. (2013) VE-cadherin and endothelial adherens junctions: active guardians of vascular integrity. *Dev Cell*, 26(5), 441-54.

Gonzalez-Brito, M. R. & Bixby, J. L. (2009) Protein tyrosine phosphatase receptor type O regulates development and function of the sensory nervous system. *Mol Cell Neurosci*, 42(4), 458-65.

Gookin, T. E. & Assmann, S. M. (2014) Significant reduction of BiFC non-specific assembly facilitates in planta assessment of heterotrimeric G-protein interactors. *Plant J*, 80(3), 553-67.

Grazia Lampugnani, M., Zanetti, A., Corada, M., Takahashi, T., Balconi, G., Breviario, F., Orsenigo, F., Cattelino, A., Kemler, R., Daniel, T. O. & Dejana, E. (2003) Contact inhibition of VEGF-induced proliferation requires vascular endothelial cadherin, beta-catenin, and the phosphatase DEP-1/CD148. *J Cell Biol*, 161(4), 793-804.

Hayashi, M., Majumdar, A., Li, X., Adler, J., Sun, Z., Vertuani, S., Hellberg, C., Mellberg, S., Koch, S., Dimberg, A., Koh, G. Y., Dejana, E., Belting, H. G., Affolter, M., Thurston, G., Holmgren, L., Vestweber, D. & Claesson-Welsh, L. (2013) VE-PTP regulates VEGFR2 activity in stalk cells to establish endothelial cell polarity and lumen formation. *Nat Commun*, 4, 1672.

Holsinger, L. J., Ward, K., Duffield, B., Zachwieja, J. & Jallal, B. (2002) The transmembrane receptor protein tyrosine phosphatase DEP1 interacts with p120(ctn). *Oncogene*, 21(46), 7067-76.

Horstman, A., Tonaco, I. A., Boutilier, K. & Immink, R. G. (2014) A cautionary note on the use of split-YFP/BiFC in plant protein-protein interaction studies. *Int J Mol Sci*, 15(6), 9628-43.

Hower, A. E., Beltran, P. J. & Bixby, J. L. (2009) Dimerization of tyrosine phosphatase PTPRO decreases its activity and ability to inactivate TrkC. *J Neurochem*, 110(5), 1635-47.

Hu, C. D., Chinenov, Y. & Kerppola, T. K. (2002) Visualization of interactions among bZIP and Rel family proteins in living cells using bimolecular fluorescence complementation. *Mol Cell*, 9(4), 789-98.

Hu, C. D., Grinberg, A. V. & Kerppola, T. K. (2005) Visualization of protein interactions in living cells using bimolecular fluorescence complementation (BiFC) analysis. *Curr Protoc Protein Sci*, Chapter 19, Unit 19.10.

Hunter, T. (1995) Protein kinases and phosphatases: the yin and yang of protein phosphorylation and signaling. *Cell*, 80(2), 225-36.

Jensen, L. J., Gupta, R., Blom, N., Devos, D., Tamames, J., Kesmir, C., Nielsen, H., Staerfeldt, H. H., Rapacki, K., Workman, C., Andersen, C. A., Knudsen, S., Krogh, A., Valencia, A. & Brunak, S. (2002) Prediction of human protein function from post-translational modifications and localization features. *J Mol Biol*, 319(5), 1257-65.

Jensen, O. N. (2004) Modification-specific proteomics: characterization of post-translational modifications by mass spectrometry. *Curr Opin Chem Biol*, 8(1), 33-41.

Jeon, M. & Zinn, K. (2015) R3 receptor tyrosine phosphatases: conserved regulators of receptor tyrosine kinase signaling and tubular organ development. *Semin Cell Dev Biol*, 37, 119-26.

Jiang, G., den Hertog, J. & Hunter, T. (2000) Receptor-like protein tyrosine phosphatase alpha homodimerizes on the cell surface. *Mol Cell Biol*, 20(16), 5917-29.

Jiang, G., den Hertog, J., Su, J., Noel, J., Sap, J. & Hunter, T. (1999) Dimerization inhibits the activity of receptor-like protein-tyrosine phosphatase-alpha. *Nature*, 401(6753), 606-10.

Kang, T.H. & Kim, K.T. (2006) Negative regulation of ERK activity by VRK3-mediated activation of VHR phosphatase. *Nat Cell Biol,* 8, 863-869.

Kerppola, T. K. (2006) Design and implementation of bimolecular fluorescence complementation (BiFC) assays for the visualization of protein interactions in living cells. *Nat Protoc*, 1(3), 1278-86.

Kerppola, T. K. (2008) Bimolecular fluorescence complementation (BiFC) analysis as a probe of protein interactions in living cells. *Annu Rev Biophys*, 37, 465-87.

Kerppola, T. K. (2009) Visualization of molecular interactions using bimolecular fluorescence complementation analysis: characteristics of protein fragment complementation. *Chem Soc Rev*, 38(10), 2876-86.

Kerppola, T. K. (2013a) Bimolecular fluorescence complementation (BiFC) analysis of protein interactions in live cells. *Cold Spring Harb Protoc*, 2013(8), 727-31.

Kerppola, T. K. (2013b) Design of fusion proteins for bimolecular fluorescence complementation (BiFC). *Cold Spring Harb Protoc*, 2013(8), 714-8.

Kerppola, T. K. (2013c) Multicolor bimolecular fluorescence complementation (BiFC) analysis of protein interactions with alternative partners. *Cold Spring Harb Protoc*, 2013(9), 798-803.

Kerppola, T. K. (2013d) Simultaneous visualization of multiple protein interactions using multicolor bimolecular fluorescence complementation (BiFC) analysis. *Cold Spring Harb Protoc*, 2013(9), 892-5.

Kim, M., Kim, H. & Jho, E. H. (2010) Identification of ptpro as a novel target gene of Wnt signaling and its potential role as a receptor for Wnt. *FEBS Lett*, 584(18), 3923-8.

Kodama, Y. & Hu, C. D. (2010) An improved bimolecular fluorescence complementation assay with a high signal-to-noise ratio. *Biotechniques*, 49(5), 793-805.

Kohanski, R.A. & Lane, M.D. (1986) Kinetic evidence for activating and non-activating components of autophosphorylation of the insulin receptor protein kinase. *Biochem Biophys Res Commun.* 134, 1312-1318.

Kolmodin, K. & Aqvist, J. (2001) The catalytic mechanism of protein tyrosine phosphatases revisited. *FEBS Lett*, 498(2-3), 208-13.

Kotani, T., Murata, Y., Saito, Y. & Matozaki, T. (2016) Future therapeutic potential of SAP-1 in inflammatory bowel diseases. *Expert Rev Gastroenterol Hepatol*, 10(12), 1313-1315.

Krebs, E.G. (1992) Protein phosphorylation and cellular regulation I. *Nobel Lect.*72-89.

Krejsa, C. M., Nadler, S. G., Esselstyn, J. M., Kavanagh, T. J., Ledbetter, J. A. & Schieven, G. L. (1997) Role of oxidative stress in the action of vanadium phosphotyrosine phosphatase inhibitors. Redox independent activation of NF-kappaB. *J Biol Chem*, 272(17), 11541-9.

Krueger, N. X., Streuli, M. & Saito, H. (1990) Structural diversity and evolution of human receptor-like protein tyrosine phosphatases. *EMBO J*, 9(10), 3241-52.

Kuppers, V., Vockel, M., Nottebaum, A. F. & Vestweber, D. (2014) Phosphatases and kinases as regulators of the endothelial barrier function. *Cell Tissue Res*, 355(3), 577-86.

Lampugnani, M. G., Corada, M., Caveda, L., Breviario, F., Ayalon, O., Geiger, B. & Dejana, E. (1995) The molecular organization of endothelial cell to cell junctions: differential association of plakoglobin, beta-catenin, and alpha-catenin with vascular endothelial cadherin (VE-cadherin). *J Cell Biol*, 129(1), 203-17.

Lampugnani, M. G., Orsenigo, F., Gagliani, M. C., Tacchetti, C. & Dejana, E. (2006) Vascular endothelial cadherin controls VEGFR-2 internalization and signaling from intracellular compartments. *J Cell Biol*, 174(4), 593-604.

Laramee, M., Chabot, C., Cloutier, M., Stenne, R., Holgado-Madruga, M., Wong, A. J. & Royal, I. (2007) The scaffolding adapter Gab1 mediates vascular endothelial growth factor signaling and is required for endothelial cell migration and capillary formation. *J Biol Chem*, 282(11), 7758-69.

Le Roy, C. & Wrana, J. L. (2005a) Clathrin- and non-clathrin-mediated endocytic regulation of cell signalling. *Nat Rev Mol Cell Biol*, 6(2), 112-26.

Le Roy, C. & Wrana, J. L. (2005b) Signaling and endocytosis: a team effort for cell migration. *Dev Cell*, 9(2), 167-8.

Lee, H., Noh, H., Mun, J., Gu, C., Sever, S. & Park, S. (2016) Anks1a regulates COPII-mediated anterograde transport of receptor tyrosine kinases critical for tumorigenesis. *Nat Commun*, 7, 12799.

Lee, J. R. (2015) Protein tyrosine phosphatase PTPRT as a regulator of synaptic formation and neuronal development. *BMB Rep*, 48(5), 249-55.

Lee, S. R., Kwon, K. S., Kim, S. R. & Rhee, S. G. (1998) Reversible inactivation of protein-tyrosine phosphatase 1B in A431 cells stimulated with epidermal growth factor. *J Biol Chem*, 273(25), 15366-72.

Lemmon, M. A. & Schlessinger, J. (1998) Transmembrane signaling by receptor oligomerization. *Methods Mol Biol*, 84, 49-71.

Lemmon, M. A., Treutlein, H. R., Adams, P. D., Brunger, A. T. & Engelman, D. M. (1994) A dimerization motif for transmembrane alpha-helices. *Nat Struct Biol*, 1(3), 157-63.

Lievens, S., Lemmens, I. & Tavernier, J. (2009) Mamalian two-hybrids come of age. *Trends Biochem. Sci.* 34(11), 579-588.

Lin, M.F. & Clinton, G.M. (1988) The epidermal growth factor receptor from prostate cells is dephosphorylated by a prostate-specific phosphotyrosyl phosphatase. *Mol Cell Biol.* 8, 5477-5485.

Lin, H. P., Vincenz, C., Eliceiri, K. W., Kerppola, T. K. & Ogle, B. M. (2010) Bimolecular fluorescence complementation analysis of eukaryotic fusion products. *Biol Cell*, 102(9), 525-37.

Liu, T., Qian, W. J., Gritsenko, M. A., Camp, D. G., Monroe, M. E., Moore, R. J. & Smith, R. D. (2005) Human plasma N-glycoproteome analysis by immunoaffinity subtraction, hydrazide chemistry, and mass spectrometry. *J Proteome Res*, 4(6), 2070-80.

Magliery, T. J. & Regan, L. (2006) Reassembled GFP: detecting protein-protein interactions and protein expression patterns. *Methods Biochem Anal*, 47, 391-405.

Mahadev, K., Zilbering, A., Zhu, L. & Goldstein, B. J. (2001) Insulin-stimulated hydrogen peroxide reversibly inhibits protein-tyrosine phosphatase 1b in vivo and enhances the early insulin action cascade. *J Biol Chem*, 276(24), 21938-42.

Mann, M. (2009) Comparative analysis to guide quality improvements in proteomics. *Nat Methods*, 6(10), 717-19.

Martino, M. M. & Hubbell, J. A. (2010) The 12th-14th type III repeats of fibronectin function as a highly promiscuous growth factor-binding domain. *FASEB J*, 24(12), 4711-21.

Matozaki, T., Murata, Y., Mori, M., Kotani, T., Okazawa, H. & Ohnishi, H. (2010) Expression, localization, and biological function of the R3 subtype of receptor-type protein tyrosine phosphatases in mammals. *Cell Signal*, 22(12), 1811-7.

Matozaki, T., Suzuki, T., Uchida, T., Inazawa, J., Ariyama, T., Matsuda, K., Horita, K., Noguchi, H., Mizuno, H. & Sakamoto, C. (1994) Molecular cloning of a human transmembrane-type protein tyrosine phosphatase and its expression in gastrointestinal cancers. *J Biol Chem*, 269(3), 2075-81.

McLachlan, R. W., Kraemer, A., Helwani, F. M., Kovacs, E. M. & Yap, A. S. (2007) E-cadherin adhesion activates c-Src signaling at cell-cell contacts. *Mol Biol Cell*, 18(8), 3214-23.

McLachlan, R. W. & Yap, A. S. (2007) Not so simple: the complexity of phosphotyrosine signaling at cadherin adhesive contacts. *J Mol Med (Berl)*, 85(6), 545-54.

Mellberg, S., Dimberg, A., Bahram, F., Hayashi, M., Rennel, E., Ameur, A., Westholm, J. O., Larsson, E., Lindahl, P., Cross, M. J. & Claesson-Welsh, L. (2009) Transcriptional profiling reveals a critical role for tyrosine phosphatase VE-PTP in regulation of VEGFR2 activity and endothelial cell morphogenesis. *FASEB J*, 23(5), 1490-502.

Meng, K., Rodriguez-Pena, A., Dimitrov, T., Chen, W., Yamin, M., Noda, M. & Deuel, T. F. (2000) Pleiotrophin signals increased tyrosine phosphorylation of beta beta-catenin through inactivation of the intrinsic catalytic activity of the receptor-type protein tyrosine phosphatase beta/zeta. *Proc Natl Acad Sci U S A*, 97(6), 2603-8.

Motiwala, T., Ghoshal, K., Das, A., Majumder, S., Weichenhan, D., Wu, Y. Z., Holman, K., James, S. J., Jacob, S. T. & Plass, C. (2003) Suppression of the protein tyrosine phosphatase receptor type O gene (PTPRO) by methylation in hepatocellular carcinomas. *Oncogene*, 22(41), 6319-31.

Motiwala, T., Kutay, H., Zanesi, N., Frissora, F. W., Mo, X., Muthusamy, N. & Jacob, S. T. (2015) PTPROt-mediated regulation of p53/Foxm1 suppresses leukemic phenotype in a CLL mouse model. *Leukemia*, 29(6), 1350-9.

Murata, Y., Kotani, T., Supriatna, Y., Kitamura, Y., Imada, S., Kawahara, K., Nishio, M., Daniwijaya, E. W., Sadakata, H., Kusakari, S., Mori, M., Kanazawa, Y., Saito, Y., Okawa, K., Takeda-Morishita, M., Okazawa, H., Ohnishi, H., Azuma, T., Suzuki, A. & Matozaki, T. (2015a) Protein tyrosine phosphatase SAP-1 protects against colitis through regulation of CEACAM20 in the intestinal epithelium. *Proc Natl Acad Sci U S A*, 112(31), E4264-71.

Murata, Y., Kotani, T., Supriatna, Y., Kitamura, Y., Imada, S., Kawahara, K., Nishio, M., Daniwijaya, E. W., Sadakata, H., Kusakari, S., Mori, M., Kanazawa, Y., Saito, Y., Okawa, K., Takeda-Morishita, M., Okazawa, H., Ohnishi, H., Azuma, T., Suzuki, A. & Matozaki, T. (2015b) Protein tyrosine phosphatase SAP-1 protects against colitis through regulation of CEACAM20 in the intestinal epithelium. *Proc Natl Acad Sci U S A*, 112(31), E4264-71.

Murata, Y., Mori, M., Kotani, T., Supriatna, Y., Okazawa, H., Kusakari, S., Saito, Y., Ohnishi, H. & Matozaki, T. (2010) Tyrosine phosphorylation of R3 subtype receptor-type protein tyrosine phosphatases and their complex formations with Grb2 or Fyn. *Genes Cells*, 15(5), 513-24.

Mustelin, T., Feng, G. S., Bottini, N., Alonso, A., Kholod, N., Birle, D., Merlo, J. & Huynh, H. (2002) Protein tyrosine phosphatases. *Front Biosci*, 7, d85-142.

Mustelin, T., Vang, T. & Bottini, N. (2005) Protein tyrosine phosphatases and the immune response. *Nat Rev Immunol*, 5(1), 43-57.

Nagano, H., Noguchi, T., Inagaki, K., Yoon, S., Matozaki, T., Itoh, H., Kasuga, M. & Hayashi, Y. (2003) Downregulation of stomach cancer-associated protein tyrosine phosphatase-1 (SAP-1) in advanced human hepatocellular carcinoma. *Oncogene*, 22(30), 4656-63.

Nakagawa, C., Inahata, K., Nishimura, S. & Sugimoto, K. (2011) Improvement of a Venus-based bimolecular fluorescence complementation assay to visualize bFos-bJun interaction in living cells. *Biosci Biotechnol Biochem*, 75(7), 1399-401.

Nawroth, R., Poell, G., Ranft, A., Kloep, S., Samulowitz, U., Fachinger, G., Golding, M., Shima, D. T., Deutsch, U. & Vestweber, D. (2002) VE-PTP and VE-cadherin ectodomains interact to facilitate regulation of phosphorylation and cell contacts. *EMBO J*, 21(18), 4885-95.

Neuberg, M., Adamkiewicz, J., Hunter, J. B. & Muller, R. (1989) A Fos protein containing the Jun leucine zipper forms a homodimer which binds to the AP1 binding site. *Nature*, 341(6239), 243-5.

Noguchi, T., Tsuda, M., Takeda, H., Takada, T., Inagaki, K., Yamao, T., Fukunaga, K., Matozaki, T. & Kasuga, M. (2001) Inhibition of cell growth and spreading by stomach cancer-associated protein-tyrosine phosphatase-1 (SAP-1) through dephosphorylation of p130cas. *J Biol Chem*, 276(18), 15216-24.

Noordman, Y. E., Augustus, E. D., Schepens, J. T., Chirivi, R. G., Rios, P., Pulido, R. & Hendriks, W. J. (2008) Multimerisation of receptor-type protein tyrosine phosphatases PTPBR7 and PTP-SL attenuates enzymatic activity. *Biochim Biophys Acta*, 1783(2), 275-86.

Nottebaum, A. F., Cagna, G., Winderlich, M., Gamp, A. C., Linnepe, R., Polaschegg, C., Filippova, K., Lyck, R., Engelhardt, B., Kamenyeva, O., Bixel, M. G., Butz, S. & Vestweber, D. (2008) VE-PTP maintains the endothelial barrier via plakoglobin and becomes dissociated from VE-cadherin by leukocytes and by VEGF. *J Exp Med*, 205(12), 2929-45.

Ostergaard, H.L., Shackelford, D.A., Hurley, T.R., Johnson. P., Hyman, R., Sefton, B.M. & Trowbridge, I.S. (1989) Expression of CD45 alters phosphorylation of the lck-encoded tyrosine protein kinase in murine lymphoma T-cell lines. *Proc Natl Acad Sci USA*, 86, 8959-8963.

Ostman, A., Hellberg, C. & Bohmer, F. D. (2006) Protein-tyrosine phosphatases and cancer. *Nat Rev Cancer*, 6(4), 307-20.

Ostman, A., Yang, Q. & Tonks, N. K. (1994) Expression of DEP-1, a receptor-like protein-tyrosine-phosphatase, is enhanced with increasing cell density. *Proc Natl Acad Sci U S A*, 91(21), 9680-4.

Petschnigg, J., Groisman, B., Kotlyar, M., Taipale, M., Zheng, Y., Kurat, C. F., Sayad, A., Sierra, J. R., Mattiazzi Usaj, M., Snider, J., Nachman, A., Krykbaeva, I., Tsao, M. S., Moffat, J., Pawson, T., Lindquist, S., Jurisica, I. & Stagljar, I. (2014) The mammalian-membrane two-hybrid assay (MaMTH) for probing membrane-protein interactions in human cells. *Nat Methods*, 11(5), 585-92.

Pixley, F. J., Lee, P. S., Dominguez, M. G., Einstein, D. B. & Stanley, E. R. (1995) A heteromorphic protein-tyrosine phosphatase, PTP phi, is regulated by CSF-1 in macrophages. *J Biol Chem*, 270(45), 27339-47.

Ransone, L. J., Visvader, J., Wamsley, P. & Verma, I. M. (1990) Trans-dominant negative mutants of Fos and Jun. *Proc Natl Acad Sci U S A*, 87(10), 3806-10.

Rose, R. H., Briddon, S. J. & Holliday, N. D. (2010) Bimolecular fluorescence complementation: lighting up seven transmembrane domain receptor signalling networks. *Br J Pharmacol*, 159(4), 738-50.

Sadakata, H., Okazawa, H., Sato, T., Supriatna, Y., Ohnishi, H., Kusakari, S., Murata, Y., Ito, T., Nishiyama, U., Minegishi, T., Harada, A. & Matozaki, T. (2009) SAP-1 is a microvillus-specific protein tyrosine phosphatase that modulates intestinal tumorigenesis. *Genes Cells*, 14(3), 295-308.

Sakuraba, J., Shintani, T., Tani, S. & Noda, M. (2013) Substrate specificity of R3 receptor-like protein-tyrosine phosphatase subfamily toward receptor protein-tyrosine kinases. *J Biol Chem*, 288(32), 23421-31.

Sallee, J. L. & Burridge, K. (2009) Density-enhanced phosphatase 1 regulates phosphorylation of tight junction proteins and enhances barrier function of epithelial cells. *J Biol Chem*, 284(22), 14997-5006.

Salmeen, A., Andersen, J. N., Myers, M. P., Tonks, N. K. & Barford, D. (2000) Molecular basis for the dephosphorylation of the activation segment of the insulin receptor by protein tyrosine phosphatase 1B. *Mol Cell*, 6(6), 1401-12.

Saltiel, A. R. & Kahn, C. R. (2001) Insulin signalling and the regulation of glucose and lipid metabolism. *Nature*, 414(6865), 799-806.

Schlessinger, J. (2002) Ligand-induced, receptor-mediated dimerization and activation of EGF receptor. *Cell*, 110(6), 669-72.

Seimiya, H. & Tsuruo, T. (1998) Functional involvement of PTP-U2L in apoptosis subsequent to terminal differentiation of monoblastoid leukemia cells. *J Biol Chem*, 273(33), 21187-93.

Sekar, R. B. & Periasamy, A. (2003) Fluorescence resonance energy transfer (FRET) microscopy imaging of live cell protein localizations. *J Cell Biol*, 160(5), 629-33.

Seo, Y., Matozaki, T., Tsuda, M., Hayashi, Y., Itoh, H. & Kasuga, M. (1997) Overexpression of SAP-1, a transmembrane-type protein tyrosine phosphatase, in human colorectal cancers. *Biochem Biophys Res Commun*, 231(3), 705-11.

Shelley, C. S., Remold-O'Donnell, E., Davis, A. E., Bruns, G. A., Rosen, F. S., Carroll, M. C. & Whitehead, A. S. (1989) Molecular characterization of sialophorin (CD43), the lymphocyte surface sialoglycoprotein defective in Wiskott-Aldrich syndrome. *Proc Natl Acad Sci U S A*, 86(8), 2819-23.

Shen, J., Frye, M., Lee, B.L., Reinardy, J.L., McClung, J.M., Ding, K., Kojima, M., Xia, H., Seidel, C., Lima e Silva, R., Dong, A., Hackett, S.F., Wang, J., Howard, B.W., Vestweber, D., Kontos, C.D., Peters, K.G. and Campochiaro,

P.A. (2014) Targeting VE-PTP activates TIE2 and stabilizes the ocular vasculature. *J. Clin. Invest*. 124, 4564–4576

Shintani, T., Higashi, S., Takeuchi, Y., Gaudio, E., Trapasso, F., Fusco, A. & Noda, M. (2015) The R3 receptor-like protein tyrosine phosphatase subfamily inhibits insulin signalling by dephosphorylating the insulin receptor at specific sites. *J Biochem*, 158(3), 235-43.

Singer, S. J. & Nicolson, G. L. (1972) The fluid mosaic model of the structure of cell membranes. *Science*, 175(4023), 720-31.

Singh, P., Carraher, C. & Schwarzbauer, J. E. (2010) Assembly of fibronectin extracellular matrix. *Annu Rev Cell Dev Biol*, 26, 397-419.

Spring, K., Chabot, C., Langlois, S., Lapointe, L., Trinh, N. T., Caron, C., Hebda, J. K., Gavard, J., Elchebly, M. & Royal, I. (2012) Tyrosine phosphorylation of DEP-1/CD148 as a mechanism controlling Src kinase activation, endothelial cell permeability, invasion, and capillary formation. *Blood*, 120(13), 2745-56.

Spring, K., Lapointe, L., Caron, C., Langlois, S. & Royal, I. (2014) Phosphorylation of DEP-1/PTPRJ on threonine 1318 regulates Src activation and endothelial cell permeability induced by vascular endothelial growth factor. *Cell Signal*, 26(6), 1283-93.

Stanford, S.M. and Bottini, N. (2017) Targeting Tyrosine Phosphatases: Time to End the Stigma. *Trends in Pharmacological Sciences*, 38(6), 524-540.

Stoker, A. (2005a) Methods for identifying extracellular ligands of RPTPs. *Methods*, 35(1), 80-9.

Stoker, A. W. (2005b) Protein tyrosine phosphatases and signalling. *J Endocrinol*, 185(1), 19-33.

Strous, G. J. & Gent, J. (2002) Dimerization, ubiquitylation and endocytosis go together in growth hormone receptor function. *FEBS Lett*, 529(1), 102-9.

Sung, M. K. & Huh, W. K. (2010) In vivo quantification of protein-protein interactions in Saccharomyces cerevisiae using bimolecular fluorescence complementation assay. *J Microbiol Methods*, 83(2), 194-201.

Suter, B., Kittanakom, S. & Stagljar, I. (2008) Two-hybrid technologies in proteomics research. *Curr Opin Biotechnol*, 19(4), 316-23.

Sorby, M., Sandstrom, J. & Ostman, A. (2001a) An extracellular ligand increases the specific activity of the receptor-like protein tyrosine phosphatase DEP-1. *Oncogene*, 20(37), 5219-24.

Sorby, M., Sandstrom, J. & Ostman, A. (2001b) An extracellular ligand increases the specific activity of the receptor-like protein tyrosine phosphatase DEP-1. *Oncogene*, 20(37), 5219-24.

Takagi, J., Strokovich, K., Springer, T. A. & Walz, T. (2003) Structure of integrin alpha5beta1 in complex with fibronectin. *EMBO J*, 22(18), 4607-15.

Takahashi, K., Mernaugh, R. L., Friedman, D. B., Weller, R., Tsuboi, N., Yamashita, H., Quaranta, V. & Takahashi, T. (2012) Thrombospondin-1 acts as a ligand for CD148 tyrosine phosphatase. *Proc Natl Acad Sci U S A*, 109(6), 1985-90.

Takahashi, T., Takahashi, K., Mernaugh, R., Drozdoff, V., Sipe, C., Schoecklmann, H., Robert, B., Abrahamson, D. R. & Daniel, T. O. (1999) Endothelial localization of receptor tyrosine phosphatase, ECRTP/DEP-1, in developing and mature renal vasculature. *J Am Soc Nephrol*, 10(10), 2135-45.

Takahashi, T., Takahashi, K., Mernaugh, R. L., Tsuboi, N., Liu, H. & Daniel, T. O. (2006) A monoclonal antibody against CD148, a receptor-like tyrosine phosphatase, inhibits endothelial-cell growth and angiogenesis. *Blood*, 108(4), 1234-42.

Tangye, S. G., Phillips, J. H., Lanier, L. L., de Vries, J. E. & Aversa, G. (1998) CD148: a receptor-type protein tyrosine phosphatase involved in the regulation of human T cell activation. *J Immunol*, 161(7), 3249-55.

Tautz, L., Pellecchia, M. & Mustelin, T. (2006) Targeting the PTPome in human disease. *Expert Opin Ther Targets*, 10(1), 157-77.

Teese, M. G. & Langosch, D. (2015) Role of GxxxG Motifs in Transmembrane Domain Interactions. *Biochemistry*, 54(33), 5125-35.

Tertoolen, L. G., Blanchetot, C., Jiang, G., Overvoorde, J., Gadella, T. W., Hunter, T. & den Hertog, J. (2001) Dimerization of receptor protein-tyrosine phosphatase alpha in living cells. *BMC Cell Biol*, 2, 8.

Thomas, P. E., Wharram, B. L., Goyal, M., Wiggins, J. E., Holzman, L. B. & Wiggins, R. C. (1994) GLEPP1, a renal glomerular epithelial cell (podocyte) membrane protein-tyrosine phosphatase. Identification, molecular cloning, and characterization in rabbit. *J Biol Chem*, 269(31), 19953-62.

Thomas, M.L. & Brown, E.J. (1999) Positive and negative regulation of Src-family membrane kinases by CD45. *Immunol Today,* 20, 406-411.

Tian, J., Wang, H. P., Mao, Y. Y., Jin, J. & Chen, J. H. (2007) Reduced glomerular epithelial protein 1 expression and podocyte injury in immunoglobulin A nephropathy. *J Int Med Res*, 35(3), 338-45.

Tonks, N. K. (2006) Protein tyrosine phosphatases: from genes, to function, to disease. *Nat Rev Mol Cell Biol*, 7(11), 833-46.

Tonks, N. K. (2013) Protein tyrosine phosphatases--from housekeeping enzymes to master regulators of signal transduction. *FEBS J*, 280(2), 346-78.

van der Wijk, T., Blanchetot, C. & den Hertog, J. (2005) Regulation of receptor protein-tyrosine phosphatase dimerization. *Methods*, 35(1), 73-9.

Vestweber, D. (2008) VE-cadherin: the major endothelial adhesion molecule controlling cellular junctions and blood vessel formation. *Arterioscler Thromb Vasc Biol*, 28(2), 223-32.

Walchli, S., Espanel, X. & Hooft van Huijsduijnen, R. (2005) Sap-1/PTPRH activity is regulated by reversible dimerization. *Biochem Biophys Res Commun*, 331(2), 497-502.

Walter, M., Chaban, C., Schutze, K., Batistic, O., Weckermann, K., Nake, C., Blazevic, D., Grefen, C., Schumacher, K., Oecking, C., Harter, K. & Kudla, J. (2004) Visualization of protein interactions in living plant cells using bimolecular fluorescence complementation. *Plant J*, 40(3), 428-38.

Waters, M. L. (2016) Post-translational modifications: Bonds that bind. *Nat Chem Biol*, 12(10), 768-9.

Wharram, B. L., Goyal, M., Gillespie, P. J., Wiggins, J. E., Kershaw, D. B., Holzman, L. B., Dysko, R. C., Saunders, T. L., Samuelson, L. C. & Wiggins, R. C. (2000) Altered podocyte structure in GLEPP1 (Ptpro)-deficient mice associated with hypertension and low glomerular filtration rate. *J Clin Invest*, 106(10), 1281-90.

Whiteford, J. R., Xian, X., Chaussade, C., Vanhaesebroeck, B., Nourshargh, S. & Couchman, J. R. (2011) Syndecan-2 is a novel ligand for the protein tyrosine phosphatase receptor CD148. *Mol Biol Cell*, 22(19), 3609-24.

Wilde, A., Beattie, E. C., Lem, L., Riethof, D. A., Liu, S. H., Mobley, W. C., Soriano, P. & Brodsky, F. M. (1999) EGF receptor signaling stimulates SRC kinase phosphorylation of clathrin, influencing clathrin redistribution and EGF uptake. *Cell*, 96(5), 677-87.

Wong, K. A. & O'Bryan, J. P. (2011) Bimolecular fluorescence complementation. *J Vis Exp*(50).

Xu, Y. & Fisher, G. J. (2012) Receptor type protein tyrosine phosphatases (RPTPs) - roles in signal transduction and human disease. *J Cell Commun Signal*, 6(3), 125-38.

Xu, Z. & Weiss, A. (2002a) Negative regulation of CD45 by differential homodimerization of the alternatively spliced isoforms. *Nat Immunol*, 3(8), 764-71.

Xu, Z. & Weiss, A. (2002b) Negative regulation of CD45 by differential homodimerization of the alternatively spliced isoforms. *Nat Immunol*, 3(8), 764-71.

Yu, K.R., Kim, Y.J., Jung, S.K., Ku, B., Park, H., Cho, S.Y. *et al* (2013) Structural basis for the dephosphorylating activity of PTPRQ towards phosphatidylinositide substrates. *Acta Crystallogr D*: *Biol Crystallogr*, 69, 1522-9

Zhang, Z. Y. (2002) Protein tyrosine phosphatases: structure and function, substrate specificity, and inhibitor development. *Annu Rev Pharmacol Toxicol*, 42, 209-34.

Zhang, Z. Y., Thieme-Sefler, A. M., Maclean, D., McNamara, D. J., Dobrusin, E. M., Sawyer, T. K. & Dixon, J. E. (1993) Substrate specificity of the protein tyrosine phosphatases. *Proc Natl Acad Sci U S A*, 90(10), 4446-50.

Zlatkine, P., Mehul, B. & Magee, A. I. (1997) Retargeting of cytosolic proteins to the plasma membrane by the Lck protein tyrosine kinase dual acylation motif. *J Cell Sci*, 110 (Pt 5), 673-9.